FLUID MECHANICS FOR ENGINEERS

FLUID MECHANICS FOR ENGINEERS

P. S. BARNA, M.E., A.F.R.Ae.S.

Senior Lecturer in Mechanical Engineering
New South Wales University of Technology
Sydney

LONDON
BUTTERWORTHS SCIENTIFIC PUBLICATIONS
1957

PREFACE

THIS text was planned primarily to provide in one volume adequate coverage for undergraduates studying for a degree or diploma in Mechanical or Civil Engineering. It is hoped that parts will be useful for Higher National Certificate courses.

Emphasis is laid upon the broad representation of the fundamentals, leaving certain topics not included in the text for the choice of individual teachers. A large number of examples with complete solutions are given and these have been carefully selected to illustrate the preceding theory. In some cases more than one example illustrates the theory and wherever possible simple examples precede the more complex ones.

It is suggested that students in Mechanical Engineering may omit Flow in Open Channels whilst students in Civil Engineering may omit some details of Rotodynamic Machinery and of Compressible Fluid Flow.

The text is subdivided into self-contained chapters each covering the relevant field as completely as it was thought practicable. So far as possible theory was kept in the neighbourhood of its application. For example, manometers are dealt with in the chapter on Fluid Metering, and moment of momentum and free vortex are treated in the later chapter on Rotodynamic Machinery. For similar reasons, Wing Theory, although an independent field, may be linked with Axial Flow Machinery and may serve as a forerunner to that chapter.

It is anticipated that certain elementary concepts such as density, pressure, force etc., have already been introduced in physics and their detailed discussion is omitted from the text.

The author expresses sincere appreciation to Messrs R. A. Bryant, B. Langevad, C. Sapsford, R. Vallentine, and A. D. Owen of the University of Technology, Sydney, to Messrs J. Palmer and K. Moore of the College of Aeronautics, Cranfield, and Royal Aircraft Establishment, Bedford, respectively, for their critical examination of the manuscript and for their useful suggestions. It is acknowledged that some of the examples and problems were adopted from past examination papers of the N.S.W. University of Technology.

Any suggestions which might improve the text will be welcomed by the author.

Cranfield, Buckinghamshire
March, 1957

CONTENTS

PART 2

PART 3

PART 1

1

FLUID STATICS

1.1 Introduction

WHEN fluids are at rest the associated problems fall into the category which is generally termed Fluid Statics. These problems are far simpler and fewer than those associated with Fluid Motion. Since no relative movement is experienced between fluid layers any mutual action due to viscosity is non-existent, and calculations may ignore viscosity effects completely; because of this, solutions may be obtained by simple methods without the aid of complex experiments.

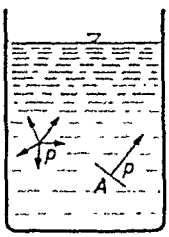

Figure 1.1

The free surface of liquids at rest lies in the gravitational equipotential planes. This is the reason why the surfaces of oceans follow the earth's curvature. For practical purposes the free surface of a liquid in a container may be considered perfectly plane provided the dimensions of the container are small (relative to the diameter of the earth). When we consider a longer channel, however, say 1,000–2,000 ft. long like the modern towing tanks used for model ship research, the curvature must be considered, as the deviation from the straight line may be of the order of, say, 1/10 of an inch.

Pressure, p, in fluids is a scalar quantity, that is a quantity without any direction, so that at any point of a fluid aggregate the pressure may not be represented by a vector. In other words, at any one point the pressure is the same in all directions. Once a surface, A, is specified the pressure acting on the surface produces a force, which is a vector of a magnitude $p \cdot A$, and direction normal to the surface (*see Fig. 1.1*).

1.2 Fundamentals of Fluid Statics

The fundamental problem of fluid statics is the determination of the distribution of pressure in a homogeneous fluid.

Consider a tank of cross-section S filled with liquid of specific weight w as shown in *Fig. 1.2.* Going down from the free surface each layer of liquid of thickness Δh rests on the next layer, the weight of each layer being $w \,.\, \Delta hS$. It may be seen therefore that the pressure continuously increases with depth by an amount

$$\Delta p = \frac{\text{weight}}{\text{area}} = \frac{w\,\Delta hS}{S} = w \,.\, \Delta h$$

for each distance Δh traversed.

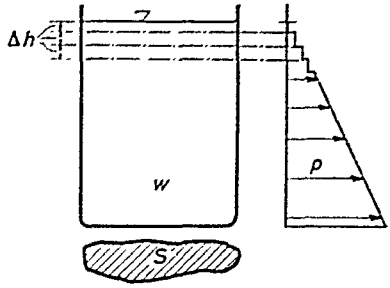

Figure 1.2—Distribution of pressure in a tank

Hence

$$w = \lim \frac{\Delta p}{\Delta h} = \frac{\mathrm{d}p}{\mathrm{d}h} \qquad \ldots.(1.1)$$

Integration yields

$$p = \int w \,\mathrm{d}h \qquad \ldots.(1.2)$$

Equation 1.2 at once brings up the question of compressibility, because in order to integrate the equation a relationship between w and h must be given. Liquids are considered incompressible so that w is independent of h. Therefore for liquids

$$p = w \,.\, h \qquad \ldots.(1.3)$$

which represents a linear relationship between depth and pressure (h being measured from the free surface).

Gaseous fluids on the other hand are compressible and follow the law of the gas equation

$$pv = RT \qquad \text{where } v = \frac{1}{w}$$

so that Eq. 1.1 becomes

$$-\frac{dp}{dh} = \frac{p}{RT} \quad \text{or} \quad \frac{dp}{p} = -\frac{dh}{RT} \qquad \ldots.(1.4)$$

The negative sign is due to p decreasing with increasing h.

Integration of Eq. 1.4 leads to the vertical pressure distribution of the atmosphere. However, in order to integrate the right hand side of Eq. 1.4 a relationship between h and T must be given.

The international standard atmosphere is defined by the assumption that the relationship between the temperature T and height h, measured from sea level, is a linear one given by the lapse rate

$$a = -\frac{dT}{dh} = 0{\cdot}00198°\text{C per ft.}$$

This holds fairly accurately up to 36,000 ft. Integration leads to

$$T = T_0 - 0{\cdot}00198h$$

Since the standard temperature at sea level is adopted as 15°C, $T_0 = 273{\cdot}2 + 15 = 288{\cdot}2°\text{K}$.

Hence $$T = 288{\cdot}2 - 0{\cdot}00198h.$$

Substituting the lapse rate into Eq. 1.4, one obtains

$$\frac{dp}{p} = \frac{1}{aR} \cdot \frac{dT}{T}$$

Integration leads to

$$\log p = \log T^{\frac{1}{aR}}$$

or

$$\frac{p}{p_0} = \left(\frac{T}{T_0}\right)^{\frac{1}{aR}}$$

Since $$1/aR = 1/0{\cdot}00198 \times 96 = 5{\cdot}256$$

one finally obtains

$$\frac{p}{p_0} = (1 - 0{\cdot}00000687h)^{5{\cdot}256} \qquad \ldots.(1.5)$$

where p_0 is the pressure at sea level. Similar relation exists for the density change with height. Values of p, based on Eq. 1.5 are given in tables published by the N.A.C.A.†

† National Advisory Committee for Aeronautics, Report 1235/1955.

1.3 Pressure Forces on Submerged Plane Surfaces. Centre of Pressure

Practical application of Eq. 1.3 may be found when pressure forces on surfaces submerged in liquids are calculated. Examples of such surfaces are lock gates and valves. The problem involves the calculation of the total force and its location which is frequently called the centre of pressure.

Consider a flat plate A–B of surface area S which may be of arbitrary shape, covering a submerged opening in the side of a reservoir (*see Fig. 1.3*). The plane of the plate makes an angle α with the free liquid surface and at a depth h, taken from the free surface, the pressure $p = wh$. The force acting on an elementary area dS of the plate dF = dSp = dSwh.

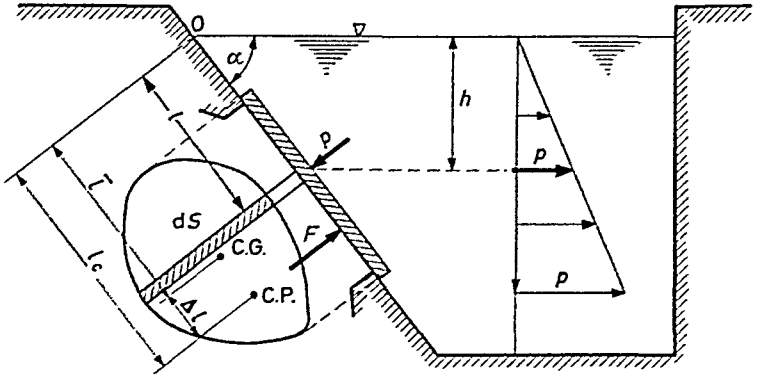

Figure 1.3—Pressures on a submerged plane surface

The total force on the plate may be obtained upon integration

$$F = w \int_0^s h \, \mathrm{d}S = w \sin \alpha \int_0^s l \, \mathrm{d}S$$

where the expression $\int l \, \mathrm{d}S = lS = I_1$ is called the first moment of area S about the horizontal axis 0.
Therefore

$$F = I_1 w \sin \alpha \qquad \ldots . (1.6)$$

The location of the total force, called the centre of pressure, may be obtained by taking moments of the force elements about the axis 0 and equating the sum of these moments to the moment of the total force about the same axis. Thus

$$\int wh \, \mathrm{d}Sl = F \cdot l_c \qquad \ldots . (1.7)$$

where l_c is the distance of the centre of pressure from 0. Since $h = l \cdot \sin \alpha$, the left hand side of Eq. 1.7 becomes $w \sin \alpha \int l^2 \, dS$. This integral is called the second moment of the area around 0. Denoting this by I_{II} we have

$$F \cdot l_c = w \sin \alpha I_{II}$$

Substituting for F from Eq. 1.6 one obtains the centre of pressure

$$l_c = \frac{I_{II}}{I_I} = \frac{\text{second moment}}{\text{first moment}} \Big| \begin{matrix} \text{of area } S \\ \text{about 0.} \end{matrix} \qquad \ldots . (1.8)$$

The depth of the centre of pressure is given by

$$h_c = l_c \sin \alpha$$

It may be shown that the centre of pressure lies always below the centre of gravity. Denoting the distance between the two by Δl and considering that $I_{II} = I_{C.G} + l^2 S$, where $I_{C.G}$ is the second moment of the area about the horizontal axis through the centre of gravity, then

$$\Delta l = \frac{I_{C.G} + l^2 S}{lS} - l = \frac{I_{C.G}}{l \cdot S} \qquad \ldots . (1.9)$$

For plane surfaces which are asymmetric about the vertical centre line, the lateral position of the C.P. or C.G. may be obtained by taking moments laterally about a convenient axis.

Example

1.1. A submerged circular opening, cut in the side of a water tank, is provided with a cover plate. The diameter of the opening is 6 ft. and its centre lies 10 ft. below the free surface of the water. Calculate the magnitude and location of the total force acting on the surface, if the angle of inclination of the side is 45°.

Solution.—The first moment of the circular area

$$I_I = \frac{10}{\sin 45} \times \frac{6^2 \pi}{4} = 400 \text{ ft.}^3$$

Hence the total force

$$F = 400 \times 62{\cdot}4 \times 0{\cdot}707 = 17650 \text{ lb.}$$

The second moment of the circular area about a diameter is given by $\frac{d^4 \pi}{64}$, hence $I_{IIC.G} = \frac{6^4 \pi}{64} = 638 \text{ ft.}^4$

The second moment about 0

$$I_{II} = 638 + \frac{6^2 \pi}{4} \times 14{\cdot}2^2 = 6320 \text{ ft.}^4$$

Distance of centre of pressure from 0

$$l_c = \frac{6320}{400} = 15{\cdot}8 \text{ ft.}$$

Hence

$$\Delta l_c = 15{\cdot}8 - 14{\cdot}2 = 1{\cdot}6 \text{ ft.}$$

1.4 Pressure Forces on Submerged Curved Surfaces

Consider now a curved surface shown in *Fig. 1.4*. The pressure forces at any point act perpendicularly to the surface and there

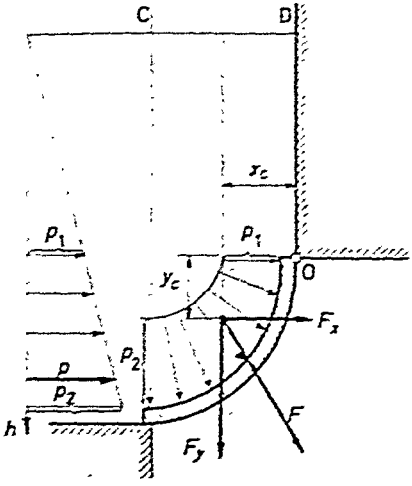

Figure 1.4

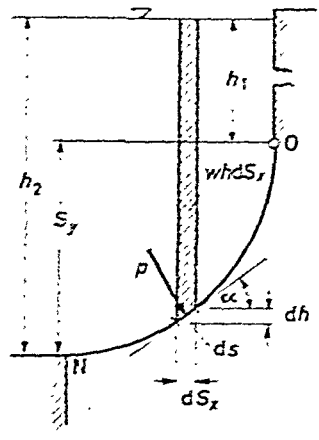

Figure 1.5

Pressures on a submerged curved surface

will be a resultant force F which may be resolved into two components, F_x being the horizontal and F_y the vertical component. These forces may be obtained from the following considerations.

At a point P of the surface an element dS is inclined to the horizontal at an angle α (*see Fig. 1.5*).

The horizontal component of the elementary pressure force $p\,dS$ (acting on unit width) is $p\,dS \cdot \sin\alpha$; and since $dS \sin\alpha = dh$ the total horizontal force

$$F_x = \int_1^2 p\,dh = w\int_{h_1}^{h_2} h \cdot dh = \frac{w}{2}(h_2^2 - h_1^2) = wS_y\bar{h} \quad \ldots\ldots(1.10)$$

where

$$\bar{h} = \frac{h_1 + h_2}{2}$$

and the projection of the curved surface onto a vertical plane

$$S_y = h_2 - h_1$$

Since $S_y \bar{h}$ is the first moment of the projected area about the axis 0, the horizontal force is identical with the result of Section 1.2 and the centre of pressure may be found on similar lines. It may be seen that the horizontal force is independent of the shape of the curved surface.

The vertical component of the elementary pressure force acting on dS is $p\, dS \cos \alpha$ and since $dS \cos \alpha = dS_x$ the total vertical force

$$F_y = \int p\, dS_x = w \int h\, dS_x \qquad \ldots.(1.11)$$

Eq. 1.11 represents the weight W of the vertical liquid column over the curved surface extending to the free liquid surface.

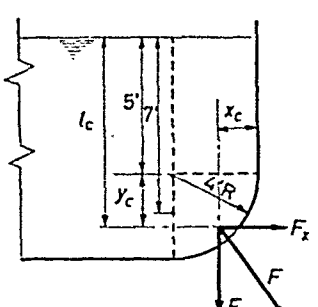

Figure 1.6

Taking moments of the vertical forces about a convenient axis gives the location of F_y. Thus

$$F_y \cdot x_c = F_x y_c$$

and

$$x_c = y_c \frac{F_x}{F_y} \qquad \ldots.(1.12)$$

Example

1.2. The dimensioned cross-section of a water tank is shown in *Fig. 1.6.* Calculate the force acting on the segment 0–N and find its location. The tank is 25 ft. long.

Solution.—Vertical area $S_y = 4 \times 25 = 100$ ft.^{2}

Horizontal force $F_x = 62{\cdot}4 \times 100 \times 7 = 43700$ lb.

$$I_{C.G} \text{ of vertical surface} = \frac{25 \times 4^3}{12} = 133{\cdot}5 \text{ ft.}^4$$

Hence vertical location of C.P.

$$l_c = 7 + \frac{133{\cdot}5}{7 \times 100} = 7{\cdot}19 \text{ ft.} \quad \therefore \quad y_c = 2{\cdot}19 \text{ ft.}$$

Vertical force

$$F_y = \left[(4 \times 5) + \frac{4^2\pi}{4}\right] 25 \times 62{\cdot}4 = 50800 \text{ lb.}$$

Equilibrium of moments about 0 gives the horizontal location of the vertical force

$$x_c = 2{\cdot}19 \times \frac{43700}{50800} = 1{\cdot}89 \text{ ft.}$$

The total force

$$F = \sqrt{(43700^2 + 50800^2)} = 67800 \text{ lb.}$$

1.5 Buoyancy of Submerged and Floating Bodies

Consider a prismatic body submerged in a fluid. (*see Fig. 1.7*). If the specific weight of the body is w_b its weight is $W = w_b V$, where V is its volume. The buoyant force $F_B = S(p_2 - p_1) = S(h_2 - h_1) \,.\, w$, where w is the specific weight of the liquid. Since $S(h_2 - h_1) = V$ the net force

$$W - F_B = V(w_b - w) \qquad \ldots\ldots(1.13)$$

and is independent of the depth of submergence.

It follows from Eq. 1.13 that if $w_b < w$ the body rises to the surface and if $w_b > w$ the body sinks in the fluid.

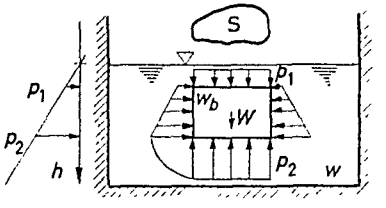

Figure 1.7—Pressures on a submerged body

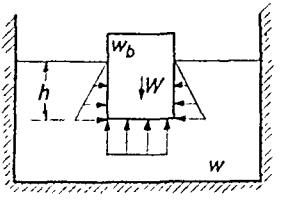

Figure 1.8—Pressures on a floating body

The weight 'lost' by the body is actually equal to the weight of the volume of fluid displaced (Archimedes' Law).

The same law applies to floating bodies (*see Fig. 1.8*) which are able to float only if the weight of the fluid displaced is equal to total weight of the body.

When a balloon filled with a gas lighter than air begins to ascend, the net buoyant force is proportional to the difference between the specific weights of air and gas. Since the air density decreases with

increasing height the balloon can only rise to the height where the air density becomes equal to that of the gas contained inside (neglecting the weight of the balloon).

1.6 Static Stability of Floating Bodies

Consider a body floating on the surface of a liquid (*Fig. 1.9*). In equilibrium the weight of the body W may be considered concentrated at the centre of gravity C.G. and the buoyant force F_B, resulting from the pressures acting on the submerged part of the body, may be considered concentrated at the centre of buoyancy

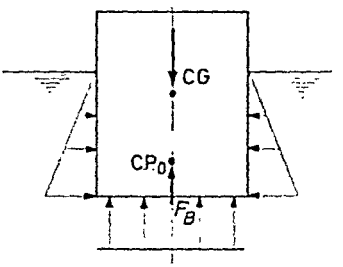

Figure 1.9

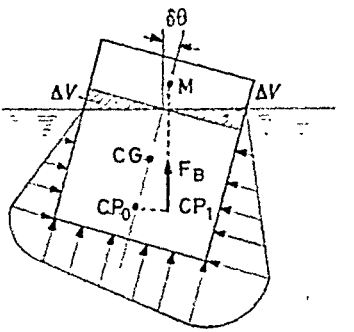

Figure 1.10

C.P.$_0$, which is the centre of gravity of the displaced water. In the equilibrium position both forces are equal and opposite and lie in a vertical line.

If the body is rolled through a small angle $\delta\theta$ as shown in *Fig. 1.10* the pressure forces acting on the sides and on the bottom set up a moment. The resultant buoyant force is of the same magnitude as prior to roll, because the list of the body causes a wedge-shaped volume (ΔV) to emerge on one side whilst a similar wedge of same volume submerges on the other side. If the submerged total volume of the body is V, the buoyant force will be wV where w is the specific weight of the liquid. This force is again vertical but the centre of buoyancy has moved from C.P.$_0$ to C.P.$_1$. The line of action of the buoyant force F_B intersects the axis of symmetry at a point M which for small angles of roll may be considered fixed and is then called the metacentre. The location of the metacentre may be calculated from the following consideration.

The submerged wedge shaped volume V sets up a buoyant force F_B. In order to calculate F_B and the resulting moment, consider

first at the water line and at a distance x from the centre line, an elementary volume dV cut out from ΔV

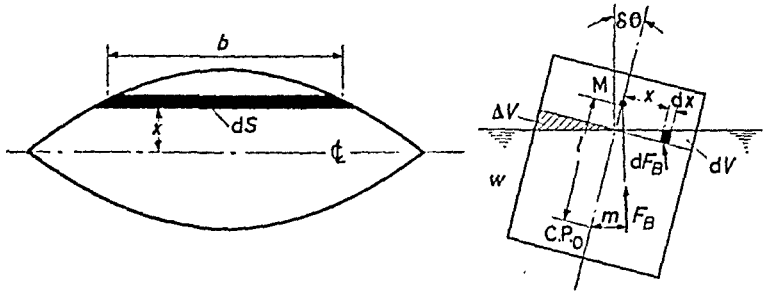

Figure 1.11

From *Fig. 1.11* it may be seen that $dV = (x\,\delta\theta)b\,dx$. An elementary buoyant force dF_B is set up by this element which yields a righting moment $dM \simeq dF_B x$ about C.P.$_0$. Since $dF_B = dVw$,

$$dM = w\,d\theta\,x^2\,dS$$

where $dS = b\,dx$. The righting moment M of the whole wedge is given by

$$M = w\,\delta\theta \int_0^S x^2\,dS \qquad \ldots.(1.14)$$

where $\int x^2\,dS$ is the second moment of the total water line area about the longitudinal centre line. (C.L.)

On the other hand the righting moment of the total submerged volume V about C.P.$_0$

$$M \simeq wVm = wVl\,\delta\theta \qquad \ldots.(1.15)$$

where l is the distance of the metacentre from C.P.$_0$.

Equating 1.14 to 1.15 yields

$$wVl\,\delta\theta = w\,\delta\theta \int x^2\,dS$$

hence

$$l = \frac{\int x^2\,dS}{V} = \frac{\text{second moment of water line area}}{\text{volume submerged}} \qquad \ldots.(1.16)$$

Note that the location of C.P.$_0$ must be known prior to calculation of l.

It appears from the above that the magnitude of the righting moment depends on the angle of roll (Eq. 1.15). The stability of the

floating body depends on the location of the metacentre. If the metacentre is above the C.G. the righting moment opposes and stabilizes the roll (*Fig. 1.12a*). If M is located below the C.G., roll and moment are of the same sense and the body rolls over (*Fig. 1.12b*). The higher the metacentre is above the C.G. the greater is the stability of the floating body.

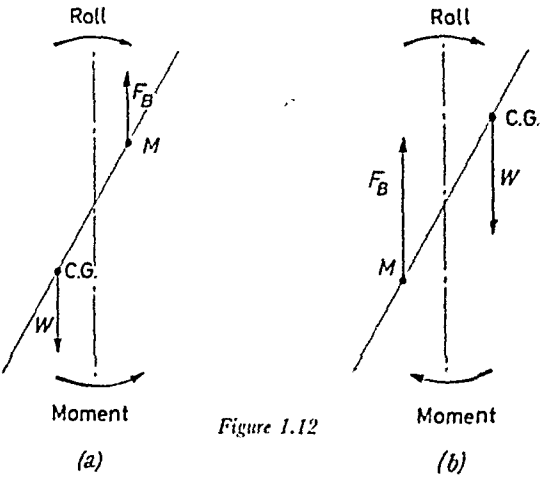

Figure 1.12

Example

1.3. A log of wood 6 in. wide, 12 in. high and 60 in. long floats on the surface of water. Assuming that its specific gravity is 0·74, calculate for two possible positions,

(*a*) the depth of immersion
(*b*) the righting moment for a 5° tilt
(*c*) the metacentric height.

The two positions are: (i) the log floats on its 6-in. side; (ii) the log floats on its 12-in. side. Comment on the stability in each case.

Solution.—

(i) (*a*) The weight of the block and weight of water displaced are equal in equilibrium, hence the depth of immersion

$$h = 12 \times 0{\cdot}74 = 8{\cdot}9 \text{ in.}$$

(*b*) The second moment of the water-line area

$$\int x^2\, dS = \frac{5 \times 0{\cdot}5^3}{12} = 0{\cdot}052 \text{ ft.}^4$$

hence the righting moment

$$M = 62{\cdot}4 \times 5 \times \frac{\pi}{180} \times 0{\cdot}052 = 0{\cdot}283 \text{ ft. lb.}$$

(*c*) The submerged volume

$$V = 8{\cdot}9 \times 6 \times 60/1728 = 1{\cdot}85 \text{ ft.}^3$$

Hence the metacentric height above C.P.$_0$.

$$l = \frac{0{\cdot}052}{1{\cdot}85} \times 12 = 0{\cdot}282 \text{ in.}$$

(ii) (*a*) Depth of immersion

$$h = 6 \times 0{\cdot}74 = 4{\cdot}45 \text{ in.}$$

(*b*) The second moment of the water-line area

$$\int x^2 \, dS = \frac{5 \times 1^3}{12} = 0{\cdot}417 \text{ ft.}^4$$

hence the righting moment.

$$M = 62{\cdot}4 \times 5 \times \frac{\pi}{180} \times 0{\cdot}417 = 2{\cdot}27 \text{ ft. lb.}$$

(*c*) The submerged volume being the same as above, the metacentric height above C.P.$_0$

$$l = \frac{0{\cdot}417}{1{\cdot}85} \times 12 = 2{\cdot}7 \text{ in.}$$

Comment on the stability: (i) The metacentre lies 1·268 in. below the centre of gravity, hence this position is unstable, and the block will turn over. (ii) The metacentre lies 1·925 in. above the centre of gravity, hence this position is stable (*See Fig. 1.13*).

REFERENCES

(1) PRANDTL, L., and TIETJENS, O.G., *Fundamentals of Hydro- and Aeromechanics*, McGraw-Hill, New York, 1934.
(2) LAMB, H., *Statics*, Cambridge University Press, 1933.
(3) BARNABY, K. C., *Basic Naval Architecture*, Hutchinson, 1948.

Problems

1.1. Calculate the magnitude and location of the total force acting on a submerged vertical gate 6 ft. wide and 12 ft. high if the water stands 10 ft. above the upper edge.

1.2. A 60-ft. wide canal 'lock' is provided with a pair of vertically hinged gates each wing being 35 ft. 'wide' and 42 ft. 'high'. Calculate, on a wing, the torque required when opening the gate, if water stands 40 ft. high on one side and 20 ft. high on the other. (Obviously, when closed the gates form a V.)

1.3. The upstream face of a dam is inclined at an angle of 60 degrees to

the horizontal. If the free surface of the water in the reservoir lies 25 feet above the base of the dam, determine the horizontal and vertical components and the line of action of the resultant force of the water per unit length of dam.

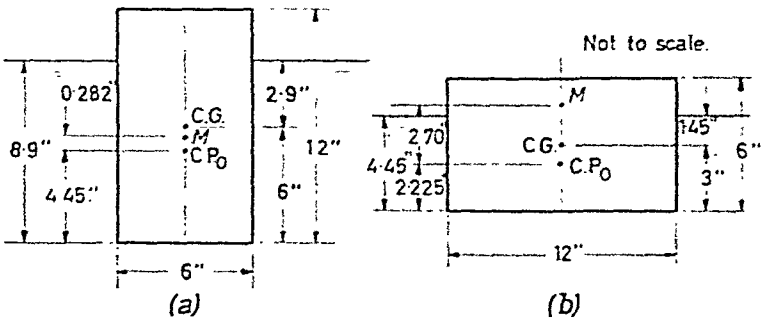

Figure 1.13

1.4. *Figure 1.14* represents a cross-section of a drum gate in a raised position. The gate is hinged at H, and is capable of rotating about H in the recess C. As water is admitted to the recess C via the connecting pipe B the gate is raised by the water to the position shown.

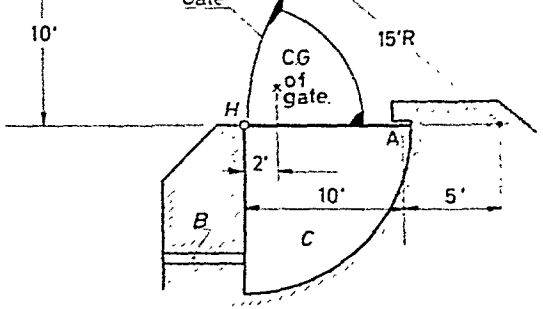

Figure 1.14

With the gate in the raised position, and the upstream water surface level with the top of the gate, determine the force per foot length exerted on the stop at A by the underside of the gate.

Weight of gate, 400 lb. per ft. length.

1.5. A pontoon 80 ft. long, 20 ft. wide and 12 ft. deep has a draught of 8 ft. What is the metacentric height? Through what distance does the water-line rise on the side if a 10-ton weight is shifted 15 ft. across the

pontoon. The centre of gravity may be assumed to be at the centre of the cross-section.

1.6. A 24-ft. diameter cylindrical caisson floats in water with the axis vertical; 18 ft. of its height is submerged. The centre of gravity is on the axis and 7 ft. above the bottom:

(*a*) Compute the metacentric height.

(*b*) It is desired to displace a structural part of half the total weight, originally located at the centre of gravity, to a higher position along the axis of the caisson. Determine the maximum permissible displacement in order that the floating stability be maintained.

2

PERFECT FLUIDS IN MOTION

2.1 Path Lines, Stream Lines and the Flow Pattern

THE study of fluids in motion commences with the visualization of the flow pattern. An entire body of fluid in motion, such as a water jet emerging from a nozzle, may be easily seen with the naked eye, but the visual observation of the movement of individual particles needs special equipment. Visual observation may be made possible

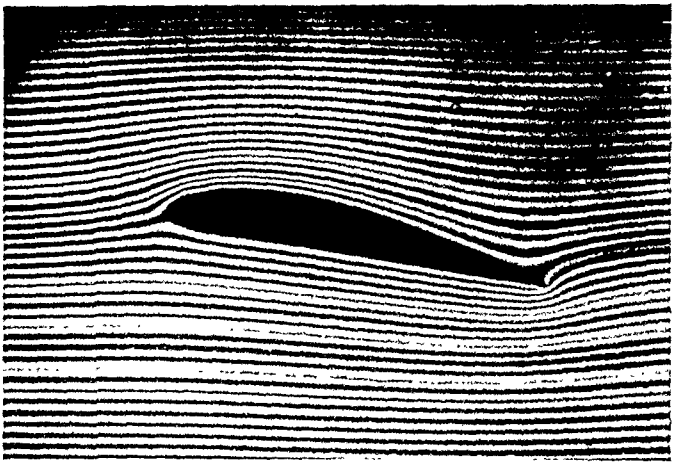

Figure 2.1—Flow pattern around a wing profile. (*From* Wind-tunnel Technique *by courtesy of Sir Isaac Pitman & Sons Limited*)

by introducing into the flow some substance, smoke into air or dye into water, and setting up a powerful light to provide the necessary contrast. An excellent record of the prevailing, instantaneous flow pattern may be made by photography. A photograph of streamlines flowing over an aerofoil placed in a smoke tunnel is shown in *Fig. 2.1.*

An individual fluid particle, moving from one point to another in the flow, follows a pathline. The pathlines of a number of individual particles could be traced, but the record obtained would not be of much value, as the individual particles wander within the fluid by

mixing. The nature of the flow is explored more satisfactorily by tracing streamlines.

The tracing of streamlines is of great value, since the determination of the flow inside a duct, or past any solid body exposed to the fluid stream, depends on the magnitude and direction of the velocity at all points of the fluid. Streamlines may be defined as tangents to the

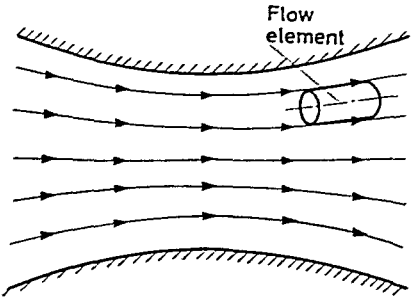

Figure 2.2—Flow pattern in a channel with constriction

fluid velocity at every point along their length. Streamlines do not cross each other, whilst individual fluid particles may move in and out of streamlines and cross each other's path frequently. A whole set of streamlines, representing the tangents of the velocities at various points of the flow, is the flow pattern.

Consider for example the flow through a channel with a constriction (*Fig. 2.2*).

A number of streamlines are drawn starting from the left with uniform spacing, so that the same quantity of fluid flows between

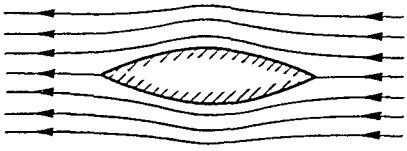

Figure 2.3

two neighbouring streamlines at all points along their length. Obviously the streamlines are crowded closer together in the constricted than in the wider portions of the channel. Since the flow of the fluid is continuous, the rate of flow at any cross section must be the same. It follows that at the minimum cross-sectional area the velocity is the highest, and the streamline spacing the least, whilst

at the largest cross-sectional area the velocity is the lowest, and the spacing of the streamlines the greatest.

A solid body placed into an open fluid flow has a similar effect on the streamlines. Far upstream from the body the streamlines are parallel and the flow unaffected, but as the flow approaches the body, the streamlines are displaced. In passing over the body the spacing first narrows and then widens, until finally, far downstream, the spacing resumes the same pattern as far upstream. The effect is shown in *Fig. 2.3.*

Although accurate flow patterns are not always easily obtained in practice, even a rough approximation may be helpful to the understanding of a particular problem.

More details of various flow patterns associated with flow phenomena will be presented in subsequent discussions.

2.2 Transformation of Energy in a Perfect, Incompressible Fluid in Motion. Bernoulli's Theorem

In going downstream along a streamline the velocity of the fluid may vary from point to point. Since the velocity changes, the associated kinetic energy must also change. It may then be anticipated that the pressure of the fluid will also change.

For the study of the energy change, a small element of the fluid, isolated from the main body (shown in *Fig. 2.2*) will be considered. The sides of the element are made up of adjacent streamlines and since the dimension in the direction of the flow is small, the sides may be considered as straight. The ends of the element may be of any geometrical form (*Fig. 2.4*). The following assumptions are made:

(a) the flow is steady, that is, the variables involved change in space only but not in time
(b) the fluid has no viscosity
(c) no heat or work is transferred to or from the fluid
(d) no fluid is added or subtracted from the flow
(e) the fluid is incompressible.

Since the element is moving and subject to a velocity change, the net force acting must have some finite value.

The forces to be considered are pressure forces, acting on all sides of the element, and gravity forces, due to the mass of the fluid enclosed in the element, and considered to act through the centre of gravity.

Resolving the pressure forces in the direction of the streamline

$$Ap + \left(p + \frac{\delta p}{2}\right)\delta A - (p + \delta p)(A + \delta A) = -A \,.\, \delta p \,.$$

The gravity force, δW, in the direction of the streamline is given by

$$-A \,.\, \delta s \,.\, \rho \,.\, g \,.\, \sin\theta = -A \,.\, \rho \,.\, g \,.\, \delta z$$

According to Newton's second law, the resultant force is equal to the mass times the acceleration,

$$-A\,\delta p - A\rho g\,\delta z = A\,\delta s \rho \frac{\mathrm{d}V}{\mathrm{d}t}$$

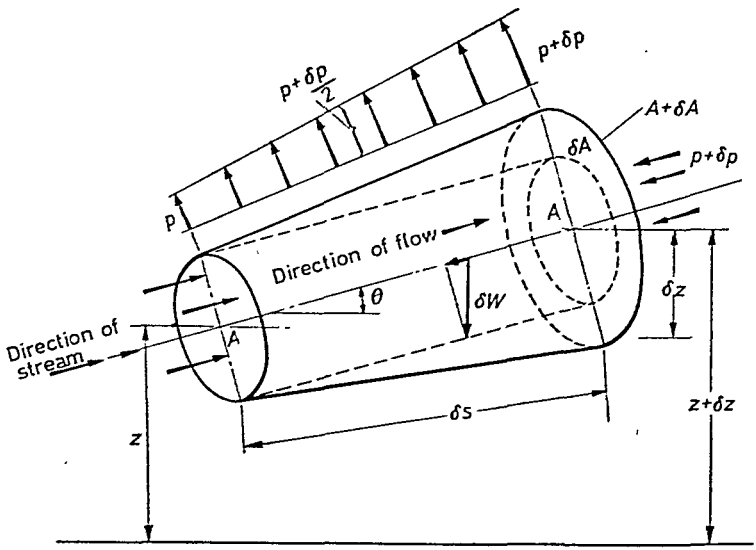

Figure 2.4—Forces on a fluid element

Since the velocity along a streamline is in general a function of both position and time, the acceleration

$$\frac{\mathrm{d}V}{\mathrm{d}t} = \frac{\partial V}{\partial s} \cdot \frac{\mathrm{d}s}{\mathrm{d}t} + \frac{\partial V}{\partial t}$$

However, by assumption (*a*) the time derivative of the velocity is zero and Newton's law becomes

$$-\delta p - \rho g\,\delta z = \rho V\,\mathrm{d}V$$

On rearranging terms Bernoulli's theorem in differential form is obtained

$$\mathrm{d}p + \rho V\,\mathrm{d}V + \rho g\,\mathrm{d}z = 0 \qquad \ldots.(2.1)$$

The original Bernoulli equation, first published in 1738, is obtained from the above upon integration and may be written in the following forms:

$$p + \tfrac{1}{2}\rho V^2 + \rho g z = \text{CONSTANT} \qquad \ldots.(2.2)$$

or, since the product of the density and gravitational acceleration g is equal to the specific weight w of the fluid

$$E = \frac{p}{w} + \frac{V^2}{2g} + z = \text{CONSTANT} \qquad \ldots.(2.3)$$

The Bernoulli equation postulates that the sum of the pressure, kinetic and potential energy† of the unit mass is constant along a specified streamline. It should be remembered, that the constant may assume different values for other streamlines. However, for practical purposes, the constant may be considered the same over the entire cross-section of a flow inside conduits.

2.3 Continuity Equation

The continuity of flow from point to point along a duct or pipe system is expressed by the equation of continuity. On the assumption that no fluid is added or removed from the flow between specified cross-sections 1 and 2, the rate of flow, often termed as 'discharge', is the product of the cross-sectional area and the mean velocity. Thus discharge

$$Q = A \,.\, V_m = A_1 V_{1m} = A_2 V_{2m} \qquad \ldots.(2.4)$$

In practice the mean velocity is often calculated from the discharge and thus the suffix m is usually omitted. The value of the mean velocity can also be obtained by measuring the velocities at several points of the cross-section and averaging the results.

The mass of fluid passing through any cross-section, termed the 'mass flow', is the product of the discharge and the density. Thus mass flow

$$W = \rho Q = A_1 V_1 \rho_1 = A_2 V_2 \rho_2 \qquad \ldots.(2.5)$$

Since liquids are incompressible $\rho_1 = \rho_2$ therefore discharge and cross-sectional area determine the mean velocity. In case of compressible fluids such as gases, however, the density may vary considerably along the flow and therefore the mean velocity will be determined from the mass flow, cross-sectional area and density.

† Energy is generally defined as the ability to do work. Since both pressure and potential head may be transformed into velocity head they may be regarded as equivalent to reservoirs from which the flow may draw energy.

In engineering practice, specific weight is used commonly for density,† the difference being that the result appears in pounds weight, instead of pounds mass.

2.4 Examples on Transformation of Energy in a Perfect, Incompressible Fluid in Motion

The transformation of pressure, kinetic and potential energy is governed by the Bernoulli and continuity equations. This can be readily demonstrated with the air of Eq. 2.3 where the variables

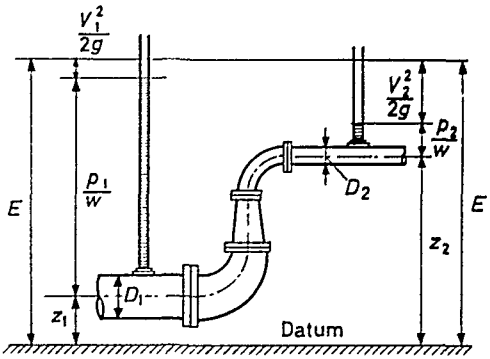

Figure 2.5—Transformation of energies along a pipeline

are expressed in 'head' of fluid flowing. The term p/w stands for (static) pressure head, $V^2/2g$ for velocity head, and z, for potential head. Since the dimension of these variables is in feet (of fluid flowing), the Bernoulli theorem may be visualized and pictured geometrically.

Consider a fluid flowing inside a duct of decreasing cross-sectional area, as shown in *Fig. 2.5.*

After an arbitrary horizontal 'datum line' is drawn, two cross-sections are selected and noted as 1 and 2.

Since the sum of the Bernoulli terms is a constant (E)

$$E = \frac{p_1}{w} + \frac{V_1^2}{2g} + z_1 = \frac{p_2}{w} + \frac{V_2^2}{2g} + z_2$$

The terms z_1 and z_2 are simply the vertical distances of the centre streamline above the datum. The terms p_1/w and p_2/w are readily obtained by 'tapping' the duct and fitting vertical glass tubes

* Slugs per ft.^{3}

(piezometers) over the holes †; the fluid will rise in these piezometers to a height of p_1/w and p_2/w above the centre line. The terms $\frac{V_1^2}{2g}$ and $\frac{V_2^2}{2g}$ are the differences between E and $p/w + z$,

$$\frac{V_1^2}{2g} = E - \left(\frac{p_1}{w} + z_1\right)$$

and

$$\frac{V_2^2}{2g} = E - \left(\frac{p_2}{w} + z_2\right)$$

Generally one of the velocities is specified so the other can be calculated from the continuity equation.

By drawing the constant energy line at a distance E above the datum line, the transformation of energy can be observed not only for points 1 and 2 but at any desired point. The following important conclusions can be drawn:

(1) The available pressure and velocity heads at certain cross-sections depend on the height of the cross-section above the datum line.

(2) The available static pressure head depends on the velocity head, which in turn is defined by the cross-sectional area. Where the cross-section is small the velocity is large and where the cross-section is large the velocity is small. It then follows from the Bernoulli equation that high velocity regions are always conspicuous for their low pressures and vice versa.

(3) In a system, the maximum velocity is attained at a cross-section where the 'available' pressure head decreases to zero. This must be avoided for several reasons, one being that liquids vaporize at low pressures and vapour pockets are formed. These collapse intermittently and cause erosions of the surfaces. Another aspect is choking. A system may be satisfactorily designed to deliver a certain quantity of fluid from a reservoir or pump, but if one cross-section in the system is of such dimensions that the pressure decreases to zero, at that particular cross-section the velocity attains a maximum value. Any further reduction in the cross-sectional area will not change the value of the maximum velocity attained, and a subsequent decrease in the flow quantity is experienced. This is termed choking.

Examples

2.1. Water flows in a circular pipe of decreasing cross-sectional area as shown in *Fig. 2.5.* At cross-section 1 the diameter of the pipe is 12 in., the

† For details on piezometers, see 'MANOMETRY' in Chapter 5.

velocity 10 ft. per sec., the pressure 30 lb./in.^{2} gauge and the elevation of the centre line is 5 ft. above the datum line. At cross-section 2 the diameter is 6 in., the elevation 10 ft. Specific weight of water $w = 62{\cdot}4$ lb./ft.^{3}

Calculate the velocity and pressure at cross-section 2.

Solution.—The area at 1 is $A_1 = \dfrac{1^2\pi}{4} = 0{\cdot}785$ ft.^{2}

The area at 2 is $A_2 = \dfrac{0{\cdot}5^2\pi}{4} = 0{\cdot}196$ ft.^{2}

From the continuity equation $A_1V_1 = A_2V_2$ and

$$\therefore \quad V_2 = V_1\frac{A_1}{A_2} = 10 \times 4 = 40 \text{ ft. per sec.}$$

Velocity at 2 $\qquad V_2 = 40$ ft./sec.

The Bernoulli 'energy' at cross-section 1

$$E = \frac{p_1}{w} + \frac{V_1^2}{2g} + z_1 = \frac{30 \times 144}{62{\cdot}4} + \frac{10^2}{64{\cdot}4} + 5 = 75{\cdot}5 = \text{ ft. lb./lb.}$$

This being constant along the pipe

$$E = 75{\cdot}5 = \frac{144p_2}{62{\cdot}4} + \frac{40^2}{64{\cdot}4} + 10$$

Hence $\qquad p_2 = 17{\cdot}7$ lb./in.^{2} gauge.

2.2. Water is discharged from an overhead tank through a 3-in. diameter horizontal pipe into the atmosphere. The free surface level in the tank is

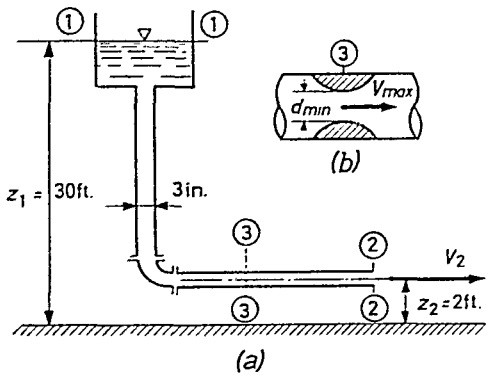

Figure 2.6

kept constant 30 ft. above the ground and the pipeline 2 ft., as shown in *Fig. 2.6a*. Use absolute pressure. Assuming the atmospheric pressure to be 14·7 lb./in.^{2} calculate the discharge.

Solution.—Choosing the ground as the datum, the Bernoulli energy at the free level (cross-section 1)

$$E = \frac{p_1}{w} + \frac{V_1^2}{2g} + z_1 = \frac{14{\cdot}7 \times 144}{62{\cdot}4} + 0 + 30 = 63{\cdot}8$$

Since the water is discharged into the atmosphere, the pressure in the jet will be the atmospheric pressure. Hence the Bernoulli energy at the exit, (cross-section 2)

$$E = \frac{14{\cdot}7 \times 144}{62{\cdot}4} + \frac{V_2^2}{2g} + 2 = 63{\cdot}8$$

From this, the velocity at exit $V_2 = 42{\cdot}5$ ft. per sec.

The discharge $Q = A_2 V_2 = \frac{0{\cdot}25^2\pi}{4} \times 42{\cdot}5 = 2{\cdot}08$ ft.^{3}/sec.

2.3. Referring to the previous example, calculate the cross-sectional area and diameter of a circular constriction placed into the pipeline, assuming that the absolute pressure at the constriction decreases to zero. What will happen if the constriction is made smaller than the calculated minimum?

Solution.—Applying the Bernoulli equation to the free water surface and the constriction (cross-section 3, *Fig. 2.6b*)

$$E = 63{\cdot}8 = 0 + \frac{V_{max}^2}{2g} + 2$$

and the maximum velocity attainable in the system

$$V_{max} = 63 \text{ ft./sec.}$$

The discharge is still of the same magnitude as computed in Example 2.2. From the continuity equation it follows that

$$A_{min} = \frac{Q}{V_{max}} = \frac{2{\cdot}08}{63} \times 144 = 4{\cdot}76 \text{ in.}^2$$

and

$$d_{min} = 2{\cdot}46 \text{ in.}$$

If the constriction is made smaller, the maximum velocity will still be of the same value, that is 63 ft./sec., as the pressure cannot fall below absolute zero. Therefore, the discharge decreases and downstream from the constriction the pipe will not run full.

2.4. Calculate the static pressure at points A, B, C, and D when water is flowing in the pipeline shown in *Fig. 2.7.* Pipe diameter is uniform. Neglect friction.

Solution.—Because of non-frictional flow the velocity at 'D', $V = \sqrt{2gh}$, where $h = 7$ ft.

hence

$$\frac{V^2}{2g} = 7$$

Assume datum 20 ft. below free surface; then Bernoulli energy $E = 20$ ft. lb./lb.

(Note *Fig. 2.7* is adopted from Vennard.)

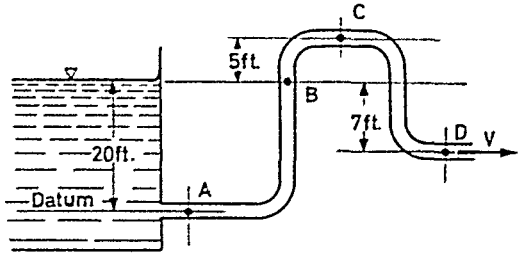

Figure 2·7

Since $$E = \frac{p}{w} + \frac{V^2}{2g} + z$$

At A

$z = 0$ $$p/w = E - \frac{V^2}{2g} = 20 - 7 = 13 \text{ ft.}$$

At B

$z = 20$ $$p/w = E - \frac{V^2}{2g} - 20 = -7 \text{ ft.} \quad \text{(VACUUM)}$$

At C

$z = 25$ $$p/w = E - \frac{V^2}{2g} - 25 = -12 \text{ ft.} \quad \text{(VACUUM)}$$

At D

$z = 13$ $$p/w = E - \frac{V^2}{2g} - 13 = 0 \quad \text{(ATMOSPHERIC)}$$

2.5. Water is flowing upwards through a vertical pipe-line which tapers from 12 in. to 8 in. diameter, in a distance of 5 ft.

If the pressure at the 12-in. section is 30 lb./in.^{2} and that at the 8-in. section 25 lb./in.^{2}, calculate the rate of flow in cusecs. Neglect friction. *(See Fig. 2.8.)*

Solution.—Write down Bernoulli's equation:

$$\frac{p_1 - p_2}{w} + z_1 - z_2 = \frac{V_2^2 - V_1^2}{2g}$$

hence

$$\frac{(30 - 25)144}{62{\cdot}4} - 5 = \frac{V_1^2}{2g}[(V_2/V_1)^2 - 1]$$

From continuity equation:

$$A_1V_1 = A_2V_2$$

$$\therefore \quad \left(\frac{V_2}{V_1}\right)^2 = \left(\frac{A_1}{A_2}\right)^2 = \left(\frac{12}{8}\right)^4 = 5{\cdot}05$$

Substituting $(V_2/V_1)^2$ into above and solving for V_1 we obtain $V_1 = 10{\cdot}5$ ft /sec.

Hence discharge

$$Q = \frac{1^2\pi}{4} \times 10{\cdot}5 = 8{\cdot}25 \text{ ft.}^3/\text{sec.}$$

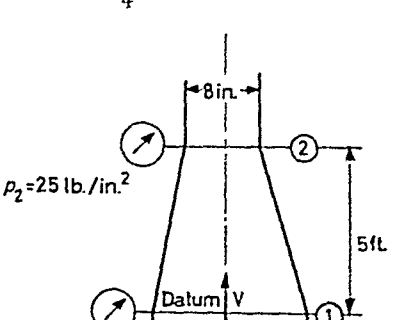

Figure 2.8

2.6. Show by graphical representation, the distribution of the pressure and velocity head along a convergent tube of circular cross-section, 20 ft. long and inclined to the horizontal, as shown in *Fig. 2.9.* At the inlet, the

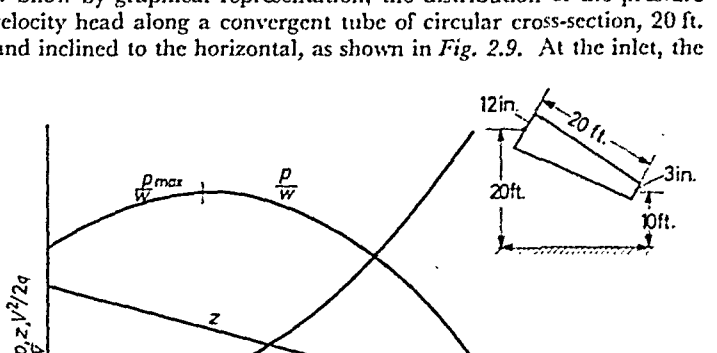

Figure 2.9

elevation above datum is 20 ft., the diameter 12 in. and the velocity 12 ft./sec. At the outlet the elevation is 10 ft. and the diameter is 3 in.

Solution.—Apply the Bernoulli and continuity equations to a number of cross-sections between inlet and outlet. Note: maximum pressure is experienced at some distance downstream from the inlet.

2.5 Momentum of Fluids in Motion

A number of problems cannot be solved by the application of the energy and continuity equations alone and the momentum equation provides the basic tool.

The momentum (impulse or impact) of solid bodies is defined as the product of the mass and the velocity

$$\vec{I} = m \cdot \vec{V} \qquad \ldots.(2.6)$$

The force changing the momentum is the time derivative of the momentum †

$$-\vec{F} = \frac{\mathrm{d}I}{\mathrm{d}t} = \frac{\mathrm{d}}{\mathrm{d}t}(m\vec{V}) = m\frac{\mathrm{d}\vec{V}}{\mathrm{d}t}$$

Since the momentum change $m \cdot \mathrm{d}V$ is equal to $F \cdot \mathrm{d}t$, for a finite change

$$\int_{t_1}^{t_2} -\vec{F}\,\mathrm{d}t = \int_{V_1}^{V_2} m\,\mathrm{d}\vec{V} = m(\vec{V}_2 - \vec{V}_1) \qquad \ldots.(2.7)$$

where V_1 is the velocity of the body before and V_2 after the application of the force.

The difference in the behaviour between solids and fluids is illustrated in the following:

Consider an elastic ball moving towards a solid wall. The ball will be repelled by the wall and the action is shown in three stages in *Fig. 2.10.* Before the ball contacts the wall its velocity is V_1 (1). At the time of the first contact the velocity is still V_1 but presently the speed is reduced to zero and the ball 'flattens' against the wall (2). Being elastic, it will 'swell' again and leave the wall, in the opposite direction, with a velocity V_2 (3). An observer recording the velocities readily estimates the 'impact' causing the change of the flight as $m[V_1 - (-V_2)] = m(V_1 + V_2)$. The negative sign of V_2 is due to the change of direction of the flight. Another observer, stationed at the wall and equipped with special apparatus, records a force increasing from zero to a maximum and back to zero again as shown in *Fig. 2.10b.* Having plotted force against time on a graph, the area under curve F is measured, and the impact $\int_1^2 F \cdot \mathrm{d}t$ obtained. The results of both observers must agree.

† The force which opposes motion will be considered positive.

The mean force F, causing the change of the momentum, depends on the duration of the contact.

Since $$\int_1^2 \vec{F}\,dt = m(\vec{V_1} - \vec{V_2}) = F(t_2 - t_1)$$

the mean force

$$F = m\frac{V_2 - V_1}{t_2 - t_1} \qquad \ldots.(2.8)$$

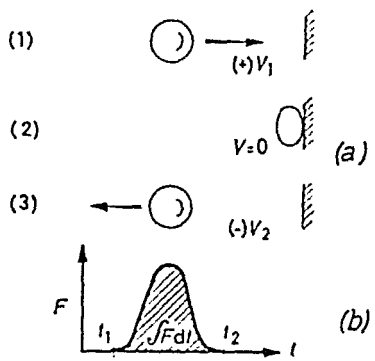

Figure 2.10—Impact of a solid object on a wall

Consider now a jet, issuing from a nozzle, directed perpendicularly against a wall. The jet may be returned by providing the the wall with a hemispherical recess, as shown in *Fig. 2.11*. The

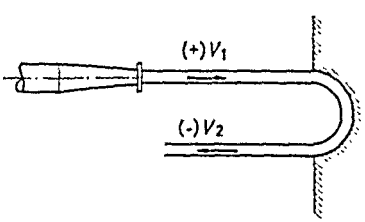

Figure 2.11—Impact of a fluid jet on a wall

observer noting the velocities again records a change in speed from V_1 to V_2, but the observer at the wall records a force of constant magnitude (independent of the duration of the contact).

The change of momentum $m(\vec{V_1} - \vec{V_2})$ being equal to $F \cdot t$, the force acting on the wall

$$\vec{F} = \frac{m}{t}(\vec{V_1} - \vec{V_2}) \qquad \ldots.(2.9)$$

As the dimension of m/t is mass per time, that is mass flow, $Q \cdot \rho$, the force exerted by fluids in steady flow is equal to the mass flow times the velocity change,

$$\vec{F} = Q\rho(\vec{V}_1 - \vec{V}_2) \qquad \ldots.(2.10)$$

Forces may be experienced by changing the direction of the flow without necessarily changing the magnitude of the velocity. This is experienced when fluids are deflected; fluids flowing inside conduits, for example, exert a force on bends.

Alternatively, a force may be experienced by changing the magnitude of the velocity without changing the direction of the flow. Velocity changes in conduit enlargements or contractions, or the propulsive force of jets generally cause a force to act opposite to the flow direction. When solving problems, the procedure is as follows: An arbitrary 'control surface' is drawn around the particular region to be investigated, and the momentum entering and leaving the control surface noted. If the flow is two-dimensional, a co-ordinate system is specified, the velocities resolved into components and the component momenta computed. Denoting the ordinates x and y, the component force

$$F_x = I_{x1} - I_{x2} = (Q\rho)(V_{1x} - V_{2x}) \qquad \ldots.(2.11)$$

and

$$F_y = I_{y1} - I_{y2} = (Q\rho)(V_{1y} - V_{2y}) \qquad \ldots.(2.12)$$

The resultant force $F = \sqrt{(F_x^2 + F_y^2)}$ $\ldots.(2.13)$

Examples

2.7. In a 3-ft. diameter pipeline carrying water, the velocity is 10 ft./sec. Calculate the magnitude and direction of the force acting on a 90° bend.

Solution.—Let x denote the ordinate in the direction of the flow before the bend and y the direction after the bend. (*Fig. 2.12.*)

Since the discharge

$$Q = AV = \frac{3^2\pi}{4} \times 10 = 70{\cdot}7 \text{ ft.}^3\text{/sec.}$$

the force in the direction of x

$$F_x = Q\rho(V_{x1} - V_{x2}) = 70{\cdot}7 \times \frac{62{\cdot}4}{32{\cdot}2} \times (10 - 0) = 1365 \text{ lb.}$$

and in the direction of y

$$Fy = Q\rho(V_{y1} - V_{y2}) = 70{\cdot}7 \times \frac{62{\cdot}4}{32{\cdot}2} \times (0 - 10) = -1365 \text{ lb.}$$

The magnitude of the resultant force

$$F = \sqrt{2} \times 1365 = 1930 \text{ lb.}$$

Since the [illegible] is [illegible], the direction of the force will be inclined [illegible] to the [illegible] as shown in Fig. [illegible].

2.8. A [illegible] jet [illegible] strikes perpendicularly against a flat plate as shown in Fig. [illegible]. If the jet diameter is [illegible] in. and the jet velocity [illegible] ft/sec, calculate the magnitude and direction of the force acting on the plate.

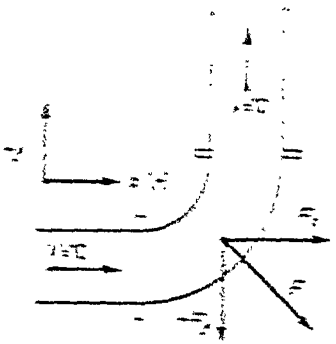

Figure [illegible]

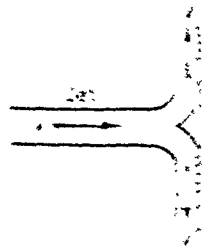

Figure [illegible]

Solution.—On the assumption that the jet is deflected in the plane of the plate, $V_{2x} = 0$, the force

$$F = [illegible] = [illegible] \text{ lb.}$$

2.9. A jet aircraft flying at a speed of [illegible] m.p.h. takes in air at a rate of [illegible] lb/sec. If the exhaust gases leave the nozzle with a velocity of [illegible] ft/sec and the fuel-air ratio is [illegible], calculate the net thrust on the aircraft.

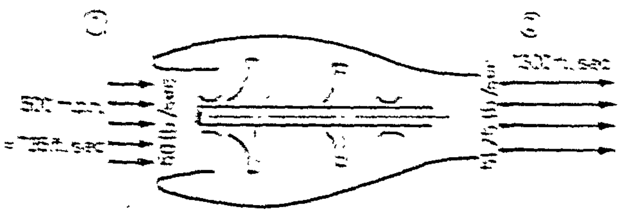

Figure [illegible]

Solution.—It is advisable to draw control surfaces in front of (1) and behind (2) the engine as shown in Fig. [illegible].

The momentum entering control surface 1

$$[illegible] = [illegible] \text{ lb.}$$

The momentum at the control surface 2 is $(Q\rho)_2 V_2$, where $(Q\rho)_2$ is the mass flow of the exhaust gases, air plus fuel, equal to $50 + 1{\cdot}25 = 51{\cdot}25$ lb./sec., and V_2 is the speed of the exhaust gases. Hence the momentum leaving control surface 2

$$(Q\rho)_2 V_2 = \frac{51.25}{32{\cdot}2} \times 1300 = 2070 \text{ lb.}$$

The net thrust is equal to the change of momentum between (1) and (2)

$$T = (Q\rho)_1 V_1 - (Q\rho)_2 V_2 = 1440 - 2070 = -630 \text{ lb.}$$

REFERENCES

(1) PRANDTL, L., and TIETJENS, O. G., *Fundamentals of Hydro- and Aeromechanics*, McGraw-Hill, New York, 1934.
(2) ECK, B., *Technische Stromungslehre*, Springer-Verlag, Berlin, 1944.

Problems

2.1. Water is flowing upwards through a vertical pipeline which tapers from 12 in. to 8 in. diameter, in a distance of 5 ft.

If the pressure at the 12-in. section is 30 lb./in.^{2} and that at the 8 in. section 25 lb./in.^{2}, calculate the rate of the flow in cusecs. Neglect friction.

2.2. Water is discharged from a 5-in. diameter horizontal pipe flowing full at the outlet, the jet striking the ground at a horizontal distance of 10 ft. and a vertical distance of 4 ft. from the end of the pipe. Calculate the rate of flow.

2.3. When a liquid is discharged from a pipe vertically, downward (towards the Earth), it may be observed that the cross-sectional area of the stream decreases downstream from the outlet.

Show that for a given discharge Q, the relation between two subsequent cross-sections A_0 and A at z distance apart, may be expressed in

$$\frac{1}{A^2} - \frac{1}{A_0^2} = \frac{2gz}{Q^2}$$

2.4. A water tender, coupled to a locomotive, 'scoops' the water from a trough between the tracks. The scoop itself consists of a vertical pipe of constant diameter with a right angle bend, the opening of which faces the fluid stream. Calculate the water flow through a 6-in. diameter scoop when travelling at a speed of 60 m.p.h. Neglect frictional losses.

2.5. Water is discharged from an overhead tank through a vertical 6-in. diameter pipe at a rate of 2·45 cusecs into a horizontal pipe of 4 in. diameter. The pipes are connected with a gradually converging bend. The height of the upper flange of the bend above the centre line of the horizontal is 1 ft. and the volume of the bend between flanges is 0·3 ft.^{3} If the pressure at the centre line of the exit section of the bend is 4·8 lb./in.^{2} gauge and the head loss in the bend is 5 ft. of water what is the magnitude and direction of the total force on the bend due to the water flow?

2.6. Fire fighting equipment in a public building consists of a nozzle, a canvas hose and a 'hydrant' globe valve.

Calculate the hydraulic force acting on the nozzle under the following conditions:

The nozzle is in a horizontal position, discharging water. The diameter at inlet to the nozzle is $2\frac{1}{2}$ in. and the exit diameter is $\frac{3}{4}$ in. The jet, leaving the nozzle, has a velocity of 96 ft./sec. and the pressure in the hose is 68 lb./in.^{2} gauge.

3

VISCOUS FLUIDS IN MOTION

3.1 Properties of Real Fluids

WHILST perfect fluids are considered to be incompressible and free from viscosity, all real fluids display compressibility to some extent and have viscous properties. In addition surface tension and vaporization effects occur on the free surfaces of liquids. These effects will now be briefly reviewed.

Compressibility

Compressibility is linked up with the elastic properties of fluids. The modulus of elasticity, E, is generally defined by the expression

$$E = -v\frac{\mathrm{d}p}{\mathrm{d}v} \sim -v\frac{\Delta p}{\Delta v}$$

where Δp denotes the pressure increase required to decrease a given volume v by the amount Δv. For example, the modulus of elasticity for water is $E = 300{,}000$ lb./in.^{2} and to cause a decrease of one in a thousand of a given volume necessitates a pressure increase of

$$\Delta p = E\frac{\Delta v}{v} = \frac{300{,}000}{1{,}000} = 300 \text{ lb./in.}^2$$

All liquids, like water, are highly elastic and only slightly compressible, whilst gaseous fluids are unelastic and therefore highly compressible.

There is marked distinction however between incompressible and compressible fluid flow. In problems, such as are met in ventilation and air conditioning, where air undergoes small density changes only, compressibility effects may be ignored. At high speeds the effects of compressibility become noticeable when the velocity of a gas approaches the speed of elastic wave propagation. At such high velocities, the laws, based on incompressibility, break down. Again, in problems such as water-hammer, where liquids undergo a high rate of velocity change, the effects of compressibility may not be ignored.

profiles. Velocity profiles are generally determined experimentally, although for isolated cases they can be derived from first principles. It may then be presumed that fluid layers slide relative to adjacent layers in the direction of the flow and that the relative 'slip' velocity between such adjacent layers varies across the flow.

On the assumption that adjacent layers slide over each other, Newton defined viscosity from the shear stress existing between the layers and their relative slip velocity.

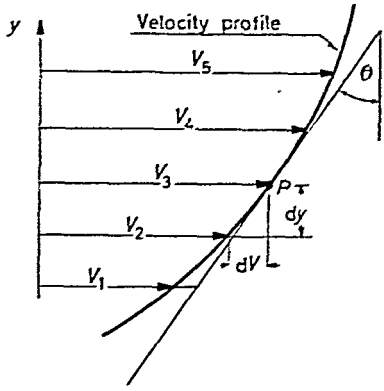

Figure 3.1

Consider two layers at an infinitesimal distance dy apart. Over this distance the velocity changes by dV. The rate of change dV/dy at a certain point P of the velocity profile is the tangent of the angle θ enclosed by the tangent drawn to the profile at P, and the perpendicular to the flow as shown in *Fig. 3.1.* According to Newton, the shear stress τ existing between the layers is proportional to the product of the coefficient of viscosity μ and the velocity gradient dV/dy,

$$\tau = \mu \frac{dV}{dy} \qquad \ldots.(3.1)$$

Since the quantity μ is a fluid property and independent of the motion, the Newtonian definition of the coefficient of viscosity is

$$\mu = \left\{ \frac{\text{shear stress}}{\text{velocity gradient}} \right\} \text{at any point of the flow}$$

It follows from Newton's law, that maximum shear stresses occur where the velocity gradient is the largest, and the shear stresses disappear where the velocity gradient is zero.

Consider a fluid flowing inside a closed conduit. Since the fluid adheres to the walls of the conduit (condition of no slip), an infinitely thin fluid layer in contact with the boundary remains stationary, whilst adjacent layers slide over it. In traversing the conduit, the velocity of the subsequent layers gradually increases from zero to a maximum, and then gradually decreases to zero as shown in *Fig. 3.2.* It is a common characteristic of all velocity profiles that the velocity gradient and thus the shear stress assumes the largest

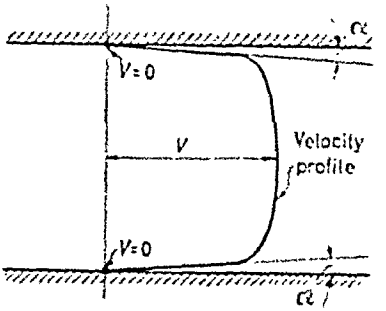

Figure 3.2

value at the boundary. Thus it is physically impossible for velocity profile to approach the boundary tangentially, as this would invoke infinitely large shear stresses. Consequently an angle of finite magnitude must always exist between the velocity profile and the boundary surface. The magnitude of the velocity gradient at the boundary becomes a deciding factor when resistance to flow is determined.

Example

7.1. Assuming the velocity distribution in a pipe as given by the approximate equation

$$V = 4y - y^2$$

where V denotes the velocity and y the distance from the solid boundary. Calculate: (*a*) the shear stress at the wall, (*b*) the shear stress at 1 ft. distance from the wall, and (*c*) the total resistance for a 4-in. diameter pipe over a length of 1000 ft., assuming the coefficient of viscosity to be 8×10^{-4} lb. sec./ft.^{2}.

Solution.—

(*a*) Differentiating V with respect to y, one obtains

$$\frac{dV}{dy} = 4 - 2y$$

At the boundary $y = 0$ and

$$\left[\frac{dV}{dy}\right]_{y=0} = 4$$

Since the velocity is also zero for $y = 4$

$$\left[\frac{dV}{dy}\right]_{y=4} = -4$$

Hence the value of the shear stress at the boundary

$$\tau_0 = \mu \left[\frac{dV}{dy}\right]_{y=0} = 8 \times 10^{-4} \times 4 = 3{\cdot}2 \times 10^{-3} \text{ lb./ft.}^2$$

(*b*) For $y = 1$ ft. the velocity gradient

$$\frac{dV}{dy} = 4 - 2 = 2$$

and the shear stress

$$\tau = \mu \left[\frac{dV}{dy}\right]_{y=1} = 8 \times 10^{-4} \times 2 = 1{\cdot}6 \times 10^{-3} \text{ lb./ft.}^2$$

(*c*) Since the total surface area of the 4 in. pipe over 1,000 ft. length

$$A_s = 1{,}000 \times 4/12 \,.\, \pi = 1050 \text{ ft.}^2$$

the force acting over this area

$$F = A_s \,.\, \tau = 1050 \times 32 \times 10^{-4} = 3{\cdot}36 \text{ lb.}$$

3.4 Viscosity Measurements. Absolute and Kinematic Viscosity

The coefficient of viscosity can be measured either by efflux or torque methods.

A small tank provided at the bottom with a small-bore tube is used for the efflux method (*see Fig. 3.3*), and from the time taken for emptying the tank, the coefficient of viscosity can be calculated. The Redwood and Saybolt viscometers are devised on this principle. The variation of viscosity with temperature may be obtained by heating the tank and measuring the efflux at different temperatures. The instruments are calibrated with fluids of known viscosities.

In the torque method a thin film of liquid to be tested is enclosed between two coaxial cylinders. The inner cyclinder is suspended by a torsion wire or spring and the outer cylinder may be rotated at a suitable speed (*see Fig. 3.4*) From the annular clearance between the

cylinders, the wetted surface, the torque and angular speed measured, the coefficient of viscosity can be calculated.

The coefficient of viscosity, μ, is frequently referred to as absolute or dynamic viscosity. Kinematic viscosity 'ν' defined by the ratio $\frac{\mu}{\rho}$, is frequently used in practice in the calculation of the Reynolds

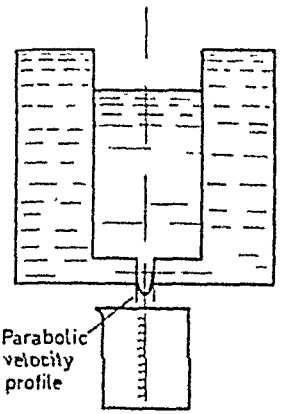

Figure 3.3

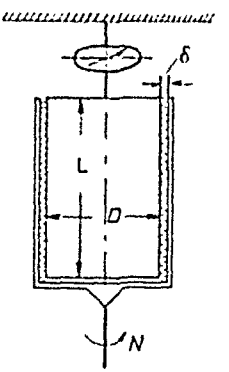

Figure 3.4

Types of viscosity meters

number. The dimension of viscosity, μ, is lb.sec/ft.^{2}, and the dimension of kinematic viscosity, ν, is ft.^{2}/sec.

Example

3.2. A cylinder of 6·05 in. diameter revolves coaxially around a fixed cylinder of 6·00 in. diameter both being 10 in. long. If the annular space is filled with glycerine and the outer cylinder revolves at a speed of 100 r.p.m., the measured torque is 6·7 ft. lb. Assuming a linear velocity distribution in the clearance and neglecting end effects, calculate the viscosity of the glycerine.

Solution.—The tangential velocity of the outer cylinder (inner surface)

$$V = \frac{D\pi N}{60} = \frac{6{\cdot}05\pi \times 100}{12 \times 60} = 2{\cdot}64 \text{ ft./sec.}$$

Since the oil adheres to both surfaces, the velocity gradient in radial direction (*see Fig. 3.5.*)

$$\frac{dV}{dr} \cong \frac{V}{\delta} = \frac{2{\cdot}64 \times 12}{0{\cdot}025} = 1{,}260 \text{ per sec.}$$

The area of the wetted surface $S = 6\pi \times 10/144 = 1{\cdot}31$ ft.^{2}. As the shear

stress is equal to the torque divided by the radius and the wetted surface area

$$\tau = \frac{T}{S \cdot R} = \frac{6{\cdot}7 \times 12}{1{\cdot}31 \times 6{\cdot}05} = 10{\cdot}1 \text{ lb./ft.}^2$$

and the coefficient of viscosity from Newton's law

$$\mu = \tau \Big/ \frac{dV}{dr} = \frac{10{\cdot}1}{1260} = 8 \times 10^{-3} \text{ lb. sec./ft.}^2.$$

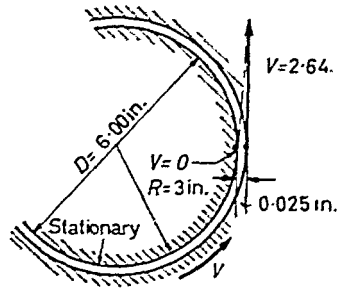

Figure 3.5

3.5 Experiments of Reynolds

Reynolds' experimental investigations first published in 1883 disclosed that fluids flowing inside pipes behave differently if the flow velocity is varied.

Reynolds' apparatus consisted essentially of a constant head tank filled with water, a small tank containing dye, a horizontal glass pipe provided with a rounded entry and a regulating valve. The layout is shown in *Fig. 3.6.* The water could flow from the tank through the glass pipe into the atmosphere and the flow velocity could be varied by adjusting the regulating valve. The dye was introduced into the flow at the bell-mouth through a small diameter tube. The experiments disclosed that the dye remained in the form of a straight and stable filament when the velocity was low. With increasing velocity a critical state was reached, the dye showed irregularities, began to waver and finally, at high velocities, rapidly diffused over the entire cross-section (*see Fig. 3.7*). Having repeated these experiments Reynolds discovered that the value of the critical velocity was governed by the relationship between the inertia (kinetic) and viscous forces. At low velocities, he reasoned, the viscous forces were predominant and the flow was largely viscous in character, adjacent fluid layers flowing in 'lamina' form. At greater velocities however, the inertia forces predominated over the viscous forces and the layers no longer remained in 'lamina' form, but diffused through fluctuations.

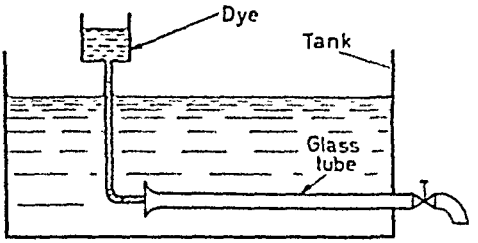

(*a*)

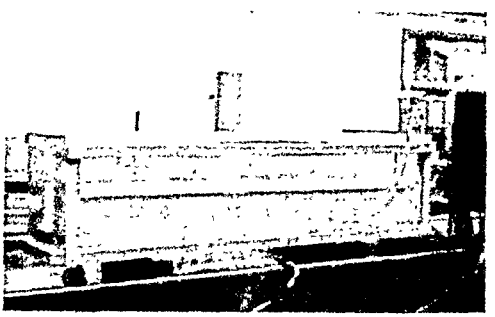

(*b*)

Figure 3.6—Reynolds' original tank. (At Manchester University)

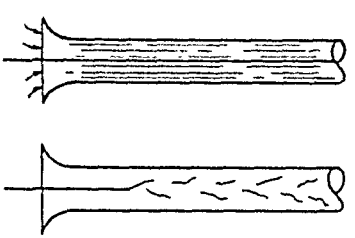

Figure 3.7—Laminar and turbulent flow in a pipe

Reynolds related the inertia to viscous forces and arrived at a non-dimensional parameter:

$$N_R = \frac{\text{inertia forces} \propto \rho V^2}{\text{viscous forces} \propto \mu V/D} = \frac{DV\rho}{\mu} \qquad \ldots.(3.2)$$

In his experiments Reynolds invariably found that critical flow occurred whenever his number (N_R) approached 12,000, and concluded that depending on the value of the parameter two types of flow were in existence, laminar and turbulent.

3.6 Laminar and Turbulent Flow

Pipe flow experiments can be carried out with increasing and decreasing velocities. With increasing velocities the 'upper critical' and with decreasing velocities the 'lower critical' Reynolds numbers

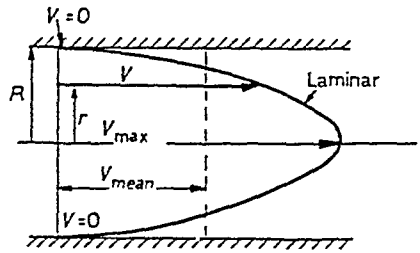

Figure 3.8—Laminar flow-velocity distribution

can be found. The upper critical number depends largely on the nature of the initial disturbance in the flow and upper critical values over 40,000 have been found with Reynolds' original equipment by increasing the stilling time, providing the pipe with a more streamlined inlet and eliminating all possible vibrations. However it is accepted that the upper critical number generally lies between 2,800 and 5,000. The lower critical number is found between 2,000 and 2,100 and at this critical value all turbulence is damped out eventually by viscous action. Between the upper and lower critical, that is for Reynolds numbers lying between 2,100 and 2,800–5,000 the flow is of transition character and is called transition flow.

It appears that the existence of laminar and turbulent flow depends primarily on the value of the Reynolds number. Investigations show further fundamental differences. Omitting details at this stage the differences appear in

(*a*) velocity distribution
(*b*) shear stress
(*c*) resistance to flow.

(*a*) The velocity distribution of a laminar flow in pipes follows a parabolic law given by the expression

$$V = V_{max}\left[1 - \frac{r^2}{R^2}\right] \qquad \ldots\ldots(3.3)$$

where the maximum velocity V_{max} attained at the centre, is exactly twice the value of the average flow velocity (*see Fig. 3.8*).

The velocity profile of a turbulent flow is much flatter than the corresponding laminar-flow parabola for the same average velocity and becomes even flatter with increasing Reynolds number (*Fig. 3.9*).

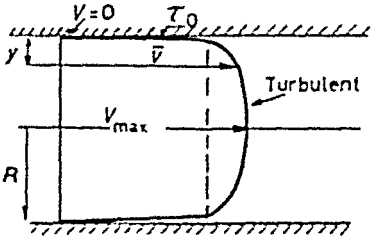

Figure 3.9—Turbulent flow-velocity distribution

Roughly, the maximum velocity is *about* 1·23 times the value of the average flow velocity. In *Fig. 3.10* a comparison between three velocity profiles at different values of N_R is shown.

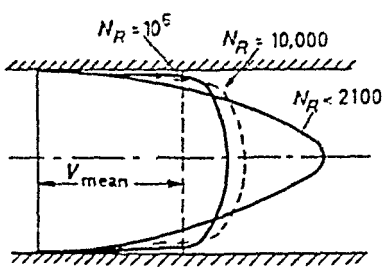

Figure 3.10—Flow pattern changes with increasing Reynolds' number

The velocity distribution for turbulent flow approximately follows a logarithmic law given by the expression

$$\frac{V_{max} - \bar{V}}{\sqrt{(\tau_0/\rho)}} = 5{\cdot}75 \log \frac{y}{R} \qquad \ldots\ldots(3.4)$$

where $\bar{V}$ is the 'temporal mean' velocity and τ_0 the boundary shear stress.

Furthermore, in turbulent flow, random speed fluctuations are superimposed on the temporal mean velocity so that the actual velocity and the velocity profile changes from instant to instant. The characteristic velocity profile shown in *Fig. 3.9* is based on the temporal mean velocity. Experimental recording of the actual movement presents an extremely difficult problem, because these random fluctuations are three dimensional. Movements in the

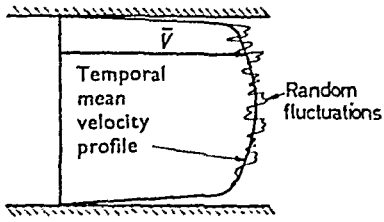

Figure 3.11

direction of the flow were successfully recorded by oscillographs, a sample record being shown in *Fig. 3.12.*

(*b*) The ever changing system of fluctuations superimposed on the 'mean' motion as shown in *Fig. 3.11* introduces stresses far in excess of that due to the viscosity alone. The shear stresses between

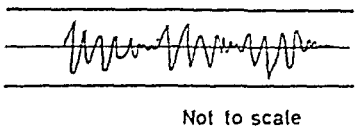

Figure 3.12—Velocity fluctuations in turbulent flow

adjacent fluid layers in turbulent flow are attributed to momentum exchanges between fluid particles moving from one layer to another by the action of the fluctuations and the phenomenon is called the turbulent mixing process. The shear stress for turbulent flow is given by the expression

$$\tau = \rho \cdot K^2 \frac{[dv/dy]^4}{[d^2v/dy^2]^2} \qquad \ldots.(3.5)$$

where K is a constant and dv/dy, d^2v/dy^2, are derivatives of the temporal mean velocity equation.

(*c*) It is apparent from the velocity distribution curves that the velocity gradient, hence the shear stress at the boundary surface, is much greater in turbulent than in laminar flow. This may be observed from the inspection of the curves shown in *Fig. 3.10.*

Actually in changing from laminar to turbulent flow the rate of energy dissipation is greatly increased, as demonstrated by a simple experiment.

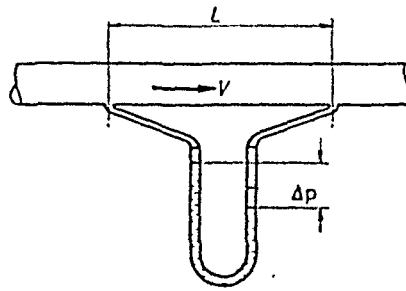

Figure 3.13—Simple pipe flow experiment

We shall pass fluid through a parallel pipe and record the pressure loss due to resistance between two cross-sections L ft. apart, as shown in *Fig. 3.13.* Plotting pressure drop $\Delta p/L$ against velocity

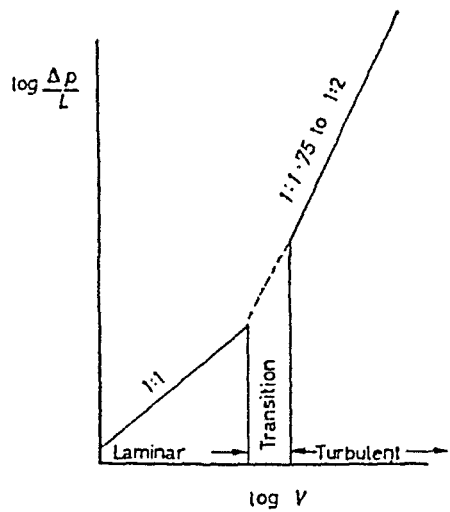

Figure 3.14—Result of pipe flow experiment

on a logarithmic graph paper we shall find: in laminar flow, the pressure drop to vary with the 1st power of the velocity (slope 1 : 1); in turbulent flow to vary approximately with 1·75–2nd power of the velocity, (slope 1 : 1·75 to 1 : 2). The results of such an experiment are shown in *Fig. 3.14.*

In conclusion, it is necessary to point out that the flow characteristics described only hold for 'fully developed' flow conditions. Neither the parabolic distribution law for laminar nor the logarithmic law for turbulent flow will hold for undeveloped flow, as found near the entrance to a pipe or at conduit transitions. The conditions under which fully developed flow can take place will be discussed in detail in Chapter 8.

Example

3.3. Oil of specific gravity 0·9 and viscosity 1×10^{-3} lb. sec./ft.^{2} flows in a 6-in. diameter pipe with a velocity of 2 ft./sec. Determine whether the flow is laminar or turbulent?

Solution.—The flow is laminar if the Reynolds number

$$N_R = \frac{DV\rho}{\mu} < 2100$$

Substituting

$$\text{for } V = 2 \text{ ft./sec.}; \quad \rho = \frac{0{\cdot}9 \times 62{\cdot}4}{32{\cdot}2} = 1{\cdot}74 \text{ slugs/ft.}^3; \quad D = 0{\cdot}5 \text{ ft.}$$

one obtains

$$N_R = \frac{0{\cdot}5 \times 2 \times 1{\cdot}74}{1 \times 10^{-3}} = 1{,}740 < 2{,}100$$

and the flow is laminar.

(Note: If the dimension of viscosity is in lb.sec./ft.^{2} density should be in 'slugs'/ft.^{3}. In case the dimension of viscosity is given in lb./ft. sec., specific weight $w = \rho \cdot g$ stands for ρ.)

REFERENCES

(1) PRANDTL, L., *The Essentials of Fluid Dynamics*, Blackie & Sons, 1952.
(2) HATSCHEK, E., *The Viscosity of Liquids*, Bell, 1928.
(3) ROUSE, H., *Elementary Mechanics of Fluids*, John Wiley & Sons, 1946.

Problems

3.1. Water flows in a pipe of 0·25 in. internal diameter at the rate of 1 g.p.m. If the viscosity of the water is $\mu = 9 \times 10^{-6}$ lb.sec/ft.^{2}, calculate the Reynolds' number and state if the flow is of laminar, turbulent or transition character.

3.2. A bush 6·5 in. long and of 4·12 in. internal diameter slides on a 4·00-inch diameter vertical column. Between the column and the bush is an oil film. Kinematic viscosity of the oil = 0·0128 ft.^{2}/sec., specific gravity S.G. = 0·89.

What must be the weight of the bush if the sliding velocity required is 3 ft./sec.?

3.3. Two horizontal circular plates of 6 in. diameter are held apart at a constant distance of 0·05 in., and have the clearance space filled with oil of dynamic viscosity 0·0019 lb. sec./ft.^{2}. The upper plate revolves at a constant speed of 200 r.p.m.

Considering viscous effects only, and assuming that the space remains filled with oil, find the torque required to maintain this speed.

3.4. Oil fills the annular space between two concentric cylinders of 18 in. height and of 12 and $12\frac{1}{4}$ in. diameter respectively. Immersed in the oil rotates an intermediate cylinder which is provided with a torque-meter. If the speed is 30 r.p.m. and a torque of 3 ft.lb. is required to maintain the rotation, calculate the viscosity of the oil. Neglect the wall thickness of the intermediate cylinder and assume a diameter of $12\frac{1}{8}$ in.

3.5. (*a*) Establish from first principles an approximate expression for the heat generated per unit time by frictional effects in a plain, oil-lubricated bearing, assuming a constant average temperature within the oil film. The clearance between the journal and bearings, the rotational speed, and the dimensions of the journal are known.

Neglect the weight of the shaft and the influence of centrifugal forces.

(*b*) Carry out a sample calculation with the following data:

Length of bearing, $L = 8$ inches.
Diameter of journal, $D = 5$ inches.
Clearance, $R_o - R_i = 0{\cdot}003$ inch.
Revolutions, $N = 11{,}000$ r.p.m.
Viscosity of the lubricant at 150° F.,
$\mu = 7{\cdot}0 \times 10^{-4}$ lb. sec./ft.^{2}.

4

FLOW IN CLOSED CONDUITS

4.1 Pressure Losses in Fluids Flowing Inside Closed Conduits

In a large number of engineering problems the loss of energy due to viscous energy dissipation has to be computed. A simple experiment demonstrates that these losses invariably occur at the expense of the available pressure head.

Consider a tank, from which a liquid can pass first to a vertical tube, then to a horizontal pipe of constant cross-section as shown in *Fig. 4.1.* The pipe is provided with a number of equally spaced

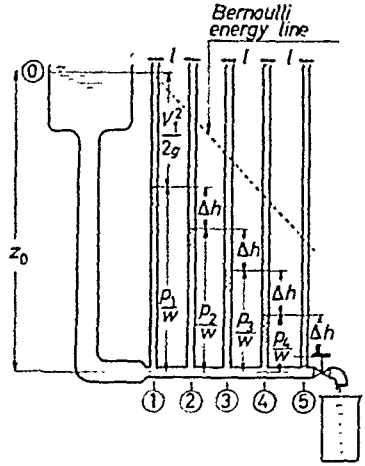

Figure 4.1—Flow from a tank

pressure tappings, over which piezometers are fitted. The flow is varied by a regulating valve situated at the end of the line, whence the fluid passes to atmosphere where the discharge is collected and measured. With the valve closed the fluid in the piezometer columns is level with the free liquid surface 0 in the tank. On opening the valve flow takes place, and the level in all piezometers falls. Neglecting losses in the vertical tube, the level in column 1 falls below the

level at 0 by a distance $V^2/2g$. Writing the Bernoulli equation for cross-section 0 and 1 one obtains

$$0 + 0 + z_0 = \frac{p_1}{w} + \frac{V_1^2}{2g} + 0$$

and

$$\frac{p_1}{w} = z_0 - \frac{V_1^2}{2g}$$

where p_1/w is the available pressure head at cross-section 1.

When the Bernoulli equation is applied between subsequent cross-sections, for example 1 and 2, or 2 and 3, and so on, a discrepancy appears between the left and right hand side of the equation. Since in steady flow neither the velocity nor the potential head varies along a horizontal pipe of uniform cross-section, the terms $V^2/2g$, p/w cancel and only the pressure head remains. For a non-viscous fluid the pressure head in all subsequent cross-sections would be equal, that is $\frac{p_1}{w} = \frac{p_2}{w} = \frac{p_3}{w} = \ldots$. The experiment shows, however, that the level in each consecutive piezometer column falls below the preceding one by a distance Δh, so that

$$\frac{p_1}{w} = \frac{p_2}{w} + \Delta h; \qquad \frac{p_2}{w} = \frac{p_3}{w} + \Delta h;$$

and so on. The quantity

$$\Delta h = \frac{p_2 - p_3}{w} = \frac{p_3 - p_4}{w} = \ldots$$

represents the *loss of head* due to viscous energy dissipation. Similar experiments can be carried out with pipes of non-uniform cross-sectional area and of varying heights above the datum line.

For two arbitrary cross-sections the discrepancy in the Bernoulli equation is balanced by the term 'head losses' which may include not only the resistance offered by long reaches of pipe, but also pipe fittings such as bends, conduit transitions, valves, and so on. Since the potential head is fixed by the layout of the pipeline and the velocity is governed by continuity, pressure remains the only energy reservoir the flow can draw on. As the flow proceeds along the line, more and more of the available pressure is converted into unavailable energy through viscous dissipation.

The Bernoulli equation corrected for *losses* becomes

$$\frac{p_0}{w} + \frac{V_0^2}{2g} + z_0 = \frac{p_x}{w} + \frac{V_x^2}{2g} + z_x + \sum_0^x \text{losses} \qquad \ldots.(4.1)$$

where the left hand side represents the 'reservoir' energy, and the

right hand side represents the sum of the energy available at x and of the energy lost between 0 and x.

4.2 Definition of the Friction Factor

It is convenient to calculate viscous losses with the aid of friction factors.

Friction between a solid surface and a flowing fluid does not exist in the same sense as it does between solid and solid, because of the absence of any rubbing or scratching action. However, the dissipation of energy through viscous action over surfaces is usually referred to as surface or skin friction.

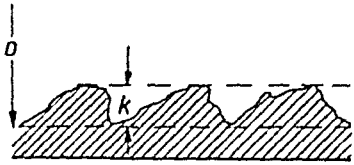

Figure 4.2—Roughness elements

The head loss due to frictional resistance in a long straight pipe is expressed by an equation of the form†

$$\Delta h_f = \frac{p_1 - p_2}{w} = f \cdot \frac{L}{D} \cdot \frac{\bar{v}^2}{2g} \qquad \ldots . (4.2)$$

where f is the friction factor, L the pipe length, D the pipe diameter and $\bar{v}^2/2g$ the mean velocity head. The expression is often referred to as the Darcy formula. Generally the friction factor depends on both the Reynolds number N_R and the surface conditions characterized by the relative roughness e,

$$f = \phi(N_R, e)$$

Surface conditions are influenced by roughness elements which are considered to be projections of similar shape, protruding from the boundary as shown in *Fig. 4.2.* The relative roughness, e, is then defined as the ratio of the height k of the roughness elements to the nominal diameter of the conduit, $e = k/D$. A surface is regarded as smooth or rough depending on the relative roughness. In the following section the influence of viscosity and surface roughness on laminar and turbulent flow will be discussed.

4.3 Friction Factor for Fully Developed Laminar Flow

The friction factor for laminar flow can be derived from first principles.

† Equation 4.2 is derived in Chapter 7.

(1) For laminar flow we can visualize the flow as large numbers of thin concentric cylinders sliding on one another (like the tubes of a telescope) as shown in *Fig. 4.3.* Consider a cylinder of length L, radius r which slides inside a concentric cylinder of a radius $r + dr$. Due to viscous shear the drag† on the outer surface S of the cylinder

$$F = S\tau = -(2\pi rL)\mu \frac{dV}{dr}$$

where $\frac{dV}{dr}$ is the velocity gradient (in radial direction) in that particular layer. In steady flow this force is balanced by a pressure

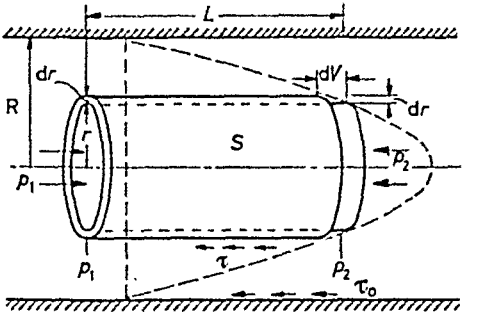

Figure 4.3

difference $p_1 - p_2$ acting on the base areas $(r^2\pi)$ of this cylinder,

$$F = (p_1 - p_2)r^2\pi = -(2\pi rL)\mu \frac{dV}{dr} \qquad \ldots.(4.3)$$

Having separated the variables, a differential equation is obtained

$$dV = -\frac{p_1 - p_2}{2\mu L} r\, dr$$

which yields upon integration

$$V = -\frac{p_1 - p_2}{2\mu L}\frac{r^2}{2} + C \qquad \ldots.(4.4)$$

The value of C can be established from the boundary conditions. At the boundary $r = R$ and $V = 0$

and $$C = \frac{p_1 - p_2}{4\mu L} R^2$$

Substituting this for Eq. 4.4, the expression for the velocity profile is obtained,

$$V = \frac{p_1 - p_2}{4\mu L} R^2 \left[1 - \frac{r^2}{R^2}\right] \qquad \ldots.(4.5)$$

† The force opposing motion is considered negative.

The expression gives a parabolic velocity distribution with a maximum at the centre ($r = 0$)

$$V_{max} = \frac{p_1 - p_2}{4\mu L} R^2 \qquad \ldots.(4.6)$$

(2) Integrating $V\,dA$ over the cross-section A the discharge

$$Q = \int_0^A V\,dA = \frac{(p_1 - p_2)R^2}{4\mu L} \int_0^{R=D/2} \left[1 - \frac{r^2}{R^2}\right] 2\pi r\,dr$$

$$= \frac{(p_1 - p_2)D^4\pi}{128\mu L} \qquad \ldots.(4.7)$$

This law was first established experimentally by Hagen and Poiseuille, and can be usefully employed for the measurement of viscosity. From Eq. 4.7

$$\mu = \frac{D^4\pi(p_1 - p_2)}{128QL} \qquad \ldots.(4.8)$$

Since the quantities on the right hand side can be measured a simple apparatus already shown in *Fig. 3.3* can be devised to obtain the value of the coefficient of viscosity.

(3) From Eq. 4.7 the mean velocity

$$\bar{V} = \frac{Q}{A} = \frac{(p_1 - p_2)D^2}{32\mu L} \qquad \ldots.(4.9)$$

Substituting Eq. 4.2 for the pressure difference, $p_1 - p_2$ the friction factor for laminar flow

$$f = \frac{64}{D\bar{V}\rho/\mu} = \frac{64}{N_R} \qquad \ldots.(4.10)$$

The friction factor for laminar flow thus appears to be independent of surface roughness and this result was accurately confirmed by experiments.

4.4 Friction Factors for Turbulent Flow

The mechanism of turbulent flow is complex and requires the study of the boundary layer theory. For this reason a detailed analysis of turbulent flow is omitted at this stage† and a summary of the experimental results, sufficient to enable the engineer to compute pipe friction losses, is presented.

† A detailed analysis is presented in Chapter 8.

Friction factors, both for laminar and smooth turbulent flow are represented by single lines; for rough turbulence, a number of lines are drawn each representing a specified roughness ratio D/k. The

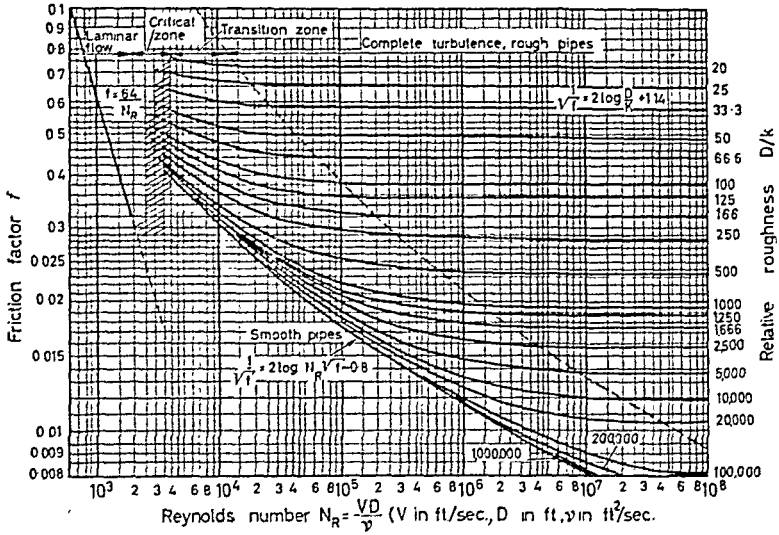

Figure 4.4—Friction factor chart. (This chart appears also on the endpapers in larger size.) (*By courtesy of* Kempe's Engineer's Year Book)

following approximate sizes of the roughness elements are given as a guide:

Boundary material (new)	k (in feet)
Glass, drawn brass, copper, lead	'smooth'
Wrought iron, steel	0·00015
Asphalted cast iron	0·0004
Galvanized iron	0·0005
Cast iron	0·00085
Wood stave	0·0006–0·003
Concrete	0·001–0·01
Riveted steel	0·003–0·03

When studying the friction-factor chart it is observed that the friction factor for laminar flow can fall below or rise above that of turbulent flow. In laminar flow, there seems to be no limit to friction with decreasing Reynolds' numbers. It should be remembered, that although the friction factor increases, the head loss being

directly proportional to the velocity increases slowly. This is shown by rearranging Eq. 4.9

$$\frac{p_1 - p_2}{w} = \frac{32\,\mu L}{D^2 w} V = \text{CONST.} \times V$$

In case of rough turbulence, when the friction factor becomes independent of the Reynolds numbers, the head loss varies with the velocity square and losses increase rapidly with increasing velocity. Again, for smooth turbulence, the head loss, for example, based on the Blasius friction factor, varies with $V^{1.75}$. Plotting head loss against velocity on logarithmic graph paper, the loss for laminar flow will show first a straight line relationship with a slope 1 : 1, then with turbulence developing the slope becomes steeper and increases to 1·75 : 1 or 2 : 1 depending on the existence of smooth or rough turbulence. Since roughness values given in the table only hold for pipes in new condition, it is advisable to allow a reasonable margin for a reserve head, depending upon the nature of the pipe material, the fluid, the sediments transported etc., which may increase the roughness over a period of time. For the same reasons the calculations need not be carried out with hair-splitting accuracy.

For head losses in air supply ducts a simple head-loss chart can be constructed and used with reasonable accuracy. In *Fig. 4.5* a chart prepared by the A.S.H. & V.E. gives head loss per 100 ft. of ducting for various air velocities and pipe diameters.

4.6 Non-Circular Ducts

Since ducts carrying fluids, especially air, are frequently of non-circular cross-section, a quantity, equivalent to the circular pipe diameter has to be substituted for D in the Darcy formula. This quantity is four times the value 'mean hydraulic radius' which acquired its name from the mean intensity of shear stresses at the boundary. The mean hydraulic radius is defined as the ratio of the area A of the flow cross-section to the wetted perimeter P. For a circular pipe of diameter D, the hydraulic radius

$$m = \frac{A}{P} = \frac{D^2\pi/4}{D\pi} = \frac{D_e}{4} \qquad \ldots\ldots(4.15)$$

and the equivalent diameter

$$D_e = 4m \qquad \ldots\ldots(4.16)$$

For a duct of rectangular cross-section, with sides a and b, the mean hydraulic radius

$$m = \frac{ab}{2(a+b)}$$

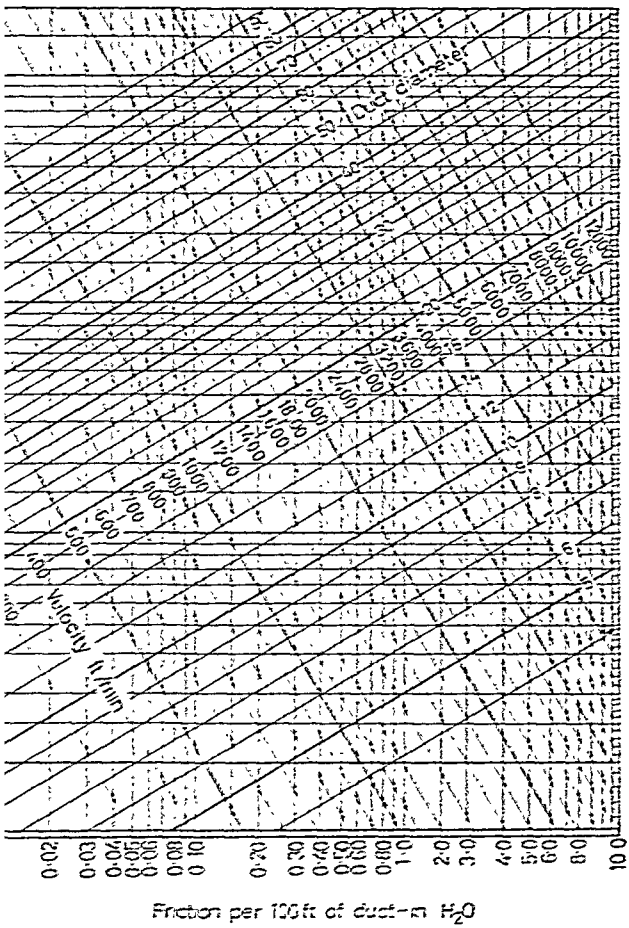

Figure 4.5—Friction chart for air. *(By courtesy of the American Society of Refrigerating Engineers)*

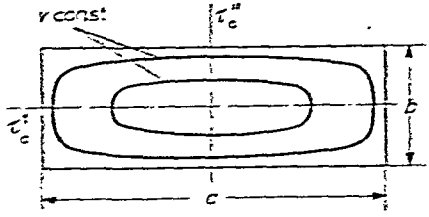

Figure 4.6

and the equivalent diameter

$$D_e = \frac{2ab}{a+b} \qquad \ldots.(4.17)$$

Consider a duct of an oblong rectangular cross-section with sides a and b as shown in *Fig. 4.6.* Since the velocity profile is no longer symmetrical the boundary shear stress τ_0 varies along the perimeter (τ_0', τ_0''). On the assumption that the mean boundary shear stress τ_{0m} is considered equal to the uniform shear stress existing in a circular duct of equivalent diameter,

$$\tau_{0m} = \frac{f}{4} \cdot \frac{\rho V^2}{2} \qquad \ldots.(4.18)$$

and

$$\tau_{0m} P \,.\, L = (p_1 - p_2)A \qquad \ldots.(4.19)$$

where P is the perimeter and A the cross-sectional area of the non-circular duct. The pressure drop over the distance L of an 'equivalent' circular duct

$$p_1 - p_2 = f \frac{L}{D_e} \frac{V^2}{2} \rho \qquad \ldots.(4.20)$$

is considered equal to the pressure drop caused by the mean boundary stress of the non-circular duct. Combination of the Eqs. 4.19 and 4.20 gives the equivalent diameter as

$$D_e = \frac{4A}{P}$$

Recent studies† disclosed the limitations of the arbitrary assumption of the mean boundary stress. It was found that the equivalent diameter may be used for turbulent flow and for cross-sections for which the width-depth ratio is not excessively great or small (say 1 : 3 as a practical limit). It may not be used however for flow between parallel plates, annular spaces or for laminar flow.

4.7 Losses in Conduit Transitions

Conduit transitions fall into three categories, (*a*) enlargements, (*b*) contractions, and (*c*) bends.

Since irreversible pressure-losses occur in all conduit transitions, the engineer's objective is to reduce these losses to a minimum. These losses may be small in comparison with skin friction losses in

† Glaser, H. 'Heat Transfer and Pressure drop in heat exchangers with laminar flow', M.A.P. Volkenrode report V.G. 96-818 March 1947. Also: Croft. 'Thermodynamics, Fluid flow and Heat transmission', p. 116, 1938, McGraw-Hill.

long pipelines. But in short lines, especially in air supply lines, where the velocity head is considerable, the losses may assume major proportions.

(*a*) *Enlargements*

The Sudden Enlargement—The losses in a sudden enlargement were first worked out by Borda and Carnot by applying the continuity, energy, and momentum equations.

A sudden enlargement is shown in *Fig. 4.7.* The fluid leaving the

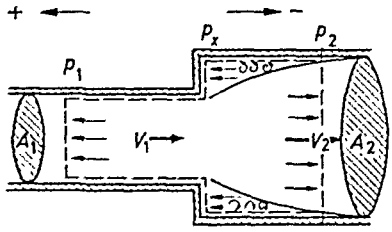

Figure 4.7—Sudden enlargement

smaller pipe with velocity V_1, (being unable to turn around the sharp corners), gradually decreases its speed to V_2. Inspection of the flow pattern shows vortices in the 'pockets' of the sudden enlargement and viscous energy losses occur in keeping these vortices in steady rotation. Due to the velocity change, there is a momentum change equal to the net force acting. Assuming the pipeline to be solidly supported, the forces acting on the fluid are opposite and equal to the forces exerted by the fluid on the pipeline. These pressure forces are indicated by arrows pointing towards the control surface.

The pressure forces are:

$$+p_1A_1 + p_x(A_2 - A_1) - p_2A_2$$

On the assumption that the pressure in the plane of the sudden enlargement (marked as x) is equal to the upstream pressure, $p_x = p_1$, the net force (equal to the momentum change)

$$-F = -(p_2 - p_1)A_2 = Q\rho(V_1 - V_2) \qquad \ldots.(4.21)$$

Writing the Bernoulli equation for cross section 1 and 2

$$p_1 + \tfrac{1}{2}\rho V_1^2 = p_2 + \tfrac{1}{2}\rho V_2^2 + \Delta p \qquad \ldots.(4.22)$$

where Δp is the pressure loss due to the sudden enlargement; hence

$$\Delta p = p_1 - p_2 + \tfrac{1}{2}\rho(V_1^2 - V_2^2) \qquad \ldots.(4.23)$$

Combining the continuity equation $Q = A_2V_2$, with Eq. 4.21

$$p_1 - p_2 = \frac{Q\rho}{A_2}(V_2 - V_1) = \rho V_2(V_2 - V_1)$$

Substituting this expression into Eq. 4.23

$$\Delta p = \rho[V_2^2 - V_1V_2 + \tfrac{1}{2}V_1^2 - \tfrac{1}{2}V_2^2] = \tfrac{1}{2}\rho[V_1 - V_2]^2 \quad \ldots.(4.24)$$

Thus the pressure loss in a sudden enlargement is proportional to the square of the difference in the velocities (not to be mixed up with the velocity square difference).

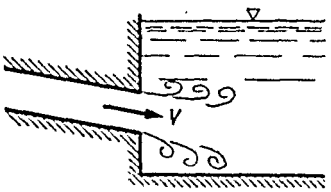

Figure 4.8—Exit loss

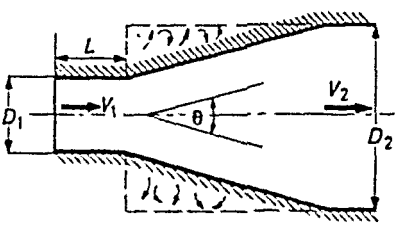

Figure 4.9—Tapered enlargement

In coefficient form

$$\frac{\Delta p}{\frac{1}{2}\rho V_1^2} = \left[1 - \frac{A_1}{A_2}\right]^2 \quad \ldots.(4.25)$$

Subsequent experiments showed that the assumption $p_x = p_1$ does not hold accurately and the expression for head loss has to be corrected. The corrected expression

$$\frac{\Delta p}{\frac{1}{2}\rho V_1^2} = C\left[1 - \frac{A_1}{A_2}\right]^2$$

where C is slightly greater than unity.

Since these losses are wasteful, the use of sudden enlargements should be avoided as far as possible.

Exit Losses—When $A_2 \gg A_1$, the pressure loss becomes equal to the velocity head $\dfrac{V^2}{2g}$. This is the case at pipe exits as shown in *Fig. 4.8* and the loss is then called exit loss.

Tapered Enlargements: Diffusers—The losses experienced in sudden enlargements (including exit losses) can be considerably decreased by the introduction of tapered enlargements, called diffusers. The reduction of the losses is due to the elimination of the eddies shown in *Fig. 4.9*. Experiments conducted on diffusers show that the loss

coefficient K depends on both the taper angle θ and the area ratio A_2/A_1 as shown in *Fig. 4.10.* The loss coefficient is defined as

$$K = \frac{\Delta p}{\frac{1}{2}\rho(V_1^2 - V_2^2)} = \frac{\Delta p}{\frac{1}{2}\rho V_1^2 \left\{1 - \left[\frac{A_1}{A_2}\right]^2\right\}} \quad \ldots . (4.26)$$

and the diffuser efficiency as

$$\eta = 1 - K$$

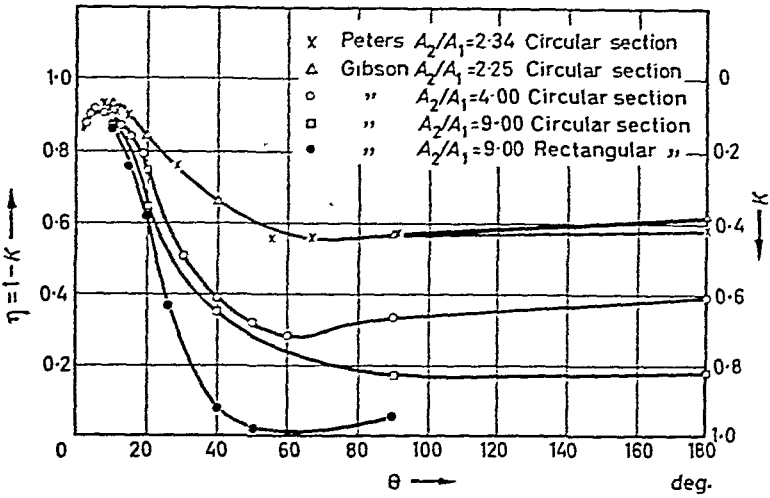

Figure 4.10—Diffuser efficiency. (*By courtesy of* Aircraft Engineering)

On the curves shown in *Fig. 4.10* the ordinate measured from 1·0 down to the curve is the loss of head expressed in terms of the change in kinetic energy during the energy transformation.

Investigations* carried out on diffusers show, that:

(1) the taper angle, which gives maximum efficiency is about 6°–8° for a conical (circular) duct, 6° for a duct with square section, and 11° for a rectangular duct with one pair of walls diverging and one pair parallel.

(2) For a given rate of expansion (A_2/A_1) a diffuser with a circular cross-section gives the best efficiency with the square section next.

(3) The length of duct preceding the diffuser should be kept as short as possible; within certain limits the efficiency is a function

* Patterson, G. Modern Diffuser Design, *Aircraft Engineering*, Sept. 1938. p. 267.

of the product 0 times L/D_1, where L/D_1 is the 'effective' entrance length†.

(4) A length of duct following the diffuser improves the efficiency; the length of outlet duct should be about 4–6 times the maximum diameter (D_2).

Since the coefficient embodies the effects of friction as well as those of eddying turbulence the behaviour of the loss curve can be explained. In an enlargement of small taper angle the head loss will result wholly from surface friction. For a specified area ratio A_2/A_1 a small angle results in a long diffuser in which the frictional losses are large. As the angle increases the enlargement approaches the sudden enlargement, the fluid no longer follows the outlines of the ducting and 'separates' from the walls, inducing vortices to appear.

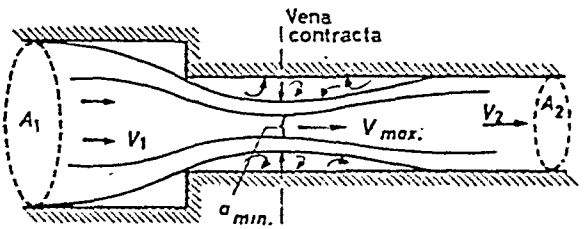

Figure 4.11—Sudden contraction

In practice diffusers are widely used for the conversion of velocity head into pressure head. When diffusers are fitted at the exit of pipelines an increase in the flow quantity is experienced. The increase is due to the reduction of the exit loss.

(b) Sudden Contractions

When fluid enters a sudden contraction, a marked decrease in the cross-sectional area is experienced as shown in *Fig. 4.11*. Inspection of the flow pattern shows that the contraction commences well upstream. Having attained a minimum cross-section (*vena contracta*), the stream expands downstream and ultimately assumes uniform flow over the entire cross-section of the pipe. The losses in a sudden contraction are largely due to the 'unsupported' expansion downstream from the *vena contracta*. Vortices appear between the main stream and the wall, thus energy is lost in keeping these in rotation.

Neglecting the losses in the contracting section and denoting the velocity at the *vena contracta* V_{max}, the loss for the expanding section is

$$\Delta p = \tfrac{1}{2}\rho[V_{max} - V_x]^2 = K_c \tfrac{1}{2}\rho V_2^2 \qquad \ldots.(4.27)$$

† Robertson, —. and Ross, —. Effect of entrance conditions on diffuser flow, *Proc. A.S.C.E.* Vol. 78. July 1952.

where K_c is the loss coefficient for the contraction.

Hence $$K_c = \left[\frac{V_{max} - V_2}{V_2}\right]^2 = \left[\frac{A_2}{A_0} - 1\right]^2 \quad \ldots.(4.28)$$

Since the value of A_2/A_0 depends on A_2/A_1, the loss coefficient is primarily a function of A_2/A_1. Some values of K are:

A_2/A_1	0·2	0·4	0·6	0·8	1·0
K_c	0·34	0·27	0·16	0·05	0

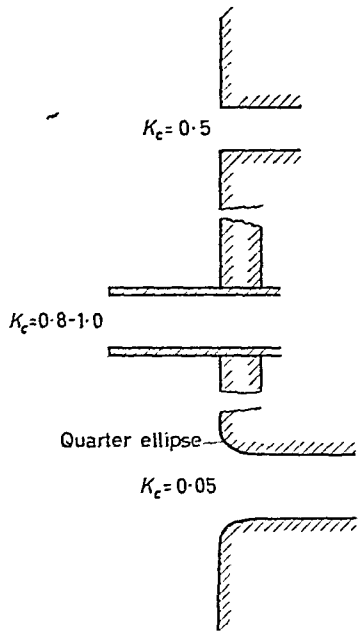

Figure 4.12—Types of pipe entrances

Pipe entrances may be sharp or rounded off as shown in *Fig. 4.12*. For sharp entrances the loss coefficient is approximately 0·5, if the pipe ends flush with the wall, and 0·8–1·0 if the pipe protrudes. The loss coefficient for a well rounded-off entrance (bell mouth) is about 0·05. These losses are frequently called 'entry' losses. Sudden contractions in pipelines are to be avoided in practice and tapered or rounded-off transitions are recommended instead. A quarter ellipse gives satisfactory transitions, such as used in nozzle designs. The loss coefficient in straight tapered contractions may be as low as 0·01–0·02, depending on design and surface finish.

c. Bends

The loss of head in bends is greater than that experienced in the same length of straight pipe. The extra loss is due to increased turbulence arising from the change in direction of the flow. The change in the flow direction results in an increase of the pressure along the outside of the bend and a decrease along the inside. The velocity profile becomes distorted and this, together with centrifugal forces produces a secondary flow as shown in *Fig. 4.13.* As a result,

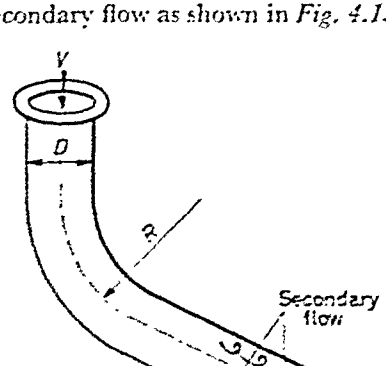

Figure 4.13

the fluid leaving the bend moves in a double spiral which diminishes in intensity only after the fluid passes well downstream. It is assumed, however, that the full effect of the loss is concentrated at the transition section, and the effects downstream are neglected.

The bend loss coefficient is defined as

$$K_B = \frac{\Delta p}{\frac{1}{2}\rho V^2} \qquad \ldots\ldots(4.29)$$

where Δp is pressure loss in the bend.

For sharp bends a complete loss of the velocity head is experienced and the value of $K_B = 1{\cdot}0$.

Generally, losses in bends depend on the ratio R/D, where D is the diameter of the pipe and R the radius of the bend and are independent of the Reynolds' number.

Investigations† on 90° bends show that the minimum loss is experienced when $R/D = 2{\cdot}5$–5 as shown in *Fig. 4.14.*

† Beij, K. H. 'Pressure losses for fluid flow in 90° pipe bends'. Research paper R.P. 1110. National Bureau of Standards. Vol. 21 p.1. July, 1938.

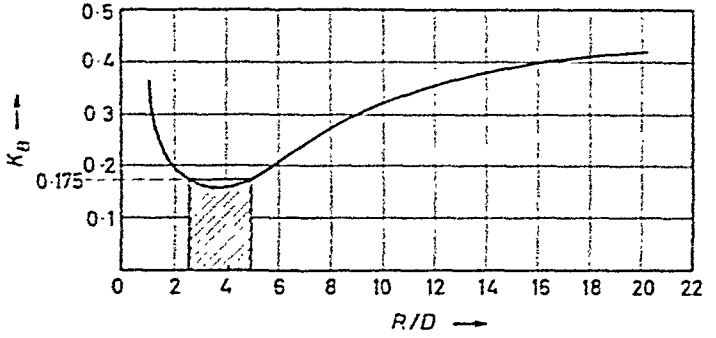

Figure 4.14—Loss coefficient for pipe bends

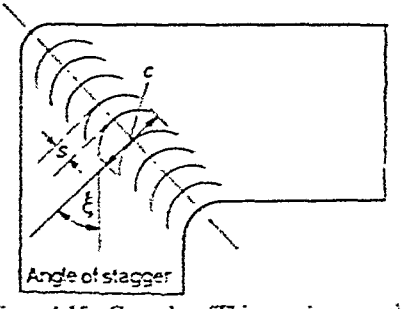

Figure 4.15—Cascade. (Thin turning vanes)

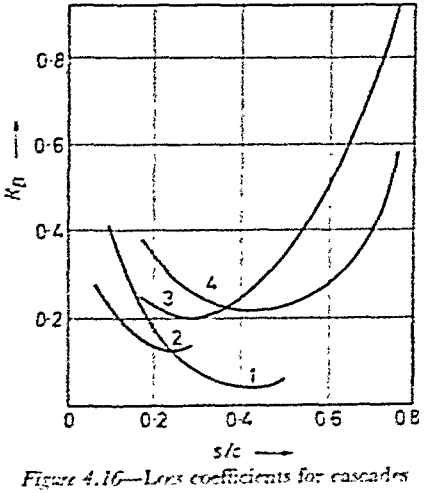

Figure 4.16—Loss coefficients for cascades

1. Collar's thick vanes
2. Salter's circular arc
3. } Circular arcs of various design
4. }

(*From* R. & M. 2469: 1952 *by permission of the Controller, H.M.S.O.*)

Because of the scarcity of data on bends less than 90°, designers are advised to rely on their own judgement. The loss coefficient of a 45° bend is given as 0·42.

The loss in sharp bends can be considerably decreased by splitting the flow into a number of streams by a series of vanes, called cascades, as shown in *Fig. 4.15.* The head loss coefficient K in such bends may be decreased to 0·05–0·2 depending on design.

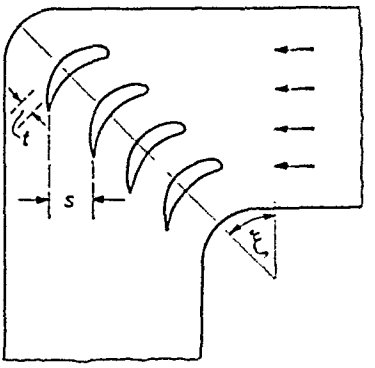

Figure 4.17

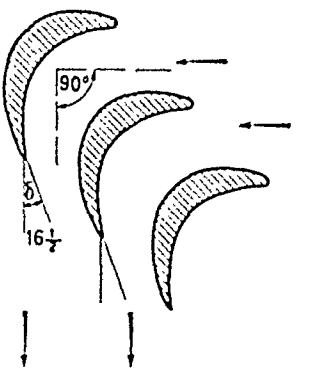

Figure 4.18

Thick turning vanes

In designing vanes for bends consideration is given to the spacing s, measured along the bend-diagonal, and to the chord c, a characteristic dimension of the vanes. Closely spaced vanes are liable to produce large frictional losses and loosely spaced vanes are ineffective. The ratio s/c, *i.e.*, the relationship of spacing to chord, has a marked influence on the loss coefficient as shown in *Fig. 4.16.* For a specific vane design, minimum loss is experienced at a certain value of s/c.

A further reduction in bend losses is obtained from considerations of the vane profile. Vanes can be made up of circular arcs† as shown in *Fig. 4.15,* or of aerofoils‡, bent around a semicircle as shown in *Fig. 4.17.* The thickness t of the vane is guided by continuity, that is, the area open for flow is equal to that of the duct. Best results are obtained with aerofoils but circular-arc vanes give satisfactory results.

Finally, consider the deflection of the stream by the vanes. A 90° arc will give a slightly less than rectangular deflection, unless vanes are closely spaced. Optimum spacing and a correct rectangular

† Salter, C. 'Experiments on thin turning vanes', Air Ministry R. & M. 2469, 1952.

‡ Collar, A. R. 'Some experiments with cascades of aerofoils', Air Ministry, R. & M. No. 1768, 1937.

deflection is obtained by extending the angle enclosed by the tangents to the leading and trailing edges of the vanes by an additional angle of 'deviation'. For a 'nominal' deflection θ, the tangents should enclose an angle $\theta - \delta$ where according to Constant†,

$$\delta = 0{\cdot}26\theta \sqrt{\frac{s}{c}} \qquad \ldots.(4.30)$$

For $s/c = 0{\cdot}5$ and nominal deflection $\theta = 90°$, $\delta = 16{\cdot}5°$ as shown in *Fig. 4.18.*

4.8 Losses in Pipe Fittings

In pipe fittings, such as valves and strainers, the losses may be several times the velocity head, depending on design. The data given in the table are not 'hard and fast', and designers are advised either to make an experimental check on a certain type of fitting or to contact the manufacturer for further information.

Losses in Pipe Fittings

Fitting	*Loss coefficient*
Globe valve	10
Angle valve (90°)	5
Gate valve fully open	0·2
Foot valve	1·5
Strainer	2
Standard T branch	1·8

4.9 The Design of Duct and Pipe Systems

In designing duct and pipe systems the cross-sections are determined on the basis of the amount of fluid to be carried. In isolated cases, the discharge has to be determined for an existing system, usually brought about by some change in the existing pump or fan set-up. In either case the determination of the losses in the various sections of the installation is required.

In going downstream in a conduit system, the losses accumulate, and the Bernoulli equation must include the summation of all losses which occur between any two sections, $(n–m)$

$$\frac{p_n}{w} + \frac{V_n^2}{2g} + z_n = \frac{p_m}{w} + \frac{V_m^2}{2g} + z_m + \Sigma \text{ losses} \qquad \ldots.(4.31)$$

† Howell, A. R. 'Cascade theory and performance', R. & M. 2095, June 1942.

The term 'losses' include all the resistance due to pipe friction, conduit transition and fittings. These in turn are computed on the basis outlined in paragraphs 4.5, and 4.7. Between any two sections n and m where the velocity of the flow is constant

$$\Sigma \text{ losses} = \frac{V_{n \text{ or } m}^2}{2g}\left[f\frac{L}{D} + K_n + K_{n+1} + \ldots K_m\right]$$

where fL/D represents the skin frictional losses and K_n, K_{n+1} . . . are the loss coefficients for the various transitions and fittings between sections n and m. For conduits of varying cross-sections and velocities, the calculations are carried out from section to section.

It is pointed out that in incompressible fluid flow the available pressure always decreases to the pressure prevailing at the discharge end of the line. Thus, for example, the pressure decreases to atmospheric if the line discharges into the atmosphere.

A knowledge of what causes pressure loss is necessary not only in determining the total pressure drop in a given system but also in avoiding arrangements which may cause excessive pressure losses. Systems carrying fluids normally consist of one or more trunk-mains leading from a pump, fan or a reservoir to distribution points. From these points the individual branches supply the fluid to the consumer. Regardless which path the fluid follows however, the pressure drop must of necessity be the same along each path. *At the distribution points the pressure is common to all lines branching off at that particular point.*

In designing a conduit system the following procedure may be followed:

(*a*) sketch a line diagram, showing each main-trunk, distribution point, length of line, conduit transitions and fittings, and mark the specified rate of flow;

(*b*) determine the sizes of all branch and trunk mains by first assigning a tentative velocity for each section. (The velocity in ducts carrying air may be chosen between 15–25 ft./sec., and for water 3–10 ft./sec.)

(*c*) calculate the pressure drop over several of the more important paths and adjust the velocities and conduit dimensions if necessary to obtain equal pressure drop for each branch. Start the calculations from the discharge end of the system and work towards the main supply trunk;

(*d*) having computed all losses, compare the total resistance of the system with the pressure available. Adjust the design if the resistance differs considerably from the available pressure. Characteristic curves of fans and pumps are helpful guides in determining the

supply in a system where the flow conditions may vary, such as are met in practice in air conditioning or in other complex pipe systems.

Designers of conduit systems often make use of the term 'equivalent length'. A fitting or conduit transition with a loss coefficient K may be represented by a length L' of straight line offering the same resistance. Writing

$$K\frac{V^2}{2g} = f\frac{L'}{D}\frac{V^2}{2g}$$

the equivalent length

$$L' = \frac{D \cdot K}{f} \qquad \ldots.(4.32)$$

Thus the equivalent length can be added to the length of conduit and substituted in the Darcy formula. For a line incorporating a number of fittings, we write

$$\Delta h_f = f\frac{L + L' + L'' + \ldots}{D}\frac{V^2}{2g} \qquad \ldots.(4.33)$$

where Δh_f is the head loss due to friction and L', L'', L''', are the equivalent lengths of the various fittings. For example a 6-in. short-radius bend is equivalent to 16·5 ft. of straight pipe. Tables and nomograms are available† for designers wishing to follow this method of calculations.

Examples

4.1. A 3 in. diameter horizontal pipeline 15 miles long carries oil at a rate of 30 gal. per min. Calculate the total resistance of the pipeline (in feet of oil) and the necessary power to maintain the flow.

Data—Viscosity of oil $= 8 \times 10^{-3}$ lb. sec./ft.^{2}
Specific gravity = 0·865.

Solution.—From the discharge and cross-sectional area, the mean velocity is found

$$V = \frac{Q}{A} = \frac{30 \times 10}{60 \times 62{\cdot}4} \Big/ \frac{3^2 \times \pi}{4 \times 144}$$

$$= \frac{0{\cdot}08}{0{\cdot}049} = 1{\cdot}63 \text{ ft. per sec.}$$

† Refrigerating Data Book, 1940 edition. p. 74.

The Reynolds' number

$$N_R = \frac{DV\rho}{\mu}$$

$$= \frac{3 \times 1{\cdot}63 \times 0{\cdot}865 \times 62{\cdot}4}{12 \times 8 \times 10^{-3} \times 32{\cdot}2}$$

$$= 85 < 2{,}100 \text{ (laminar flow)}$$

Hence the friction factor

$$f = \frac{64}{N_R} = \frac{64}{85} = 0{\cdot}75$$

Total resistance of pipeline

$$\Delta h_f = f\frac{L}{D}\frac{V^2}{2g} = 0{\cdot}75 \times \frac{15 \times 5280}{3/12} \times 1{\cdot}63^2/64{\cdot}4$$

$$\cong 10{,}000 \text{ ft. of oil.}$$

Necessary power

$$P = \frac{Qw\Delta h_f}{550} = \frac{0{\cdot}08 \times 62{\cdot}4 \times 0{\cdot}865 \times 10{,}000}{550}$$

$$= 78{\cdot}5 \text{ h.p.}$$

4.2. A pipeline is required to convey light diesel oil of specific gravity 0·86 and kinematic viscosity $5{\cdot}4 \times 10^{-5}$ ft.^{2}/sec from a tanker to a storage tank. The cast-iron pipeline is 500 feet in length and the desired discharge rate is at least 100 tons per hour. The difference in level between suction and delivery is 80 feet. If the pump is capable of developing a pressure of 50 lb./in.^{2}, what diameter of pipe will be required? Commercial sizes available are 2, 3, 4, 6, 8, and 10 in. Neglect all losses, except pipe friction.

Solution.—Write down Bernoulli's equation including losses

$$\frac{p_1}{w_{oil}} + \frac{V_1^2}{2g} + z_1 = \frac{p_2}{w_{oil}} + \frac{V_2^2}{2g} + z_2 + f\frac{L}{D}\frac{V_2^2}{2g}$$

where $\frac{p_1}{w_{oil}} = \frac{50 \times 144}{0{\cdot}86 \times 62{\cdot}4} = 135$ ft. and $z_1 = 0 \quad p_1 = 0 \quad z_2 = 80$

Hence the head loss due to friction

$$\Delta h_f = 135 - 80 = 55 = f\frac{L}{D}\frac{V_2^2}{2g}$$

Since the discharge is specified, $V_2 = \frac{Q}{A}$

Substituting this for V_2

$$\Delta h_f = 55 = f\frac{L}{D^5}\left(\frac{4}{\pi}\right)^2\frac{Q^2}{2g}$$

and

$$D = \sqrt[5]{\frac{500 \times fQ^2}{55 \times 0{\cdot}785^2 \times 64{\cdot}4}}$$

Assuming friction factor of 0·025 and substituting for discharge

$$Q = \frac{100 \times 2240}{3600 \times 0{\cdot}86 \times 62{\cdot}4} = 1{\cdot}16 \text{ cusecs.}$$

We obtain

$$D = \sqrt[5]{\frac{0{\cdot}025 \times 500 \times 1{\cdot}16^2}{55 \times 39{\cdot}7}} = (76{\cdot}5 \times 10^{-4})^{0{\cdot}2} = 0{\cdot}375 \text{ ft.} = 4{\cdot}5 \text{ in.}$$

Try a 4-in. pipe and check the friction factor.

The velocity in the pipe $V = \frac{Q}{A} = \frac{4 \times 1{\cdot}16 \times 144}{\pi \times 16} = 13{\cdot}3$ ft./sec

The Reynolds' number

$$N_R = \frac{4 \times 13{\cdot}3 \times 0{\cdot}86 \times 1{\cdot}94}{12 \times 5{\cdot}4} \times 10^5 = 1{\cdot}37 \times 10^5$$

For cast-iron $k = 0{\cdot}00085$ ft. and $\frac{D}{k} = \frac{4}{12 \times 0{\cdot}00085} = 400$

From the friction factor chart $f = 0{\cdot}026 \sim 0{\cdot}025$ (assumed).
Try a 6-in. pipe and repeat the calculation.

4.3. A 1/2-in. dia. rubber hose, 60 ft. long, is connected to a garden tap, which is fitted to a water main where the pressure is 80 lb./in.^{2} (gauge). Calculate the exit velocity of water for the following conditions:

(*a*) A nozzle attachment restricts the exit diameter to 0·125 in.

(*b*) The water flows unrestricted into the atmosphere (attachment removed)

(*c*) Calculate the kinetic energy of the jets in both cases.

Assume that the hose is in a horizontal position and smooth inside. The loss coefficient K_y of the nozzle may be taken as 0·1 and that of the tap K_T as 7·50.

Neglect the flow velocity in the main.

The kinematic viscosity of the water is $\nu = 1{\cdot}02 \times 10^{-5}$ ft.^{2}/sec.

Solution.—(*a*) Write down Bernoulli's equation including losses for cross-sections 1–1 and 3–3 (*see Fig. 4.19*):

$$\frac{p_1}{w} + \frac{V_1^2}{2g} + z_1 = \frac{p_3}{w} + \frac{V_3^2}{2g} + z_3 + \text{losses}$$

Since $z_1 = z_3$, $V_1 = 0$, and $p_3 = 0$ (discharge into atmosphere)

$$\frac{p_1}{w} = \frac{V_3^2}{2g} + \text{losses}$$

The losses are:

(1) pipe friction $\Delta h_f = f \cdot \frac{L}{D} \cdot \frac{V_2^2}{2g}$

(2) loss at the valve $= K_V \frac{V_2^2}{2g}$

(3) loss in the nozzle $= K_N \frac{V_3^2}{2g}$

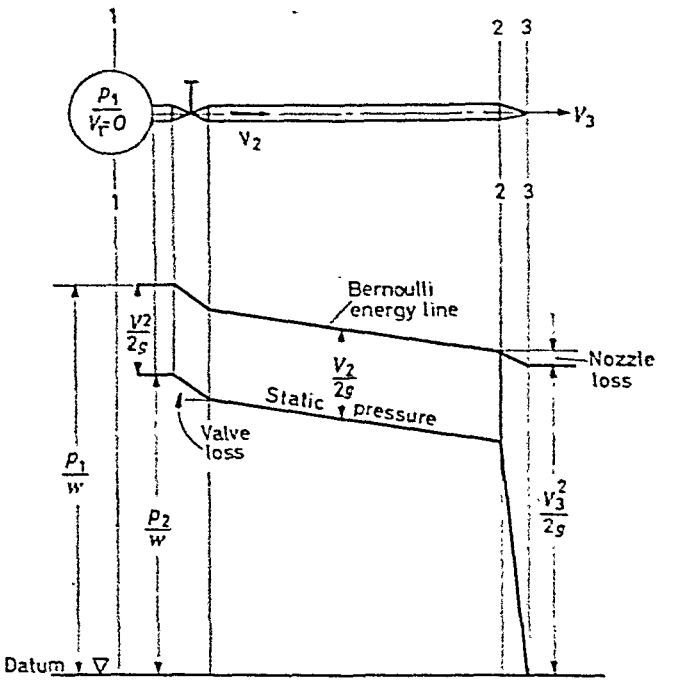

Figure 4.19

From the continuity equation

$$A_2 V_2 = A_3 V_3$$

$$\therefore \quad V_3 = \frac{A_2}{A_3} V_2$$

Hence

$$\frac{p_1}{W} = \frac{V_2^2}{2g}\left[(1 + K_N)\left(\frac{A_2}{A_3}\right)^2 + f\frac{L}{D} + K_V\right]$$

Assuming $f = 0{\cdot}025$

$$\frac{p_1}{W} = \frac{80 + 144}{62{\cdot}4} = \frac{V_2^2}{64{\cdot}4}\left[\left(\frac{0{\cdot}5}{0{\cdot}125}\right)^4 (1 + 0{\cdot}1) + 0{\cdot}025 + \frac{60 \times 12}{0{\cdot}5} + 7{\cdot}5\right]$$

Hence $$V_2 = \sqrt{\frac{184 \times 64{\cdot}4}{325}} = 6{\cdot}05 \text{ ft./sec.}$$

The velocity at exit is $16 \times 6{\cdot}05 = 97$ ft./sec.
This is only slightly less than $\sqrt{(2gh)} = \sqrt{(64{\cdot}4 \times 184)} = 109$ ft./sec., which indicates that the losses are small.
However because of the small exit area the discharge

$$Q = \frac{0{\cdot}125^2\pi}{4 \times 144} \times 98 = 8{\cdot}3 \times 10^{-3} \text{ cusecs.}$$

(*b*) If the nozzle is removed the losses become considerable. The equation may now be written:

$$\frac{p_1}{w} = \left[1 + f\frac{L}{D} + K_v\right]\frac{V_2^2}{2g}$$

Assuming $f = 0{\cdot}02$

$$184 = [1 + 28{\cdot}8 + 7{\cdot}5]\frac{V_2^2}{64{\cdot}4}$$

Hence

$$V_2 = \sqrt{\frac{184 \times 64{\cdot}4}{37{\cdot}3}} = 18 \text{ ft./sec.}$$

The discharge

$$Q = \frac{0{\cdot}5^2\pi}{4 \times 144} \times 18 = 24{\cdot}6 \times 10^{-3} \text{ cusecs.}$$

(*c*) Comparing the kinetic energies of the two jets

$$\frac{\text{Kin. Energy (1)} \propto (QV^2)_1}{\text{Kin. Energy (2)} \propto (QV^2)_2} = \frac{8{\cdot}4}{24{\cdot}6} \times \left(\frac{98}{18}\right)^2 = 10$$

Under these circumstances it is obvious that much greater *power* can be obtained from a smaller but 'faster' jet, than from a larger but much slower jet.

(See Max. Power of a Jet, in section 'Turbines').

4.4. Air is discharged from a tank, through a 25 ft. long horizontal C.I. pipe of 1 ft. diameter, into the atmosphere. Constant pressure difference of 1 in. W.G. is maintained between the tank and the ambient air.

(*a*) Calculate the exit velocity and the quantity of air flowing.

(*b*) Now consider that a diffuser is fitted to the end of the pipe which increases the exit diameter from 1 ft. to 2 ft. Recalculate the flow quantity. Assume that the pipe is provided with a well rounded entry, that the loss coefficient is 0·1 and the diffuser efficiency is 85

per cent. (taper angle 20° approx.) The kinematic viscosity of the air is $1{\cdot}6 \times 10^{-4}$ ft.²/sec.

Solution.—We write down Bernoulli's equation with losses

$$\frac{p_1}{w_{air}} + \frac{V_1^2}{2g} + z_1 = \frac{p_2}{w_{air}} + \frac{V_2^2}{2g} + z_2 + \text{losses}$$

$$\therefore \qquad \frac{p_1 - p_2}{w_{air}} = \left[0{\cdot}1 + f\frac{L}{D} + 1\right]\frac{V_2^2}{2g}$$

Assuming $f = 0{\cdot}02$ and $w_{air} = 0{\cdot}075$ lb./ft.³

$$\frac{1 \times 5{\cdot}2 \times 64{\cdot}4}{0{\cdot}075} = \left[1{\cdot}1 + 0{\cdot}02 \times \frac{25}{1}\right] V_2^2$$

Hence $$V_2 = 52{\cdot}4 \text{ ft./sec.}$$

Check for friction factor:

$$N_R = \frac{52{\cdot}4 \times 1 \times 10^4}{1{\cdot}6} = 3{\cdot}25 \times 10^5$$

Relative roughness $D/k = 1/0{\cdot}00085 = 1400$

For which $$f \cong 0{\cdot}02$$

The discharge

$$Q = V \,.\, A = 52{\cdot}4 \times \frac{1^2 \times \pi}{4} = 41{\cdot}1 \text{ ft.}^3\text{/sec.}$$

If a diffuser is fitted to the end of the pipe the exit velocity is decreased from V_2 to V_3, and

$$\frac{p_1 - p_2}{w_{air}} = \frac{V_3^2}{2g} + \frac{V_2^2}{2g}\left[0{\cdot}1 + f\frac{L}{D}\right] + 0{\cdot}15\,\frac{V_2^2 - V_3^2}{2g}$$

Since

$$V_3 = \frac{A_2}{A_3}V_2 = (\tfrac{1}{2})^2 V_2 = \frac{V_2}{4}$$

$$\therefore \quad \frac{1 \times 5{\cdot}2 \times 64{\cdot}4}{0{\cdot}075} = V_2^2\left[(\tfrac{1}{4})^2 + 0{\cdot}1 + 0{\cdot}02 \times \frac{25}{1} + 0{\cdot}15\left(1 - \frac{1}{16}\right)\right]$$

Hence $$V_2 = \sqrt{\frac{69{\cdot}5 \times 64{\cdot}4}{0{\cdot}8035}} = 74{\cdot}5 \text{ ft./sec.}$$

The discharge

$$Q = V \,.\, A = 74{\cdot}5 \times 0{\cdot}785 = 58{\cdot}5 \text{ ft.}^3\text{/sec.}$$

Thus the fitting of a diffuser at the end of this pipeline resulted in a 42% increase in the discharge.

4.5. A water supply line is to be laid between a river and a nearby factory.

It is proposed to utilize 2-in. diameter galvanized iron pipes and a centrifugal pump, both in stock in the factory stores. The difference in elevation between the water surface level of the river and a storage reservoir is estimated to average 40 feet. Data on the performance of the pump are available and it is estimated that the pipeline would have an overall length of 500 feet incorporating three 90° bends, one strainer, one non-return valve and one stop-valve.

(*a*) Calculate the discharge through the pipeline.

(*b*) Calculate the power necessary to drive the pump.

Losses in Valves and Fittings

90° Bend	$K = 0{\cdot}2$
Strainer	$K = 2{\cdot}0$
Non-return valve	$K = 1{\cdot}7$
Gate-valve (open)	$K = 0{\cdot}2$

Head, Efficiency and Discharge Data on the Pumps

Discharge cusecs	0	0·1	0·15	0·2	0·25	0·30
Head available, ft.	82	76	71	63	50	32
Efficiency	0	19	26	31	33	23

Assume kinematic viscosity of water $1{\cdot}16 \times 10^{-5}$ ft.^{2}/sec.

Solution.—(*a*) The head required to overcome level difference and losses

$$H = 40 + \left[\Sigma K + f\frac{L}{D}\right]\frac{V^2}{2g}$$

Since

$$\Sigma K = 3 \times 0{\cdot}2 + 2 + 1{\cdot}7 + 0{\cdot}2 = 4{\cdot}5$$

and

$$\frac{L}{D} = \frac{500 \times 12}{2} = 3000$$

$$H = 40 + [4{\cdot}5 + 3000f]\frac{V^2}{2g}$$

Assuming a (mean) friction factor $f = 0{\cdot}03$

$$H = 40 + 1{\cdot}57\,V^2$$

Substituting discharge for V,

$$\left(\text{cross-sectional area} = \frac{2^2\pi}{4 \times 144} = 2{\cdot}18 \times 10^{-2}\ \text{ft.}^2\right)$$

$$H = 40 + 3300Q^2$$

For various values of Q, H may be plotted on the same graph as the pump characteristics as shown in *Fig. 4.20.*

The resistance curve intersects at $Q = 0{\cdot}104$ cusecs. The corresponding head is 76 ft.

Now check the friction factor.

Velocity $$V = \frac{0{\cdot}104}{0{\cdot}0218} = 4{\cdot}8 \text{ ft./sec.}$$

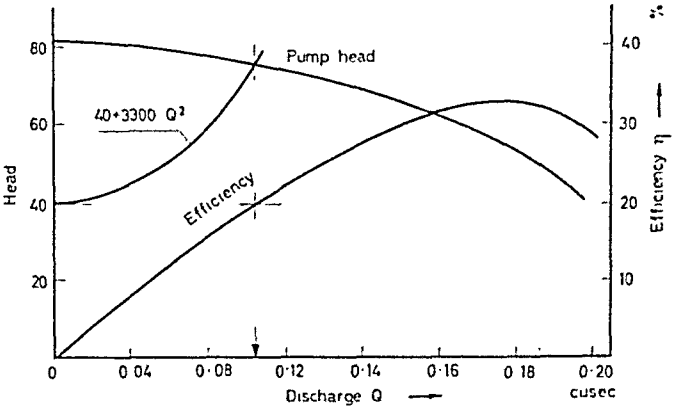

Figure 4.20

Reynolds' number

$$N_R = \frac{4{\cdot}8 \times 2 \times 10^5}{12 \times 1{\cdot}16} = 6{\cdot}9 \times 10^4$$

For galvanized iron pipe $k = 0{\cdot}0005$

and $$\frac{D}{k} = \frac{2}{12 \times 0{\cdot}0005} = 330$$

On the friction chart $f = 0{\cdot}029$, reasonably close to the assumed value.

(*b*) Power requirements†; Since the efficiency of the pump is 20% at $Q = 0{\cdot}104$.

$$\text{b.h.p.} = \frac{QwH}{550\eta} = \frac{0{\cdot}104 \times 62{\cdot}4 \times 76}{550 \times 0{\cdot}2} = 4{\cdot}5 \text{ h.p.}$$

REFERENCES

(1) Bakhmetef, —, and Allan, —., The mechanism of energy loss in fluid friction, *Trans Amer. Soc. civ. Engrs*, 1946, p. 1043.
(2) *Fan Engineering*, Buffalo Forge Co., N.Y.
(3) Lea, F. C., *Hydraulics for Engineers and Engineering Students*, Longmans, Green, 1938.

Problems

4.1. Glycerine is flowing downwards through a vertical 6-in. diameter smooth glass cylinder at a mass rate of 3·85 slugs per second. At the bottom

† See Chapter 11, Section 7.

of the cylinder a pressure gauge indicates a pressure of 2·9 lb./in.² g. Determine the height of a section of the cylinder where the pressure is atmospheric.

4.2. A 180-ft. long 4-in. diameter clean galvanized-iron pipe discharges water from a closed constant-head reservoir A to an open constant head reservoir B. The pipe has three bends and two gate valves, and the actual level difference between A and B is 22 ft. What must be the gauge pressure of the air above the water level in A if a discharge of 1·2 cusecs of water through the pipe is required?

Assume the following head loss coefficients:

For pipe entrance,	$K_e = 0{\cdot}5$
For a bend,	$K_b = 0{\cdot}8$
For a gate valve,	$K_v = 0{\cdot}2$
For pipe outlet,	$K_o = 1{\cdot}0$

Assume kinematic viscosity of water $\nu = 1{\cdot}33 \times 10^{-5}$ ft.²/sec.

4.3. A new galvanized-iron pipe, 5 in. bore, conveys water from a reservoir in which the water surface stands at a reduced level of 370 ft. At a point 7,000 ft. along the pipe from the reservoir a pressure gauge is fitted 10 ft. above the centre line of the pipe. If the gauge pressure is 20 lb./in.² and the reduced level at the centre line of the gauge is 170 ft., what is the flow rate through the pipe?

Neglect all minor losses and take $\nu = 1{\cdot}2 \times 10^{-5}$ ft.²/sec.

4.4. A large open water tank has, at a depth h_1 below the surface, a short horizontal tapered enlargement fitted as a 'spout.' The area, at the junction of the taper with the tank, is a_1 and at the large end, discharging to atmosphere, is a_2 ($a_2 > a_1$).

Show that, if the enlargement runs full and the total losses are $0{\cdot}19h_1$, C_d based on a discharge area of a_1 may exceed unity.

4·5. A vertical cement-lined stack, 75 ft. high, of 3 ft. × 3 ft. square cross-section is being erected on top of a large factory. Assuming a constant air temperature of 84° F. inside the factory and the stack, and a temperature of 50°F. in the free atmosphere determine:

(*a*) the pressure difference due to the change of specific weight on both sides of the stack wall at the bottom end;

(*b*) the air velocity in the stack due to this pressure difference.

The kinetic energy loss coefficients for the entrance and outlet of the stack are $K_e = 0{\cdot}5$ and $K_o = 1{\cdot}0$, respectively. Assume gas constant of air $R = 53{\cdot}5$ ft. per F°., and kinematic viscosity of air at 84°F., $\nu = 17 \times 10^{-5}$ ft.²/sec.

4·6. A pipeline is required to convey light diesel oil of specific gravity 0·86 and kinematic viscosity $5{\cdot}4 \times 10^{-5}$ ft.²/sec. from a tanker to a storage tank. The cast-iron pipeline is 500 ft. in length and the desired discharge rate is at least 100 tons per hour. The difference in level between suction and delivery is 80 ft.

If the pump is capable of developing a pressure of 50 lb./in.², what diameter of pipe will be required? Commercial sizes available are 2, 3, 4, 6, 8, and 10 in. Neglect all losses, except pipe friction.

4.7. For the ventilation of two rooms a certain fan is used, the characteristics of which are given in the table below.

The fan is located in the basement and supplies heated air to one room through a duct of 5 × 12 in. cross-section, 15 ft. long, and to the other room through a duct of 7 × 12 in. cross-section, 60 ft. long. The ducts may be considered smooth (*Fig. 4.21*).

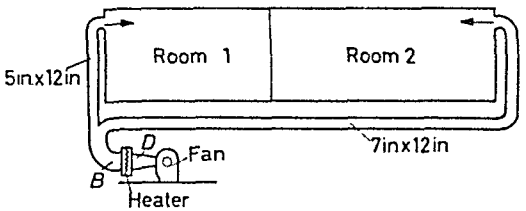

Figure 4.21

Neglecting the losses in the diffuser D and branch main B, calculate the approximate discharge of air into each room, assuming that adequate provision is made for the air supplied to escape into the atmosphere.

The loss coefficient of the bends is $K_B = 0{\cdot}9$ and that of the heater $K_H = 2{\cdot}5$. Kinematic viscosity of air, $\nu = 1{\cdot}67 \times 10^{-4}$ ft.^{2}/sec. The amount of heat added to the air may be considered as negligible. Make use of the hydraulic diameter, $d = 4 \times m$, where

$$m = \frac{\text{cross-section}}{\text{perimeter}} = \frac{ab}{2(a + b)}$$

Discharge ft.^{3}/min.	800	1000	1200	1400
Static Pressure in. W.G.	2	1·6	0·97	0·44

5

FLOW IN OPEN CHANNELS

5.1 Introduction

THE term open channel applies to any conduit in which a liquid flowing has a free surface subjected only to atmospheric pressure. The conduit may be either open to the atmosphere, like natural streams, rivers, artificial canals, or closed like the sewerage tunnels. Conduits of the latter type can only be considered as open channels if they are not running full. Various cross-sections of open channels are shown in *Fig. 5.1.*

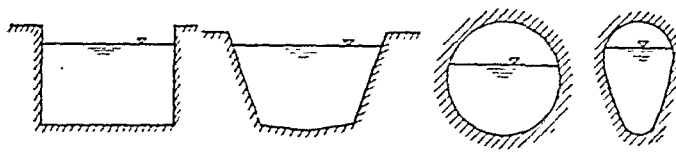

Figure 5.1—Open channel sections

Flow in open channels is generally produced under the influence of gravity. The flow may be of laminar or turbulent character, steady or unsteady, uniform or varied (non-uniform), tranquil or rapid. Except in isolated cases, laminar flow is rarely experienced† and unsteady flow is extremely complex, therefore the present discussion will be confined to steady turbulent flow under uniform or varied conditions.

5.2 Steady, Uniform Flow in Open Channels

Flow in a channel is considered uniform when the depth of the liquid along the flow is constant; in other words under uniform flow conditions the hydraulic slope‡ of the free liquid surface is parallel with the slope of the channel bed as shown in *Fig. 5.2.* Uniform flow may also be regarded as steady if the flow variables, such as velocity or pressure at any point, do not change with time.

† The critical Reynolds number based on the hydraulic radius for channel flow is around 300. A typical example of laminar flow is thin sheets of rain water coming down a flat roof.

‡ Note: $\tan \alpha_0 = i_0$ and $\tan \alpha = i$.

Consider a liquid flowing along a channel of uniform cross-section. Under steady uniform flow conditions, the gravity forces, acting in the direction of the flow are balanced by the viscous resistance forces acting in the opposite direction.

The gravity forces are obtained by considering the weight of a liquid body of length ΔL and cross-sectional area, A, concentrated as a single force at the centre of gravity as shown in *Fig. 5.3.* Since

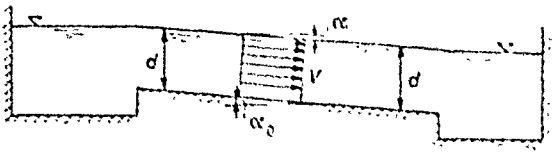

Figure 5.2—Steady uniform flow along a channel

the weight is $w.A\Delta L$, motion is produced by the component parallel to the flow $w.A\Delta L \sin \alpha$, where α is the angle of inclination of the free surface with the horizontal.

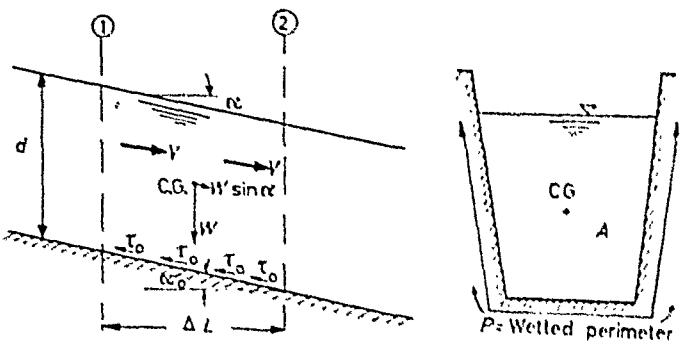

Figure 5.3—Forces on a liquid flow-element

The resistance forces are obtained by considering the mean boundary shear stresses (τ_{0m}) acting on the liquid area in contact with the 'wetted' channel walls. Since the wetted area is the product of the wetted perimeter P and length ΔL, the resistance forces equal to $P\Delta L\, \tau_{0m}$.

For equilibrium

$$P\Delta L\, \tau_{0m} = w \,.\, A \,.\, \Delta L \sin \alpha$$

Introducing

$$\tau_{0m} = \frac{f}{4} \cdot \frac{1}{2} \rho V^2 \quad (see\ Eq.\ 4.18) \qquad \text{and } m = \frac{A}{P}$$

and noting that for small angles $\sin \alpha \simeq \tan \alpha = i$, we obtain the head loss Δh_f due to friction

$$\Delta h_f = \Delta L \sin \alpha = \Delta L i = f \frac{\Delta L}{4m} \cdot \frac{V^2}{2g} \qquad \ldots . (5.1)$$

Solving Eq. 5.1 for V, we have

$$V = \sqrt{\frac{8g}{f}} \sqrt{(m \, . \, i)} \qquad \ldots . (5.2)$$

Equation 5.1 states that for a given friction factor f and hydraulic mean radius m, the flow velocity is proportional to the square root of the slope i.

Eq. 5.1, when written in the form

$$V = c\sqrt{(m \, . \, i)} \qquad \ldots . (5.3)$$

is frequently referred to as the Chezy formula, where the Chezy coefficient

$$C = \sqrt{\frac{8g}{f}} \qquad \ldots . (5.4)$$

5.3 Friction Factors for Flow in Open Channels

For the determination of the Chezy coefficient, extensive experiments have been conducted on open channel flow. The results of these investigations are represented by formulae bearing the names of their originators, amongst whom the best known are Bazin, Ganguillet and Kutter, and Manning. Although the formulae of Bazin and Ganguillet and Kutter are still commonly used in hydraulic design, in recent years the Manning formula has gained popularity because of its simplicity.†

According to Manning, the Chezy coefficient is given by

$$C = \frac{1{\cdot}49}{n} m^{1/6} \qquad \ldots . (5.5)$$

where n is the boundary roughness determined by Kutter. Values of n are presented below.

Values of the Kutter Surface Roughness, n

Smooth cement	0·01
Masonry or brickwork	0·013
Rubble masonry	0·017
Firm gravel	0·020
Rivers in good condition	0·025
Rivers in bad condition	0·035

† Also more recently correlation has been sought between friction in open channels with that in closed conduits. Up to date these investigations are not conclusive.

Substituting Eq. 5.5 into Eq. 5.3, the Manning formula is obtained

$$V = \frac{1{\cdot}49}{n} m^{2/3} \sqrt{i} \qquad \ldots.(5.6)$$

Hence the discharge

$$Q = AV = \frac{1{\cdot}49}{n} A m^{2/3} \sqrt{i} \qquad \ldots.(5.7)$$

It is apparent, on the basis of Eqs. 5.6 and 5.7 that for a given boundary roughness n and slope i the flow velocity varies with $m^{2/3}$ and discharge varies with $A \cdot m^{2/3}$.

Example

5.1. Determine the discharge in a rectangular concrete channel 20 ft. wide for uniform flow at a depth of 4 ft. The slope is 0·00025.

Solution.—The flow area is $4 \times 20 = 80$ ft.^{2} and the wetted perimeter $2 \times 4 + 20 = 28$ ft. Hence the hydraulic radius $m = \frac{A}{P} = \frac{80}{28} = 2{\cdot}86$ and $m^{2/3} = 2{\cdot}02$. Using $n = 0{\cdot}010$ and substituting into Eq. 5.7, the discharge

$$Q = \frac{1{\cdot}49}{0{\cdot}01} \times 80 \times 2{\cdot}02 \times \sqrt{0{\cdot}00025} = 382 \text{ ft.}^3\text{/sec.}$$

5.4 Best Hydraulic Cross-section

A channel offering the least resistance to flow under specified conditions yields maximum discharge.

Consider various rectangular channels (*Fig. 5.4*) with common

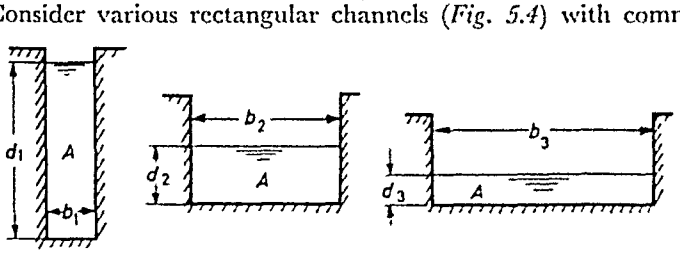

Figure 5.4

slope i, roughness n, and assume the flow area $A = b_1 d_1 = b_2 d_2 = b_3 d_3$ to be constant in each channel. Since discharge is then proportional to $m^{2/3}$ and

$$m = \frac{A}{P} = \frac{A}{b + 2d} = \frac{A}{\frac{A}{d} + 2d}, \qquad \ldots.(5.8)$$

maximum discharge will be experienced when the wetted perimeter, P, assumes minimum value.

Differentiating P with respect to d, and equating to zero yields

$$-Ad^2 + 2 = 0$$

whence $$A = 2d^2 = bd$$

and $$d = b/2 \qquad \ldots.(5.9)$$

Thus for a given flow area A, the best proportion for a rectangular channel exists when the depth of the flow is one half the width of the channel.

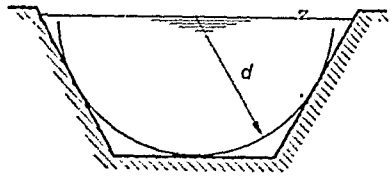

Figure 5.5

It may be shown that for trapezoidal cross-sections the best proportions exist if the sides of the channel are tangential to a semi-circle described on the water line, as illustrated in *Fig.* 5.5. Since the minimum wetted perimeter means a minimum in lining material, the best hydraulic cross-section also contributes to the economy of the construction.

Example

5.2. A rectangular channel is to carry 100 ft.^{3}/sec. Calculate the dimensions of the best hydraulic cross-section if the channel is lined with cement (smooth) and is laid on a slope of 0·0001. Assume for smooth cement lining $n = 0{\cdot}012$.

Solution.—Since for the best hydraulic cross-section

$$A = bd = 2d^2$$

and $$m = \frac{A}{P} = \frac{d}{2}$$

we have $$100 = \frac{1{\cdot}49}{0{\cdot}012} \times 2d^2 \times \left(\frac{d}{2}\right)^{2/3} \times (0{\cdot}0001)^{1/2}$$

whence $$d^{8/3} = 52{\cdot}6$$

and $$d = 4{\cdot}42 \text{ ft.} \qquad b = 8{\cdot}84 \text{ ft.}$$

5.5 Specific Energy

Certain problems in open channel flow are solved with the aid of specific energy methods.†

† The concept of specific energy was introduced by Bakhmeteff in 1911.

Consider uniform flow in a channel between specified cross-sections 1 and 2 as shown in *Fig. 5.6.* When applying the Bernoulli equation for a streamline (marked x–x) we have

$$\frac{p_1}{w} + \frac{V_1^2}{2g} + z_1 = \frac{p_2}{w} + \frac{V_2^2}{2g} + z_2 + \Delta z$$

Since $$V_1 = V_2$$

and $$p_1/w = p_2/w$$

the flow over the stretch 1–2 is maintained at the expense of the potential head drop $\Delta z = z_1 - z_2$. Obviously in going downstream the 'Bernoulli energy' decreases.

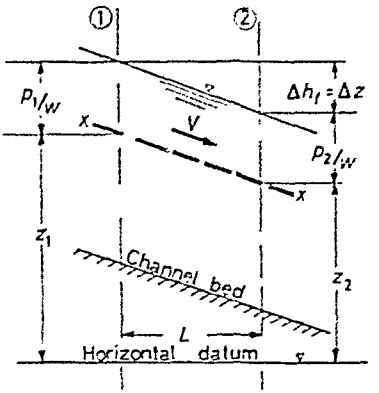

Figure 5.6

Whilst the Bernoulli energy is referred to an arbitrary horizontal datum line, the specific energy is referred to the channel bed as a datum, thus eliminating the slope of the channel bed from the picture. For any streamline, at a depth y over the channel bed, the sum of $y + p/w$ remains unchanged and equal to the depth d of the flow, as shown in *Fig. 5.7.*

The expression

$$E_s = d + \frac{V^2}{2g}$$

is called the specific energy. On the assumption that the velocity is constant across the flow, the specific energy remains unchanged for any streamline. In case of uniform flow, it also remains unchanged along the flow.

It is convenient to express the flow velocity in terms of discharge Q and flow area A, and the specific energy becomes

$$E_s = d + \frac{Q^2}{2gA^2}$$

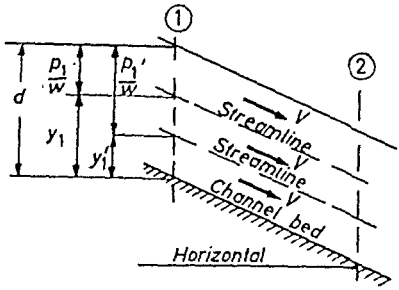

Figure 5.7

In case of rectangular channels the flow velocity is generally expressed in terms of q and depth d, where q is the discharge across a strip 1 ft. wide of depth d; the specific energy then becomes

$$E_s = d + \frac{q^2}{2gd^2} \qquad \ldots.(5.11)$$

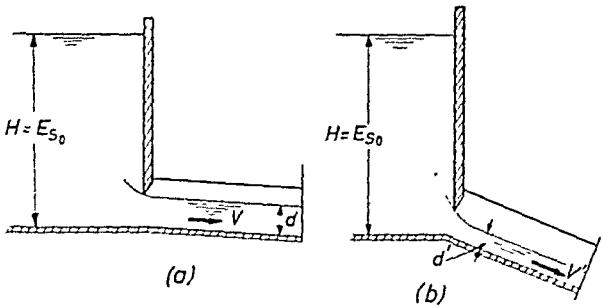

Figure 5.8

5.6 Specific Energy Diagrams

The physical aspects of the specific energy may be conveniently studied by treating Eq. 5.11 for two characteristic cases:

Rate of Discharge Constant, E_s and d Variable

Consider a constant head reservoir provided with a sluice gate as shown in *Fig. 5.8.* On opening the gate, water is allowed to flow

into a channel of adjustable slope. With the gate fixed in one position, the rate of discharge remains constant and its magnitude determined by the elevation of the free surface level, in the reservoir. It is apparent that the flow will assume greater depth d and lower velocity V if the slope of the channel is mild (*Fig. 5.8a*) and conversely, smaller depth d' and higher velocity V', if the slope is steep (*Fig. 5.8b*).

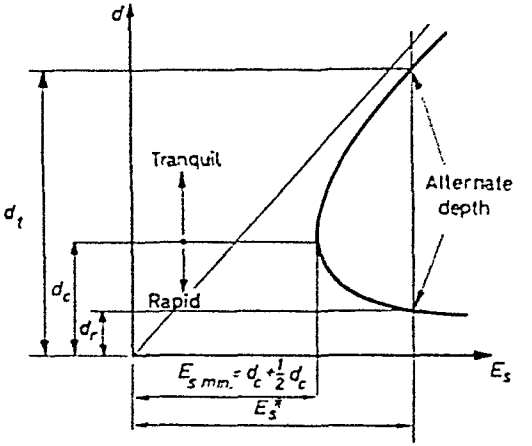

Figure 5.9—Specific energy diagram. (Showing alternate depth)

For a fixed discharge q the relationship between E and d may be shown graphically by plotting E_s against d as shown in *Fig. 5.9*. The 'potential head' d is represented by a straight line drawn through the origin.† The line of specific energy E_s is obtained by adding to the potential head the kinetic energy term $q^2/2gd^2$. When studying *Fig. 5.9* it appears that the specific energy attains a minimum value at a certain depth. This depth is called the critical depth, d_c. For a given specific energy marked E_s^*, (greater than the minimum), two alternate depths (marked d_r and d_t) exist, at which flow may take place, one greater and one less than the critical depth If the depth of flow is greater than the critical value, it is said to be 'tranquil' and the slopes which produce such flows are classed as 'mild' slopes. Conversely, if the depth is less than the critical value, the flow is said to be rapid and the slopes which produce such flows are classified as 'steep' slopes.

The critical depth for constant q may be established by differentiating Eq. 5.11 with respect to d and equating the result to zero.

† Provided the scales of E_s and d are equal the inclination will be 45°.

Then

$$\frac{dE}{dd} = \frac{d}{dd}\left[d + \frac{q^2}{2gd^2}\right] = 1 + \frac{q^2}{2g}\left(-\frac{2}{d_c^3}\right) = 0$$

where d assumed the value of d_c after the differentiation. Solving this for d_c gives the critical depth

$$d_c = \sqrt[3]{\frac{q^2}{g}} \qquad \ldots.(5.12)$$

Substituting this expression into Eq. 4.11, the minimum specific energy is given by

$$E_{s\,min} = \frac{3}{2}d_c = \frac{3}{2}\sqrt[3]{\frac{q^2}{g}} \qquad \ldots.(5.13)$$

Specific Energy Constant, q and d Variable

Consider in *Fig. 5.8* the channel fixed in a horizontal position and the discharge varied by manipulating the sluice gate. On the assumption that no energy is lost as flow passes the gate the fluid flowing in the channel will possess a constant specific energy E_s equal to the surface elevation H of the reservoir level above the channel bed.

The relation between depth d and discharge q for constant specific energy may be obtained by solving Eq. 5.11 for q,

$$q = \sqrt{(2gd^2E_s - 2gd^3)} \qquad \ldots.(5.14)$$

The critical depth for constant E_{s0} may be established by differentiating Eq. 5.14 with respect to d and equating the result to zero. Then

$$\frac{d}{dd}(q^2) = 4gE_{s0}d_c' - 6gd_c'^2 = 0$$

where d assumed the value of d_c' after the differentiation. Hence the critical depth d_c' for constant E_{S0} is given by

$$d_c' = 2/3E_{s0} = 2/3H \qquad \ldots.(5.15)$$

Plotting discharge against depth (*Fig. 5.10*) for a constant E_s shows that the maximum discharge is attained at the critical depth d_c'. Thus, by manipulating the gate the flow quantity may be varied between zero (gate closed $d' = 0$) to a maximum ($d = d_c' = 2/3H$) and back to zero (gate fully opened $d' = H$). Since the point of maximum flow for a given specific energy is the same as that of

minimum energy for a given rate of flow, that is $d_c' = d_c$, the regions of rapid and tranquil flow may also be indicated on the q curve.

The critical velocity V_c which occurs at critical depth may be obtained from Eq. 4.12 by substituting $V_c \cdot d_c$ for q. The result

$$V_c = \sqrt{(d_c \cdot g)} \qquad \ldots . (5.16)$$

may also be written as $V_c^2/d_c g = 1$, or $q^2/d_c^3 g = 1$

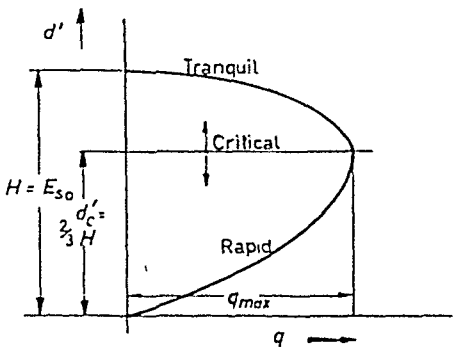

Figure 5.10—Specific energy diagram. (Showing alternate flow)

Equation 5.16 is identical with the expression which gives the velocity of propagation of a small wave† on the surface of a liquid of small depth. Under critical flow conditions the propagation of such a wave takes place exactly at the velocity of the flow and cannot progress upstream because of the equality of the velocities. In tranquil flow these surface waves can travel both upstream and downstream; in rapid flow they can only travel downstream.

The expression $V^2/gd = q^2/d^3 g$ may further be used as a criterion to establish whether the flow is tranquil or rapid. If $V^2/gd < 1$ the flow is tranquil and if $V^2/gd > 1$ the flow is rapid.

Example

5.3. A cement-lined rectangular channel 20 ft. wide carries water at a rate of 400 ft.^{3}/sec. Assuming $n = 0{\cdot}012$, calculate: (*a*) the critical depth and velocity, (*b*) the slope required to maintain a depth of 4 ft., and (*c*) the slope to maintain a depth of 1 ft.

Solution.—(*a*) Since $q = \dfrac{400}{20} = 20$, the critical depth $d_c = \sqrt[3]{\dfrac{q^2}{g}} = \sqrt[3]{\dfrac{20^2}{32{\cdot}2}} = 2{\cdot}31$ ft. The critical velocity $V_c = \sqrt{d_c g} = \sqrt{(2{\cdot}31 \times 32{\cdot}2)} = 8{\cdot}65$ ft./sec.

† A 'small' wave has a negligible depth in comparison with the depth of the liquid.

(*b*) In the case of a 4-ft. depth $q^2/gd^3 = 0{\cdot}194 < 1$, and the flow is tranquil. Since $m = \dfrac{4 \times 20}{28} = 2{\cdot}86$ and $m^{2/3} = 2{\cdot}02$ the slope required

$$i = \left(\frac{400 \times 0{\cdot}012}{1{\cdot}49 \times 80 \times 2{\cdot}02}\right)^2 = 0{\cdot}02^2 = 0{\cdot}0004$$

(*c*) In the case of a 1-ft. depth, $q^2/gd^3 = 12{\cdot}4 > 1$ and the flow is rapid. Since $m = \dfrac{1 \times 20}{22} = 0{\cdot}91$ and $m^{2/3} = 0{\cdot}932$, the slope required

$$i = \left(\frac{400 \times 0{\cdot}012}{1{\cdot}49 \times 20 \times 0{\cdot}932}\right)^2 = 0{\cdot}172^2 = 0{\cdot}030$$

5.7 Application of the Specific Energy Diagrams. Occurrence of Critical Depth

Consider a constant rate of flow in a channel passing over a rise on the channel floor as shown in *Fig. 5.11*. Upstream from the rise the flow is considered tranquil and the specific energy $E_{s0} = d_0 + V_0^2/2g$ where d_0 is the depth of flow and $V_0^2/2g$ is the kinetic energy at cross section 00. In passing over the rise of height Δ, the specific energy decreases to E_{s1} whilst the velocity increases to V_1.

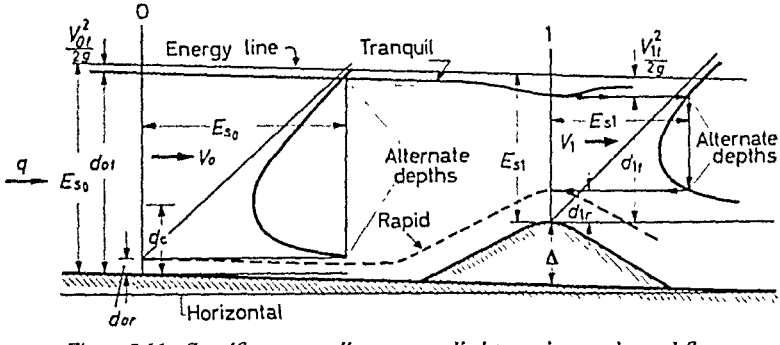

Figure 5.11—Specific energy diagram applied to a rise on channel floor

The depth of flow d_1 over the rise may be obtained from the specific energy equation by substituting $E - \Delta$ for E_1 and solving for d_1. Inspection of *Fig. 5.11* shows the specific energy diagram constructed for the specified d_0 and q. The same diagram is also shown on the top of the rise.†

If the height Δ of the rise above the channel bed is increased until the depth of the flow attains critical value, d_c, (shown in *Fig. 5.12*), the minimum specific energy, at which the fixed rate of flow is

† The alternate rapid flow appears by a dotted line.

physically possible, is reached. Any further increase in Δ would be simultaneously accompanied by an increase in d_0 upstream.

When the alternate rapid flow is considered, shown by a dotted line in *Fig. 5.11*, the presence of the rise causes an increase in depth, from d_{0r} to d_{1r} and a decrease in the velocity from V_{0r} to V_{1r}. When the rise reaches the critical height (Δ_c) (*Fig. 5.12*), the depth

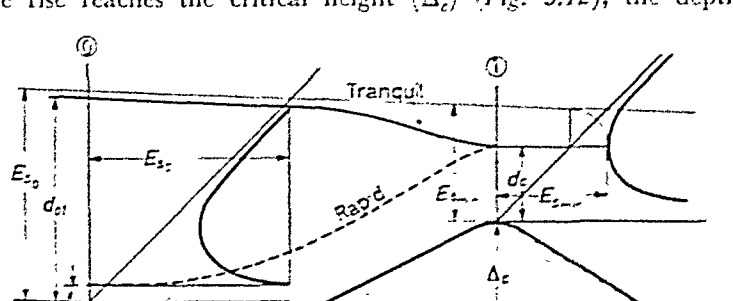

Figure 5.12—Specific energy diagram applied to a rise on channel floor

increases to d_c and the velocity decreases to V_c. It is of interest to note that once a rapid stream has attained critical flow in a channel of *mild slope*, depth continues to increase and the velocity to decrease until alternate tranquil flow conditions are reached downstream.

The critical height of the rise may be obtained by equating E_{s0} with $E_{s\,min} + \Delta_c$

Since $$E_{s\,min} = d_c + \frac{q}{2gd_c^2} = \frac{3}{2}d_c$$

the critical height,

$$\Delta_c = E_{s0} - \frac{3}{2}d_c \qquad \ldots.(5.17)$$

Example

5.4. With the data given in Example 5.4, calculate the critical height of a rise (*a*) for tranquil flow ($d_{0t} = 4$ ft.) (*b*) for rapid flow $d_{0r} = 2$ ft. (Note: In this problem d_{0t} and d_{0r} are not alternate depths.)

Solution.—(*a*) Tranquil flow: specific energy upstream from the rise,

$$E_{s0} = 4 + \frac{20^2}{64{\cdot}4 \times 16} = 4{\cdot}39 \text{ ft.}$$

Since critical depth is 2·31 ft. the critical velocity

$$V_c = \frac{20}{2{\cdot}31} = 8{\cdot}65 \text{ ft./sec.}$$

and the critical velocity head

$$V_c^2/2g = 1{\cdot}17 \text{ ft.}$$

Substituting these values into Eq. 5.17 yields

$$\Delta_c = 4{\cdot}39 - 3/2 \times 2{\cdot}31 = 0{\cdot}9 \text{ ft.}$$

The velocity increased from $20/4 = 5$ ft./sec. to critical, $V_c = 8{\cdot}65$ ft./sec.

(b) Rapid flow: specific energy upstream from the rise

$$E_0 = 1 + \frac{20^2}{64{\cdot}4 \times 1} = 7{\cdot}2 \text{ ft.}$$

hence $$\Delta_c = 7{\cdot}2 - 3/2 \times 2{\cdot}31 = 3{\cdot}71 \text{ ft.}$$

In this case the velocity decreased from $q/d = 20/1 = 20$ ft./sec. to the critical 8·65 ft./sec.

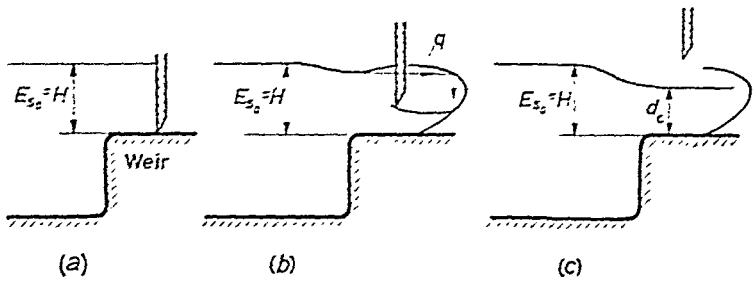

Figure 5.13—Specific energy diagram applied to a flow controlled by a sluice gate

Flow at critical depth occurs over the crest of a broad-crested weir. We may assume again a sluice gate regulating the flow. With the gate closed the flow is zero and the total specific energy may be taken as equal to the height of the free surface over the weir as shown in *Fig. 5.13a.* On opening the gate alternate depths will be established on the upstream and downstream sides as shown in *Fig. 5.13b.* Finally the maximum rate of flow will occur when $d = d_c$ and raising the gate beyond the critical depth will have no further effect upon the discharge as shown in *Fig. 5.13c.* Since $d = d_c$ the discharge over a broad-crested weir of width b is given approximately by

$$Q \cong b d_c V_c = b \frac{2}{3} H \sqrt{\left(g \frac{2}{3} H\right)} = \frac{2}{3\sqrt{3}} b \sqrt{2g} H^{3.2}$$

A further example of critical depth may be found at the entrance to a steep channel. The flow from a reservoir into a channel is controlled by the critical depth at the entrance as shown in *Fig. 5.14,*

provided that the slope of the bed is such that the channel is capable of taking away all incoming flow at a depth *less* than the critical.

A channel with a sudden change in the slope is shown in *Fig. 5.15.* Upstream from the change of slope, the normal (uniform) depth is greater than d_c whilst downstream the depth is less than d_c owing to the steeper grade. At some distance x upstream from the change in the slope the depth is equal to d_c.

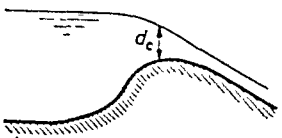

Figure 5.14

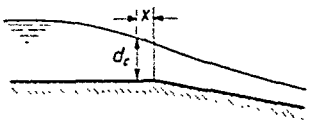

Figure 5.15

5.8 Varied Flow

When the depth along the flow continually varies, the type of fluid motion is termed varied or non-uniform flow. Whilst under uniform flow conditions constant velocity is attained when frictional losses balance the gravity force, under varied flow conditions this balance is upset by either a change of channel form or bed slope, resulting in

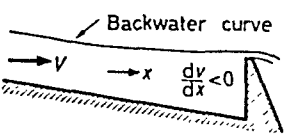

Figure 5.16

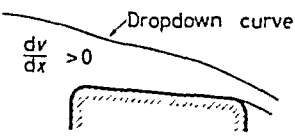

Figure 5.17

a positive or negative velocity gradient. If depth increases downstream, the velocity gradient is negative (retarded flow), producing a 'backwater curve' as shown in *Fig. 5.16.* If depth decreases downstream, the velocity gradient is positive (accelerated flow) and a dropdown curve is produced as shown in *Fig. 5.17.*

5.9 Calculation of Water Surface Curve

Consider a short channel-element of length ΔL over which the surface may be assumed straight, as shown in *Fig. 5.18.* Equating the energies at section 1 and 2, we have

$$\frac{V_1^2}{2g} + d_1 + z_1 = \Delta h_f + \frac{V_2^2}{2g} + d_2 \qquad \ldots.(5.18)$$

The slopes of the energy line and channel bed are i and i_0 respectively. Since the energy loss caused by frictional effects

$$\Delta h_f = i\Delta L$$

and

$$z_1 = i_0 \Delta L,$$

Eq. 5.18 may be written as

$$\frac{V_1^2}{2g} + d_1 + i_0 \Delta L = \frac{V_2^2}{2g} + d_2 + i\Delta L.$$

Solving for ΔL gives

$$\Delta L = \frac{\left[d_1 + \frac{V_1^2}{2g}\right] - \left[d_2 + \frac{V_2^2}{2g}\right]}{i - i_0} \qquad \ldots\ldots(5.19)$$

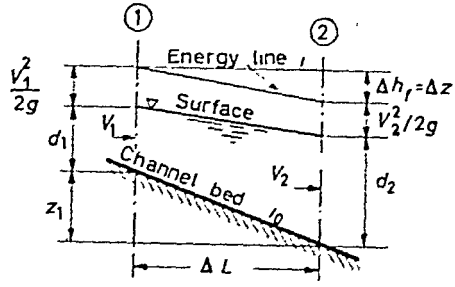

Figure 5.18

If ΔL is short enough, the energy gradient may be computed in the same manner as for uniform flow. Expressing i from Eq. 5.6 we have

$$i = \frac{(nV)^2}{2{\cdot}2m^{4/3}} \qquad \ldots\ldots(5.20)$$

where both the velocity V and the hydraulic radius m are the arithmetic mean of the values entering and leaving the section considered; that is

$$V = \frac{V_1 + V_2}{2} \qquad \text{and} \qquad m = \frac{m_1 + m_2}{2}$$

When varied flow profiles are calculated, the usual procedure is to start at a point along the flow where the depth and velocity are known. Then assuming equal depth increments, the velocities are calculated from section to section from continuity and the mean hydraulic radii from the mean depths. Substituting these into Eq. 5.19 and 5.20, the length of the sections between the equal depth increments are obtained.

Example

5.5. An overflow dam is installed in a rectangular channel carrying water at a rate of 250 ft.^{3}/sec. The bed is 10 ft. wide and its slope is 1 : 1000. Just upstream from the weir, the depth of flow is 7 ft. The channel is lined with an unfinished concrete surface, ($n = 0{\cdot}015$).

Calculate the approximate length of the backwater curve.

Solution.—Find the depth where the flow is uniform. Substituting the above values into Eq. 5.7

$$250 = 10d \times \frac{1{\cdot}49}{0{\cdot}015} \times \left(\frac{10d}{10 + 2d}\right)^{2/3} \times (0{\cdot}001)^{1/2}$$

and solving for d (by trial) gives $d = 4{\cdot}5$ ft. Assume six equal depth increments each; $\delta d = \dfrac{7 - 4{\cdot}5}{6} = 0{\cdot}5$ ft.

The result of the calculations is tabulated:

d	A	P	m	V	$V^2/2g$	E	Average m	Average V	$n.V$	$i \times 10^5$	$i_0 - i / 10^5$	ΔE	ΔL
7·0	70	24	2·91	3·57	0·20	7·20							
							2·87	3·71	0·0557	33	67	0·47	700
6·5	65	23	2·82	3·85	0·23	6·73							
							2·77	4·01	0·0603	43	57	0·46	807
6·0	60	22	2·72	4·17	0·27	6·27							
							2·67	4·36	0·0655	54	46	0·45	978
5·5	55	21	2·62	4·55	0·32	5·82							
							2·56	4·77	0·0717	67	33	0·43	1300
5·0	50	20	2·50	5·00	0·39	5·39							
							2·44	5·28	0·0793	86	14	0·41	2920
4·5	45	19	2·37	5·56	0·48	4·98							
							Total extent of backwater 6705 ft.						

5.10 Hydraulic Jump

It was shown in Section 5.7 that transition of rapid to tranquil flow may occur over a rise in the channel floor.

Transition from rapid to tranquil flow may also be experienced without having any device on the channel floor. The phenomenon, accompanying such a transition, is called the hydraulic jump. In a hydraulic jump, transition takes place over a relatively short distance, over which the height of the liquid increases rapidly, and considerable energy losses are experienced because of the eddying turbulence accompanying the abrupt transition. The critical depth occurs within the jump.

Hydraulic jump may be produced in a channel of mild slope by releasing water from under a sluice gate at a high velocity as shown in *Fig. 5.19.* The relation between the depths and velocities

upstream and downstream from the jump can be established by applying the continuity and momentum equations.

Consider a profile taken through a hydraulic jump in a horizontal (rectangular) channel as shown in *Fig. 5.20.* Denoting the velocities

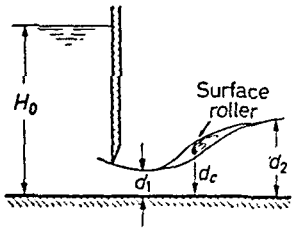

Figure 5.19

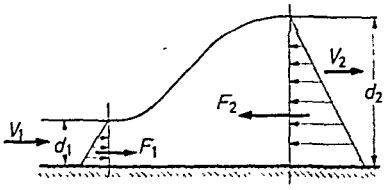

Figure 5.20

Hydraulic jump

and depths as V_1, d_1 and V_2, d_2, in front of and downstream from the jump respectively, we have:

the continuity equation

$$q = V_1 d_1 = V_2 d_2 \qquad \ldots.(5.21)$$

and the momentum equation

$$F_2 - F_1 = \frac{1}{2} d_2 w(d_2) - \frac{1}{2} d_1 w(d_1) = \frac{qw}{g} (V_1 - V_2) \ldots.(5.22)$$

where the term $(1/2\ dw)$ is the average hydrostatic pressure acting on the flow cross-section d.

Substituting for $V_1 = \frac{q}{d_1}$ and for $V_2 = \frac{q}{d_2}$ into Eq. 5.22 we obtain

$$\frac{d_2^2 - d_1^2}{2} = \frac{q^2}{g} \left(\frac{1}{d_1} - \frac{1}{d_2} \right) = \frac{q^2}{g} \frac{d_2 - d_1}{d_1 d_2}$$

Dividing by $d_2 - d_1$, multiplying by 2, and rearranging terms yields

$$d_2^2 + d_1 d_2 - \frac{2q^2}{g d_1} = 0 \qquad \ldots.(5.24)$$

Solution of Eq. 5.24 gives

$$d_2 = -\frac{d_1}{2} + \sqrt{\left(\frac{2q^2}{g d_1} + \frac{d_1^2}{4} \right)} \qquad \ldots.(5.25)$$

With this value of d_2 the downstream velocity V_2 can be found and

and the energy ΔE dissipated in the jump may be calculated. From the energy equation

$$d_1 + \frac{V_1^2}{2g} = d_2 + \frac{V_2^2}{2g} + \Delta E$$

whence

$$\Delta E = -(d_2 - d_1) + \frac{V_1^2 - V_2^2}{2g} \qquad \ldots.(5.26)$$

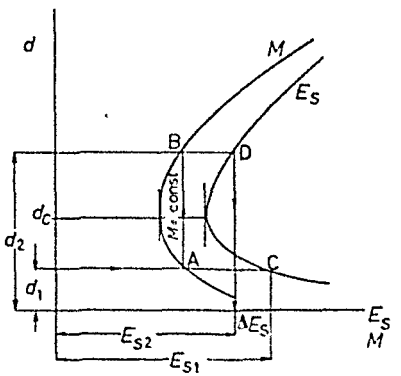

Figure 5.21—Specific energy diagram showing energy loss in jump

In Eq. 5.25, d_2 is always the larger depth following the jump. Because of the energy loss, d_2 and d_1 are not alternate depths†; for this reason before and after the jump are referred to as conjugate depths.

The length of the hydraulic jump is estimated to be approximately between 4½–7 times its height, d_2–d_1.

The energy loss ΔE may also be demonstrated graphically. Since the momentum upstream equals the momentum downstream from the jump it follows from Eq. 5.22 that

$$\frac{d_1^2}{2} + \frac{q^2}{gd_1} = \frac{d_2^2}{2} + \frac{q^2}{gd_2}$$

Generally for a given rate of flow q, the expression $M = \frac{d^2}{2} + \frac{q^2}{gd}$ depends on d only, thus M may be plotted against d as shown in *Fig. 5.21*. The M curve is similar in shape to the specific energy curve E_s which is plotted in *Fig. 5.21*. It is of interest to note that minimum M is experienced at the critical depth.

† Alternate also means reversible.

To find the energy loss, the procedure is as follows: by drawing a vertical (M = constant) line through the intersection of the known d_1 with the lower branch of the M curve (point a), the conjugate depth d_2 is found on the upper branch of the M curve (point b). Then drawing horizontal lines through these points the specific energies E_{s1} and E_{s2}, corresponding to depth d_1 and d_2, are obtained from the intersection of the horizontal lines with the E_s curve (points c and d). The energy loss ΔE_s appears as $E_{s1}-E_{s2}$.

Although the calculation of the change of depth and energy loss may be obtained with ease, the exact location of the jump is still an unsolved engineering problem.

The hydraulic jump, being a powerful energy dissipator, is frequently used for absorbing kinetic energy and thereby reducing the velocity where high speeds would otherwise scour the channel lining.

Example

5.6. In a rectangular channel the discharge is 40 ft.^{3}/sec. per ft. width. If a hydraulic jump occurs at a depth of 3 ft., calculate the height of the jump and the energy dissipated per foot width.

Solution—From Eq. 5.25

$$d_2 = -\frac{3}{2} + \sqrt{\left(\frac{2 \times 40^2}{32{\cdot}2 \times 3} + \frac{3^2}{4}\right)} = 4{\cdot}44 \text{ ft.}$$

hence the height of the wave $= d_2 - d_1 = 4{\cdot}44 - 3 = 1{\cdot}44$ ft.
Since $V_1 = q/d_1 = 40/3 = 13{\cdot}3$ ft./sec. and $V_2 = 40/4{\cdot}44 = 9$ ft./sec., the dissipated energy per pound of water (Eq. 5.26)

$$\Delta E_s = -(4{\cdot}44 - 3) + \frac{177 - 81}{64{\cdot}4} = 0{\cdot}05 \text{ ft. lb./lb.}$$

For the discharge specified, the energy loss

$$(Qw)\Delta E_s = 40 \times 62{\cdot}4 \times 0{\cdot}05 = 125 \text{ ft. lb./sec.}$$

5.11 Velocity Distribution in Open Channels

Velocity distribution in open channels is more complex and less accessible for observations than in closed conduits. In isolated cases the channels may be straight over an appreciable distance, but generally they follow an irregular course. Measurements in straight open channels disclose a symmetrical velocity distribution as shown in *Fig. 5.22.* A characteristic feature of all open-channel flow is the fact that the maximum velocity is experienced at some distance from the free surface. In case of a symmetrical velocity distribution the maximum velocity occurs in the centre plane.

At a bend the velocity is greater and the surface slightly higher, at the outside, because of the centrifugal forces. Then, due to the velocities distribution, this is accompanied by a secondary flow, with an outward component of the velocity in the layers near the surface and an inward component in the layers near the channel floor.

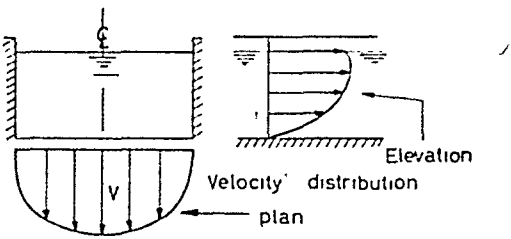

Figure 5.22—Velocity distribution in an open channel

The existence of a velocity distribution across the flow, as opposed to the simplified assumption of uniform velocity for specific energy calculations introduces errors. These errors are not considered sufficiently great to upset the theory and measurements in rectangular channels with mild slopes show that the simplified theory yields reasonably accurate numerical values for the phenomena discussed.

REFERENCES

1. Bakhmeteff, B., *Hydraulics of Open Channels*, McGraw-Hill, 1932.
2. Rouse, H., (Ed.), *Engineering Hydraulics*, J. Wiley and Sons, 1950.
3. Woodward, —., and Posey, —., *Hydraulics of Steady Flow in Open Channels*, J. Wiley and Sons, 1941.

Problems

5.1 Water flows from a storage reservoir into a channel which is 20 ft. wide. The channel is rectangular and the bottom is 4 ft. below the surface of the pond. Calculate the maximum discharge and the minimum slope required.

5.2 Calculate the specific energy in a trapezoidal channel, which has a bottom 10 ft. wide and the sides slope 1 : 1. The rate of flow is 180 ft.^{3}/sec. at a depth of 3 ft.

5.3 Establish the character of the flow (tranquil or rapid) in a rectangular channel 20 ft. wide, if the depth is 4 ft. The rate of flow is 550 ft.^{3}/sec.

5.4 Calculate the power dissipated in a hydraulic pump in a rectangular channel 25 ft. wide, if the flow is 500 ft.^{3}/sec. and the depth of stream is 1 ft.

5.5 For the same specific energy, calculate the alternative depth of flow in channel which is 10 ft. wide and the depth of stream is 10 ft. The rate of flow is 400 ft.^{3}/sec.

5.6 A cement-lined trapezoidal channel is to be constructed with the bottom and sides of the channel cross-section tangential to a circular arc. The centre of the arc is located on the centre-line of the channel cross-section at the water surface (*i.e.*, radius of arc is equal to the depth of water).

If the side slopes are 60° and the bed slope is 4×10^{-4}, determine the depth of flow and bed width for a steady uniform flow of 500 cusecs.

Adopt $n = 0{\cdot}015$ in the Manning's equation

$$V = \frac{1{\cdot}486}{n} m^{2/3} . i^{1/2},$$

where V = flow velocity,

m = mean hydraulic radius of the cross-section,

i = bed slope.

How does this cross-section compare with the 'Best Hydraulic Cross-section'?

5.7 A piece of drift-wood and a fallen leaf from a tree float side-by-side on the surface of a river. Which one travels faster?

6

FLUID METERING AND MANOMETRY

6.1 Introduction

In considering flow meters it is convenient to group them under two headings:

(*a*) Meters for measuring the flow of fluids through closed conduits

(*b*) Meters for measuring the flow through open conduits.

Under group (*a*) all fluids are included; under group (*b*), since they are open to the atmosphere, the fluids are limited to liquids.

The discussion in this text will be limited to those meters most frequently used in practice and which can be simply treated from the basic laws of fluid mechanics. For this reason positive displacement and special mechanical meters will not be considered.

6.2 The Orifice Meter

The basic principle underlying the operation of the orifice meter is an increase in the velocity of flow, accompanied by a decrease in the pressure of the fluid under consideration. Thus the quantity of fluid flowing can be computed from the measured pressure drop across the orifice.

Consider a plate provided with a sharp-edged circular orifice, fitted into a conduit between two flanges as shown in *Fig. 6.1.*

Upstream from the plate the stream velocity is V_1, and the pressure p_1; downstream from the plate a *vena contracta* is formed and the cross-sectional area decreases to a minimum value (A_{min}). At the *vena contracta* the velocity attains its maximum value and the pressure decreases to p_2. Further downstream the stream gradually expands and resumes normal flow.

Neglecting small pressure losses, the Bernoulli equation may be applied for cross-sections 1 and 2.

$$\frac{p_1}{w} + \frac{V_1^2}{2g} = \frac{p_2}{w} + \frac{V_{max}^2}{2g} \qquad \ldots\ldots(6.1)$$

From the continuity equation, the discharge

$$Q = A_1 V_1 = AV = A_{min} \cdot V_{max} \qquad \ldots\ldots(6.2)$$

where, owing to contraction,

$$A_{min} = C_c A_2 \qquad \ldots\ldots(6.3)$$

Substituting in Eq. 6.1

$$V_1 = \frac{A_{min}}{A_1} V_{max} = \frac{C_c A_2}{A_1} V_{max}$$

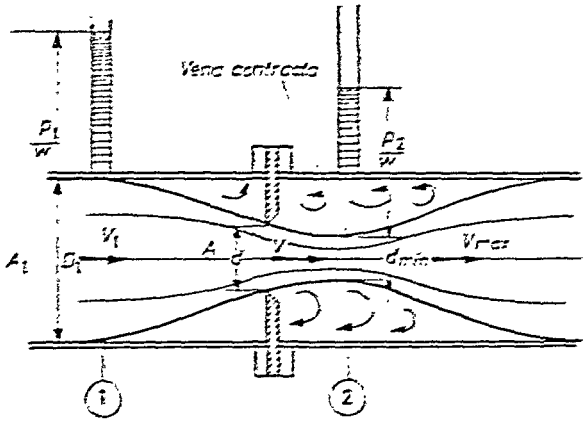

Figure 6.1—Pattern of flow across orifice meter

after rearranging terms we obtain

$$\frac{p_1 - p_2}{w} = \frac{V_{max}^2}{2g}\left[1 - \left(\frac{C_c A_2}{A_1}\right)^2\right] \qquad \ldots\ldots 6.4$$

and

$$V_{max} = \sqrt{\left(2g\frac{p_1 - p_2}{w}\left[\frac{1}{1 - \left(\frac{C_c A_2}{A_1}\right)^2}\right]\right)}$$

Hence the discharge,

$$Q = A_{min} \cdot V_{max} = C_c \frac{d_2^2 \pi}{4} \sqrt{\frac{1}{1 - \left(\frac{C_c A_2}{A_1}\right)^2}} \sqrt{2g\frac{p_1 - p_2}{w}}$$

It is convenient to write this expression in the following form

$$Q = C_d \cdot \frac{d^2\pi}{4} \cdot E \sqrt{2g\frac{p_1 - p_2}{w}} \qquad \ldots.(6.5)$$

where C_d is the discharge coefficient and E the approach factor.

$$E = \frac{1}{\sqrt{1 - \left(\frac{A}{A_1}\right)^2}} = \frac{1}{\sqrt{1 - \left(\frac{d}{D}\right)^4}} = \frac{1}{\sqrt{1 - m^2}} \qquad \ldots.(6.6)$$

In practice the discharge coefficient C_d is experimentally obtained; thus the error due to the omission of the coefficient of contraction C_c under the square root sign and the small loss experienced between sections 1 and 2 is automatically adjusted.

For a specified design the discharge coefficient is a function both of the Reynolds' number, based on the diameter of the orifice, and the ratio $m = \left(\frac{d}{D}\right)^2$. The British Standard Code† presents three graphs for the calculation of the discharge coefficient, which is considered to be a product of C, Z_1 and Z_2

$$C_d = C \cdot Z_1 \cdot Z_2 \qquad \ldots.(6.7)$$

where Z_1 and Z_2 are correction factors (multipliers); In the first graph C is plotted against m; in the second graph the multiplier Z_1 is given as a function of both m and the Reynolds' number; in the third graph, the multiplier Z_2 is given as a function of both m and the pipe diameter as shown in *Fig. 6.2* and *Fig. 6.3.* Since orifice meters may be provided with D and $D/2$, or corner tappings a set of curves for each design is given.

According to the Flow Code the calculations are carried out in two steps:

(1) The multipliers Z_1 and Z_2 are taken as unity and with the value of C obtained from the first graph, the approximate discharge is calculated. From the discharge the flow velocity through the orifice opening is found and the Reynolds' number obtained.

(2) With the value of the Reynolds' number the multiplier Z_1 is obtained from the second graph; and having found Z_2 from the third graph the approximate discharge is corrected.

† British Standard Code B.S. 1042: 1943, Flow Measurements. Extracts from B.S. 1042: 1943, are published by kind permission of the British Standards Institution, 2 Park Street, London, W.1., from whom official copies of the standard can be obtained, price 12s. 6d.

When the dimension of the orifice opening is determined, it is advisable to compare the pressure difference with the available

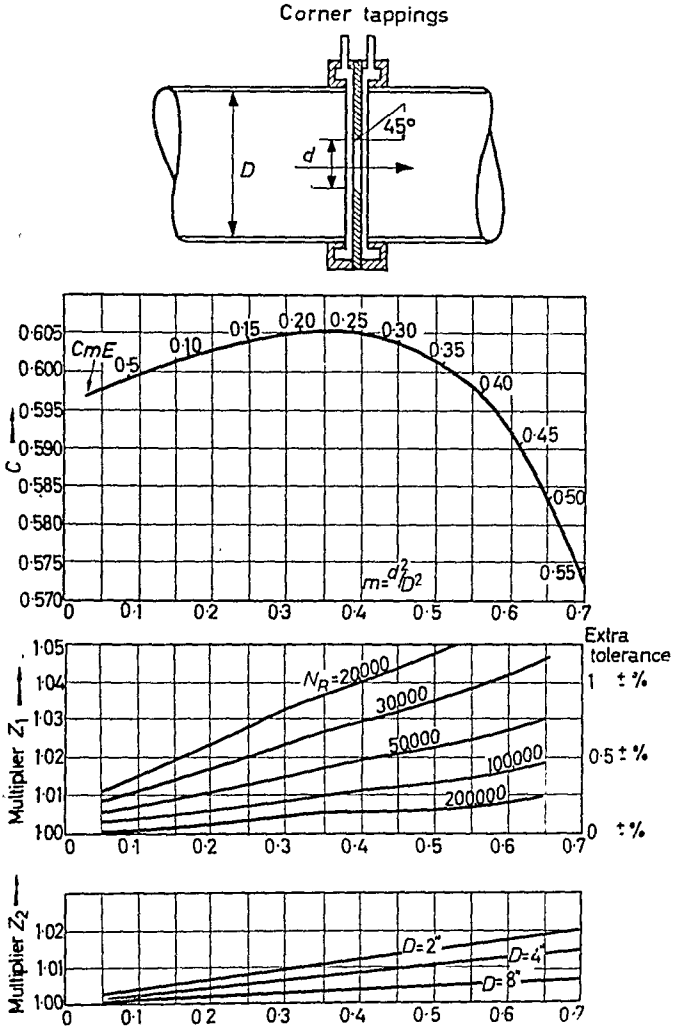

Figure 6.2—Discharge coefficients for orifice plate with corner tappings. (*From* B.S. 1042:1943)

pressure in the line. It should be remembered that all orifices are restrictions and cause a certain decrease in the flow quantity. Large orifices offer least resistance, but the accuracy of the meter suffers

slightly; small orifices choke the flow. It is convenient to calculate the orifice from a pressure drop specified in advance, and to facilitate

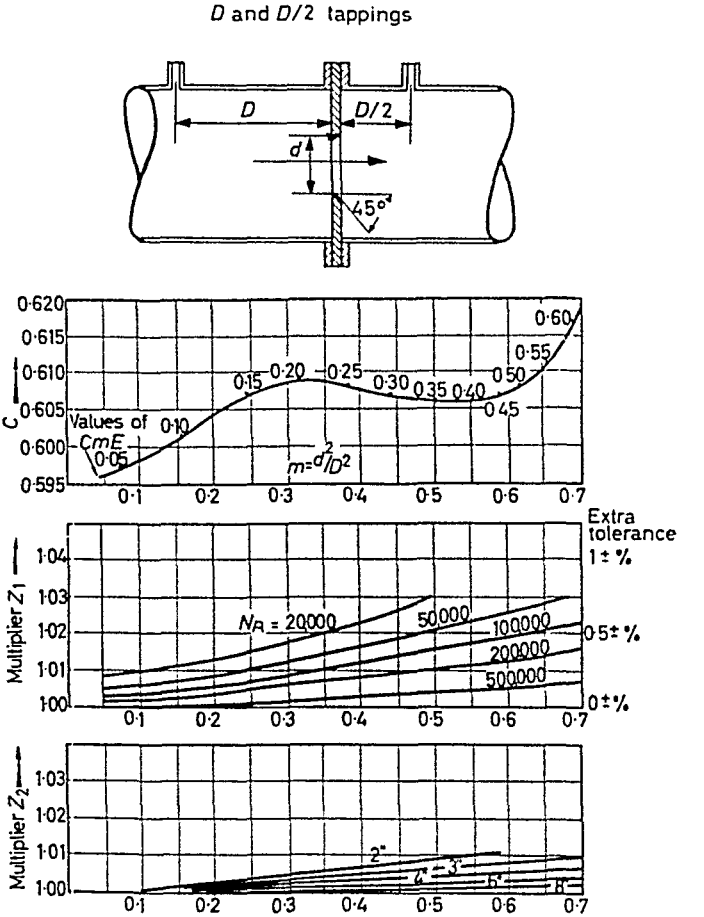

Figure 6.3—Discharge coefficients for orifice plates with D and $D/2$ tapping. (*From* B.S.1042:1943)

this calculation, different values of the product $C.m.E.$ are noted on the C curves. Since for $Z_1 = Z_2 = 1$

$$C.m.E. = \frac{4Q}{\pi D^2 \sqrt{\left(2g\frac{p_1 - p_2}{w}\right)}} \qquad \ldots . (6.8)$$

the corresponding point on the curve C determines m and thus the diameter of the opening from the expression $d = \sqrt{m} \cdot D$ may be found.

In order to damp out large scale turbulence, orifice meters built into pipelines require straight lengths of calming sections, at least 10 pipe-diameters long upstream and 5 pipe-diameters downstream from the plate, depending on the magnitude of the disturbance.

Pressure Losses in Orifice Meters

The pressure difference, $p_1 - p_2$, across the orifice is not entirely lost and a pressure recovery is experienced downstream. The results

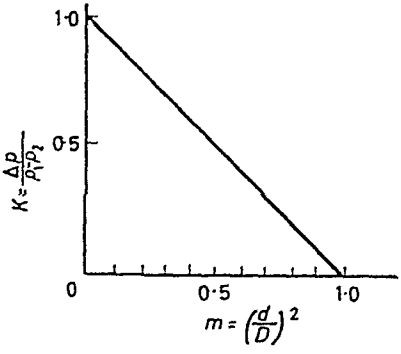

Figure 6.4

of experiments indicate that the pressure loss Δp is proportional to the pressure difference existing across the plate,

$$\Delta p = K(p_1 - p_2)$$

where the loss coefficient K is a function of m. The relationship between K and m was found to be approximately linear†, as shown in *Fig. 6.4.*

Thus the pressure loss

$$\Delta p = (1 - m)(p_1 - p_2) \qquad \ldots . (6.9)$$

The location of the correct position of the pressure tappings was also found experimentally. The so-called minimum upstream static pressure was found to occur approximately at a distance of one pipe-diameter upstream from the orifice; the position of the minimum downstream static pressure and the position of the *vena*

† Head loss and pressure recovery in orifice plates. A.S.M.E. Research Report on Fluid Meters, 1937. Mechanical World Monographs (39) 1948 p. 67.

contracta was found approximately half a pipe-diameter downstream. Just in front of, and right behind the orifice, both the upstream and the downstream static pressures were found to increase slightly, the increments (δp) being nearly equal. The pressure recovery was found to attain its maximum value at a

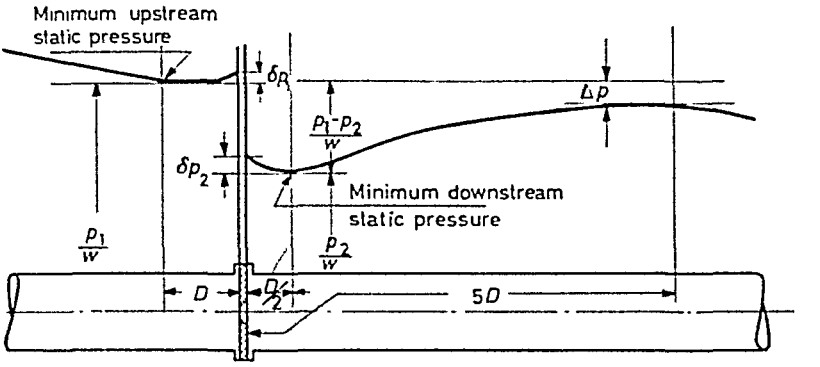

Figure 6.5—Pressure distribution upstream and downstream from an orifice plate

distance of five pipe-diameters downstream from the orifice. The distribution of the static pressure in the vicinity of an orifice is shown in *Fig. 6.5.*

Orifice Nozzles—Orifice nozzles are frequently used in practice in lieu of orifice plates. Since the discharge coefficient which depends

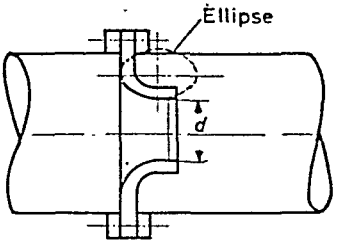

Figure 6.6—Orifice nozzle

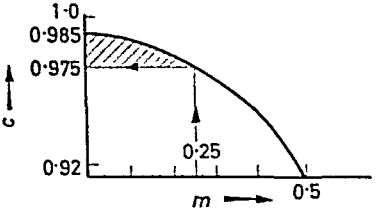

Figure 6.7

mainly on the area ratio $(d/D)^2$ and is practically independent of Reynolds' numbers exceeding 50,000, this type of flow meter presents an advantage over the orifice meter. Below this value the coefficient decreases† with the decreasing velocity.

The British Standard Flow Code recommends nozzles designed with a quarter ellipse profile as shown in *Fig. 6.6.* For (m) equal or

† Data from Regeln für die Durchflussmessung mit genormten Düsen und Blenden, V.D.I. 1935.

less than 0·25 the discharge coefficient may be taken as 0·98 as shown in *Fig. 6.7.* For highly accurate work, the reader is referred to the B.S. Code. The discharge may also be calculated from Eq. 6.5.

The Venturi Meter—The Venturi meter is a standard rate of flow meter, offering low flow losses. It consists of converging, parallel and

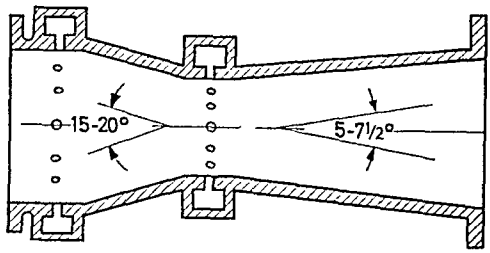

Figure 6.8—Venturi meter

diverging sections as shown in *Fig. 6.8.* In standard designs the parallel section is short, 1/4–1/2 pipe-diameter; the converging section has a taper angle of 15–20° whilst the diverging section is

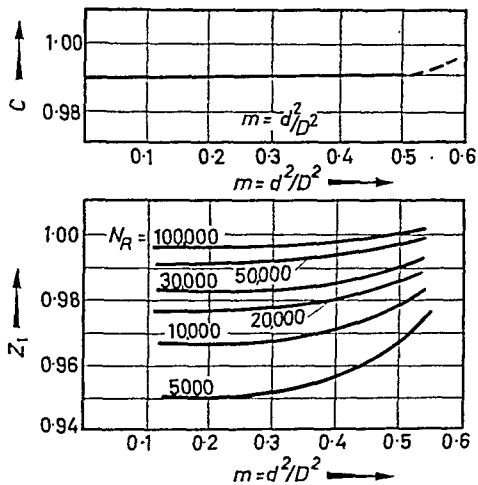

Figure 6.9—Discharge coefficients for Venturi meter.
(*From* B.S. 1042:1943)

longer, having a taper angle 5–7½°. The pressure tappings both upstream and at the throat, usually end in piezometer rings where the fluid is free from any disturbance. The discharge coefficient varies between 0·95 and 0·99 depending on the Reynolds' number,

as shown in *Fig. 6.9.* The discharge may again be calculated from Eq. 6.5.

6.3 Weirs and Notches

For measuring delivery in open channels weirs find wide application. A longitudinal cross-section and essential features of a sharp-crested weir installation is shown in *Fig. 6.10.*

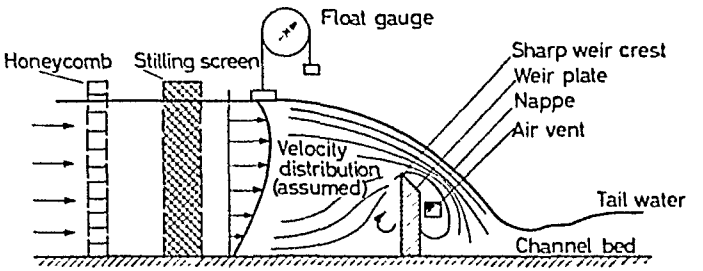

Figure 6.10—Typical weir installation

Upstream from the weir, the flow is calmed by stilling screens, and the height of the level H above the weir crest is measured by a float gauge. As the flow approaches the weir, the stream contracts, the liquid level gradually drops and the flow velocity increases. Downstream from the weir, a jet, called the nappe is formed, which

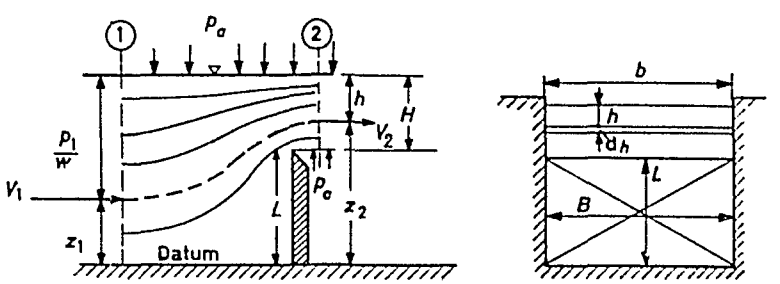

Figure 6.11

strikes the tail water creating large eddies. In sharp-crested weirs the atmospheric pressure is maintained under the nappe by ventilation which enables the nappe to spring free from the crest.

The calculation of the jet velocity is based on a simplified flow pattern as shown in *Fig. 6.11.* It is assumed that

(1) The approach velocity V is uniform and parallel
(2) The streamlines above the weir are horizontal

(3) The pressure under the nappe is atmospheric
(4) The losses are negligible.

With the notation shown the Bernoulli equation is applied to a single streamline drawn with a dotted line.

Substituting

$$\text{for} \quad \frac{p_1}{w} = \frac{p_a}{w} + (H + L) - z; \quad \text{for} \quad \frac{p_2}{w} = \frac{p_a}{w};$$

$$\text{for} \quad z_2 = H + L - h$$

we obtain

$$\frac{V_1^2}{2g} = \frac{V_2^2}{2g} - h$$

and

$$V_2 = \sqrt{\left[2g\left(h + \frac{V_1^2}{2g}\right)\right]}$$

The transformation of energy is clearly manifested. Stream filaments liberated from greater depths attain a higher velocity because of the greater pressure above them. Since V_2 depends on h, the discharge dQ across an elementary area dh high and b wide,

$$dQ = V_2 b dh = b\sqrt{2g} \cdot \sqrt{h + \frac{V_1^2}{2g}} \cdot dh$$

Integration of this equation between the limits O and H yields the theoretical discharge

$$Q_{TH} = b\sqrt{2g} \int_0^H \left[h + \frac{V_1^2}{2g}\right]^{1/2} dh =$$

$$= \frac{2}{3} b\sqrt{2g} \left\{\left[H + \frac{V_1^2}{2g}\right]^{3/2} - \left[\frac{V_1^2}{2g}\right]^{3/2}\right\} \quad \ldots.(6.10)$$

Introducing the discharge coefficient the actual discharge

$$Q_A = C_d Q_{TH} \quad \ldots.(6.11)$$

The value of C_d depends primarily on the parameters H and L/H, where L is the height of the crest above the channel bed. The influence of viscosity is normally negligible since the viscous resistances are small in comparison with inertia effects.

6.4 Weir Designs

Sharp Crested Weir

The characteristic feature of the sharp crested weirs is the smooth vertical weir plate provided with interchangeable sharp edges.

In the suppressed weir, the horizontal weir plate extends from wall to wall of an open channel as shown in *Fig. 6.12.* Since the contraction of the stream appears in the vertical dimension only, the weir can be used for large variations of head. The coefficient C

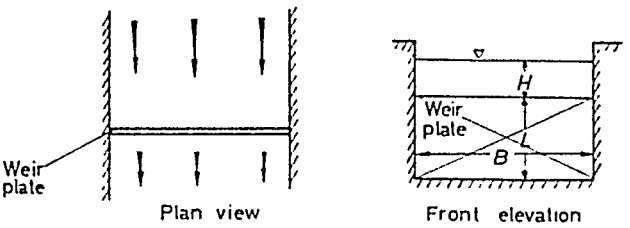

Figure 6.12—Suppressed weir

depends on both L/H and H as shown† in *Fig. 6.13.* It appears that (1) for a given head the weir coefficient increases with decreasing weir height; (2) for a weir of fixed height the coefficient increases with increasing head. The disadvantage of the use of suppressed

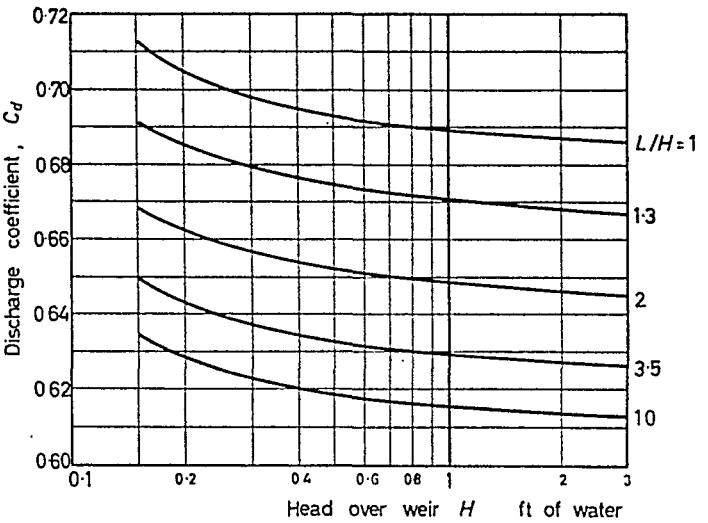

Figure 6.13—Discharge coefficients for suppressed weirs

weirs appears at low rates of flow when viscosity and surface tension effects cause the liquid of cling to the weir plate, thus preventing the formation of a nappe.

† Based on the Rehbock formula, see *Trans. Amer. Soc. civ. Engrs,* Vol. 93, p. 999.

Contracted Weirs

In the contracted weir the plate is provided with an opening of b width and the liquid allowed to flow through it. In the symmetrical design, two side contractions are formed as shown in *Fig. 6.14.* The side contractions were estimated by Francis to reduce the width on each side of the nappe by one-tenth of the prevailing head H. Since

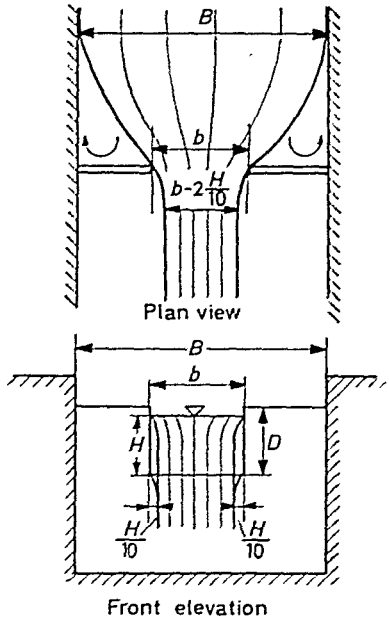

Figure 6.14—Contracted weir

the area open for flow is considerably less than that of the suppressed weir, the effect of the approach velocity may be ignored and the delivery calculated from the expression

$$Q = C\frac{2}{3}\sqrt{2g}\left(b - \frac{2}{10}H\right)H^{3/2} \qquad \ldots.(6.12)$$

where the value of the coefficient of discharge is approximately 0·622. The rectangular contracted weir is more suitable for measuring small delivery than a suppressed weir, except for very low deliveries when viscosity and surface tension prevent the formation of the nappe. High deliveries may cause the liquid to rise higher than the opening and the weir becomes flooded.

V-notch Weirs

In the V-notch weirs the opening is triangular as shown in *Fig. 6.15*. Since the crest of the weir coincides with the apex, V-notches prove advantageous for measuring small deliveries.

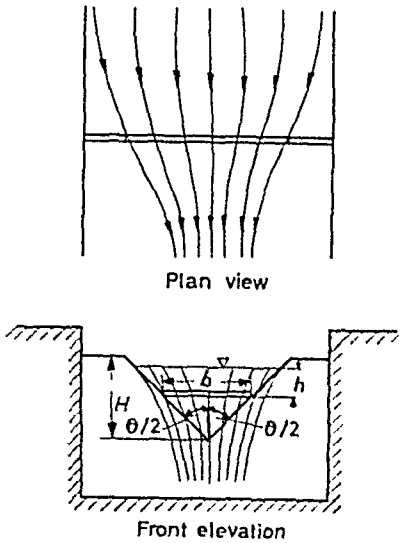

Figure 6.15—V-notch weir

Neglecting the approach velocity, an expression for the delivery can be derived on lines similar to those presented previously. With the notation shown,

$$b = 2(H - h) \,.\, \tan \theta/2$$

and

$$\mathrm{d}Q = C_d 2(H - h) \tan \frac{\theta}{2} \sqrt{(2gh)} \,.\, \mathrm{d}h$$

Integration between limits H and 0 yields

$$Q = C_d 2 \tan \frac{\theta}{2} \sqrt{2g} \int_0^H (H - h) h^{1/2} \,\mathrm{d}h =$$

$$= C_d 2 \tan \frac{\theta}{2} \sqrt{2g} \left[\frac{2}{3} H h^{3/2} - \frac{2}{5} h^{5/2} \right]_0^H =$$

$$= C_d \frac{8}{15} \tan \frac{\theta}{2} \sqrt{2g}\, H^{5/2} \qquad \ldots\ldots (6.13)$$

For 90° notches (2 tan 45° = 2) and the expression reduces to

$$Q = 4{\cdot}28 \,.\, C_d \,.\, H^{2{\cdot}5} \qquad \ldots\ldots (6.14)$$

Experiments conducted on notches show that the value of the discharge coefficient mainly depends† on the height H, and on the angle θ, as shown in *Fig. 6.16*. The dependence of the coefficient with the Reynolds' number, is shown in *Fig. 6.17*.

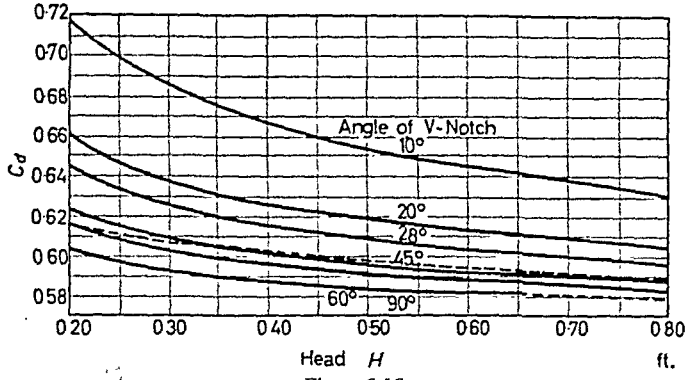

Figure 6.16
(By courtesy of the American Society of Civil Engineers)

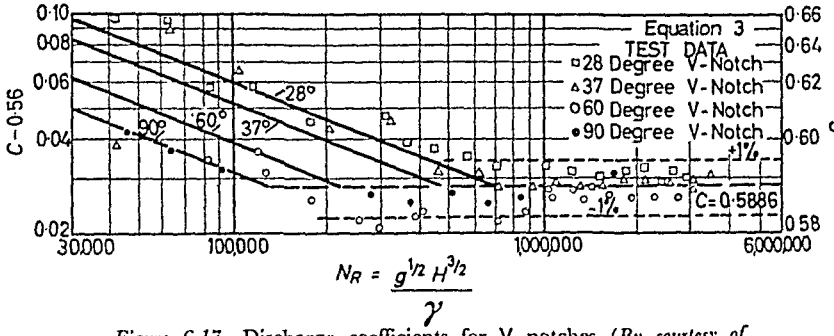

Figure 6.17—Discharge coefficients for V notches *(By courtesy of the American Society of Civil Engineers)*

6.5 Pitot Tube

The Pitot tube consists essentially of a tube with the open end facing the stream as shown in *Fig. 6.18*. The velocity of the stream along streamline 'x–y' is decreased to zero and transformed into pressure. The point of contact y is called the stagnation point and the pressure the stagnation pressure. Applying Bernoulli's equation for sections 1 and 2 we have

$$\frac{p_1}{w} + \frac{V_1^2}{2g} = \frac{p_0}{w} + 0 \qquad \ldots.(6.15)$$

† Trans. A.S.C.E. Vol. 107. 1943. A. T. Lenz "Viscosity and surface tension effects on V-notch weirs."

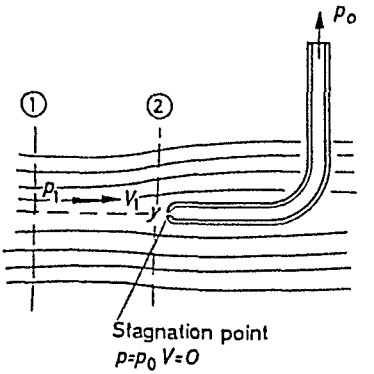

Figure 6.18—Pitot tube

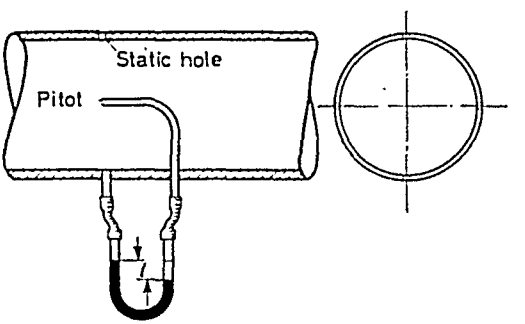

Figure 6.19—Pitot tube and static hole

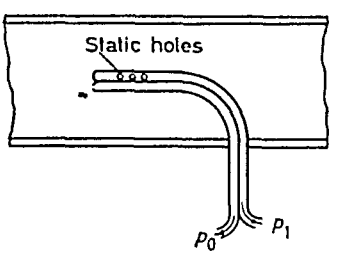

Figure 6.20—Pitot and static tube

where p_1 denotes the upstream pressure and V_1 the approach velocity. The stagnation head, $\frac{p_0}{w}$ is measured by the Pitot tube. The static head, may be measured either by pressure tappings located on the conduit walls (*Fig. 6.19*) or through small holes located at the side of a separate static tube placed parallel to the stream as shown in *Fig. 6.20.* From Eq. 6.15 the velocity head of the stream

$$\frac{V_1^2}{2g} = \frac{p_0 - p_1}{w}$$

and

$$V_1 = \sqrt{2g\frac{p_0 - p_1}{w}} \qquad \ldots.(6.16)$$

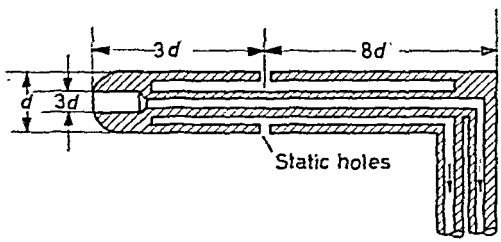

Figure 6.21—Combined Pitot–static tube (Prandtl type)

The Pitot tube may be combined with the static tube as shown in *Fig. 6.21.* In this design, first used by Prandtl, the static pressure tube jackets the Pitot tube, resulting in a compact meter. The static holes in the Prandtl type (and in the N.P.L. design) are so located that the slight pressure decrease caused in the stream by the tube is exactly compensated by the slight pressure increase due to stagnation on the stem. The relative dimensions of the Prandtl Pitot–static tube is given in *Fig. 6.21.* These meters are reasonably insensitive to yaw; for example the Prandtl tube may enclose an angle with the stream as large as 19° resulting only in 1 per cent error.

A conduit, open or enclosed, may be traversed with a Pitot–static tube and with the velocity distribution obtained, the discharge can be calculated. In conduits the cross-sectional area is usually divided into equal areas A and by plotting the velocity distribution curve obtained from the traverse method, the flow quantity can be computed. The method presented in the B.S.S. Flow Code for circular cross-sections is shown in *Fig. 6.22.*

Pitot–static meters made of fine tubes, such as hypodermic needles can be employed when the velocity distribution in the vicinity of solid boundaries is explored. To get as near the boundary

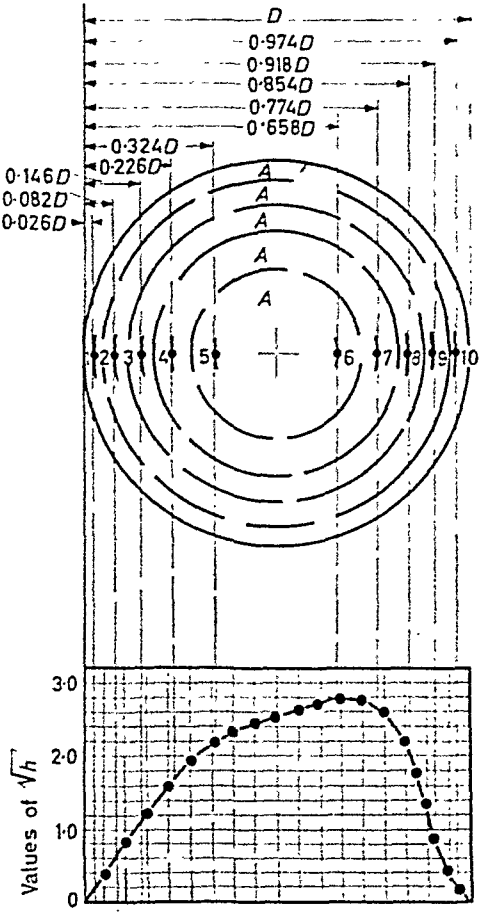

Figure 6.22—Arrangement of Pitot traverse measuring points in a circular duct

as possible, the Pitot tube may be flattened, and velocities as close as 0·02 in. from the wall, measured. An apparatus showing such a special arrangement is shown in *Fig. 6.23.*

6.6 Special Meters: Bend Meter, Rotameter, Anemometer

Bend Meters

Bend meters may be used for measuring the discharge in a pipe-line. The flow bend utilizes the difference in pressures existing between the inside and outside of a deflected flow. The favourable

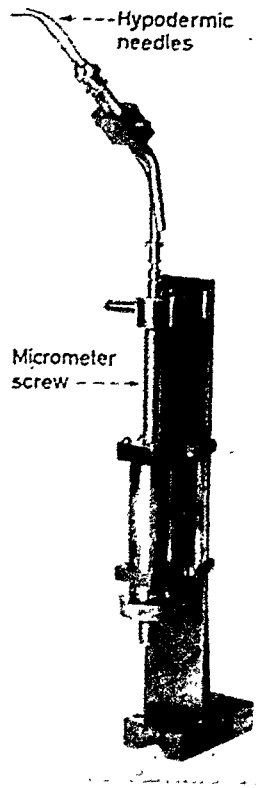

Figure 6.23—Special Pitot-static tubes

feature of such a meter is the small cost of installation and low resistance to flow. Any bend incorporated in a system may be used by fitting two pressure tappings, one at the inside and one at the outside as shown in *Fig. 6.24.*

The discharge is calculated from the expression

$$Q = \phi \cdot \frac{d_2^2 \pi}{4} \sqrt{\frac{p_0 - pi}{w}} \qquad \ldots.(6.17)$$

where $p_0 - p_i$ is the pressure difference created by the centrifugal forces and ϕ a discharge coefficient. The value of the coefficient depends on the bend-radius to diameter ratio and surface roughness. Since the surface roughness of commercial pipes varies a great deal and the ratio R/d may also be subject to variation, calibration of the

bend is necessary if reliable results are required. For circular 90° bend the following approximate data may serve as a guide.†

$2R/d$	2	3	4	5	6
ϕ	0·71	0·87	1·0	1·12	1·2

The Rotameter

The rotameter consists essentially of an accurately ground glass tapered tube set in vertical position with the larger end at the top.

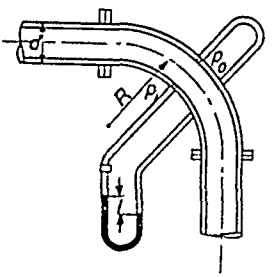

Figure 6.24—Bend meter

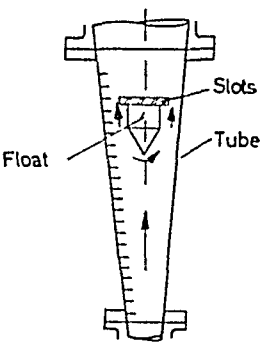

Figure 6.25—Rotameter

The liquid flowing upwards steadily supports a float, its position being determined by the rate of flow. The float is provided with a conical end and a head as shown in *Fig. 6.25.* Slots are cut in the head slantwise, which stabilize the centre position by setting the float in rotation. The meter is calibrated, and the rate of flow figures etched on the outside of the tube.

Rotameters are used in many practical fields‡ where high accuracy is not essential and the discharge varies to a limited extent only.

The Anemometer

The anemometer consists essentially of a small windmill and revolution counter as shown in *Fig. 6.26.* When exposed to air currents the anemometer registers the velocity by measuring the time with the aid of a timeclock. Anemometers are calibrated

† Lansford: Bull. Univ. Ill. No. 289.

‡ Rotameters are not recommended for accurate metering of liquid containing dissolved gases.

against a standard flow meter and the calibration should be carried out from time to time since the fine mechanism incorporated in the revolution counter is subject to wear.

Current Meters

Current meters are used to measure the delivery of rivers by means of traversing the stream and measuring the velocity at different points.

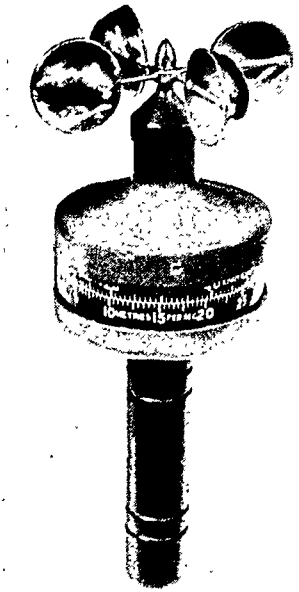

Figure 6.26—Cup type anemometer. (*By courtesy of Kelvin Hughes Ltd.*)

6.7 Manometers

For the measurement of pressures a variety of manometers are in use, each designed to suit individual requirements.

Bourdon Pressure Gauge

The Bourdon pressure gauge consists essentially of a bent tube held rigidly at one end, and the free end is connected to a pointer as shown in *Fig. 6.27.* When pressure is admitted to the tube it tends to

straighten, thus actuating a lever system which moves the pointer over a graduated scale.

Piezometer Tubes

Piezometer tubes, already mentioned earlier in the text, are the simplest type of manometers using a liquid as indicating fluid. If the

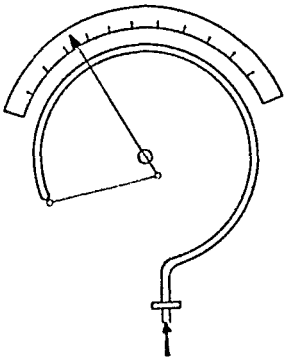

Figure 6.27—Bourdon gauge

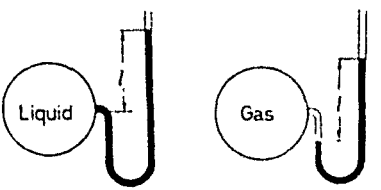

Figure 6.28—Piezometer tubes

fluid in the conduit is a liquid, it will fill the piezometer tube to a height depending upon the pressure at the tapping point as shown in *Fig. 6.28.* If the conduit transmits gas, the piezometer is filled with a suitable liquid, for example water or alcohol.

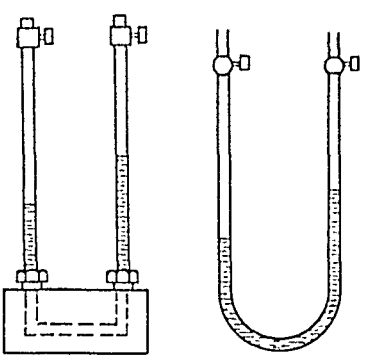

Figure 6.29—Standard U-tubes

U-*Tube*

The U-tube is the simplest type of differential manometer, made up by either two separate glass tubes, fitted into a block, or by one single U-shaped glass tube as shown in *Fig. 6.29.* U-tubes are partly

0

filled with a liquid having a greater density than that of the metered fluid. Mercury is used as an indicating fluid for water, and water or alcohol for flowing gases.

Inverted U-Tube

The inverted U-tube is a combination of two piezometers connected at the top as shown in *Fig. 6.30.* Air can be introduced into

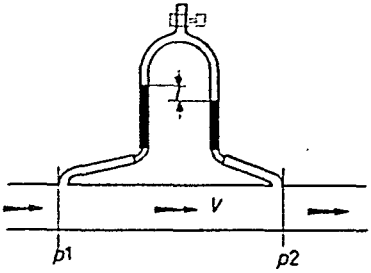

Figure 6.30—Inverted U-tube

the manometer at the top to compensate for the static pressure and drive the two liquid surfaces down to a required position. The advantage of using inverted manometers is that the fluid flowing can be used as indicating fluid.

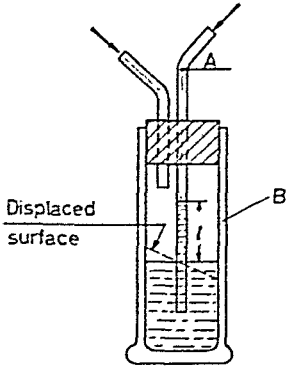

Figure 6.31—Coaxial U-tube

Coaxial Tubes

Coaxial tubes can be successfully used when the measurement of pressures is carried out under unsteady conditions, for example in a moving vehicle. One tube (A) is placed inside the other (B) of generally much larger diameter. Vibration or acceleration displaces

the free surface of the liquid in the outer tube, but the height of liquid inside the inner tube above the neutral axis of the displaced free surface is practically unaffected by the movements as shown in *Fig. 6.31.*

Inclined Manometer

Inclined manometers consist essentially of a sloping glass tube and a reservoir. Compared with the bore of the tube d the cross-sectional area A of the reservoir is large. The manometer shown in

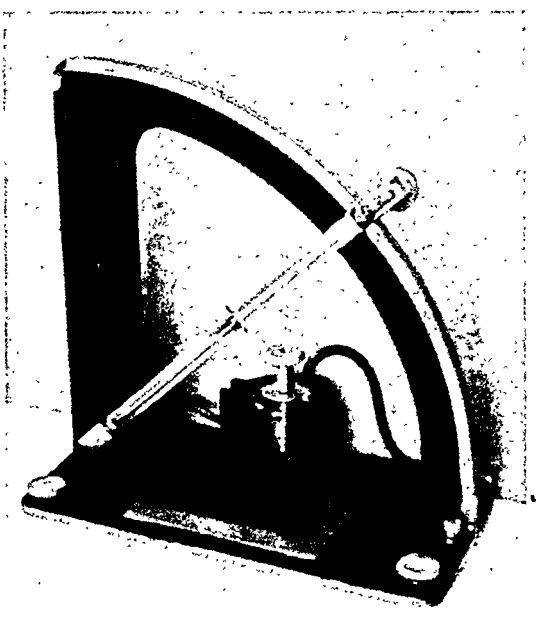

Figure 6.32—Inclined tube manometer

Fig. 6.32 is so designed that the inclination of the tube may be varied from a few degrees to a vertical position, and the magnified differential head can be directly observed on the tube. The actual pressure is given by the expression

$$h = R\left[\sin\theta + \left(\frac{d}{D}\right)^2\right] \qquad \ldots\ldots(6.18)$$

where R = reading, θ = angle inclination and $\frac{d^2}{D^2}$ tube–container area ratio.

Micromanometers

Micromanometers are used for measuring pressure differences from, say, 1/2 in. water gauge down to a fraction of an inch. Amongst the various designs, the Small† type incorporates two glass reservoirs (A and B), a micrometer screw, a float, a short-distance telescope, and a light source, as shown in *Fig. 6.33.* A small mirror is fitted on

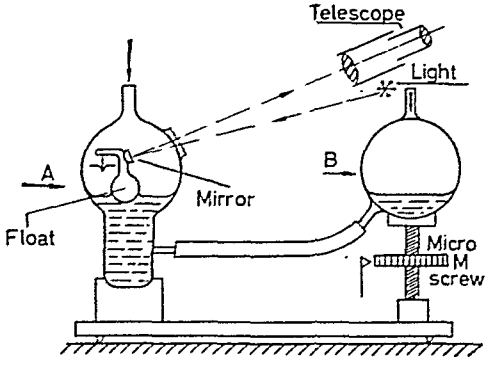

Figure 6.33—'Small' type micromanometer

the float which hinges on a knife edge. The light beam emerging from the point source is reflected by the mirror onto the telescope. Any change in the pressures alters the levels in both reservoirs thereby affecting the position of the float and mirror. By turning the micrometer screw the surface level in reservoir A is brought back to its original position by raising or lowering reservoir B, until the image of light source reappears in the telescope. From the number of turns of the screw, the pressure difference is obtained. Depending on design, this manometer may register pressures as low as 0·0002 in. water gauge.

Other types of micromanometers used in aeronautical research are the Chattock‡ and the Ower§, which may register pressures as low as 10^{-5} in. water gauge. These have a restricted use because of their slow response to pressure changes.

6.8 Conversion of Pressure Measurements

Manometer readings are usually converted into 'head of fluid flowing'.

From the law of hydrostatics, a pressure is equivalent to the height

† R. & M. Report No. 1430.
‡ Phil. Mag. 1901, p. 83.
§ R. & M. No. 1308, 1930.

of a liquid multiplied by its specific weight. For the same pressure, liquids of different specific weights will rise to different levels.

The conversion of manometer reading into head of fluid flowing will be shown for two typical cases.

(1) Consider a fluid of specific weight w, flowing inside a conduit as shown in *Fig. 6.34*. A U-tube, filled with an indicating liquid of

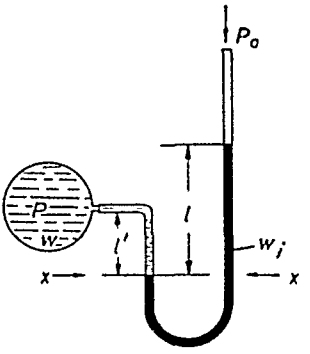

Figure 6.34

specific weight w_i, is connected to a pressure tapping where the pressure is p. Assuming one leg of the gauge to be open to the atmosphere, we write

$$p + l'w = p_a + lw_i$$

where l is the deflection of the manometer and l' the distance between the lower meniscus and the pressure tapping. Converted into head of fluid flowing,

$$h = \frac{p}{w} = \frac{p_a}{w} + l\frac{w_i}{w} - l' \qquad \ldots.(6.19)$$

(2) Consider a fluid flowing inside a horizontal pipe. Two pressure tappings L ft. apart are connected to a U-tube which registers a deflection of l (*Fig. 6.35*). To calculate the pressure difference between the tappings we write

$$p_1 + l'w = p_2 + (l' - l)w + lw_i$$

Hence

$$p_1 - p_2 = l(w_i - w) \qquad \ldots.(6.20)$$

Converted into head of fluid flowing

$$h = \frac{p_1 - p_2}{w} = l\left(\frac{w_i}{w} - 1\right) = l(\sigma - 1) \qquad \ldots.(6.21)$$

where $\sigma = w_i/w$. For water flowing and mercury as indicating liquid $\sigma = 13{\cdot}6/1$ and $\sigma - 1 = 12{\cdot}6$. For air flowing and alcohol as indicating liquid $\sigma = 62{\cdot}4 \times 0{\cdot}8/0{\cdot}075 = 866$. In this case $\sigma - 1 \sim \sigma$.

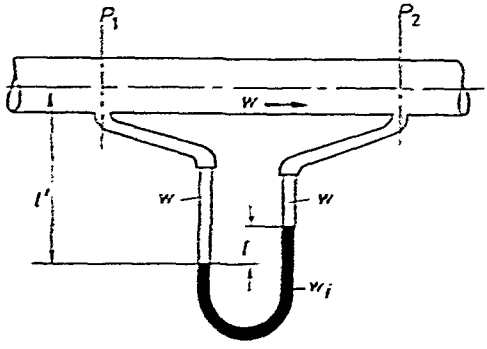

Figure 6.35

6.9 Absolute and Gauge Pressures

With the aid of a barometer the magnitude of the atmospheric pressure is obtained. Pressures in excess of the atmospheric are called gauge pressures and pressures relative to the absolute zero are called absolute pressures. Frequently it is advisable to work with

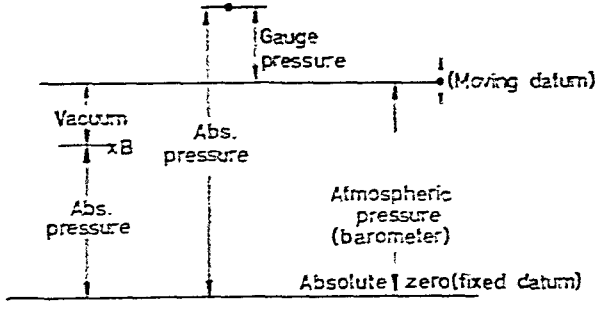

Figure 6.36

absolute pressures as the atmospheric pressure varies with the weather conditions and altitude. Pressures less than the atmospheric are usually measured in inches of mercury vacuum relative to the atmosphere. The effect is shown in *Fig. 6.36.*

Examples

6.1. Calculate accurately the rate of water flowing (in cusecs) in a
pipeline fitted with a 4-in. orifice plate provided with D and $D/2$ tappi
The mercury manometer registers a deflection of 10 in. Kinematic visc
of water $\nu = 10^{-5}$ ft.^{2}/sec.

Solution.—Discharge $Q = C_d \cdot \frac{d^2\pi}{4} \cdot E\sqrt{2gh}$

where

$$E = \frac{1}{\sqrt{(1 - m^2)}} = \frac{1}{\sqrt{[1 - (4/6)^4]}} = \frac{1}{\sqrt{0{\cdot}804}} = 1{\cdot}11$$

$$\frac{d^2\pi}{4} = \frac{4^2\pi}{4 \times 144} = 0{\cdot}0874 \text{ ft.}^2$$

and

$$h = R(\sigma - 1) = \frac{10}{12}(13{\cdot}6/1 - 1) = 10{\cdot}5 \text{ ft. of water}$$

Assuming $Z_1 = Z_2 = 1$, from *Fig. 6.3.* $C = 0{\cdot}607$ for $m = \left(\frac{4}{6}\right)^2 = 0{\cdot}$

$$\therefore \quad Q = 0{\cdot}607 \times 0{\cdot}0874 \times 1{\cdot}11 \times \sqrt{(64{\cdot}4 \times 10{\cdot}5)} =$$

$$= 1{\cdot}535 \text{ ft.}^3\text{/sec.}$$

Calculation of Z_1

Velocity across orifice

$$V = \frac{Q}{A} = \frac{1{\cdot}535}{0{\cdot}0874} = 17{\cdot}6 \text{ ft./sec.}$$

Reynolds' number $N_R = \frac{4 \times 17{\cdot}6}{12 \times 10^{-5}} = 5{\cdot}85 \times 10^5$

From *Fig. 6.3.* $Z_1 = 1{\cdot}005$

also $Z_2 = 1{\cdot}003$

the corrected discharge

$$Q = 1{\cdot}535 \times 1{\cdot}005 \times 1{\cdot}003 = 1{\cdot}55 \text{ ft.}^3\text{/sec.}$$

6.2. Determine the size of orifice plate, which will be fitted with co
tappings, to be inserted into a 6-in. diameter pipe to meter 60,000 cubic
of town's gas per hour if the maximum allowable differential is 3 in.

Dynamic (absolute) viscosity of town's gas $\mu = 3 \times 10^{-7}$ lb. sec./ft.^{2}
Specific gravity of town's gas $s = 0{\cdot}5$ (air = 1)
Temperature $t = 60°\text{F.}$
Pressure $p = 14{\cdot}7$ lb./in.^{2}

Solution.—Assume $Z_1 = Z_2 = 1$

$$C.m.E. = \frac{Q}{A\sqrt{(2gH)}} = \frac{60{,}000}{3600 \times 0{\cdot}196 \times \sqrt{(64{\cdot}4 \times 410)}} = 0{\cdot}523$$

From the gas equation

$$w_{air} = \frac{p}{RT} = \frac{14{\cdot}7 \times 144}{53{\cdot}3 \times 520} = 0{\cdot}076 \text{ lb./ft.}^3$$

$$w_{gas} = 0{\cdot}5 \times 0{\cdot}076 = 0{\cdot}038 \text{ lb./ft.}^3$$

Head of gas flowing

$$H = 3/12 \times \frac{62{\cdot}4}{0{\cdot}038} = 410 \text{ ft.}$$

from *Fig. 6.2* for $C.m.E. = 0{\cdot}523$

$C = 0{\cdot}581$

the corresponding $m = 0{\cdot}67$

the diameter of the orifice $d = D\sqrt{m} = 6\sqrt{0{\cdot}67} = 4{\cdot}9$ in., say 5·0 in.

Correction for N_R and D

As $$\frac{d^2\pi}{4} = \frac{5^2\pi}{144 \times 4} = 0{\cdot}136 \text{ ft.}^2$$

the velocity across orifice, $V = \frac{16{\cdot}6}{0{\cdot}136} = 122$ ft./sec.

The Reynolds' number:

$$N_R = \frac{5 \times 122 \times 0{\cdot}038 \times 10^7}{12 \times 3 \times 32{\cdot}2} = 2 \times 10^5$$

Correction for N_R: $Z_1 = 1{\cdot}005$

Correction for D $Z_2 = 1{\cdot}001$

Check

$$m' = \left(\frac{5}{6}\right)^2 = 0{\cdot}695 \qquad m'^2 = 0{\cdot}482$$

$$c' = 0{\cdot}573 \qquad E' = \frac{1}{\sqrt{1 - m'^2}} = \frac{1}{\sqrt{1 - 0{\cdot}482}} = 1{\cdot}38$$

hence

$$C'Z_1Z_2m'E' = 0{\cdot}573 \times 1{\cdot}005 \times 1{\cdot}001 \times 0{\cdot}695 \times 1{\cdot}38 = 0{\cdot}558$$

the actual pressure drop

$$H = \frac{Q^2}{2g(C'Z_1Z_2m'E'A)^2} = \frac{(60{,}000)^2}{(3{,}600 \times 0{\cdot}558 \times 0{\cdot}196)^2 \times 64{\cdot}4} = 360 \text{ ft.} < 410$$

6.3. It is desired to insert an orifice plate fitted with corner tappings into a 4-in. diameter water-main to meter an estimated maximum rate of flow of 8,000 gallons per hour. If the maximum allowable differential is 50 in. water gauge, find the diameter of the orifice. Assume $\nu = 10^{-5}$ ft.^{2}/sec.

Solution.—Assume $Z_1 = Z_2 = 1$

From B.S.S. Code

$$C.m.E. = \frac{G}{2239 D^2 \sqrt{h} \frac{1}{\sqrt{w}}}$$

where G = discharge in gallons per hour
h = pressure differential in inches of water
w = specific weight of liquid in lb./per ft.^{3}
D = diameter of pipe

The product

$$C.m.E. = \frac{8000}{2239 \times 16 \times \sqrt{50} \times 1/\sqrt{62{\cdot}4}} = 0{\cdot}25$$

from graph C versus m we find (for $C.m.E. = 0{\cdot}25$) $m = 0{\cdot}38$ and $C = 0{\cdot}605$

hence $d = D\sqrt{m} = 4\sqrt{0{\cdot}38} = 2{\cdot}47$ in, say 2·5 in.

Check: Proceed as in Example 6.2.

6.4. The deflection of an inclined manometer using alcohol of specific gravity 0·80 is 10 in. when connected to a pitot-static tube which is inserted in an air stream. The barometric pressure is 770 mm. Hg and temperature 70°F. ($R = 53{\cdot}3$). The inclination of the manometer to the horizontal is 15°. Find the velocity of the airstream.

Solution.—To find the specific weight of air, assume the air to be dry, and apply the gas equation.

Thus $$pv = RT$$

and specific weight $$w = \frac{p}{RT}$$

Since $$p = \frac{770 \times 13{\cdot}6 \times 62{\cdot}4}{25{\cdot}4 \times 12} = 2140 \text{ lb./ft.}^2$$

$$w = \frac{2140}{53{\cdot}3 \times (460 + 70)} = 0{\cdot}071 \text{ lb./ft.}^3$$

The air velocity

$$V = \sqrt{2g \frac{p_1 - p_2}{w}}$$

where $\frac{p_1 - p_2}{w} = h$, is the head of air flowing.

Neglecting the area ratio a/A

$$h = R\frac{\sin\theta}{12} \times \frac{w_{alcohol}}{w_{air}} =$$

$$= \frac{10 \sin 15}{12} \times \frac{0{\cdot}80 \times 62{\cdot}4}{0{\cdot}0761} = 142 \text{ ft. of air}$$

Hence air velocity

$$V = \sqrt{(64{\cdot}4 \times 142)} = \sqrt{9160} = 96 \text{ ft./sec.}$$

6.5. Calculate the rate of flow over a sharp crested rectangular suppressed weir 6 ft. wide and 3 ft. high, if the head over the weir $H = 10$ in.

Solution.—Since $\frac{L}{H} = \frac{3 \times 12}{10} = 3{\cdot}6$ the corresponding point on *Fig. 6.13* yields $Cd = 0{\cdot}63$

To obtain the velocity of approach, the approximate discharge is calculated

$$Q = Cd\tfrac{2}{3}b\sqrt{2g}\,.\,H^{3/2}$$

$$= 0{\cdot}63 \times 2 \times 6 \times \sqrt{2g} \times \left(\frac{10}{12}\right)^{3/2} =$$

$$= 15{\cdot}4 \text{ ft.}^3\text{/sec.}$$

Hence

$$V_1 = \frac{Q}{A} = \frac{15{\cdot}4}{\left(3 + \frac{10}{12}\right) \times 6} = 0{\cdot}672 \text{ ft./sec.}$$

and

$$\frac{V_1^2}{2g} = \frac{0{\cdot}672^2}{64{\cdot}4} = 0{\cdot}007 \text{ ft.}$$

Since the velocity of approach is small, the discharge may be taken as 15·4 cusecs.

REFERENCES

1 LINFORD, A., *Flow Measurements and Meters*, E. and F. Spon, London, 1949.
2 ADDISON, H., *Hydraulic Measurements*, Chapman and Hall, London, 1946.

Problems

6.1. A venturi meter is installed for metering the flow of benzene. The meter is fitted to a pipeline which is downwardly inclined at 30° to the horizontal. The inlet and throat diameters are 12 and 6 in. respectively and the distance between the upstream and throat pressure-tappings is 4 ft., measured along the line. Assuming a coefficient of discharge $C_d = 1$, calculate the rate of flow through the meter when the pressure difference between the tappings is 10 in. mercury. S.G. of benzene is 0·82.

6.2. A sharp-edged orifice plate with corner tappings inserted in a circular air duct is connected to an inclined differential manometer with kerosene as the indicating liquid. The diameters of the duct and the orifice plate are 12

and 8·5 in., respectively. Determine the velocity in the duct if the measuring tube of the manometer is inclined to an angle of 20° to the horizontal and the displacement of the liquid level along the tube is 43 mm. S.G. of kerosene is 0·79.

6.3. A Pitot tube is placed in an airstream flowing with a speed of 200 ft./sec. If the pressure of the air is 30 lb./in.², abs. and its temperature is 85°F, calculate the differential height of the free surfaces in a U-tube filled with mercury. (S.G. = 13·6)

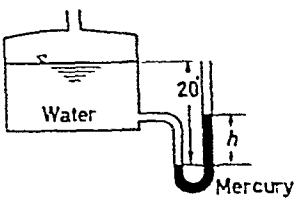

Figure 6.37 (*From* Elementary Fluid Mechanics *by courtesy of John Wiley & Sons*)

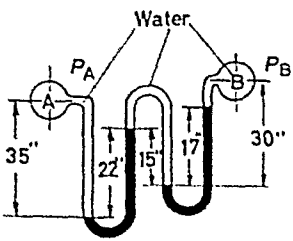

Figure 6.38 (*From* Fluid Mechanics *by courtesy of Constable & Co. Ltd. and Prentice-Hall, Inc.*)

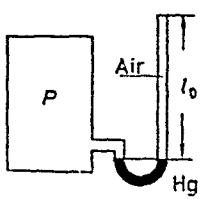

Figure 6.39

6.4. A manometer stands as shown in *Fig. 6.37*. Calculate the manometer reading when:

(*a*) the air space is open to atmosphere

(*b*) the air space is closed and the pressure is raised to 20 lb./in.²

6.5. The pressure is a gas holder installed at sea level (14·7 lb./in.² absolute) is 7 in. w.g. Find the pressure in the distribution system under no flow conditions at a point 500 feet above the outlet of the holder. The specific gravity of the gas = 0·5 (air = 1). Take the specific weight of air as 0·077 lb./ft.³

6.6. Calculate the pressure difference between sections A and B. Use the data shown in detail on *Fig. 6.38*.

6.7. The absolute pressure of air, p, in a container is to be measured by means of a closed type manometer (*see Fig. 6.39*). Air is enclosed in the upper part of the manometer and mercury is the indicating liquid.

When both mercury levels in the manometer are at the same height, the air in the closed manometric tube occupies a length of $l = 22{\cdot}5$ inches. The following are the results of a calibration test:

When the air pressure in the container is—	p_1	$p_2 = 8p_1$
THEN		
the air in the closed tube occupies a length of	$l_1 = \frac{4}{3}l_0$	$l_2 = \frac{2}{3}l_0$

Assuming that the change of state of air in the manometric tube is isothermal, determine the pressures p_1 and p_2 and also the pressure at which both mercury levels will be at the same height.

7

DIMENSIONAL ANALYSIS OF FLUID FLOW PHENOMENA

7.1 Purpose and Principles of Dimensional Analysis

DIMENSIONAL analysis gives certain information about the relations which hold between the measurable quantities associated with various physical phenomena. The method employed in dimensional analysis is the grouping of quantities involved into a definite number of independent dimensionless products so that the results of experimental observations may be expressed in terms of such non-dimensional products.

Application of dimensional methods to the analysis of problems is of particular interest to fluid mechanics. To illustrate the method, consider first an elementary example well known from mechanics: the simple pendulum. The measurable quantities are: length of the pendulum, time of swing, gravitational acceleration and mass of the pendulum. The relation,

$$t = 2\pi \sqrt{(l/g)}$$

expresses the time of swing in terms of the square root of the length of the pendulum, and gravitational acceleration. By introducing a proportionality factor 2π the equation is satisfied. The mass of the pendulum apparently does not enter into the formula.

The above relation may be written in the following way;

$$\frac{t\sqrt{g}}{\sqrt{l}} = 2\pi$$

If it is desired to confirm the formula, experiments may be carried out with pendulums of various lengths, measuring the times of swing. We shall find that, provided the amplitude of the swing is small, the times of swing t_1, t_2, $t_3 \ldots$ and lengths l_1, l_2, $l_3 \ldots$ invariably yield

$$t_1\sqrt{\frac{g}{l_1}} = t_2\sqrt{\frac{g}{l_2}} = t_3\sqrt{\frac{g}{l_3}} = \ldots = 2\pi \qquad \ldots . (7.1)$$

Whilst the formula may be derived by applying the basic principles of motion, certain information leading to a relation may also

be obtained without going through a detailed investigation of the problem.

Consider the dimensions on the left and right hand side of Equation 7.1. Since the right hand side is a pure number, the left hand side must yield a pure number *if* dimensional homogeneity is to be satisfied. Substituting into Eq. 7.1 the dimensions of length, time and gravitational acceleration, one obtains

$$T\sqrt{\frac{LT^{-2}}{L}} = 1 = \text{pure number.}$$

Thus, by replacing the variables in the equation with their appropriate dimensions, the formula was found dimensionally correct.

Assume now, that the formula quoted is not known *a priori*, and it is desired to arrive at a relationship from dimensional considerations. The procedure is then as follows:

(1) List *all* the independent variables which may enter the physical picture.
(2) Write down the dimensions of these variables.
(3) Combine the variables into a functional relationship in such a way that dimensional homogeneity is satisfied.

In case of the pendulum, the independent variables which may enter the physical picture and the relevant dimensions are:

Variable	Symbol	Dimensions
length	l	L
time	t	T
mass	m	M
gravitational acceleration	g	LT^{-2}

Assume that the functional relation is expressed in the form of a product of powers of the variables†, and that a prototype relation is of the form

$$t = \text{CONST.} \times l^{\alpha} \cdot m^{\beta} \cdot g^{\gamma} \qquad \ldots\ldots(7.2)$$

where the exponents α, β and γ are not known. By replacing the variables with their dimensions, one obtains

$$T = L^{\alpha} \cdot M^{\beta} \cdot (LT^{-2})^{\gamma}$$
$$= L^{\alpha+\gamma} \cdot M^{\beta} \cdot T^{-2\gamma}$$

Since the left hand side of the equation may also be written as $L^0M^0T^1$, we have

$$L^0M^0T^1 = L^{\alpha+\gamma}\, M^{\beta}\, T^{-2\gamma}$$

† Often referred to as the Rayleigh method.

A solution for the unknown α, β, and γ is found by 'equating the exponents'. Thus:

$$\begin{aligned} \alpha + \gamma &= 0 \quad \text{(Condition on } L\text{)} \\ \beta &= 0 \quad \text{(Condition on } M\text{)} \\ -2\gamma &= 1 \quad \text{(Condition on } T\text{)} \end{aligned}$$

Solving the equation gives

$$\begin{aligned} \alpha &= \tfrac{1}{2} \\ \gamma &= -\tfrac{1}{2} \end{aligned}$$

and substituting these values into Eq. 7.2 yields

$$f = \text{CONST.} \times l^{\frac{1}{2}} \cdot g^{-\frac{1}{2}}$$

or

$$f\sqrt{(g/l)} = \text{CONST.}$$

The value of the non-dimensional constant does not appear in the solution and must, be determined experimentally.

Consider now another problem, for example, the frequency of vibration of a structure. The independent variables which may enter the physical picture and their dimensions are:

Variables	Symbol	Dimension
Frequency	f	T^{-1}
Length of span	l	L
Density of material	ρ	ML^{-3}
Elasticity	E	$ML^{-1}T^{-2}$

Assuming that the relation is of the form

$$f = \text{CONST.} \times l^{\alpha} \cdot E^{\beta} \cdot \rho^{\gamma} \qquad \ldots\ldots(7.3)$$

and replacing the variables with their relevant dimensions one obtains

$$T^{-1} = L^{\alpha}(ML^{-1}T^{-2})^{\beta}(ML^{-3})^{\gamma}$$

or

$$M^0L^0T^{-1} = L^{\alpha-\beta-3\gamma} \cdot M^{\beta+\gamma} \cdot T^{-2\beta}$$

Equating the indices gives:

$$\begin{aligned} \alpha - \beta - 3\gamma &= 0 \qquad \text{Condition on } L \\ \beta + \gamma &= 0 \qquad \text{Condition on } M \\ -2\beta &= -1 \qquad \text{Condition on } T \end{aligned}$$

Solving the equation yields

$$\alpha = -1 \qquad \beta = \tfrac{1}{2} \qquad \gamma = -\tfrac{1}{2}$$

With these values

$$f = \text{CONST.} \times \frac{\sqrt{(E/\rho)}}{l} \qquad \ldots.(7.4)$$

Let us now confront the task of estimating the frequency of vibration of a large steel structure, for example a bridge. Assuming that the structure is in the design stage, so that no direct measurements on the structure are possible, but that facilities for the building of a model structure are available and we are allowed to use some other convenient material, for example, brass, we may then estimate, from the measurements on the model, the frequency of the prototype. Writing Eq. 7.4 in the form

$$\frac{f \cdot l}{\sqrt{E/\rho}} = \text{CONST.}$$

and providing the variables relating to the model with the suffix 'm' and those relating the prototype with the suffix 'p', we have

$$\frac{f_m l_m}{\sqrt{(E_m/\rho_m)}} = \frac{f_p \cdot l_p}{\sqrt{(E_p/\rho_p)}}$$

Hence, the frequency of vibration of the prototype

$$f_p = f_m \cdot \frac{l_m}{l_p} \cdot \sqrt{\frac{E_p \rho_m}{E_m \rho_p}} \qquad \ldots.(7.5)$$

Since the linear scale ratio l_m/l_p and the ratios of the physical constants E_p/E_m, ρ_m/ρ_p are specified, the experiment calls for the measurement of the frequency of vibration f_m of the model only.

Perfect geometric similarity between model and prototype is a condition for obtaining correct results. This calls for the construction of a model 'scaled down' to minute details, including similarity between rivets, joints and frictional effects.

The simple pendulum and the structure are typical examples of a class of phenomena which is more or less free of the size of the sample on which the experiment is carried out. One may, in fact, experiment on a moderate scale and establish the value of the constant. In the case of the pendulum, one invariably obtains the same value for the constant, irrespective of what length we choose. Neither the mass nor the material of the filament, on which the mass is suspended, enters the formula and as long as the experiment is carried out in still atmosphere and the amplitude of the swing is small, one arrives at consistent results. It appears that all simple pendulums are geometrically similar and complete independence of the constant is observed.

The constant obtained for the structure, however, may vary with the design. The large variety of structures met in practice, being geometrically dissimilar, will yield a different value of the constant for each particular design.

In a larger class of problems, such as encountered in fluid mechanics, the constant varies with the geometry as well as with other variable quantities. With the aid of dimensional analysis, these variables are grouped to form a non-dimensional number, which may no longer be considered a constant. These non-dimensional (variable) groups are called parameters. We have already met such a non-dimensional parameter, the Reynolds' number. In fluid mechanics, besides the Reynolds' number, there are other non-dimensional numbers in use, such as the Froude number, the Mach number, the Euler number and so on.

Consider now a problem in which the Reynolds' number plays an important role, for example, the pressure losses in pipes caused by friction. The variables involved and their dimensions are:

Variable	Symbol	Dimension
Pressure loss per foot length	$\Delta p/L$	$ML^{-2}T^{-2}$
Diameter of pipe	d	L
Velocity of fluid	V	LT^{-1}
Kinematic viscosity	ν	L^2T^{-1}
Density of fluid	ρ	ML^{-3}

Assuming that the relation is of the form

$$\frac{\Delta p}{l} = \text{CONST.} \times d^{\alpha} \cdot V^{\beta} \cdot \nu^{\gamma} \cdot \rho^{\delta}$$

and replacing the variables with their relevant dimensions, one obtains

$$ML^{-2}T^{-2} = L^{\alpha}(LT^{-1})^{\beta} \cdot (L^2T^{-1})^{\gamma} \cdot (ML^{-3})^{\delta}$$
$$= M^{\delta} \cdot L^{\alpha+\beta+2\gamma-3\delta} \cdot T^{-\beta-\gamma}$$

Equating the indices, yields

$$\delta = 1$$
$$\alpha + \beta + 2\gamma - 3\delta = -2$$
$$\beta + \gamma = 2$$

As it appears, the number of variables are more numerous than in the preceding examples, and, in fact, one has four unknown quantities and only three equations. Hence, one of the unknowns

remains arbitrary and one may select this one to be γ. Solving the equations in terms of γ yields

$$\beta = 2 - \gamma$$
$$\alpha = -1 - \gamma$$

Hence, the product becomes

$$\text{CONST.} \times d^{-1-\gamma} \cdot V^{2-\gamma} \cdot \nu^{\gamma} \cdot \rho$$

Upon re-arranging terms, one obtains

$$\frac{\Delta p}{l} = \text{CONST.} \times \frac{\rho V^2}{d} \left(\frac{\nu}{dV}\right)^{\gamma} \qquad \ldots.(7.6)$$

In this equation, the non-dimensional product is obviously the reciprocal of the Reynolds' number and since no numerical value for γ was found, the function $(\nu/Vd)^{\gamma}$ must be determined experimentally. The numerical constant may be absorbed in this function so that we may generally write $(\nu/Vd)^{\gamma} = \Phi(N_R)$. Further, since the friction factor is defined by the Darcy equation as being $f = \dfrac{2\Delta p d}{\rho V^2 l}$ (Eq. 4.2, Chapter 4), we may write $f = \Phi(N_R)$. For laminar flow, $\Phi(N_R)$ was found to be $64/N_R$, and for turbulent flow $\Phi(N_R) = 0{\cdot}316/N_R{}^{0{\cdot}25}$ (Blasius).

Inspection of Eq. 7.6 shows that actually two non-dimensional products form the solution of the problem: $\dfrac{2\Delta p d}{\rho V^2 l}$ represented by f and Vd/ν represented by N_R. We may specify N_R to be the independent parameter and f the dependent one and plot f against N_R. The experiment calls for a large number of observations on the variables, which are then grouped into these two non-dimensional parameters and the functional relationship between the parameters established. The results of such experiments are presented on friction factor charts.

Again, the experiments may be carried out on model pipes and the results obtained used for the calculation of frictional losses in other pipes. Geometric similarity is satisfied by using pipes, for example, of similar circular cross-section and of geometrically similar surface finish.

RECAPITULATION

It was suggested that the standard procedure used in solving problems be set aside and a method of analysing the dimensions be

introduced. The guiding principle in this analysis was dimensional homogeneity, which must be maintained if dimensionally correct results are to be obtained. In making such analysis, all variables which possibly may enter the final equation were listed. With these variables a hypothetical equation was formed and the variables subsequently replaced by their respective dimensions. Then the principle of dimensional homogeneity was applied whereby the exponents of the variables were found.

The information thus obtained by the analysis leads to the form of the equation describing the phenomenon, but since the information lacks completeness, certain measurements are necessary to complete the relationship between the variables.

It is further suggested that these measurements might not necessarily be carried out on a large scale and measurements on conveniently scaled models might suffice. In this way, all information needed might be obtained with much less trouble and expense than would otherwise be required. Indeed, one finds in modern engineering practice an extensive use of models, the results being employed for the prediction of the behaviour of the prototype.

The salient feature of the method which furnishes such a powerful tool for the engineer lies in the grouping of the variables into non-dimensional parameters. A change in the magnitude of the variables does not affect the value of the parameter provided certain similarity conditions are satisfied.

In case of the single pendulum, the parameter $t\sqrt{\frac{g}{l}}$ is invariably found equal to 2π. Any change in the length l is compensated by a change in t in such a way that the parameter remains constant. Similarity conditions are not required because all simple pendulums are similar. In the case of a structure, the parameter $f \cdot l/\sqrt{E/\rho}$ yields the same constant for all geometrically similar designs. Any change in the length and the material used for the construction is compensated by f in such a way that the parameter remains constant. Geometric similarity is required because structures vary in design. Again, in the case of friction in pipes, the similarity conditions to be satisfied are extended. To maintain the parameter $\frac{2\Delta p d}{\rho V^2 \cdot l}$ at a constant value, in addition to geometric similarity, a certain fixed value of the parameter $\frac{V \cdot d}{\nu}$ (Reynolds' number) is also required. Once these two similarity conditions are satisfied, any change in the pipe diameter, d, length, l, and dynamic head $\frac{1}{2}\rho V^2$,

is compensated by Δp in such way that the parameter $\frac{2\Delta p d}{\rho V^2 . l}$ remains constant. Thus, in the case of friction in pipes, the constancy of one parameter depends on the similarity of another parameter plus geometric similarity.

Since the method of dimensional analysis is based on the formation of suitable parameters, followed by the application of similarity, these two issues will be discussed again separately and in detail.

7.2 The Π Theorem

In the preceding section, it was shown that if a dimensionally homogeneous relationship between variables $x_1, x_2, \ldots x_n$ of the general form $f(x_1, x_2, \ldots x_n) = 0$, exists, then, according to Rayleigh, a solution of the form $x_1^{\alpha}, x_2^{\beta}, x_3^{\gamma} \ldots$ may be advanced where the exponents α, β, γ etc. may be determined from dimensional considerations.

The dimensions of the variables $x_1, x_2, \ldots x_n$ are formed with the aid of the 'fundamental' or 'prime concepts' in mechanics known as mass, length, and time; where heat transfer enters the problem, temperature is an additional prime concept. An inspection of a table presented below shows the dimensions of most common variables met in fluid mechanics.

Variables and their Dimensions

Variable	Symbol	Dimension	
Mass	m	M	Prime Concepts
Length	l, d	L	
Time	t	T	
Temperature	0	0	
Velocity	V	LT^{-1}	Kinematic
Acceleration	a	LT^{-2}	
Rate of flow	Q	L^3T^{-1}	
Kinematic viscosity	ν	L^2T^{-1}	
Rotational speed	N	T^{-1}	
Density	ρ	ML^{-3}	
Viscosity	μ	$ML^{-1}T^{-1}$	Dynamic
Surface tension	S	MT^{-2}	
Force	F	MLT^{-2}	
Torque	T	ML^2T^{-2}	
Power or rate of heat in transit	P	ML^2T^{-3}	
Heat quantity	q	ML^2T^{-2}	
Heat conduction	γ, κ	$MLT^{-3}0^{-1}$	

From the table of dimensions, it appears that the different variables are all based on a suitable combination of the prime concepts M, L, T and θ. Some of the variables incorporate purely geometric terms characterized by L; others incorporate kinematic terms such as T^{-1}, LT^{-1}, L^2T^{-1}; while those which include M as well as L and T may be regarded as dimensions of a dynamic character. Hence, we note that the dimensions generally indicate the nature of the variable.

It also appears that the dimension of a variable does not necessarily incorporate all prime concepts.

The Rayleigh method may be applied without difficulty to the dimensional analysis of certain problems where the number of variables does not exceed the available number of prime concepts. In order to analyse a problem, however, where the number of variables p is greater than the number of prime concepts r, $p - r$ exponents must be chosen arbitrarily. For example, in the 'friction in pipe' problem, the number of variables is four and the number of prime concepts employed three. Hence, one amongst the exponent is to be chosen arbitrarily. Again, if the variables are more numerous, the number of exponents to be chosen arbitrarily increases. Evidently this method leaves us undecided in the choice of these exponents.

A different approach to this problem is due to Buckingham†, who introduced the pi theorem, which may be stated as follows:

> 'Given a set of variables $x_1, x_2 \ldots x_p$, p in number and relating to a physical phenomenon, in the dimensions of which r prime concepts are expressed, then provided the equation $f(x_1, x_2, x_3 \ldots x_p) = 0$ is dimensionally homogeneous, it may be reduced to the form
>
> $$F(\Pi_1, \Pi_2, \ldots \Pi_{p-r}) = 0 \qquad \ldots.(7.7)$$
>
> where the parameters Π_1, $\Pi_2 \ldots \Pi_{p-r}$ are independent and dimensionless products formed from the variables.'

The pi theorem asserts that, since the equation is dimensionally homogeneous, f is rather a function of a set of dimensionless products of the variables than a function of separate variables. The parameters can thus be regarded as new variables in a reduced number. A reduction of the variables is desirable because—(1) The graphical representation of dimensionless parameters furnishes information in a more comprehensive way than a graph in which the co-ordinates have dimensions, and (2) dimensionless graphs can frequently be determined by tests on models.

† E. Buckingham: 'On Physically Similar Systems', *Phys. Review*, Vol. IV No. 4, p. 345, 1914.

Whilst the pi theorem introduces a rule relating to the number of independent parameters to be formed, it does not impose a restriction on the method of formation nor does it furnish complete information with regard to the variables to be incorporated in the parameters. Since, however, the independence of parameters is a condition of primary importance, we are, in fact, at liberty to select variables at random to a limited extent only. In a specified field, one may either be guided by established practice based on experience, or, in the absence of this, one may form parameters which fit the experimental requirements.

Typical Π's may be of the form

$$\Pi_i = \frac{x_i}{x_1^{\alpha_1} x_2^{\alpha_2} \ldots} \qquad \Pi_j = \frac{x_j}{x_1^{\beta_1} x_2^{\beta_2} \ldots} \qquad \Pi_k = \frac{x_k}{x_1^{\gamma_1} \cdot x_2^{\gamma_2} \ldots}$$

where the variables $x_i, x_j, x_k \ldots$ in the numerator are selected from the available set of variables in such a way that they are dimensionally balanced by the products of powers of variables in the denominator; *i.e.*, each Π is a dimensionless group of variables.

The solution in the form given in Eq. 7.7 may be solved explicitly for any one of the products, or for any one of the variables contained in the products. Thus, for the parameter Π_i, we write

$$\frac{x_i}{x_1^{\alpha_1} x_2^{\alpha_2} \ldots} = \phi(\Pi_2, \Pi_3 \ldots \Pi_{p-r}) \qquad \ldots . (7.8)$$

and for a selected variable x

$$x_i = x_1^{\alpha_1} x_2^{\alpha_2} \ldots \phi(\Pi_2, \Pi_3 \ldots \Pi_{p-r}) \qquad \ldots . (7.9)$$

The general method of procedure adopted in some field, for example, in fluid mechanics, is as follows:

(1) Select a fixed set of variables for the denominator, preferably equal in number to the prime concepts. In fluid mechanics, the number of prime concepts generally does not exceed three.

(2) Select, for geometric similarity purposes, a characteristic linear dimension, l or d; for kinematic similarity purposes, a speed (linear or rotational); for dynamic similarity purposes, the density of the fluid, ρ, but any variable which incorporates mass may be suitable.

(3) Take from the set of variables each variable in turn and place these in the numerator and balance dimensionally. In order to obtain $p-r$ parameters, none of the variables selected for the denominator must appear in the numerator.

For the illustration of the pi theorem, consider now the problem of measuring the rate of discharge by means of an orifice plate. The

variables are: quantity of fluid flowing Q, diameter of pipe D, diameter of orifice d, velocity of fluid across the orifice V, kinematic viscosity ν, density of fluid ρ, and pressure difference across orifice Δp. As the number of variables $p = 7$ and the number of prime concepts $r = 3$, the number of parameters to be formed $p - r = 7 - 3 = 4$. Accordingly

$$\Pi_1 = \frac{Q}{\rho^{\alpha_1} d^{\alpha_2} V^{\alpha_3}}; \quad \Pi_2 = \frac{D}{\rho^{\beta_1} d^{\beta_2} V^{\beta_3}}; \quad \Pi_3 = \frac{\nu}{\rho^{\gamma_1} d^{\gamma_2} V^{\gamma_3}};$$

$$\Pi_4 = \frac{\Delta p}{\rho^{\delta_1} d^{\delta_2} V^{\delta_3}}.$$

Substituting the dimensions for the variables

$$\Pi_1 = \frac{L^3 T^{-1}}{(ML^{-3})^{\alpha_1} . L^{\alpha_2} (LT^{-1})^{\alpha_3}} = \frac{M^0 L^3 T^{-1}}{M^{\alpha_1} L^{-3\alpha_1 + \alpha_2 + \alpha_3} . T^{-\alpha_3}} = \frac{Q}{d^2 V}$$

Following similar lines of calculations

$$\Pi_2 = \frac{D}{d}; \qquad \Pi_3 = \frac{\nu}{dV}; \qquad \Pi_4 = \frac{\Delta p}{\rho V^2}$$

Hence, the reduced equation is of the form

$$F\left(\frac{Q}{d^2 V}, \frac{D}{d}, \frac{dV}{\nu}, \frac{\Delta p}{\rho V^2}\right) = 0$$

Inspection of the parameters shows that Δp and V are inter-dependent and one parameter may be eliminated by substituting $\sqrt{\Delta p/\rho}$ for V. Hence, the equation further reduces to

$$F\left(\frac{Q}{d^2\sqrt{\frac{\Delta p}{\rho}}}, \frac{d\sqrt{\Delta p/\rho}}{\nu}, \frac{D}{d}\right) = 0 \qquad \ldots.(7.10)$$

It appears from the result that the discharge coefficient C_d, defined as $\frac{Q}{d^2\sqrt{\Delta p/\rho}}$ is a function of both the diameter ratio, $\left(\frac{d}{D}\right)^2$, and the Reynolds' number, $N_R = \frac{d\sqrt{\Delta p/\rho}}{\nu}$. Expressing C_d in explicit form

$$C_d = \phi\left(N_R, \frac{d}{D}\right) \qquad \ldots.(7.11)$$

Consider Eqs. 6.5 and 7.11. It is apparent that whilst Eq. 6.5 furnishes the correct formula for the calculation of the discharge, Eq. 7.11 furnishes the functional dependence of the discharge coefficient. The information given by Eq. 7.11 leads to the plotting of the discharge coefficient C_d against the Reynolds number N_R, using the diameter ratio d/D as an additional parameter, as shown in the graphs presented in Chapter 6 (*Figs. 6.2* and *6.3*).

An example analogous to the above is the discharge over a weir. The variables are: discharge Q, head over weir H, gravitational acceleration g, velocity of water over weir plate V, width of the weir b, height of the weir over the channel bed l and kinematic viscosity of water ν. As the number of variables $p = 7$ and the number of prime concepts $r = 2$ (notice the absence of mass), the number of parameters to be formed $p - r = 7 - 2 = 5$. The selection of a geometric and kinematic term for the denominator is first to be considered. Since the quantities b and l may be constant for a specified weir, the only variable which may be used for a 'length' is H. Assuming the kinematic term to be V, the following parameters are formed:

$$\Pi_1 = \frac{Q}{H^{x_1}V^{x_2}}, \quad \Pi_2 = \frac{\nu}{H^{\beta_1}V^{\beta_2}}, \quad \Pi_3 = \frac{b}{H^{\gamma_1}V^{\gamma_2}}, \quad \Pi_4 = \frac{l}{H^{\delta_1}V^{\delta_2}}$$

$$\Pi_5 = \frac{g}{H^{\epsilon_1}V^{\epsilon_2}}$$

The interdependence between H and V appears from the last parameter. One finds

$$\Pi_5 = \frac{g}{V^2H^{-1}} \qquad \text{or} \qquad V = \Pi_5\sqrt{gH}$$

Substituting $\sqrt{gH}$ for V leads to

$$\Pi_1 = \frac{Q}{H^{5/2}g^{1/2}}, \quad \Pi_2 = \frac{\nu}{H^{3/2}g^{1/2}}, \quad \Pi_3 = \frac{b}{H}, \quad \Pi_4 = \frac{L}{H}$$

Hence

$$F\left(\frac{Q}{H^{5/2}g^{1/2}}, \frac{\nu}{H^{3/2}g^{1/2}}, \frac{b}{H}, \frac{l}{H}\right) = 0 \qquad \ldots.(7.12)$$

From the results, it appears that the discharge coefficient, C_d, defined as $Q/H^{5/2}g^{1/2}$ is a function of both the Reynolds' number $N_R = \frac{H^{3/2}g^{1/2}}{\nu}$ and the 'geometry' of the weir specified by the ratios l/H and

b/H. The information given by Eq. 7.12 leads to the plotting of C_d against N_R and l/H for a given b/l†. (*See Figs. 6.13, 6.16,* and *6.17* in Chapter 6.)

As shown in the foregoing, the pi theorem proves to be a most useful and simple method for the formation of non-dimensional parameters.

7.3 Similarity

Information obtained from dimensional analysis leads to the selection and grouping of relevant variables in a prescribed way, so that experimentally measured quantities may be employed for the prediction of similar phenomena which may occur on any other scale.

Examples quoted in the preceding section show that actually dimensional analysis furnishes additional and most useful information to formulae derived from first principles. The formulae, for example, giving the discharge across an orifice or over a weir do not specify the functional dependence of the discharge coefficient: dimensional analysis readily provides this additional information.

Similarity conditions, as pointed out before, may be (1) geometric; (2) kinematic; (3) dynamic; and/or a combination of the three. Let us discuss these conditions separately.

Geometric Similarity

Geometric similarity means similarity of shape. To satisfy geometric similarity, the model must be a perfect replica of the prototype. This implies that all corresponding linear dimensions of model and prototype must be related by the same scale factor, k_g. For example, two spheres of different diameters are usually regarded as geometrically similar bodies; strictly speaking, however, *perfect* geometric similarity can be claimed only if the ratio of relative roughness of model and prototype yields the same number (k_g) as the diameter ratio. Obviously a scale model must have a smoother surface than the prototype. Geometrically similar surface finish is most important in fluid mechanics; one may, for example, be satisfied with a rough casting for a marine propeller or for a turbine runner, but any experiment on a scaled down model must be carried out with a correspondingly smooth surface finish. This frequently entails painstaking work.

Any variation in the scale factor relating dimensions of a specific model and prototype leads to a distorted model. One may, for

† The π theorem allows the investigator to combine parameters provided such combinations fit the experimental results better.

example, have geometrically similar body shapes with distorted surface finish or one may have a model in which the horizontal and vertical dimensions are reduced by different scales. In some cases, perfect similarity must be observed; in others, close similarity will suffice; the degree of perfection depends on the type of problem and the accuracy required in the final results.

Kinematic Similarity

Kinematic similarity means the similarity of motions. Kinematic similarity is satisfied if the time rate of change of motions in the

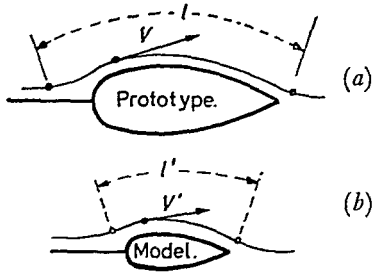

Figure 7.1

prototype 'system' corresponds to a similar change in the model 'system'. If points that correspond to each other on model and prototype are called corresponding points, and particles in motion that correspond to each other are called corresponding particles, then the motions in the two systems are similar if corresponding particles move at corresponding points at corresponding times.

Consider the flow pattern around a prototype and model and select corresponding streamlines. Since the corresponding streamlines of similar fluid motions are corresponding curves, components of velocity and acceleration are also corresponding.

The kinematic (velocity, acceleration) scale factors (k_V and k_a) may be established from the geometric similarity of streamlines and the time similarity of motions. Consider the flow pattern around a prototype and model. If a particle moves along path ABC (*Fig. 7.1a*) and a corresponding particle moves along A'B'C' (*Fig. 7.1b*), the ratio of the respective path lengths, l/l', yields the geometric similarity factor k_g.

Expressing length in terms of velocity and time

$$l = V \cdot t \qquad \text{and} \qquad l' = V' \cdot t'$$

respectively, and denoting $V/V' = k_V$ and $t/t' = k_t$, we obtain

$$k_a = \frac{l}{l'} = \frac{V \cdot t}{V' \cdot t'}$$

or

$$k_a = k_V \cdot k_t$$

Hence, the velocity scale factor

$$k_V = \frac{k_a}{k_t} \qquad \ldots.(7.13)$$

Similarly the acceleration scale factor k_a may be obtained by considering

$$V = a \cdot t \quad \text{and} \quad V' = a't', \quad \text{whence}$$

$$k_a = \frac{a}{a'} = \frac{V}{V'} \cdot \frac{t'}{t} = \frac{k_a}{k_t^2} \qquad \ldots.(7.14)$$

For example, a model is built to a 1/5 scale and it is desired to maintain kinematic similarity between model and prototype. Assuming we are permitted to choose $k_t = 1$, then, according to Eq. 7.13, $k_V = 1/5$. This means that the velocity in the model system must be a fifth of the velocity in the prototype system. If, however, one desires to choose $k_V = 1$, the corresponding time must be 1/5 in the model system.

Dynamic Similarity

Dynamic similarity means the similarity of forces. Dynamic similarity is satisfied if corresponding points of the prototype and model system experience dynamically similar forces. Similar forces do not necessarily mean equal forces.

The dynamic similarity factor k_F may be obtained by considering that force equals mass times acceleration so that the force factor

$$k_F = \frac{F}{F'} = \frac{m \cdot a}{m' \cdot a'}$$

Denoting m/m' by k_m, one obtains

$$k_F = k_m \frac{k_a}{k_t^2} \qquad \ldots.(7.15)$$

Assume, for example, that a one-tenth scale model of a certain reciprocating mass performs three times as many cycles per second

as the prototype and both model and prototype are made of the same material. Since $k_a = \frac{k_g}{k_l^2} = \frac{10}{9}$ and $k_m = \left(\frac{\rho l}{\rho' l'}\right)^3 = 10{,}000$, the force scale factor

$$k_F = \frac{10{,}000}{9}$$

Hence, the inertia forces acting on the model are only 9/10,000 as great for the model as for the prototype. Under the specified conditions, any force of different magnitude could not be considered as a dynamically similar force.

7.4 Dimensional Analysis of Drag of Bodies Fully or Partially Submerged in Fluids. Corresponding Speed

Any relative motion between a fluid and a body fully or partially submerged in the fluid causes a drag force on the body. The mathematical formula in Chapter 8 (Eqs. 8.10, 8.27) may be derived by dimensional analysis.

Consider first the drag on a fully submerged body. The variables are: drag force F, relative velocity V, characteristic linear dimension l, surface roughness k, fluid density ρ and viscosity μ. Since the number of variables $p = 6$ and the number of prime concepts $r = 3$, the number of parameters to be formed $p - r = 6 - 3 = 3$. Choosing ρ, l and V as variables for the denominator, F, k and μ for the numerator, we have

$$\Pi_1 = \frac{F}{\rho^{\alpha_1} l^{\alpha_2} V^{\alpha_3}}, \quad \Pi_2 = \frac{\mu}{\rho^{\beta_1} l^{\beta_2} V^{\beta_3}}, \quad \Pi_3 = \frac{k}{\rho^{\gamma_1} l^{\gamma_2} V^{\gamma_3}}$$

Substituting for the variables their respective dimensions gives

$$\Pi_1 = \frac{MLT^{-2}}{(ML^{-3})^{\alpha_1} L^{\alpha_2} (LT^{-1})^{\alpha_3}}, \quad \Pi_2 = \frac{ML^{-1}T^{-1}}{(ML^{-3})^{\beta_1} L^{\beta_2} (LT^{-1})^{\beta_3}},$$

$$\Pi_3 = \frac{k}{(ML^{-3})^{\gamma_1} L^{\gamma_2} (LT^{-1})^{\gamma_3}}.$$

Equating the indices and solving the equations yields

$$\alpha_1 = 1 \qquad \beta_1 = 1 \qquad \gamma_1 = 0$$
$$\alpha_2 = 2 \qquad \beta_2 = 1 \qquad \gamma_2 = 1$$
$$\alpha_3 = 2 \qquad \beta_3 = 1 \qquad \gamma_3 = 0$$

Hence

$$\phi\left(\frac{F}{\rho l^2 V^2}, \frac{\mu}{\rho l V}, \frac{k}{l}\right) = 0 \qquad \ldots.(7.16)$$

Introducing the drag coefficient C_D, defined as $F/\frac{1}{2}\rho l^2 V^2$ and substituting for $\frac{\rho l V}{u}$ the Reynolds' number N_R and for k/l the relative roughness ϵ, and expressing C_D in explicit form, one obtains

$$C_D = \phi(N_R, \epsilon) \qquad \ldots.(7.17)$$

Graphs showing the functional relationship between C_D and N_R are shown in *Figs. 8.20, 8.21* (Chapter 8).

The necessary condition to satisfy all similarity requirements for bodies fully submerged in fluids rests on the equivalence of the Reynolds number

$$N_{R_{\text{model}}} = N_{R_{\text{prototype}}} \qquad \ldots.(7.18)$$

It then follows that, provided k/l is constant,

$$C_{D_{\text{prototype}}} = C_{D_{\text{model}}} \qquad \ldots.(7.19)$$

or

$$\left[\frac{F}{\frac{1}{2}\rho l^2 V^2}\right]_{\text{m}} = \left[\frac{F}{\frac{1}{2}\rho l^2 V^2}\right]_{\text{p}} \qquad \ldots.(7.20)$$

Consider now the geometric, kinetic and dynamic similarity factors. Writing Eq. 7.20 in the form

$$\frac{F_{\text{p}}}{F_{\text{m}}} = \frac{\rho_{\text{p}}}{\rho_{\text{m}}} \cdot \left(\frac{V_{\text{p}}}{V_{\text{m}}}\right)^2 \cdot \left(\frac{l_{\text{p}}}{l_{\text{m}}}\right)^2 \qquad \ldots.(7.21)$$

and substituting for $F_{\text{p}}/F_{\text{m}}$, $\rho_{\text{p}}/\rho_{\text{m}}$, $V_{\text{p}}/V_{\text{m}}$, $l_{\text{p}}/l_{\text{m}}$ their respective scale ratios, one obtains

$$k_F = \frac{k_m}{k_\rho^3}\left(\frac{k_g}{k_t}\right)^2 k_\rho^2 = k_m \frac{k_g^2}{k_t^2}$$

Since the geometric scale factor k_g includes the similarity of shape and the similarity of surface roughness as well, our statement is well proved. Thus, if one experiments on geometrically similar models at the corresponding speed and corresponding force, the same drag coefficient is obtained as if a similar experiment on a full prototype is carried out. The term 'corresponding speed' for fully submerged bodies is thus defined by Eq. 7.18.

Consider now the drag on a body partially immersed in a fluid. Obviously, any relative speed between body and fluid will give rise to surface waves, the magnitude of which depends on certain variables such as the gravitational acceleration g, surface tension and depth of fluid. Neglecting surface tension and providing adequate

depth, the only additional variable to be considered is the gravitational acceleration g.

One now has $p = 7$ variables, namely: F, V, l, k, ρ, μ, and g, and $r = 3$ prime concepts, so that the number of parameters to be formed $p - r = 7 - 3 = 4$. The parameters established for the fully submerged body may be accepted and an additional parameter may be formed by considering g. Thus

$$\Pi_4 = \frac{g}{\rho^{\delta_1} l^{\delta_2} V^{\delta_3}}$$

and substituting for the variables the relevant dimensions gives

$$\Pi_4 = \frac{LT^{-2}}{M^{\delta_1} L^{3\delta_1+\delta_2+\delta_3} T^{-\delta_3}}$$

Equating the indices and solving the equations yields

$$\delta_1 = 0 \qquad \delta_2 = -1 \qquad \delta_3 = 2$$

and

$$\Pi_4 = \frac{gl}{V^2}$$

Hence, the general resistance equation for partially submerged bodies is given by

$$\phi\left(\frac{F}{\rho V^2 l^2}, \frac{\rho l V}{\mu}, \frac{V^2}{l \cdot g}, \frac{k}{l}\right) = 0 \qquad \ldots.(7.22)$$

The parameter written in the form $V^2/l \cdot g$ is known as the Froude number

$$N_F = \frac{V^2}{l \cdot g} \qquad \ldots.(7.23)$$

Thus, the total drag coefficient expressed in explicit form in terms of the Reynolds', Froude numbers and the relative roughness

$$C_D = \phi(N_R, N_F, e) \qquad \ldots.(7.24)$$

From Eq. 7.24, it appears that the drag coefficient of bodies partially submerged in fluids depends on both the Reynolds' and the Froude numbers and the relative roughness. Froude showed that this drag is the sum of the skin friction drag, form drag and the drag due to wave making. Froude also showed that since skin friction and form drag are functions of the Reynolds' number and the

wave-making drag is a function of the Froude number, these two functions are independent. Hence, Eq. 7.24 may also be written as

$$C_D = \phi_1(N_R, e) + \phi_2(N_F) \qquad \ldots.(7.25)$$

or

$$C_D = C_{D(N_R)} + C_{D(N_F)}$$

where

$$C_{D(N_R)} = \phi_1(N_R, e)$$

and

$$C_{D(N_F)} = \phi_2(N_F)$$

The total drag force is generally given by

$$F = \tfrac{1}{2}\rho V^2 S \{C_{D(N_R)} + C_{D(N_F)}\} \qquad \ldots.(7.26)$$

where S is the 'wetted' area. The relation plays an important role in predicting drag of ships.

The determination of the drag coefficient from model experiments is more complex for bodies partially submerged than for bodies fully submerged. The difficulty arises when dynamically similar conditions are sought. According to Eq. 7.25, dynamic similarity is satisfied if:

(1) $N_{R_{\text{model}}} = N_{R_{\text{prototype}}}$

(2) $N_{F_{\text{model}}} = N_{F_{\text{prototype}}}$.

Towing tests are generally carried out in water, so that viscosity and gravitational acceleration for both model and prototype are the same. It then follows that if condition (1) is satisfied and $V_m l_m = V_p l_p$, condition (2) cannot be satisfied simultaneously, because

$$\frac{V_{\text{m}}^2}{l_{\text{m}}} = \frac{V_{\text{p}}^2\, l_{\text{p}}}{l_{\text{m}}^2} \neq \frac{V_p^2}{l_{\text{p}}}$$

In other words, the corresponding speed obtained by equating the Reynolds' numbers differs from the corresponding speed obtained by equating the Froude numbers.

The difficulty is overcome by first calculating the skin frictional resistance with the equation established for flat plates (See Eqs. 8.22 and 8.25, Chapter 8), then adding the estimated value of the form resistance and deducting the sum of these two from the total drag. The wave making or residual drag coefficient

$$C_{D(N_F)} = C_D - C_{D(N_R)}$$

may then be plotted against the Froude number.

In *Fig. 7.2*, the residual drag coefficients of various types of ships are shown. Inspection of the curves shows that below $N_F = 0{\cdot}2$, the residual coefficient is substantially constant; above 0·2 it begins to build up gradually and when a value of $N_F = 0{\cdot}3$–$0{\cdot}4$ is attained, it increases rapidly. It follows that at low Froude numbers, the wave-making resistance is small and the skin friction and form drag

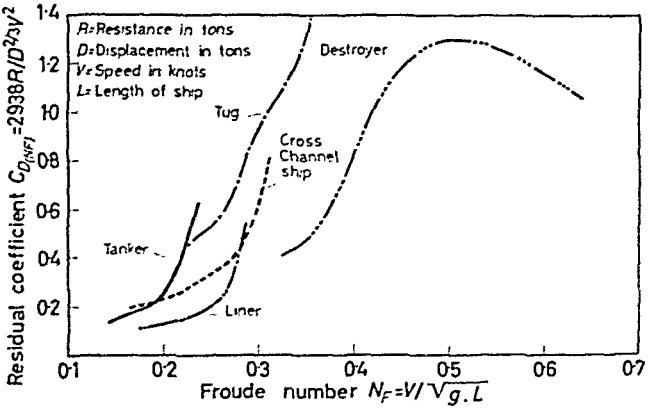

Figure 7.2—Residual drag of various ships

are in excess, whilst at higher Froude numbers, the wave-making resistance predominates. The rapidly increasing drag at higher Froude reflects the building up of wave size.

The irregular shape of the curves, the 'humps and hollows', may be accounted for when considering the relation between wave length and wave-making drag. Generally, the wave pattern surrounding a ship, which advances at a certain speed into undisturbed water, does not change with time. It is found however, that the wave pattern moves with the same speed as the ship, even though the water as a whole does not advance. The relation between wave length and ship length is given by†

$$\frac{\lambda}{l} = 0{\cdot}557\,\frac{V^2}{l}$$

where λ is the length of the wave and l is the length of the ship. Accordingly, the wave length and the size of the wave pattern also increase with increasing speed.

† See for example: Ref. 3. Chapter I.

Waves generated by a ship are shown in *Fig. 7.3* for three different speeds. It may be observed that the 'humps' in the residual drag coefficient curve occur when the surface level about the stern is relatively low and the 'hollows' occur when this level is relatively high. Hence, the residual drag may also be considered as some function of the pressure forces acting on the hull, the latter being a

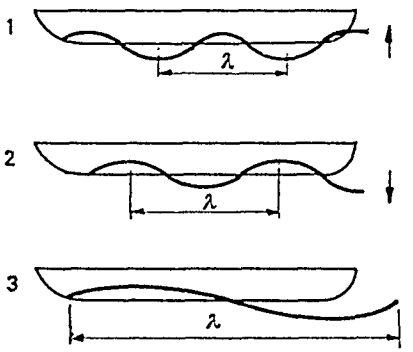

Figure 7.3

function of the wave train initiated at the bow. The intensity of the bow-wave depends a great deal on the shape of the bow, so that the bow shape makes an important contribution towards the wave-making resistance. The form drag, on the other hand, depends largely on the shape of the stern.

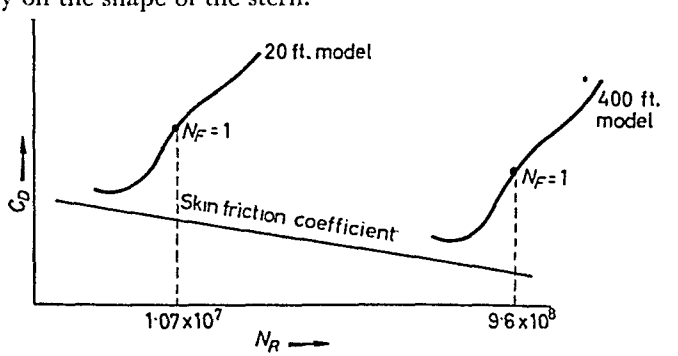

Figure 7.4
(By courtesy of the Society of Naval Architects and Marine Engineers)

The approximate value of the form drag may be estimated when the residual resistance dies out at low Froude numbers and the total drag becomes equal to the sum of the skin frictional drag and eddy-making drag. In calculations, it is assumed that the form drag remains constant over a practical range.

Since flow patterns and wave trains about similar ship forms are similar under dynamically similar flow conditions (specified by a fixed Froude number), the total drag of a full scale prototype can be calculated from measured values on a model. A practical graphical method is obtained by superimposing the residual drag curve over the skin friction curve. Since the residual drag coefficient is independent of the Reynolds' number, the curve retains its shape and may thus be drawn over any desired range of Reynolds' numbers.

In *Fig. 7.4*, the results obtained for a 20 ft. model are used for the prediction of drag of a 400 ft. prototype. The Froude numbers, noted on the residual drag curve, are related to the Reynolds' number by the length of the ship. For example, omitting g from the calculations, Froude number $N_F = 1$ for the 20 ft. model gives $V_m = \sqrt{l} = 4{\cdot}46$ ft./sec. Assuming kinematic viscosity $\nu = 0{\cdot}84 \times 10^{-5}$ ft.^{2}/sec., the related Reynolds' number $N_R = \dfrac{20 \times 4{\cdot}46 \times 10^5}{0{\cdot}84}$ $= 1{\cdot}07 \times 10^7$. The same Froude number yields for the 400 ft. prototype $V_p = \sqrt{400} = 20$ ft./sec., giving $N_R = \dfrac{20 \times 400 \times 10^5}{0{\cdot}84}$ $= 9{\cdot}6 \times 10^8$.

7.5 Scale Effect

Variation of the drag coefficient with the Reynolds number is known as 'scale effect'. More generally, variation of any related parameters may be denoted with the same name. The variation of the drag coefficients (as shown in *Figs. 8.20* and *8.21*) of the sphere and circular cylinders with Reynolds' number are typical examples of scale effect. Inspection of these curves shows, however, that in the case of the circular cylinder the drag coefficient is free of the scale effect in the region of $N_R = 10^4$–10^5. Again, in the case of the sphere, the drag coefficient is free of the scale effect in the region of $N_R = 10^3$–10^4. The friction factor for rough pipes is also free of scale effect at high Reynolds numbers.

Inability to produce dynamically similar conditions in the laboratory may also be regarded as scale effect. This is of particular interest in all model testing of aircraft. Models tested in wind-tunnels are generally exposed to artificial airstreams of the same viscosity and density as the prototype, so that dynamic similarity is satisfied if the wind velocity $V_m = V_p \dfrac{l_p}{l_m}$. To test a 1/10 scale model plane under dynamically similar conditions requires velocity $V_m = 10V_p$. This requirement creates difficulty even with a prototype

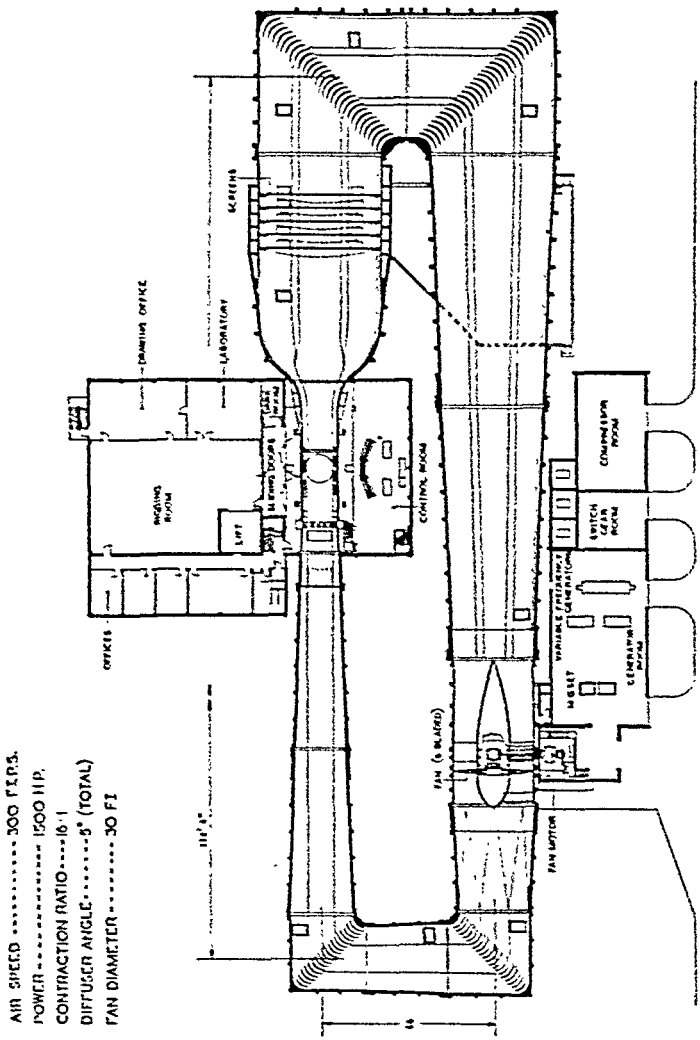

Figure 7.5—Modern subsonic wind-tunnel. *(By courtesy of the Director, Royal Aircraft Establishment, Bedford)*

aircraft flying at as low as 100–200 m.p.h., because the speed of the wind in the tunnel must then be 1,000–2,000 m.p.h. At such high speeds, the air may no longer be considered incompressible. In fact, compressibility effects begin to develop noticeably around 500 m.p.h., whilst around 780 m.p.h. the sonic speed is reached†; beyond the sonic speed a complete change in the flow pattern is experienced. Thus the testing of air plane models with air at standard pressure and at reasonable speeds inevitably leads to scale effects, and the resulting Reynolds' numbers will be at different points of the 'scale' both for model and prototype. One way to overcome this difficulty in practice

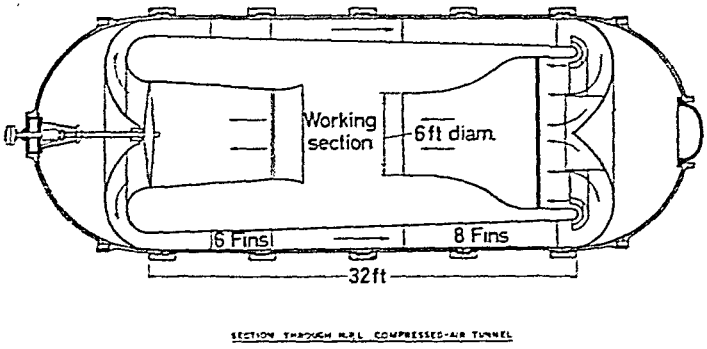

Figure 7.6—Variable (air) density wind-tunnel.
(*By courtesy of N.P.L. Crown copyright reserved*)

is to build model planes as large as possible; for example, to 1/3–1/2 scale, or even to full scale. The other way is to build pressurized wind-tunnels, in which the air density can be increased. Both types of wind tunnels have been built and typical designs are shown in *Figs. 7.5* and *7.6*.

From the point of view of scale effects, practical problems may be divided into two categories. One category deals with problems in which similarity is sought on the basis of corresponding force. The mathematical solution of such problems is relatively simple, as it requires the equation of certain parameters only. On a two-dimensional graph, by fixing the two parameters, we may find the position of a point P (see *Fig. 7.7a*). Dimensional similarity is satisfied if the curve (A) given by the functional relationship $\Pi_2 = f(\Pi_1)$ passes through the specified point, *P*. The curve, in fact, need not be drawn at all and the solution is obtained by writing

$$\Pi_{1_{\text{model}}} = \Pi_{1_{\text{prototype}}}$$

$$\Pi_{2_{\text{model}}} = \Pi_{2_{\text{prototype}}}$$

† At sea level conditions.

It is assumed that adequate information is supplied with the problem, so that the calculation of the parameters may be effected. Illustrative Examples Nos. 1, 2, and 3 are typical examples for this category. On a similar basis, the treatment can be extended to problems involving more than two parameters. One may regard these problems as more or less free of scale effect.

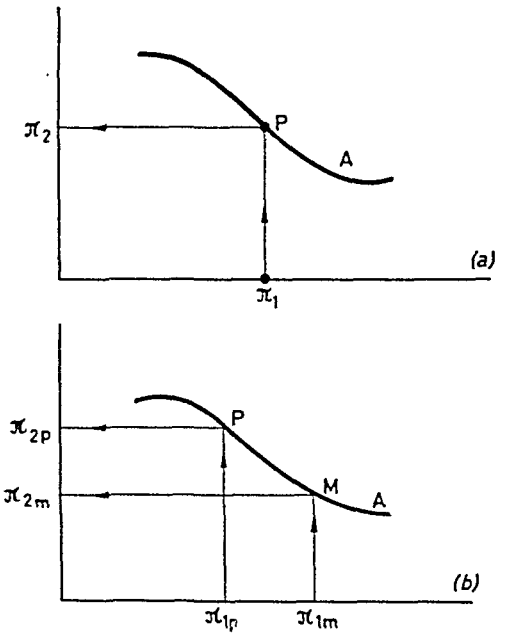

Figure 7.7

The second category is more general, as it deals with problems in which similarity is sought in a certain range of values of the relevant parameters. Curve (A) given by the functional relationship is then used and adequate information must be supplied for the plotting of the curve. Since 'corresponding' similarity between model and prototype is not required, the solution of these problems is not 'free of of scale effect'. In other words, points P, M, specified by values of the parameters Π_1 and Π_2, fall on the curve A at different positions for both model and prototype (*Fig. 7.7b*). Illustrative Examples 4, 5, and 6 are typical examples for this category. We may add that information furnished to such problems is frequently the result of extensive research.

7.6 Conclusions

In the preceding discussions, it was shown that dimensional analysis furnishes a powerful tool for the engineer and simplifies solutions to problems in which the number of variables is large, so that exact mathematical solution, if any, would present difficulties. It is pointed out, however, that simplicity must not be underestimated. Errors may be introduced, even if greatest care is exercised. The general rule to follow, in order to reduce possibilities leading to errors, is to include all variables which may enter a certain problem. In fact, one should include rather more than less variables and discard later those which have negligible influence on the final result. This way, the possibility that answers to a problem will be out of scale is reduced.

For example, when considering flow over a weir, viscosity and surface tension effects may be ignored, provided that 'head' over the weir is relatively high. Again, surface tension does not influence ocean waves as a whole, but if the waves in a model harbour are small (say, less than one inch long), their behaviour may be considerably influenced by surface tension if water is used as fluid. The drag of submerged bodies may be conveniently explored on models placed in wind-tunnels; wind-tunnels, however, are never free of some turbulence in the stream. Thus, the result applied to the prototype may be out of scale by an amount depending upon the difference in the turbulence levels surrounding model and prototype. Similarity conditions thus must also include the turbulence level parameter, because the Reynolds' number, being based on the mean velocity, does not include this factor. In model-towing-tests, the distribution of mass in the model must be similar to the distribution of the mass in the full scale vessel.

From the examples quoted above, it appears that the scale of the model is of great importance and one should endeavour to construct models as large as possible. Naturally, there may be other factors to be considered as well.

Thus, we may realise that, whilst dimensional methods appear to be simple, the elimination of all sources leading to errors necessitates careful planning.

Dimensional analysis will be used again in connection with rotodynamic machinery and compressible fluid flow.

Examples

7.1. A geometrically similar model of an air duct is built to 1 : 30 scale and tested with water which is 50 times more viscous and 800 times more

dense than air. When tested under dynamically similar conditions, the pressure drop is 33 lb./in.^{2} in the model.

Find the corresponding pressure drop in the full scale prototype and express it in inches of water.

Solution.—Since viscosity effects predominate, conditions are dynamically similar if $(N_R)_p = (N_R)_m$

or
$$\frac{\rho_p L_p V_p}{\mu_p} = \frac{\rho_m L_m V_m}{\mu_m}$$

Hence,
$$\frac{V_p}{V_m} = \frac{\rho_m}{\rho_p} \cdot \frac{L_m}{L_p} \cdot \frac{\mu_p}{\mu_m} = \frac{800}{30 \times 50} = \frac{8}{15}$$

Since pressure loss due to friction $\Delta_p = f \frac{L}{D} \frac{1}{2} \rho V^2$ we have

$$\frac{\Delta p_p}{\Delta p_m} = \frac{f_p}{f_m} \cdot \frac{L_p}{L_m} \cdot \frac{D_m}{D_p} \cdot \frac{\rho_p}{\rho_m} \cdot \left(\frac{V_p}{V_m}\right)^2$$

This reduced to
$$\frac{\Delta p_p}{\Delta p_m} = \frac{\rho_p}{\rho_m} \left(\frac{V_p}{V_m}\right)^2$$

because
$$f_m = f_p, \text{ and } \frac{L_p}{D_p} = \frac{L_m}{D_m}$$

Hence
$$\Delta p_p = \Delta p_m \frac{\rho_p}{\rho_m} \left(\frac{V_p}{V_m}\right)^2 = 33 \times \frac{1}{800} \times \left(\frac{8}{15}\right)^2 = 0{\cdot}01174 \text{ lb./in.}^2$$

and
$$\Delta H_p = \frac{\Delta p_p}{w} = \frac{0{\cdot}01174 \times 144}{5{\cdot}2} = 0{\cdot}33 \text{ in. W.G.}$$

7.2. It may be shown (by dimensional analysis) that

$$\frac{T}{\rho \omega^2 D^5} = \phi \left(\frac{\rho D^2 \omega}{\mu}\right)$$

where T = torque, D = characteristic linear dimension, ω = angular velocity, ρ = density, μ = viscosity.

Calculate the horse power required to drive a 30-in. diameter disc rotating in air, if it requires a torque of 0·8 ft./lb. to rotate a similar disc of 9-in. diameter in water at a corresponding speed of 1400 r.p.m.

Data:

	Air	Water
Viscosity	$1{\cdot}86 \times 10^{-4}$	$1{\cdot}01 \times 10^{-2}$
Density	1.2×10^{-3}	1·0 (c.g.s. units)

Solution.—Substituting N for ω, we obtain at the corresponding speed

$$\frac{\rho_a D_a^2 N_a}{\mu_a} = \frac{\rho_w D_w^2 N_w}{\mu_w}$$

hence,

$$N_a = N_w \cdot \left(\frac{D_w}{D_a}\right)^2 \left(\frac{\rho_w}{\rho_a}\right) \left(\frac{\mu_a}{\mu_w}\right)$$

$$= 1400 \times \left(\frac{9}{30}\right)^2 \times \frac{10^3}{1{\cdot}2} \times \frac{1{\cdot}86 \times 10^{-4}}{1{\cdot}01 \times 10^{-2}} = 1920 \text{ r.p.m.}$$

At corresponding torque

$$\frac{T_a}{\rho_a N_a^2 D_a^5} = \frac{T_w}{\rho_w N_w^2 D_w^5}$$

hence,

$$T_a = T_w \cdot \frac{\rho_a}{\rho_w} \cdot \left(\frac{N_a}{N_w}\right)^2 \left(\frac{D_a}{D_w}\right)^5 = 0{\cdot}8 \times \frac{1{\cdot}2 \times 10^{-3}}{1} \times \left(\frac{1920}{1400}\right)^2 \times \left(\frac{30}{9}\right)^5$$

$$= 0{\cdot}73 \text{ ft.lb.}$$

Since power

$$P = \frac{2\pi \cdot T \cdot N}{33{,}000}$$

the power required to drive the 30 in. disc in air

$$P_a = \frac{2\pi T_a N_a}{33{,}000} = \frac{6{\cdot}28 \times 1920 \times 0{\cdot}73}{33{,}000} = 0{\cdot}27 \text{ h.p.}$$

7.3. A spillway section of a hydro-electric project is to be studied by means of a geometrically similar model, constructed to scale of 1 : 10.

Neglecting viscous and surface tension effects, calculate:

(*a*) the rate of flow through the model if the corresponding discharge in the prototype is 50,000 ft.^{3}/sec.;

(*b*) the corresponding velocity in the prototype if at a corresponding point in the model the velocity is 10 ft./sec.;

(*c*) the dissipation of energy in a hydraulic jump in the tailwater of the prototype if the jump in the model dissipates 0·5 horse power.

Solution.—(*a*) Since viscosity effects may be neglected and only gravitational effects are to be considered

$$\frac{Q}{bg^{1/2}H^{2/3}} = \phi\left(\frac{b}{H}\right)$$

where Q = discharge, b = width of spillway, H = head of water over weir and g = gravitational acceleration.

Kinematic similarity is satisfied if $\left(\frac{b}{H}\right)_m = \left(\frac{b}{H}\right)_p$

hence $$\frac{Q_m}{Q_p} = \frac{b_m}{b_p} \cdot \left(\frac{H_m}{H_p}\right)^{3/2}$$

Substituting for b and H a characteristic linear dimension L, we have $b = C_1 L$, $H = C_2 L$, so that $bH^{\frac{3}{2}} = C_1 C_2^{\frac{3}{2}} L^{\frac{5}{2}}$. Accordingly

$$Q_m = Q_p \left(\frac{L_m}{L_p}\right)^{5/2} = 50{,}000 \times \left(\frac{1}{10}\right)^{5/2} = 158 \text{ ft.}^3\text{/sec.}$$

(*b*) On the basis of kinematic similarity, we have $\frac{b_m}{b_p} = \frac{H_m}{H_p}$ and since $V \propto \sqrt{(gH)}$

$$\frac{b_m}{b_p} = \left(\frac{V_m}{V_p}\right)^2; \quad \text{and } V_p = V_m \left(\frac{L_p}{L_m}\right)^{1/2} = 10\sqrt{10} = 31{\cdot}6 \text{ ft./sec.}$$

(*c*) Since power $\propto Q.w.H.$

$$\frac{P_p}{P_m} = \frac{Q_p w_p H_p}{Q_m w_m H_m}$$

Substituting

$$\frac{Q_p}{Q_m} = \frac{b_m}{b_p} \cdot \left(\frac{H_m}{H_p}\right)^{3/2} = \left(\frac{L_m}{L_p}\right)^{5/2}$$

and noting that $w_p = w_m$, we obtain

$$\frac{P_p}{P_m} = \left(\frac{L_p}{L_m}\right)^{5/2} \cdot \frac{L_p}{L_m} = \left(\frac{L_p}{L_m}\right)^{7/2}$$

and

$$P_p = 0{\cdot}5 \times 10^{7/2} = 1580 \text{ h.p.}$$

7.4. A model vessel having a submerged surface area of 8 ft.^{2} and length 7 ft. has a total drag of 0·95 lb. when towed at a velocity of 5·14 ft./sec. Assuming the friction drag of the submerged part of the hull to follow the same law as flat plate of the same length covered completely with a turbulent boundary layer, calculate:

(*a*) the friction drag on the model hull;

(*b*) the total drag of a geometrically similar hull 25 times as long as the model, when moving at the corresponding speed.

Data:

Density of water $\rho = 1{\cdot}94$ slugs/ft.^{3}

Kinematic viscosity $\nu = 1{\cdot}2 \times 10^{-5}$ ft.^{2}/sec.

Solution.—Neglecting the eddy making resistance

$$F = \tfrac{1}{2}\rho V^2 S\{C_D(N_R) + C_D(N_F)\}$$

where S is the wetted surface.

For the model

$$N_{R_m} = \frac{5{\cdot}14 \times 7 \times 10^5}{1{\cdot}2} = 3 \times 10^6$$

and

$$C_D = \frac{0{\cdot}455}{[\log_{10} 3 \times 10^6]^{2{\cdot}58}} = 3{\cdot}65 \times 10^{-3} \qquad \textit{See} \text{ Eq. 8.25, Chapter 8.}$$

Since $\frac{1}{2}\rho V^2 = 25{\cdot}4$

the residual drag coefficient

$$C_{D(N_F)} = \frac{0{\cdot}95 - 3{\cdot}65 \times 10^{-3} \times 25{\cdot}4 \times 8}{25{\cdot}4 \times 8} = 1{\cdot}03 \times 10^{-3}$$

The corresponding speed is calculated on the basis of similarity of wave making. Hence

$$N_{Fm} = \frac{V_m^2}{l_m} = \frac{5{\cdot}14^2}{7} = 3{\cdot}75 = \frac{V_p^2}{25 \times 7}$$

and the corresponding speed of the prototype $V_p = \sqrt{25 \times 5{\cdot}14^2} = 25{\cdot}7$ ft./sec.

For the prototype, the Reynolds' number

$$N_R = \frac{25 \times 7 \times 25{\cdot}7 \times 10^5}{1{\cdot}2} = 3{\cdot}76 \times 10^8$$

and

$$C_D = 0{\cdot}0018$$

As the wetted surface

$$S = 25^2 \times 8 = 5{,}000 \text{ ft.}^2$$

the total drag:

$$F = 9{,}000 \text{ lb.}$$

7.5. The values below relate to an investigation of the drag experienced by a cylinder placed in the working section of a wind-tunnel, the axis of the cylinder being perpendicular to the direction of air flow.

With the aid of the drag coefficient curve (to be established from the data), estimate the force exerted on a smoke stack of 3 ft. diameter and 30 ft. high during a 17 m.p.h. wind.

Neglecting the influence of surface roughness, comment on the result and in what respect will it be out of scale?

Model dimensions; Diameter 3 in.

Wind tunnel working section data:

Air pressure, lb./in.^{2} abs.	14·5	87	87
Air temperature, °F	60	72	72
Air flow velocity, ft./sec.	62·6	53·4	64·1
Drag force, lb.	1·38	3·74	2·12

Viscosity of air at 60°F $= 3{\cdot}67 \times 10^{-7}$ lb.sec./ft.^{2}

Viscosity of air at 72°F $= 3{\cdot}88 \times 10^{-7}$ lb. sec./ft.^{2}

Atmospheric pressure 14·7 lb./in.^{2} Temperature 60°F.

Solution.—From the given data, the Reynolds' numbers and the drag coefficients are calculated and the curve is drawn (*Fig. 7.8*).

Air pressure	Temperature	Density (slugs)	Viscosity $\times 10^{-7}$	$N_R \times 10^{-4}$	C_D
14·5	60	0·00234	3·67	9·88	1·2
87	72	0·001375	3·88	48·5	0·765
87	72	0·00138	3·88	58·8	0·298

The Reynolds' number for the smoke stack in a 17 m.p.h. wind

$$N_R = \frac{3 \times 17 \times 1{\cdot}47 \times 0{\cdot}00234}{3{\cdot}67 \times 10^{-7}} = 4{\cdot}75 \times 10^5$$

From the graph

$$C_D = 0{\cdot}76$$

Hence the drag

$$D = C_D A \tfrac{1}{2}\rho V^2 =$$
$$= 0{\cdot}76 \times 3 \times 30 \times 0{\cdot}00117 \times 25^2 =$$
$$= 56 \text{ lb.}$$

The data do not specify the length of the model cylinder and it may be assumed to extend from wall to wall of the working section so that two

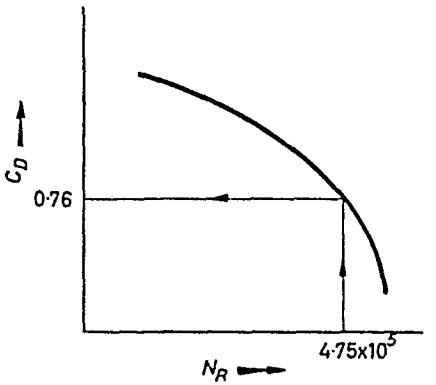

Figure 7.8

dimensional flow is maintained during the tests. The finite aspect ratio of the stack, 10 : 1 may not introduce large errors, but a considerable discrepancy may be attributed to the mode of anchorage of the stack. Further discrepancy may be expected due to the difference in the turbulence level in the natural wind and the turbulence level of the wind-tunnel.

REFERENCES

1. Bridgeman, P. W., *Dimensional Analysis*, Yale University Press, 1931.
2. Langhaar, H. L., *Dimensional Analysis and Theory of Models*, J. Wiley, 1951.

Problems

7.1. By dimensional analysis, show that C_D given in Eq. 6.5 is some function of Reynolds' number and d/D where d = diameter of orifice, D is diameter of pipe. Use Rayleigh's method.

7.2. Two balls made of lead (S.G. 11·34) and aluminium (S.G. 2·7) are allowed to sink freely in water. Determine the ratio of the diameters of the balls if dynamic similarity must be obtained when the balls have arrived at their terminal sinking velocities.

7.3. A new type of flow meter when tested in a pipe carrying water, yields a differential pressure of 7·6 lb./in.^{2} The power absorbed in the meter was found to be 80·5 lb. ft./sec. What differential pressure would the flow meter indicate if atmospheric air flows through the same system at dynamically similar conditions, and what would be the corresponding power loss in the meter?

7.4. A mass of floating ice in a channel has a momentum of 1000 slugs ft./sec. In a model 1/20 of the size what will be the momentum of a similar mass?

7.5. The frequency of the surface waves (*i.e.*, the number of waves passing through a station per unit time), caused by the motion of a floating body is proportional to V/l, where V is the velocity of the body and l is a characteristic length of the body, the coefficient of proportionality being some function of the Froude number.

(*a*) Prove this statement by making a dimensional analysis of the problem.

(*b*) A 1 : 100 scale ship model is being tested in a towing tank at a certain velocity. The frequency of the waves behind the model is $n_m = 4{\cdot}5$ waves per second. What would be the frequency of the waves behind the ship when moving at the corresponding velocity?

7.6. A thin liquid film is flowing uniformly downwards along a rectangular flat plate under its own weight. The width of the plate is b, the inclination to the horizontal is α. The flow is steady laminar, the velocity distribution in the film is linear with respect to the distance from the plate. The specific weight and the absolute viscosity of the liquid are w and μ, respectively.

(*a*) *Show by dimensional analysis that the rate of flow of the liquid may* be expressed as

$$Q = \frac{\delta^4 \cdot w}{\mu} \times \phi \left(\frac{\delta}{b} \cdot \alpha \cdot \frac{w\delta^2_2}{g^{\frac{1}{2}}} \right)$$

Where

δ = thickness of the liquid film; and
g = gravitational acceleration.

(*b*) Using the above relationship, show by a simple reasoning that the thickness of a liquid film at a given rate of flow

$$\delta = K \cdot \sqrt[3]{\frac{Q \cdot \mu}{(b \cdot w \cdot \sin \alpha)}}$$

where $K = \phi_1 \left(\frac{w\delta^{3/2}}{\mu g^{1/2}} \right)$

7.7. The coefficient of discharge of an overflow dam is to be determined by means of a model. The crest length is 40 feet and the approximate discharge 4,000 cusecs at 10 feet head. The supply available in the laboratory is 1 cusec. Determine the head of water in model and length of model crest.

7.8. The length of a ship is 175 ft. and the submerged surface area is 7,700 ft.^{2}

Calculate the engine power required to maintain a speed of 10 knots, assuming that the combined propulsive and propeller efficiency is 60 per cent.

The residual drag† coefficient may be obtained from *Fig. 7.2* and the skin friction coefficient from the formula

$$C_D = \frac{0{\cdot}455}{(\log_{10} N_{RL})^{2{\cdot}58}}$$

† Residual drag is the combined form drag and wave-making drag.

8

BOUNDARY LAYER THEORY

The theory of skin friction, form drag and turbulence

8.1 General Description of the Boundary Layer

THE previous discussion has been focused on the establishment of certain laws of fluid aggregates. The fluid was considered as a mass of homogeneous particles flowing either in closed ducts or in open conduits. In the following discussion, it is intended to have a closer look at the behaviour of viscous fluids in the vicinity of solid boundaries.

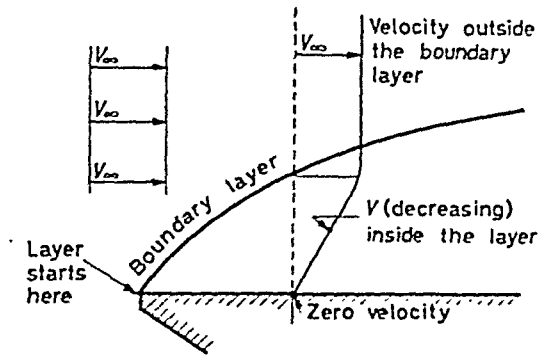

Figure 8.1—Boundary layer over a flat plate

It is observed experimentally that when a fluid passes along a solid surface a thin fluid layer is formed next to the boundary. Inside this layer, which is known as the boundary layer, the velocity of the stream falls to zero at the boundary surface. Outside this layer, the velocity appears to be of the same *order* as the velocity of approach (V_∞), as shown in *Fig. 8.1*.

It is also observed experimentally that boundary layers formed on solid surfaces exposed to a free fluid stream become thicker in going downstream. Further, the flow inside the boundary layer may be of laminar or turbulent character.

Consider a flat plate with one surface exposed parallel to a fluid stream, as shown in *Fig. 8.2*. At the leading edge the thickness of

the boundary layer is zero; downstream, the thickness of the layer increases and the main stream is somewhat displaced by the gradually thickening layer. The 'smooth' increase of the layer continues only to a certain distance from the leading edge; beyond this point a more rapid increase occurs, which continues until the end of the plate is reached.

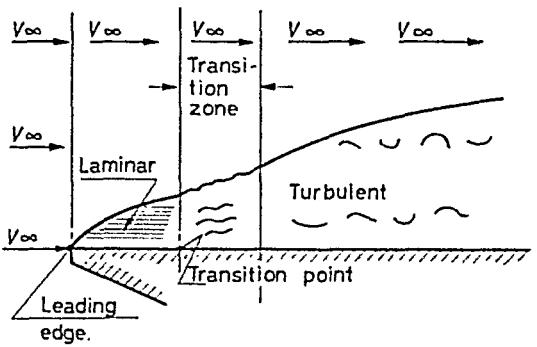

Figure 8.2—Laminar and turbulent boundary layers (flat plate)

Experiments disclose two types of boundary layer flow. Near the leading edge, the boundary layer flow is laminar; downstream the laminar flow changes at a point called the transition point, and after going through a transition zone of finite length, the boundary layer flow assumes a fully developed turbulent character. Within the turbulent boundary layer, a thin, laminar *sublayer* is formed next to the boundary. Outside the boundary layer, the main fluid flow may be either laminar or turbulent. In the former case, one may find a turbulent boundary layer sandwiched between laminar external flow and laminar sublayer. In the latter case, one may have a laminar layer (near the leading edge) sandwiched between a turbulent main fluid body and the solid surface.

The establishment of 'fully-developed' flow conditions inside a tube takes place similarly. Downstream from the entrance to the tube, the thickness of the annular boundary layer increases until at a certain point it is equal to the radius of the tube, as shown in *Fig. 8.3.* Between the entrance to the tube and this point the flow in the boundary layer may be either laminar or turbulent. As the layer thickens, the main fluid body accelerates. Beyond a distance L^* the flow becomes fully developed, and is laminar if the Reynolds' number $N_R = (V \cdot d)/\nu$, based on the tube diameter and the 'mean'

velocity, is less than 2,100. Fully-developed turbulent flow may be observed beyond the distance L^*, provided the Reynolds' number is greater than about 3,000. If the Reynolds' number falls between

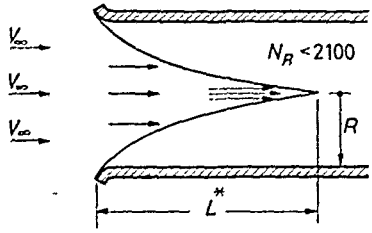

Figure 8.3—Boundary layer at pipe inlet

2,100–3,000, the entire flow is of transition character. Note that in the case of turbulent flow with turbulent boundary layer there exists, nevertheless, a laminar boundary layer near the entry to the tube, as shown in *Fig. 8.4*. The entry length in this case is L^{**}.

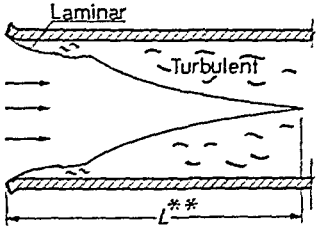

Figure 8.4—Types of boundary layers at pipe inlet

The characteristic velocity distribution of fully developed laminar and turbulent flow inside pipes has been shown in *Figs. 22* and *23*.

The entry length L^* for a laminar boundary layer (*Fig. 8.3*) is estimated to be

$$L^* = 0{\cdot}5 \,.\, D \,.\, N_R$$

where D is the diameter of the tube and N_R is the Reynolds' number based on the mean velocity and the diameter.

Boundary layer investigations are concerned with the determination of:

(*a*) the thickness of the layer,

(*b*) the velocity distribution in the layer, and

(*c*) the shear stresses set up in the layer and the associated frictional drag forces experienced over the surface.

The triple task will be carried out for both laminar and turbulent flow over flat plates and in circular pipes.

8.2 The Thickness of the Boundary Layer. Momentum Theorem

It follows from the definition of the boundary layer that marked velocity changes take place within the layer. The velocity gradient is largest at the wall and gradually diminishes towards the main stream. The flow, in the immediate vicinity of the wall is markedly affected (by the presence of the solid surface) while far away the effects become negligible.

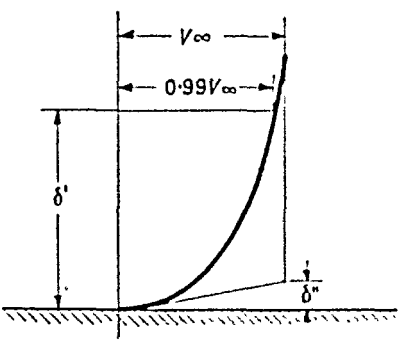

Figure 8.5—Thickness of boundary layer

Difficulty is experienced in defining the boundary layer thickness because of the increase of velocity from zero (at the boundary) to the main stream velocity V takes place asymptotically. One may define the thickness as the distance from the boundary to the point where the velocity differs, say, by 1 per cent from the main stream velocity (shown as δ' in *Fig. 8.5*). Another possibility is to find the intersection of the asymptote and the tangent to the velocity profile drawn at the origin (shown as δ''). Obviously, the two methods yield different results.

A more satisfactory definition, which leads to an expression of greater mathematical use is the 'displacement thickness' given by

$$\delta_d V_\infty = \int_0^\infty (V_\infty - V)\, dy \qquad \ldots.(8.1)$$

where δ_d is the displacement thickness, V_∞ is the approach or main stream velocity, and V is the velocity at a distance y from the surface. The integration is taken along a normal across the stream. It is

apparent that the area $\delta_d V_\infty$ is equal to $\int_0^\infty (V_\infty - V)\, dy$ represented by the shaded area, as shown in *Fig. 8.6.*

Since the mathematical methods for handling boundary flows analytically are complex, it is proposed to arrive at results by means of approximate methods. Such methods were first used by Kármán, who introduced the momentum theorem to solve boundary layer problems.

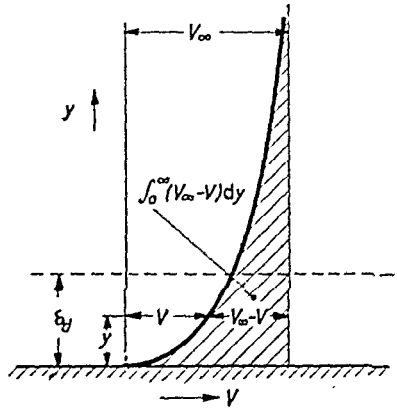

Figure 8.6—Displacement thickness of boundary layer

Consider a flat plate of unit width exposed parallel to a free fluid stream. Over this plate, boundary layers are formed on each side, as shown in *Fig. 8.7.* Application of the theorem of momentum expresses the fact that frictional drag between a fluid and the solid is accompanied by an equivalent change of momentum carried by the fluid. Compare the momentum carried by the fluid at a cross-section 1 upstream from the leading edge of the plate with that at a cross-section 2, distance x downstream from the leading edge. Assume that the velocity is uniform over the first cross-section and has the value V_∞. The velocity normal to the second cross-section at an arbitrary point will be denoted by V. The fluid mass passing in unit time through a layer of thickness dy at the second cross-section is evidently $\rho V\, dy$, where ρ denotes the density of the fluid. This fluid mass had the momentum V_∞ per unit mass passing through the first cross-section and has the momentum V per unit mass when passing through the second cross-section. Hence, the loss of momentum of the fluid mass considered amounts to $\rho V(V_\infty - V)\, dy$ and the total loss of momentum of the fluid in

unit time is $\int_0^\infty \rho V(V_\infty - V)\,dy$, the integral being taken at x across the boundary layer. This amount must be equal to the total frictional force acting on the portion of the plate extending from the leading edge to the distance x. Denoting the boundary stress at the surface of the plate by τ_0, the resistance (drag force) per unit

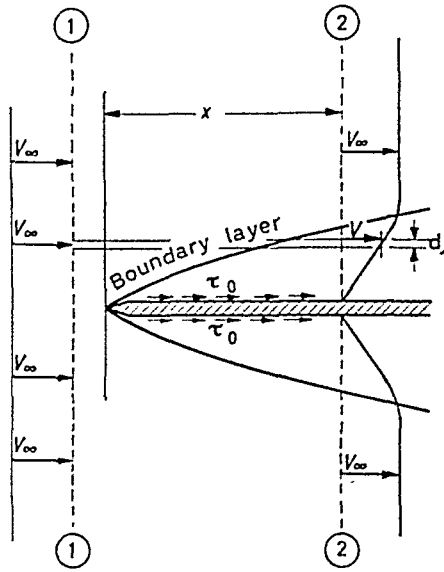

Figure 8.7

width of one side of the plate between the leading edge ($x = 0$) and second cross-section will be

$$D = \int_0^x \tau_0\,dx$$

According to the momentum theorem

$$\int_0^x \tau_0\,dx = \int_0^\infty \rho V(V_\infty - V)\,dy$$

Hence, the local shearing stress at the wall

$$\tau_0 = \frac{d}{dx}\int_0^\infty \rho V(V_\infty - V)\,dy \qquad \ldots.(8.2)$$

Assume now that the boundary layer has a definite thickness δ and that the velocity distribution in the boundary layer follows a general law

$$V = V_\infty \cdot f\left(\frac{y}{\delta}\right)$$

where the function $f(y/\delta)$ is unknown. Putting $y/\delta = \eta$, one has $y = \delta\eta$ and $\mathrm{d}y = \delta\,\mathrm{d}\eta$. Substituting these in Eq. 8.2,

$$\tau_0 = \frac{\mathrm{d}}{\mathrm{d}x}\int_0^\delta \rho V_\infty f(\eta)[V_\infty - V_\infty f(\eta)]\,\delta\,\mathrm{d}y =$$

$$= \frac{\mathrm{d}}{\mathrm{d}x}\rho V_\infty^2\,\delta\int_0^1 [f(\eta) - f(\eta)^2]\,\mathrm{d}\eta$$

Since the integral, for a given velocity distribution, yields a finite value, and the quantity ρV_∞^2 is independent of η, the local shear stress at x

$$\tau_0 = \alpha\rho V_\infty^2 \frac{\mathrm{d}\delta}{\mathrm{d}x} \qquad \ldots.(8.3)$$

where

$$\alpha = \int_0^1 [f(\eta) - f(\eta)^2]\,\mathrm{d}\eta \qquad \ldots.(8.4)$$

The application of the momentum theorem replaces the problem of skin friction by the problem of velocity distribution in the boundary layer. The frictional drag may be determined by measurement of the velocity distribution across the boundary layer.

Example

8.1. Experiments carried out on a flat plate set parallel to the direction of flow of a uniform air current yielded the following associated values of the distance y in., and the velocity of flow V ft./sec. for a station 9 in. back. from the leading edge:

y = 0·025,	0·05,	0·075,	0·1,	0·125	
V = 2·7,	4·6,	7·4,	8·4,	9·1	
y = 0·15,	0·175,	0·2,	0·225,	0·25	and over
V = 9·7,	10·2,	10·6,	10·74,	10·8,	10·8

For this station determine:

(*a*) the displacement thickness of the boundary layer;

(*b*) the drag experienced by the two sides of the plate between the leading edge and the station. The plate is 2 ft. wide.

Data:

Approach velocity: V_∞ = 10·8 ft./sec.

Specific weight of air: 0·075 lb./ft.

Kinematic viscosity: 1·67 × 10^{-4} ft.²/sec.

Solution.—In the following table the quantities $V_\infty - V$ and $V(V_\infty - V)$ are shown as functions of distance y.

Y	0·025	0·05	0·075	0·1	0·125	0·15	0·175	0·20	0·225	0·250
$V_\infty - V$	8·1	6·2	3·4	2·4	1·7	1·1	0·6	0·2	0·6	0·0
$V(V_\infty - V)$	21·9	28·5	25·2	20·2	15·5	10 7	6·1	2·12	0·64	0·0

Plot $V_\infty - V$ and $V(V_\infty - V)$ against V (*see Fig. 8.8.*) and obtain the areas

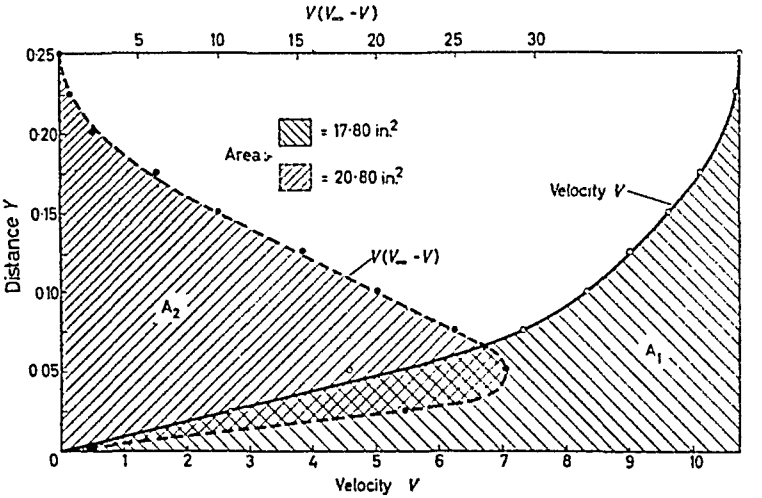

Figure 8.8

under the curves. Thus one finds that $A_1 = 17{\cdot}8$ in.^{2} and (*a*) the displacement thickness

$$\delta_d = \frac{17{\cdot}8 \times 0{\cdot}04}{10{\cdot}8} = 0{\cdot}066 \text{ in.}$$

(*b*) For the drag one finds $A_2 = 20{\cdot}8$ in.^{2} hence the drag

$$D = bpA_2 = 2 \times \frac{0{\cdot}075}{32{\cdot}2} \times 20{\cdot}8 \times \frac{0{\cdot}04}{12} \times 4 = 0{\cdot}0012 \text{ lb.}$$

8.3 The Properties of the Laminar Boundary Layer

In the case of laminar motion, we may also write for the boundary stress

$$\tau_0 = \mu \left[\frac{\mathrm{d}V}{\mathrm{d}y}\right]_{y=0}$$

Substituting $V = V_\infty f(\eta)$ and $\mathrm{d}y = \delta\, \mathrm{d}\eta$

$$\tau_0 = \mu \frac{V_\infty}{\delta} \left[\frac{\mathrm{d}f(\eta)}{\mathrm{d}\eta}\right]_{\eta=0} \qquad \ldots\ldots(8.5)$$

Denoting $\dfrac{df(\eta)}{d\eta_{\eta=0}} = \beta$ and equating 8.3 with 8.5

$$\alpha\rho V_\infty^2 \frac{d\delta}{dx} = \mu \frac{V_\infty}{\delta}\beta \qquad \ldots.(8.6)$$

Eq. 8.6 can be readily integrated, giving the thickness of the boundary layer as

$$\delta = \sqrt{\left(2\frac{\beta}{\alpha}\frac{\mu}{V_\infty \rho}x\right)} \qquad \ldots.(8.7)$$

With this value of δ the boundary shear stress becomes (Eq. 8.3)

$$\tau_0 = \sqrt{\frac{\alpha\beta}{2} \cdot \frac{\mu\rho V_\infty^3}{x}} \qquad \ldots.(8.8)$$

and the surface drag D, acting between 0 and x, on one side of the plate, for unit width,

$$D = \int_0^{x_0} \tau_0 \, dx = 2\sqrt{2\alpha\beta\mu\rho V_\infty^3 x} \qquad \ldots.(8.9)$$

For a plate of length $x = l$, the laminar drag

$$D = KV^{\frac{3}{2}}$$

where $K = 2\sqrt{2\alpha\beta\mu\rho l}$.

In modern practice, the shear stress is frequently replaced by the non-dimensional skin-friction drag coefficient, defined as

$$C_D = \frac{\text{drag force}}{\frac{1}{2}\rho V_\infty^2 \times \text{wetted area}} \qquad \ldots.(8.10)$$

For unit width, $A = x$ and

$$C_D = \frac{D}{\frac{1}{2}\rho V_\infty^2 x} = 2\sqrt{2\alpha\beta \frac{\mu}{xV_\infty\rho}}$$

Introducing the Reynolds' number of the plate,

$$N_{Rx} = \frac{V_\infty \cdot x}{\nu}$$

the drag coefficient becomes

$$C_D = \frac{2(2\alpha\beta)^{\frac{1}{2}}}{N_{Rx}^{\frac{1}{2}}} \qquad \ldots.(8.11)$$

It follows from the foregoing that the displacement thickness given by Eq. 8.1 becomes

$$\delta_d = \int_0^\infty \left(1 - \frac{V}{V_\infty}\right) dy = \delta \int_0^1 [1 - f(\eta)] \, d\eta \qquad \ldots.(8.12)$$

By assuming various forms for $f(\eta)$, Eqs. 8.7, 8.11 and 8.12 yield approximate values of δ, δ_d and C_D. For example, experiments indicate that the velocity distribution near the surface varies almost proportionally with the distance. Assume that in this region

$$V = a + b\frac{y}{\delta}$$

From the boundary conditions: $V = 0$ where $y = 0$ and $V = V_\infty$ where $y = \delta$. Thus

$$V = V_\infty \frac{y}{\delta} = V_\infty \cdot \eta$$

Hence, the value of the numerical form factors α and β can be calculated, giving

$$\alpha = \int_0^1 (\eta - \eta^2)\, \mathrm{d}\eta = \frac{\eta^2}{2} - \frac{\eta^3}{3}$$

$$= \frac{1}{2} - \frac{1}{3} = \frac{1}{6}$$

and

$$\beta = f'(\eta)_{\eta=0} = 1$$

With these values, the effective thickness of the laminar boundary layer

$$\delta = 3{\cdot}46\, \frac{x}{N_{Rx}^{\frac{1}{2}}}$$

and the displacement thickness

$$\delta_d = \delta \int_0^1 (1 - \eta)\, \mathrm{d}\eta = \frac{\delta}{2}$$

giving

$$\delta_d = \frac{1{\cdot}73x}{N_{Rx}^{\frac{1}{2}}} \qquad \ldots.(8.13)$$

Other assumed forms of $f(y)$ yield the following values:

$f(\eta)$	$\delta_d \cdot (N_{Rx}^{\frac{1}{2}}/x)$
$2\eta - \eta^2$ . . .	1·83
$\frac{3}{2}\eta - \frac{1}{2}\eta^3$ . . .	1·74
$2\eta - 2\eta^3 + \eta^4$ . . .	1·75
Exact solution . . .	1·73

For the skin-friction drag coefficient, we calculate $2(2\alpha\beta)^{1/2} = 1{\cdot}155$, whilst the correct numerical constant was found to be 1·328; hence for laminar flow over plates

$$C_D = \frac{1{\cdot}328}{N_{Rx}^{\frac{1}{2}}} \qquad \ldots.(8.14)$$

It is noted that the drag coefficient given by Eq. 6.14 represents the 'mean' of the local skin-frictional drag for a plate of length x.

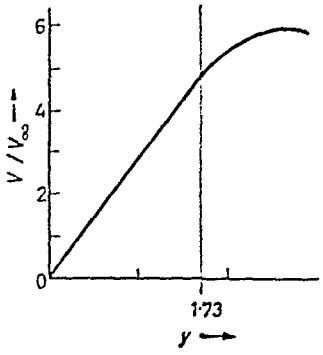

Figure 8.9

The 'local' skin-frictional drag C_f may then be derived from the mean drag C_d considering that

$$\int_0^x C_f \, \mathrm{d}x = C_D x$$

whence

$$C_f = \frac{\mathrm{d}}{\mathrm{d}x}(C_D x)$$

For laminar flow

$$C_f = \frac{\mathrm{d}}{\mathrm{d}x}\left[\frac{1{\cdot}328}{N_{Rx}^{\frac{1}{2}}} x\right] = \frac{0{\cdot}664}{N_{Rx}^{\frac{1}{2}}}$$

The velocity distribution in the laminar boundary layer was analytically solved by Blasius and the result is given in graphical form in *Fig. 8.9*. It appears that up to $yN_{Rx}^{\frac{1}{2}}/x = 1{\cdot}73$ the ratio V/V_∞ is approximately proportional to η, which explains why such a simple function as $f(\eta) = \eta$ furnishes an almost correct numerical constant for the displacement thickness. The free stream velocity is practically reached for $\eta = 6{\cdot}0$ and, therefore, an approximate formula for 'effective' thickness of the boundary layer† is given by

$$\delta = 6{\cdot}0 \frac{x}{N_{Rx}^{\frac{1}{2}}} \qquad \ldots.(8.15)$$

† Prandtl suggests 5·2, others 5·85.

The results given by Eqs. 8.13 and 8.15 may be summarized as follows:

(*a*) The increase in the thickness of the laminar boundary layer is proportional to the square root of the distance from the leading edge and inversely proportional to the square root of the relative velocity between plate and fluid.

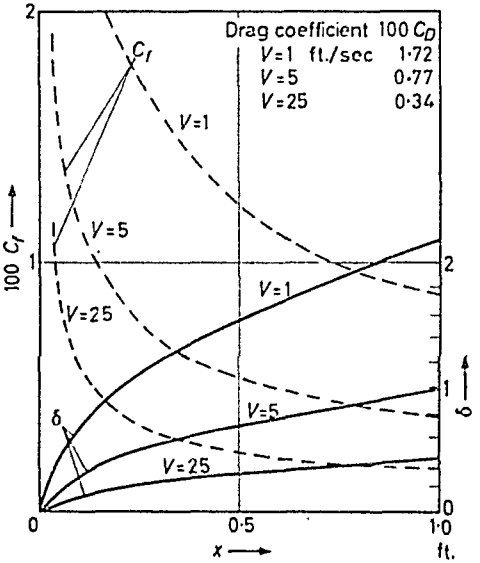

Figure 8.10—Boundary layer thickness and local skin friction over a flat plate. (Air flowing)

(*b*) The drag coefficient of the plate is inversely proportional to the square root of the Reynolds' number of the plate and the local skin friction is half of this value.

(*c*) The drag force acting on the plate is proportional to the 3/2 power of the velocity.

Depending on the turbulence level in the outer stream laminar boundary layers are found up to $N_R = 700{,}000$. Transition starts earlier if the turbulence level is high and $N_R = 200{,}000$ may be assumed as approximately the lower critical value.

In *Fig. 8.10*, the local skin-friction coefficient and the boundary layer thickness are shown over a plate for velocities 1, 5, and 25 ft./sec. (Air flowing.)

8.4 The Properties of the Turbulent Boundary Layer

When considering a turbulent boundary layer, the assumption

is made that the layer is turbulent right from the leading edge. On earlier experimental evidence obtained, V/V_∞ may be assumed to be proportional to the seventh root of the distance y from the wall. Accordingly

$$V/V_\infty = (y/\delta)^{1/7} \qquad \ldots.(8.16)$$

With this expression, the value of the numerical form factor

$$\alpha = \int_0^1 [f(\eta) - f(\eta)^2]\,\mathrm{d}\eta = \int_0^1 \eta^{1/7}\,\mathrm{d}\eta - \int_0^1 \eta^{2/7}\,\mathrm{d}\eta$$
$$= \frac{7}{8} - \frac{7}{9} = \frac{7}{72}$$

Substituting this into Eq. 8.4,

$$\frac{\tau_0}{\rho V_\infty^2} = \frac{7}{72}\frac{\mathrm{d}\delta}{\mathrm{d}x} \qquad \ldots.(8.17)$$

The calculation of form factor β may not be carried out with Eq. 8.5, as the seventh root law approaches the wall with a tangent of zero angle. The difficulty may be overcome by assuming analogy between turbulent boundary layer flow over surfaces and turbulent flow in pipes. In this case, the wall friction based on Blasius' empirical formula may be used (Eq. 4.11), which is regarded as reliable for a limited range of Reynolds' number.

Combining Eqs. 4.11 and 4.18, (Chapter 4)

$$\frac{\tau_0}{\rho \bar{V}^2} = \frac{f}{8} = \frac{0{\cdot}316}{8N_R^{1/4}} \qquad \ldots.(8.18)$$

where the Reynolds' number is based on the diameter of the pipe and on the average velocity, $\bar{V}$. In making use of the formula, imagine that the pipe is cut longitudinally and its surface unrolled so as to form a plane. The thickness of the boundary layer will then be equal to half the diameter of the pipe $\delta = d/2$ and the velocity V_∞ at the boundary of the layer will be equal to the maximum velocity prevailing at the pipe centre *i.e.*, $V_\infty = V_{max}$. The latter may be taken as $V_{max} = 1{\cdot}235\bar{V}$ for a considerable range of Reynolds' numbers. Substituting these values into Eq. 8.17,

$$\frac{\tau_0}{\rho V_\infty^2} = \frac{0{\cdot}023}{N_{R\delta}^{1/4}} \qquad \ldots.(8.19)$$

where $N_{R\delta} = \dfrac{V_\infty \delta}{\nu}$.

Equating 8.17 and 8.19, one obtains

$$\frac{7}{72}\frac{\mathrm{d}\delta}{\mathrm{d}x} = 0{\cdot}023\nu^{1/4}V_\infty^{1/4}\delta^{-1/4}$$

which, upon rearranging terms, yields a differential equation

$$\delta^{1/4}\,\mathrm{d}\delta = 0{\cdot}236\nu^{1/4}V_\infty^{-1/4}\,\mathrm{d}x$$

Integration between limits δ and x yields

$$\frac{4}{5}\delta^{5/4} = 0{\cdot}236\nu^{1/4}V_\infty^{-1/4}x$$

Introducing the Reynolds' number of the plate $\frac{V_\infty x}{\nu}$ and rearranging terms gives

$$\delta = \frac{0{\cdot}377x}{N_{Rx}^{0{\cdot}2}} \qquad \ldots.(8.20)$$

With Eq. 8.20, the drag coefficient can be calculated. Since

$$D = \int_0^x \tau_0\,\mathrm{d}x = \alpha\rho V_\infty^2\,\delta$$

the drag coefficient

$$C_D = \frac{D}{\frac{1}{2}\rho V_\infty^2 x} = \frac{2\alpha\delta}{x} = \frac{0{\cdot}072}{N_{Rx}^{0{\cdot}2}} \qquad \ldots.(8.21)$$

For Reynolds' numbers greater than 3×10^6, the velocity distribution deviates from the 1/7 power law. It has been found that the exponent decreases with increasing Reynolds' numbers. In order to find laws valid in the whole range and especially valid for large Reynolds numbers, allowing extrapolation to 'full scale' conditions, a more systematic investigation of the nature of turbulent flow becomes inevitable. These investigations lead to the replacement of the seventh power law, by the logarithmic velocity distribution law, and details of such investigations are discussed in article 8.10. The main results, concerning turbulent flow over flat plates, are summarized here as follows:

(1) the drag coefficient is given by†

$$\frac{0{\cdot}242}{\sqrt{C_D}} = \log_{10}(N_{Rx}C_D) \qquad \ldots.(8.22)$$

† Eq. 8.22 is called the 'Schoenherr' formula. Results of more recent experiments on the frictional resistance of smooth plane surfaces in turbulent flow is given by G. Hughes, Institute of Naval Architects, 1954. It appears that there is no single friction line, but a family of lines varying with the length/breadth ratio of the flat plates.

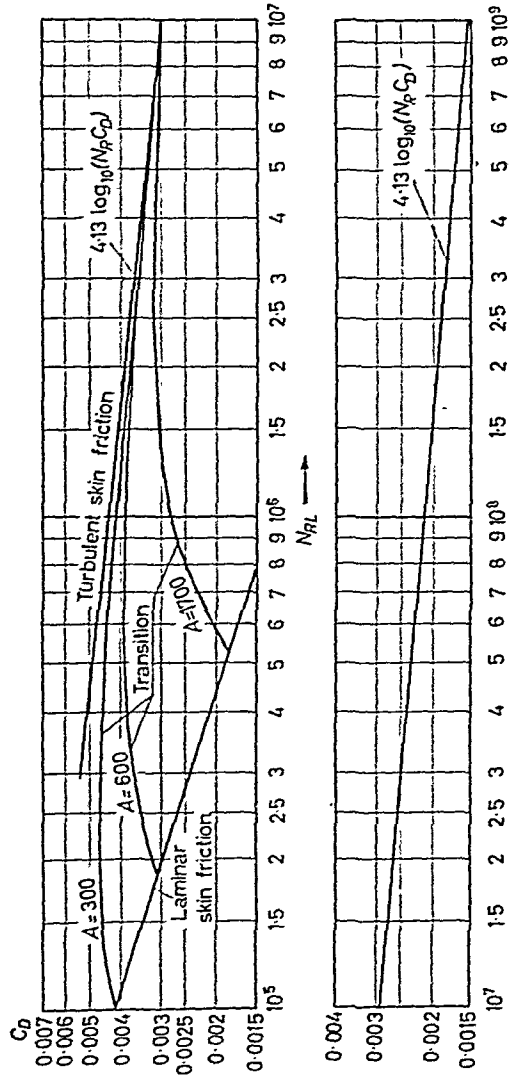

Figure 8.11—Drag coefficient (two dimensional) of flat plate surfaces.
(*From* Modern Developments in Fluid Mechanics *by courtesy of The Aeronautical Research Council*)

(2) the thickness of the boundary layer is given by

$$\delta = 0{\cdot}38x(C_D)^{\frac{1}{2}} \qquad \ldots.(8.23)$$

(3) the velocity distribution in the boundary layer is logarithmic and approximately given by

$$V/V_\infty = 1 - 4{\cdot}15C_D^{\frac{1}{2}} \log_{10} \frac{\delta}{y} \qquad \ldots.(8.24)$$

Thus, with the aid of the drag coefficient, both the velocity distribution and the layer thickness may be calculated. In order to facilitate such calculation, the drag coefficients for both laminar and turbulent flow are presented in graphical form in *Fig. 8.11.*

The transition between laminar and turbulent boundary layers is also shown in *Fig. 8.11.* It appears that there is no definite critical value of N_R for the transition. The critical value depends on the turbulence level in the outside stream. It is to be expected, however, that under similar conditions the transition depends on the Reynolds' number based on the boundary layer thickness $N_\delta = \frac{V\delta}{\nu}$. Critical values of N_δ were found to lie between 1,650 and 6,000. A family of transition curves are shown in *Fig. 8.11.*

Since the formula for the drag coefficient given by Eq. 8.22 is complex for numerical computations, an empirical interpolation formula has been developed by Prandtl and Schlichting that agrees with the values of Eq. 8.22 up to $N_R = 10^9$. The Prandtl–Schlichting formula for turbulent flow developed from the leading edge is

$$C_D = \frac{0{\cdot}455}{[\log_{10} N_{Rx}]^{2{\cdot}58}} \qquad \ldots.(8.25)$$

Since the total skin friction of smooth surfaces consists of the skin friction of the forward portion where the flow is laminar and that of the rear portion where the flow is turbulent, it is desirable to obtain a formula which covers the laminar zone at the leading edge as well as the transition and the turbulent zone. So far, such a formula has not been derived analytically but it is suggested that an empirical formula of the form

$$C_D = C_{D\text{turb.}} - \frac{A}{N_{Rx}} \qquad \ldots.(8.26)$$

would represent the average drag-coefficient, where C_D is given by Eq. 8.25 and the constant A depends on the turbulence level in the outside stream. It is further suggested that taking 1,700 for A would characterize the state of affairs in which there is little or no disturbance in the stream and it must be altered for other cases. The formula Eq. 8.26 may be used in the range of Reynolds'

numbers 10^5–10^6 when the two different skin frictions contribute to drag in about the same order. If, however, the Reynolds' number is much larger, the skin friction in the laminar and in the transition zone may be replaced by the turbulent one and the drag computed with the aid of Eq. 8.25.

In concluding this chapter, it is necessary to emphasize that drag due to skin friction is the smallest possible resistance experienced by any body exposed to a fluid stream.

Examples

8.2. A thin flat plate 1 ft. wide and 2 ft. long is suspended and exposed parallel to air flowing with a velocity of 10 ft./sec.
Calculate the drag force on the plate in

(a) when the 1 ft. edge is parallel to the stream
(b) when the 2 ft. edge is parallel to the stream
(c) account for the difference between the drags under the two conditions,

$$\nu = 1{\cdot}6 \times 10^{-4}\ \text{ft}^2/\text{sec.}, \quad \rho = 0{\cdot}00233\ \text{slugs/ft}^3.$$

Solution.—Assuming laminar flow, the drag coefficient is given by equation

1-ft. edge parallel to stream	2-ft. edge parallel to stream
Reynolds' number $N_R = \dfrac{10 \times 1 \times 10^4}{1{\cdot}6} = 6{\cdot}2 \times 10^4$	$N_R = \dfrac{10 \times 2 \times 10^4}{1{\cdot}6} = 12{\cdot}4 \times 10^4$
Drag coefficient $C_D = \dfrac{1{\cdot}328}{10^2\sqrt{6{\cdot}2}} = 5{\cdot}32 \times 10^{-3}$	$C_D = \dfrac{1{\cdot}328}{10^2\sqrt{12{\cdot}4}} = 3{\cdot}8 \times 10^{-3}$
Drag (on both sides) $D = \frac{1}{2} \times 0{\cdot}00233 \times 2 \times 2 \times 10^2 \times 5{\cdot}32 \times 10^{-3} = 2{\cdot}48 \times 10^{-3}$ lb.	$D = \frac{1}{2} \times 0{\cdot}00233 \times 2 \times 2 \times 10^2 \times 3{\cdot}8 \times 10^{-3} = 1{\cdot}77 \times 10^{-3}$ lb.

The reason for the difference is the local skin friction C_f which is large at the leading edge; C_D is average value of C_f.

8.3. A 'honeycomb' mesh is to be fitted into a duct as an air straightener. It is made up of flat perpendicular metal strips 1 in. wide, and the pitch of the mesh in both directions is also 1 in.

Calculate the pressure drop across the straightener (in. W.G.), at an air velocity of 100 ft./sec.

Neglect the thickness of the metal and assume laminar flow over the plates.

Kinematic viscosity of air is $\nu = 16 \times 10^{-4}$ ft.^{2}/sec.

Solution.—Reynolds' number $N_R = \dfrac{100 \times 1}{12 \times 1{\cdot}6} \times 10^4 \therefore N_R^{1/2} = 228$

Drag coefficient $C_D = \dfrac{1{\cdot}328}{228} = 5{\cdot}82 \times 10^{-3}$

Drag over surface of wall enclosing 1 in.^{2} of opening, expressed in terms of skin friction

$$D = 5{\cdot}82 \times 10^{-3} \times \tfrac{1}{2} \times \frac{0{\cdot}075}{32{\cdot}2} \times 100^2 \times \frac{4 \times 1}{144} \simeq 0{\cdot}0019 \text{ lb.}$$

On the other hand, drag expressd in terms of pressure drop across the mesh

$$D = (p_1 - p_2)A$$

Hence pressure drop

$$p_1 - p_2 = \frac{D}{A} = \frac{0{\cdot}0019 \times 144}{5{\cdot}2} = 0{\cdot}0527 \text{ in. W.G.}$$

(A being ·1 in.^{2})

8.5 Flow over Curved Surfaces, Boundary-layer Separation

In the discussion on flow over flat plates it was assumed that no pressure gradient existed in the main flow. We shall now consider

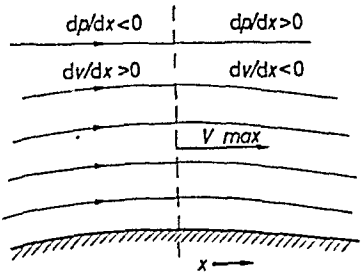

Figure 8.12—Flow over a slightly curved surface

the course of events when the fluid is moving with an increasing or decreasing pressure. It is noted that since the pressure is nearly constant across any section of the boundary layer, the pressure gradient is operative right across the layer.

Consider first the flow over a slightly curved plate as shown in *Fig. 8.12*. As the flow passes over the surface, the streamlines are displaced near the plate and fluid particles are first subject to acceleration, then after passing through a region where the velocity attains a maximum value, deceleration takes place. The maximum

velocity is attained somewhere near the minimum cross-sectional area open for flow. In such a flow a negative pressure gradient exists upstream ($dp/dx < 0$) and a positive pressure gradient downstream ($dp/dx > 0$). Far away from the body, the main fluid velocity (V_∞) may be considered constant and equal to the approach velocity.

On the forward portion of the body, the rate of increase of the boundary-layer thickness is retarded because of the favourable

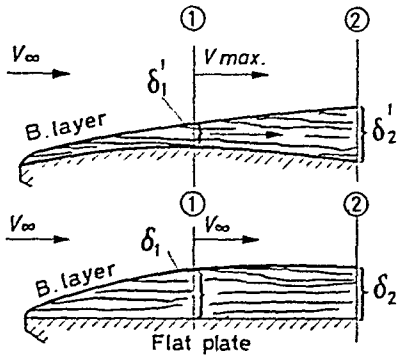

Figure 8.13

pressure gradient (increasing velocity). In comparison with the *flat* plate, for a given approach velocity the increase is smaller at corresponding cross-sections. Downstream from the maximum velocity region, however, the rate of increase of the boundary layer becomes more pronounced because of deceleration (adverse pressure gradient). In comparison with a flat plate, for a given approach velocity the rate of increase of the boundary layer is greater at corresponding cross-sections, as shown in *Fig. 8.13. Provided, however, that the surface curvature is only slight, the boundary layer will follow the surface outline right along the body.*

Consider now a body with a substantial curvature, for example a cylinder or a sphere. Again on the forward portion of the body a thin boundary layer is formed, but further downstream the increase of the boundary-layer thickness may be so rapid that the fluid is unable to flow along the surface, and breaks away instead of following the body outline.

The particular point where the break away or 'separation' occurs is called the separation point. Separation can occur only in an adverse pressure gradient, its location depending on the nature of the boundary layer. Laminar layers separate much more readily

than turbulent layers do, which 'stick' to the surface over considerable distances in an adverse gradient before they separate.

The mechanism of separation may be studied by considering the velocity distribution outside and within the boundary layer. An approximate representation of the events is shown (in two dimensions) in *Fig. 8.14*, when the flow passes over a cylindrical body. It is assumed that separation takes place downstream from the vertical centre line (C.L.).

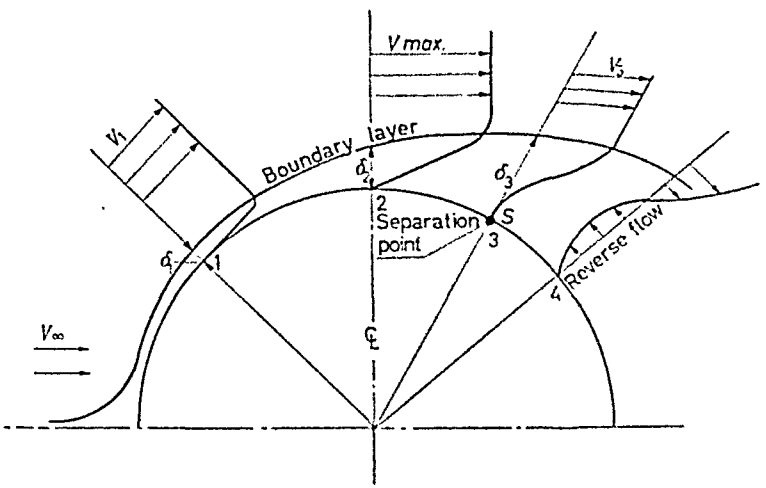

Figure 8.14—Flow separation from a cylindrical surface

On the forward portion of the body the velocity in the main flow increases (1) and a favourable pressure gradient retards the growth of the boundary layer. In going downstream, the layer naturally continues to thicken (2) and passes into a region where rapid thickening occurs (2–3). In this region the velocity profile within the boundary layer changes considerably. Finally at some point (3) the tangent drawn to the velocity profile at the surface becomes normal to the surface. This is the point where the boundary layer separates from the surface. Downstream (4) from the separation point a slow reverse flow, in the direction of the pressure gradient, sets in. The phenomenon may be comprehended by considering the rapidly decreasing energy and momentum of the fluid *in the boundary layer* working against an adverse pressure gradient.

A well-known example in which the flow separates from the walls in this way is that of flow through a diffuser, or pipe of increasing cross-section. In this case, since in steady flow the same

amount of fluid must pass through any cross-section, if the fluid followed the walls the velocity would decrease and the pressure would increase as the cross-section increased. The fluid in the boundary layers at the walls is moving all the way along against an adverse pressure gradient. After a certain distance, which decreases with increasing pressure gradient, the stream leaves the walls (at point S) and forms a jet as shown in *Fig. 8.15a*. In a well

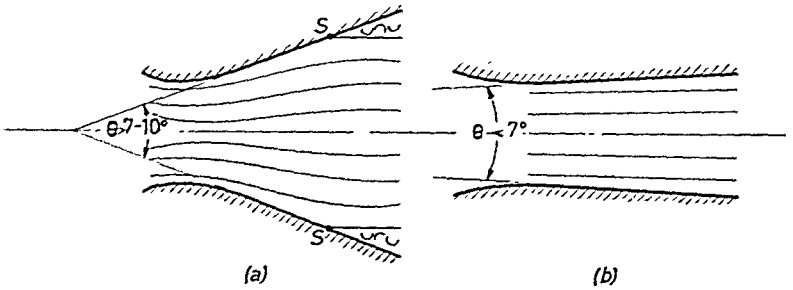

Figure 8.15—Separated and attached flow in diffusers

designed diffuser, with a taper of 5–7° included angle, no separation takes place, and frictional losses are reduced to a minimum (*see Fig. 8.15b*).

8.6 Form Drag. The Wake

In all cases where separation occurs, large frictional forces tangential to the flow initiate the generation of eddies and vortices downstream from the separation point. The affected downstream region is called the wake. In maintaining these eddies and vortices energy is continuously dissipated which gives rise to a drag in addition to the skin friction. This additional drag will be called 'form' drag, and is of quite different nature from the skin friction. The magnitude of the form drag is closely associated with the size and frequency of the eddies, the width of the wake, and this in turn with the position of the separation point. For streamlined bodies, separation takes place near the rear of the body, the form drag is then small and drag due to skin friction predominates. This may, in fact, be taken as a definition of a streamlined body. For 'bluff' obstacles, on the other hand, the skin friction drag is small compared with the form drag.

In *Fig. 8.16* the points of separation and the wake behind streamlined and bluff bodies are shown. In case of a streamlined body, the separation point is positioned near the trailing edge and the

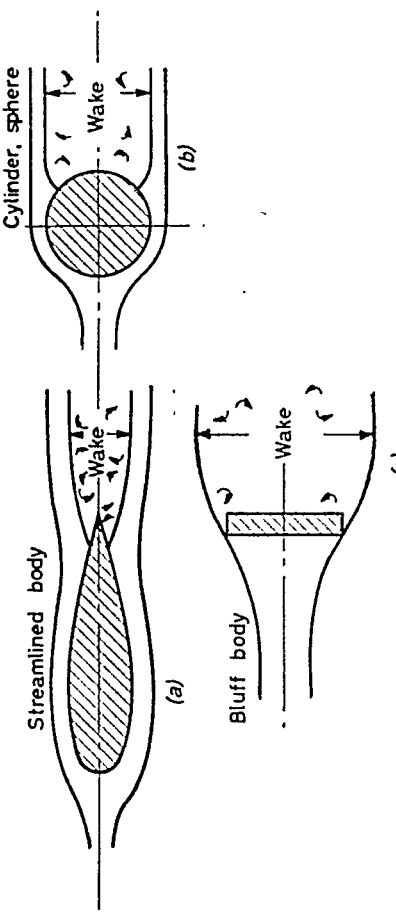

Figure 8.16—Approximate representation of flow separation from various bodies

width of the resulting wake is small (*Fig. 8.16a*). The size of the wake appears to be greater in the case of a cylinder (*Fig. 8.16b*) or a sphere and greater still in the case of a flat plate (*Fig. 8.16c*) or a disc placed perpendicular to the stream.

We will now consider:

(1) the origin and mechanism of the wake, and (2) the factors affecting separation.

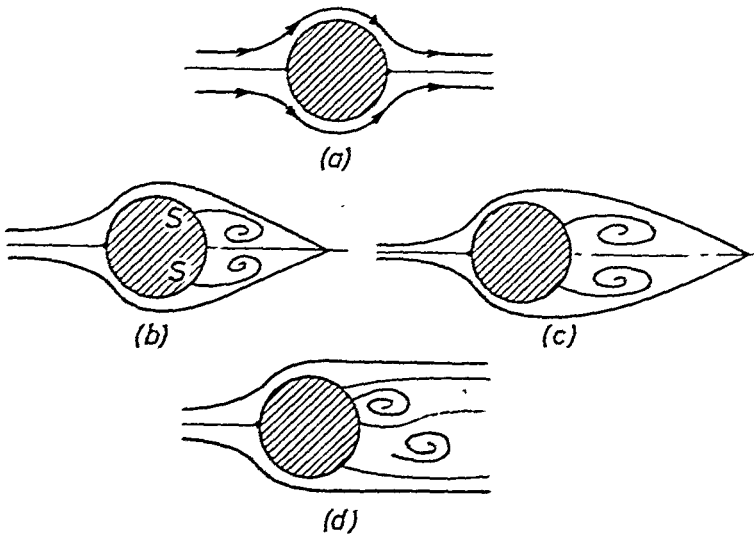

Figure 8.17—Development of separation

Photographic studies show that the flow pattern in the wake changes with the Reynolds' number and with the time counted from the beginning of the motion. First consider the 'origination' of the wake when the motion is starting from rest. The discussion will be limited to two dimensional flow around a bluff body (*e.g.*, a cylinder placed perpendicularly to the flow and extending to infinity).

Immediately after the motion starts, the streamlines close behind the body (*Fig. 8.17a*) and a forward and rear stagnation point may be observed. After a short time, separation points make their appearance with the associated reverse flow behind the body.

As a result of the reverse flow, two vortices with opposite rotation are formed (*Fig. 8.17b*) which increase their intensity with time. Gradually the shape of the vortices changes and

becomes longer and longer in the direction of the flow (*Fig. 8.17c*). Finally the vortices break away from the body surface (*Fig. 8.17d*) and continue to move and to spread downstream. When steady conditions are reached the final flow-pattern will depend on the flow velocity, more accurately, on the Reynolds' number.

Figure 8.18—Vortex street

For a certain range of Reynolds' number, the vortices are alternately shed from the body and form a vortex 'street'.†

The vortex street consists of a double row of vortices arranged in such a way that the vortices in one row are opposite the points half way between the vortices in the other row (see *Fig. 8.18*).

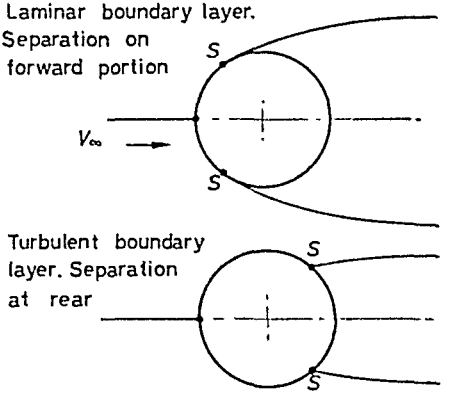

Figure 8.19

However, the vortex street may only be observed over a certain distance downstream, after which the regularity disappears and the motion in the wake becomes irregular.‡

At very low Reynolds' numbers (*e.g.*, 20) the vortices shed behind the body remain stationary and form a trailing vortex pair. The flow closes behind these and the length of the wake becomes limited

† This vortex street is generally called the Kármán Vortex Street.
‡ Richards; R & M 1590, 1934.

to the neighbourhood of these vortices (as shown in *Fig. 8.17c*). On the other hand at higher Reynolds' numbers (about 2,500) the vortices diffuse so rapidly after the formation that it is no longer possible to observe a vortex street. In the absence of individual eddies, one may consider the wake as a form of turbulent zone.

Experiments show that the width of the wake depends principally on the type of boundary layer formed on the body surface. It was pointed out earlier that turbulent boundary layers resist separation whilst laminar boundary layers separate readily, so that separation points of a turbulent layer are positioned further downstream. It then follows that the wake is broader in the case of a laminar boundary layer. The effect is shown in *Fig. 8.19.*

The same mechanism that controls transition along a flat plate holds for a body. For a specified surface roughness and fluid velocity, the transition occurs at a constant value of the Reynolds' number (approximately),

$$N_R = \frac{V_\infty L}{\nu} = \text{CONSTANT}$$

where L is the distance along the surface between stagnation point and transition point, and V_∞ is the approach velocity. With increasing approach velocity, the transition point moves forward, but as long as the transition point would occur downstream from the separation point the flow will have laminar boundary layer character. When the transition point moves upstream from the separation point, however, the boundary layer becomes turbulent and resists separation; so that the separation point moves downstream, resulting in a smaller wake. Experiments conducted on circular cylinders and spheres show that the contraction of the wake occurs around $N_R = 1{\cdot}20\text{–}3{\cdot}80 \times 10^5$, depending on surface roughness and turbulence level in the outer stream. The drag falls considerably over this 'critical' range although the velocity increases.

8.7 Profile Drag

The profile drag of a body is the sum of skin friction and form drag. Since both skin friction and separation depend primarily on the Reynolds' number so also does the profile drag.

Dimensional considerations† suggested that the drag be expressed as

$$D = C_D \times \tfrac{1}{2}\rho V_\infty^2 \times A_P \qquad \ldots.(8.27)$$

where $\frac{1}{2}\rho V_\infty^2$ is the dynamic head of the main stream, A_P is the *projected* area‡ of the body (perpendicular to the flow) and C_D is

† See Chapter 7.
‡ In the case of skin friction A is the wetted area.

the drag coefficient. This latter, in turn, may then be expressed as a function of the Reynolds' number, and we write $C_D = f(N_R)$; more generally, since surface roughness and turbulence levels both affect the location of the separation points, we write $C_D = f$ (N_R, surface roughness, turbulence level). In *Fig. 8.20*, drag coefficients

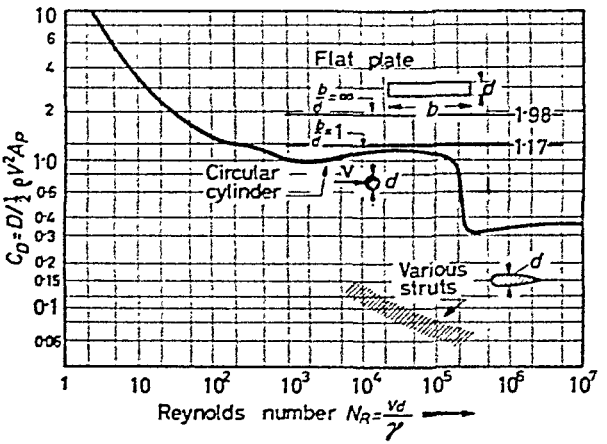

Figure 8.20—Drag coefficients of some two dimensional bodies

of various two dimensional bodies are plotted against Reynolds' number. For a specified fluid velocity the Reynolds' number is first calculated and the drag coefficient found from *Fig. 8.20*; the drag of the body is then obtained with the aid of Eq. 8.27.

For a circular cylinder, the drag coefficient falls rapidly with increasing Reynolds' number and at first the drag is approximately proportional to the velocity. The value of N_R at which the shedding of vortices commences is uncertain, but it is probably about 50. As N_R increases, C_D falls steadily to the minimum value of 0·95 at $N_R = 1{,}800$ and then rises to 1·2 at $N_R = 30{,}000$. In the region of N_R between 3×10^4 and 18×10^4, C_D appears to be independent of N_R and the quadratic resistance law is found to hold with reasonable accuracy. A marked fall from 1·2 to 0·36 occurs at about $N_R = 10^5$. This is the critical state when the boundary layer becomes turbulent and the separation point moves downstream.

Streamlined bodies appear to have considerably lower drag coefficients than cylinders, whereas the flat plate, placed perpendicularly to the flow, has higher resistance. Perforated plates have higher resistances still.

Drag coefficients for bodies of revolution, like spheres, ellipsoids, airship hulls, are presented in *Fig. 8.21*. The curves show a similar trend to that obtained for two dimensional bodies.

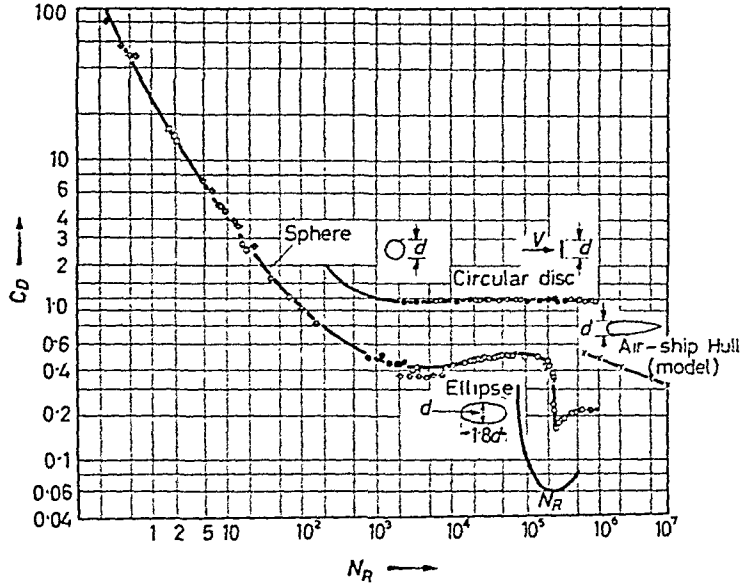

Figure 8.21—Drag coefficients of some bodies of revolution

The values of drag coefficients presented in *Figs. 8.20* and *8.21* are obtained from experiments conducted in low-turbulence wind-tunnels on bodies with smooth surface-finish. Changes in the surface

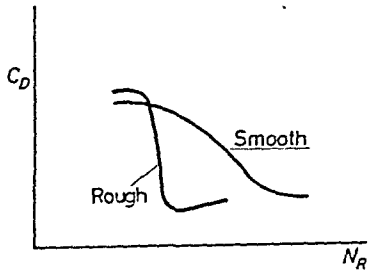

Figure 8.22—Effects of surface roughness on transition

roughness, however, cause considerable variation in these values.

In *Fig. 8.22*, the results of experiments† carried out on both smooth and sand-coated cylinders in the critical range, are shown.

† Fage and Warsap: A.R.C. Reports and Memoranda No. 1283, 1930.

The rough surfaces were obtained by wrapping sheets of sandpaper around the cylinder. It appears that a decrease in C_D occurs at a lower value of N_R and becomes smaller as the surface roughness is increased.

Finally, the effect of turbulence in the stream on the drag in the critical range is considered. Investigations on a cylinder placed downstream from a screen, consisting of wire-rope netting disclose a lateral shift of the curve in the direction of decreasing Reynolds'

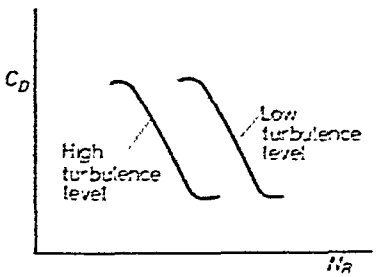

Figure 8.23—Effects of turbulence on transition

numbers as the distance from the screen decreases. Obviously, with an increase in turbulence level in the outer stream the downstream shift of the separation points (accompanied by the drop in C_D) occurs at a lower Reynolds' number. The effect is shown in *Fig. 8.23.* In other words, increasing turbulence level in the outer stream produces turbulent boundary layers.

8.8 Control of Separation

The fact that separation originates eddies and these in turn consume energy calls for the control of separation.

Energy losses in pipelines—apart from the frictional resistance—may be considerably reduced by relatively simple means. Losses in bends may be reduced by using large radii or by introducing suitably shaped vanes; losses in valves may be satisfactorily controlled by using either gate valves or 'streamlined' valves, through which the fluid can pass with the minimum amount of obstruction; losses in diffusers may be kept to a minimum by using an included taper angle of about 7 degrees; entry losses may be reduced by carefully rounding off the sharp corners and so on.

For the aircraft designer, the control of separation becomes an all important design principle. The high speed modern aeroplane must be carefully streamlined because the power requirements and the

fuel consumed by the engine, and subsequent top speed attained, depend largely on the aerodynamic shape. *Useless* energy consumption must be reduced to an absolute minimum and this naturally calls for thorough knowledge of the prevailing flow-pattern. All the components of the aircraft body exposed to the airstream are shaped to ensure aerodynamically 'clean' surfaces. Clean surfaces, however, do not prevent the natural growth of the boundary layer and since thick layers lead to instability and ultimately to separation, artificial means are sought to control the natural growth of the boundary layer. Earlier, attempts were made

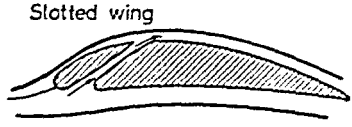

Figure 8.24

by Handley Page who introduced the slotted wing (*Fig. 8.24*) and controlled separation by the air current coming out of the slot and blowing into the boundary layer on top of the wing, imparting fresh momentum to the particles which have been slowed down by the action of viscosity. Thus the particles are able to hold on to the surface over a longer distance without separation; by blowing air through little nozzles from the interior of the wing into the boundary layer a certain amount of artificial turbulence is produced and separation delayed. Another attempt in this direction is the

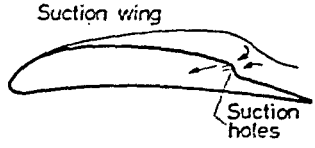

Figure 8.25

suction wing, where thick boundary layers are sucked into the interior of the wing through slots. *Fig. 8.25.*

Another striking example showing the reduction of air resistance by streamlining is the development of the motor-car body. The resistance of earlier models was extremely high because of the box-shaped body and the large projected area. The drag coefficient was near to the value of the flat plate set perpendicular to the flow. Streamlining brought about radical changes in the body design. By lowering the 'silhouette', the projected area was decreased and

further modifications, such as the proper setting of the angle of inclination of the windscreen and the tapering of the rear end of the body, brought about a gradual reduction of the wind resistance. As a result of progressive development, the wind resistance of well streamlined modern motor car bodies dropped to about one quarter of the earlier figures. Comparative values of the resistance coefficients are shown in *Fig. 8.26*.

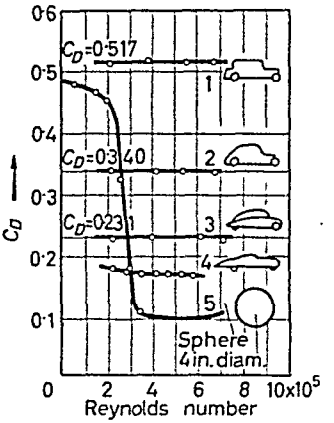

Figure 8.26—Drag coefficient of motor cars

From the large volume of research work carried out on the control of separation, it appears that a thorough understanding of this field of fluid mechanics is of extreme importance.

8.9 Drag and Pressure Distribution Relationship for Bluff Bodies

It was stated earlier that profile drag may be divided into two parts: form drag associated with separation, and skin friction.

The results of profile-drag measurements in wind-tunnels include both form drag and skin friction. With the aid of pressure plotting on the body, however, the form drag can be separated from skin friction and its magnitude obtained by integration of the downstream component of the pressure forces around the body.

In the case of bluff bodies the drag due to skin friction is small in comparison with the form drag, and in this case the form drag may be taken as equal to the profile drag. Such a procedure only requires an adequate number of holes drilled into the surface through which the static pressure can be measured.

The pressure distribution around axi-symmetric objects, such as spheres and cylinders, is symmetrical as shown in *Fig. 8.27a* and the force then points downstream. In the case of asymmetric bodies,† such as motor cars (*Fig. 8.27b*), or buildings (*Fig. 8.27c*), the pressure distribution yields a force which generally makes an angle with the

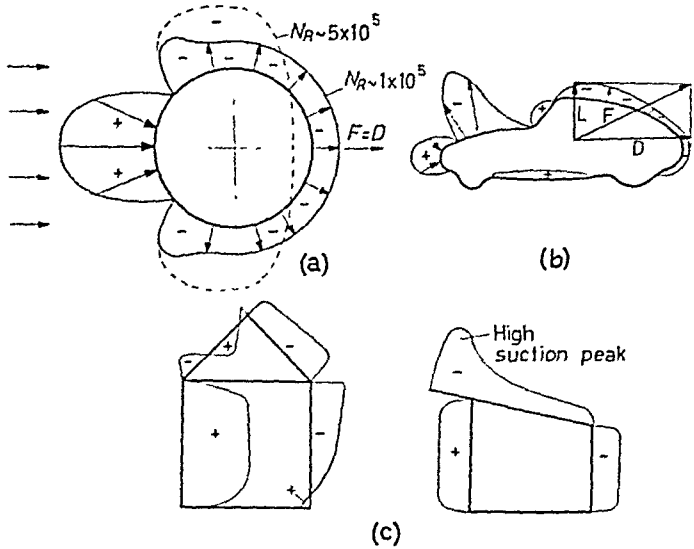

Figure 8.27—Pressure distribution around bodies. (+ positive, − negative pressure field relative to ambient) (*By courtesy of McGraw-Hill, New York*)

stream. This force may be resolved into two components, one being parallel and the other perpendicular to the stream. The former is the drag and the latter is called the 'lift' L.

An intimate knowledge of pressure distribution around bodies is important to the engineer for the purpose of load calculations. Under heavy wind-loads buildings have been known to collapse and roofs be lifted up. Large eddies shed downstream from flexible structures may cause periodic oscillations in the force which may lead to serious damage or even complete failure of the structure. The collapse of the Tacoma bridge is a classic example.

Example

8.4. Calculate the drag force and power required to pull the following objects at 100 m.p.h. through still air: (*a*) circular disc; (*b*) sphere; (*c*) ellipsoid; (*d*) airship hull.

† Wings are discussed in Chapter 9.

The diameter is 1 ft. Density of air = 0·00234 slugs/ft.^{3} Kinematic viscosity = 1·67 10^{-4} ft.^{2}/sec.

Solution.—Dynamic head = $\frac{1}{2}\rho V^2 = 0{\cdot}00117 \times (100 \times 1{\cdot}47)^2 = 25{\cdot}2$.
Projected area = $\pi/4 \times 1^2 = 0{\cdot}785$
Hence drag force = $25{\cdot}2 \times 0{\cdot}785 \times C_D = 19{\cdot}8\, C_D$

$$\text{Power required} = \frac{19{\cdot}8 \times 147}{550} C_D = 5{\cdot}29\, C_D$$

The Reynolds' number based on the diameter is

$$N_R = \frac{147 \times 1}{1{\cdot}67} \times 10^4 = 8{\cdot}8 \times 10^5$$

The drag coefficients may be obtained from *Fig. 8.21.* The results are tabulated below:

Object	C_D Drag coefficient	Drag force (lb.)	Power (h.p.)
Disc	1·02	20·20	5·40
Sphere	0·22	4·35	1·16
Ellipsoid	0·08	1·58	0·42
Airship hull	0·045	0·89	0·24

Exercise

(*a*) What is the definition of the boundary layer and the fundamental cause of its existence?

(*b*) If flow takes place over a flat plate exposed parallel to a fluid stream draw a picture of the laminar and turbulent boundary layer and the transition zone separating them.

(*c*) If flow takes place over a curved surface describe the effect of the curvature on the flow pattern.

(*d*) Draw the approximate flow pattern around a sphere, an aerofoil and a flat plate, the latter placed perpendicular to the stream.

Problems

8.1. A motor car travels at a speed of 60 m.p.h. Calculate the air resistance if the drag coefficient is 0·34 and the projected area is 25 ft.^{2}

8.2. Calculate the (constant) terminal velocity of a spherical object dropped from an aircraft at great height. The diameter of the object is 3 feet and its weight 300 lb. (Neglect the effect of the speed of the aircraft.) The density of the air is 0·00233 slugs/ft.^{3}, kinematic viscosity $1{\cdot}67 \times 10^{-4}$ ft.^{2}/sec.

8.3. A rising spherical weather balloon is filled with hydrogen. At a certain altitude the specific weight of the hydrogen is 0·006 lb./ft.^{3}, the diameter 6 feet and the specific weight of the surrounding air 0·0600 lb./ft.^{3}

If the combined weight of the rubber envelope and the instrument is 6 lb., estimate the steady upward velocity of the balloon.

Take kinematic viscosity of air $= 1{\cdot}5 \times 10^{-4}$ ft.^{2}/sec.

8.4. A 3-ft diameter mine is dropped from an aircraft and hits the water surface at a (vertical) speed of 200 ft./sec. Calculate the depth the mine reaches before starting to rise, if the average specific gravity of its shell and contents is 0·95.

8.5. A spherical object placed in a 'wide' fluid stream shows a symmetrical pressure distribution similar to that shown in *Fig. 8.28.* If such a spherical object is placed in a 'narrow' fluid stream, such as one issuing from a vertical jet, it is possible to keep the object 'suspended' in

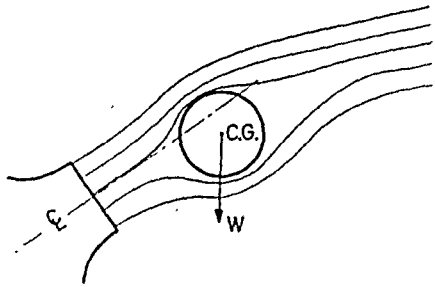

Figure 8.28

the fluid against gravity force by adjusting the stream velocity. If the jet is inclined to the vertical the suspension will still hold under controlled conditions. It may be observed, however, that the sphere adjusts its relative position to the jet by displacing its C.G. from the centre line of the jet as shown in *Fig. 8.28.*

Explain, what changes must take place in the pressure distribution and draw a vector diagram showing equilibrium of forces.

8.6. A train consists of ten carriages and is travelling at a speed of 60 m.p.h. If each carriage is 75 ft. long, 10 ft. wide, and 8 ft. high what will be the drag force due to skin friction? Neglect the frictional effects under the floor and assume that each carriage starts a fresh boundary layer which is substantially turbulent. Compare your results with data given in Ref. 3.

8.10 On the Mechanism of Turbulence

Turbulence makes its appearance in fluids when they flow past solid surfaces or when neighbouring streams of the same fluid pass over one another. The motion is irregular and experiments show that the irregularity is caused by velocity fluctuations, superimposed

on the main fluid flow. These fluctuations cause a continuous interchange of minute masses between the neighbouring layers, the mass interchange being accompanied by a respective loss or gain of momentum.

It is emphasized that the expression turbulence is often applied to phenomena which have little in common with the turbulence outlined in the foregoing. For example, it is observed that if a fluid passes around a body not carefully streamlined, regular vortices appear in its wake. Vortex motion, however, is not necessarily turbulent motion. Turbulent motion is solely characterized by the irregular fluctuations of minute magnitude accompanied by permanent mixing of fluid particles between adjacent fluid layers.

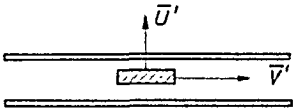

Figure 8.29

Considering energy losses in pipes with laminar flow, compared with turbulent flow, one finds a greater rate of energy dissipation with turbulence present. Also, the skin friction drag acting on flat plates exposed to parallel streams is greater if the boundary layer is turbulent.

The question arises: what causes the larger energy dissipations in turbulent flow and how could a theoretical study of such irregular motions lead to practical results? The answer lies in a simplified and reasonably close representation of the actual phenomena supported by continuous experimental checking on the validity of the assumptions made.

Among the various investigators who studied the turbulence problem, Reynolds was the first to show that the momentum transport due to the fluctuations originates a tangential force between adjacent layers. Reynolds considered one component of the fluctuations, V', as superimposed on the mean flow velocity whilst the other component, U', was considered as a cross-current pulsation. The function of U' is to cause an exchange of particles from one layer to the other. Assuming that these pulsating cross-current velocities are uniformly distributed over a surface S (separating two adjacent layers), the mass transported in unit time would be $\rho\bar{U}'S$, where $\bar{U}'$ is temporal mean of U'. Because of the relative velocity V' between the layers, the average momentum carried into the neighbouring layer (*see Fig. 8.29*) would be $\rho S\bar{U}'\bar{V}'$.

This momentum is considered to be lost in the adjacent layer and the loss of momentum results in a tangential force F equal to the momentum change,

$$F = S \cdot \rho \bar{U}' \cdot \bar{V}' \qquad \ldots\ldots(8.28)$$

and the Reynolds' stress

$$\tau = \frac{F}{S} = -\rho U' V' \qquad \ldots\ldots(8.29)$$

The negative sign corresponds to the definition of positive friction in such a way that τ is considered as positive if the fluid layer at the distance y from the wall is accelerated by the outside flow; accordingly, the momentum transfer produces friction of positive amount if the fluid portions moving towards the wall (*i.e.*, having negative components) carry positive excess momentum.

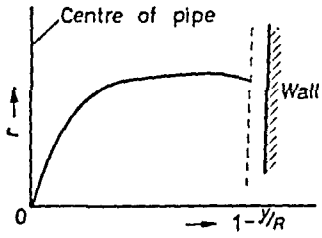

Figure 8.30

The question naturally arises: could the velocity fluctuations be considered as random movements if there was a positive 'trend' of momentum transfer towards the wall? In the case of random distribution of the U' and V' components, the product $V' \cdot U'$ has the mean value zero $\bar{U}' \cdot \bar{V}' = 0$. This kind of turbulent flow actually does exist in practice, but it does not give rise to tangential forces. The type of turbulence referred to is called isotropic turbulence and may be found behind screens, grids, etc. Tangential forces are encountered only if the mean of $U' \cdot V'$ differs from zero, that is, a correlation exists between V' and U'. Such correlation may be expressed by a correlation factor, a term widely used in statistical mathematics. Accordingly, the correlation between V' and U' is measured by the ratio $r = \bar{U}'\bar{V}'/\sqrt{(\bar{U}'^2\bar{V}'^2)}$ where $\sqrt{\bar{U}'^2}$ and $\sqrt{\bar{V}'^2}$ are the square roots of the mean squares of the particular components. Correlation between turbulent velocity fluctuations is shown in *Fig. 8.30*, where the correlation factor r, obtained from measurements, is plotted against the quantity $(1 - y/R)$, R being the radius of the pipe. Since the velocity fluctuations in the direction

of the flow can be measured†, the value of $\overline{U'^2}$ may be obtained. From measurements of pressure drop, the value of $\overline{U'V'}$ can be calculated, assuming that $\tau = -\rho\overline{U'V'}$ and taking into consideration that the shearing stress in a channel is proportional to distance from the centre‡. The curves show the following results:

(*a*) $\overline{U'V'}/\sqrt{\overline{U'^2}}$ is almost constant over the main part of the cross-section, corresponding with constant correlation.

(*b*) $\overline{U'V'}/\sqrt{\overline{U'^2}} = 0$ near the centre; this is evident by symmetry considerations, since in the centre isotropic turbulence prevails.

(*c*) The curve drops near the wall, but in this range the fluctuations are damped out by viscous forces predominating in the laminar sublayer.

The expression derived for the turbulent stress may be considered an important step towards the understanding of the forces set up by the momentum transfer. The relation, as given by Eq. 8.29, does not provide a useful formula for stress calculations since the magnitude of the fluctuations and their mean values in question are unknown. Considering the flow pattern in the neighbourhood of a certain point, Prandtl introduced a characteristic parameter of turbulent flow, namely, a length which is characteristic for the size of the region involved in the turbulent exchange. According to Prandtl, the fluid masses displaced perpendicular to the direction of the mean flow carry their momentum over a certain length, l, perpendicular to the mean flow. Although the actual mechanism may be more complicated, it is useful to have a length parameter connected with the turbulence phenomena, as the magnitude of the fluctuations may vary considerably. For example, the magnitude of turbulent fluctuations in the boundary layer of an airfoil placed

† Dryden and Kuethe: 'The measurement of fluctuations of air speed by the hot-wire anemometer', N.A.C.A. Report 320, 1929.

‡ The expression

$$\tau = \tau_0(1 - y/R)$$

at times referred to as the 'shear harness' equation, holds for all pipe flow conditions (laminar and turbulent).

Since $$(p_1 - p_2)\frac{D^2\pi}{4} = \tau_0 \cdot 2R\pi \cdot L$$

or $$\tau_0 = \frac{p_1 - p_2}{L} \cdot \frac{R}{2}$$

it follows that for any other radius r,

$$\tau = \frac{p_1 - p_2}{L}\frac{r}{2}$$

Hence

$$\tau = \tau_0 \frac{r}{R} = \tau_0\left(\frac{R - y}{R}\right) = \tau_0(1 - y/R)$$

in the wind tunnel may be much smaller than fluctuations produced by natural wind near the ground. On the other hand, the term 'large scale' and 'small scale' turbulence is connected with time, that is, with fluctuations of large or short period.

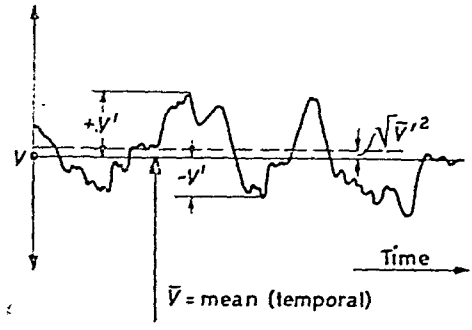

Figure 8.31

The length of parameter l, called the mixing length, may also represent a connection between the mean value of V' and the gradient of the mean velocity at a particular point, $\frac{d\bar{V}}{dy}$. According to Prandtl†,

$$V' = l\left(\frac{d\bar{V}}{dy}\right)$$

Information concerning the mean value of U' is now required. The transverse fluctuations are probably smaller than V', but one may anticipate the same order of magnitude, so that

$$V' = \text{number} \times \bar{U}' = l\frac{d\bar{V}}{dy}$$

where $d\bar{V}/dy$ is the mean velocity gradient‡ (*see Fig. 8.31*). Hence

† Durand: *Aerodynamic Theory*, Vol. III, p. 129.

‡ At any *fixed point* of the stream, the *temporal* mean velocity is defined as

$$\bar{V} = \frac{1}{t}\int (V + V')dt = \frac{1}{t}\int V\,dt + \frac{1}{t}\int V'\,dt$$

where

$$\int V'\,dt = 0$$

Similarly

$$\int U'\,dt = 0$$

It is obvious that the root mean square $\sqrt{\bar{V}'^2}$ or $\sqrt{\bar{U}'^2}$ of the instantaneous velocity fluctuations may assume a finite value. (See *Fig. 8.31.*)

The average velocity, V_{av}, on the other hand, is obtained by considering $\int \bar{V}\,dA$ where the integration is taken over the entire cross-sectional area A of the pipe.

the product

$$\overline{V'U'} = \text{number} \times l^2 \left(\frac{d\bar{V}}{dy}\right)^2$$

Absorbing the 'number' into the mixing length, it follows that

$$\tau = \rho \overline{V'U'} = \rho l^2 . \left(\frac{d\bar{V}}{dy}\right)^2 \qquad \ldots . (8.30)$$

Thus, with the introduction of the mixing length, two unknown variables (V' and U') have been replaced by a single variable, l. The mixing length varies across the flow, but the variation may be readily established by calculating from measured values of the pressure drop in pipes or the skin friction of plates and by finding the values of dV/dy from the measured velocity profile. Since the shear stress in a pipe is proportional to the distance from the centre, (*see* footnote p. 197)

$$\tau = \tau_0(1 - y/R) = \rho l^2 \left(\frac{dV}{dy}\right)^2 \qquad \ldots . (8.31)$$

from which the mixing length

$$l = \frac{\sqrt{\tau_0/\rho}}{dV/dy} \sqrt{1 - y/R} \qquad \ldots . (8.32)$$

The quantity $(\tau_0/\rho)^{1/2}$ has evidently the dimension of a velocity. In fluid mechanics, it is usual to characterize a velocity by the corresponding pressure head; in the inverse way, one may characterize pressure by the corresponding velocity. Similarly, one may relate the velocity $(\tau_0/\rho)^{1/2}$ to the shear stress τ_0. Henceforth, the quantity $(\tau_0/\rho)^{1/2}$ will be called the 'friction velocity', denoted with V^*; the ratio y/R will be called the relative distance from the centre.

The distribution of the mixing length in a tube for moderate and high Reynolds numbers is shown in *Fig. 8.32*. It can be seen that l tends to zero as the wall is approached and that all curves have a near common tangent at the wall, the value of the slope being 0·4. The effects of viscosity appear to decrease with increasing Reynolds numbers and both very high N_R and rough surfaces yield the same curve.

The distribution of the mixing length in pipes obtained from experiments may be regarded as a step forward in the understanding of the turbulence problem, but a general law showing the variation of the mixing length across a fluid stream has not yet been found.

Additional experiments conducted by Fritsch† on rectangular

† Fritsch: Abhandlungen aus dem Aerodynamischen Institut an der Technischen Hochschule Aachen. Heft 8.

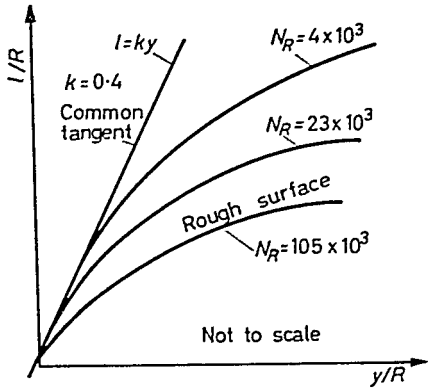

Figure 8.32

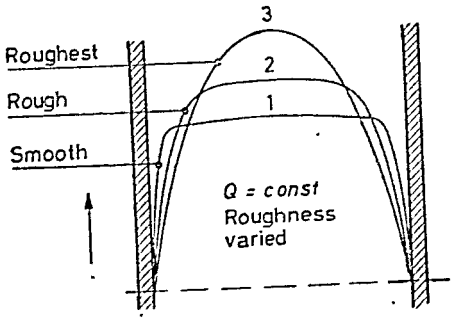

Figure 8.33

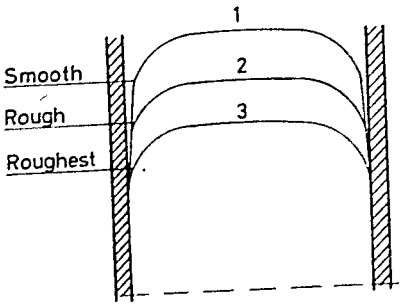

Figure 8.34

conduits show that (*a*) for a specified discharge (Q = CONST.) the velocity distribution curves undergo substantial changes if the roughness of the pipe is varied (*Fig. 8.33*), (*b*) for a specified resistance (τ_0 = CONST. obtained by adjusting discharge Q and roughness k), all velocity distribution curves are similar—in fact, identical over a substantial portion of the conduit. (*Fig. 8.34.*)

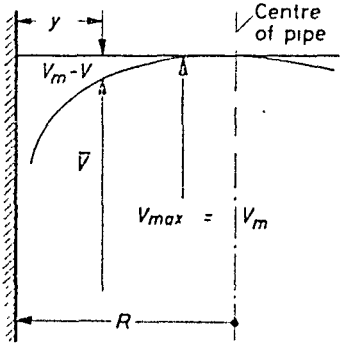

Figure 8.35

It follows that the velocity distribution curves, when traced from a common centre velocity point, become congruent except for a narrow region near the wall. The influence of the wall affects the velocity distribution curve only in the vicinity of the boundary.

Hence the velocity difference $V_m - V$ (*see Fig. 8.35*), called the 'velocity defect,' at any point appears to be independent of the surface conditions. Kármán suggested that for high Reynolds' numbers the ratio $\frac{\text{(friction defect)}}{\text{(velocity velocity)}}$ is independent of the Reynolds' number and surface roughness and is a general function of y/R alone. According to Kármán†

$$\frac{V_m - V}{V^*} = f(y/R) \qquad \ldots . (8.33)$$

where the function $f(y/R)$ has to be determined.

In order to bridge the gap between theory advanced so far and the final solution, Kármán suggested that the mixing length at a point might be taken as proportional to the ratio of the first and second derivative of the velocity distribution at that particular point. His idea was conceived from the similarity of the flow pattern. Kármán assumed that the internal mechanism of the

† Kármán: 'Turbulence and Skin Friction.' *J. aero. Sci.* 1, 1934.

turbulence at any two places differs only to the extent of a change of the units of length and time. Exact similarity of the flow pattern can be expected for a constant shear stress. Looking at the flow pattern from the point of view of two observers, one travelling with the fluid and the other with a velocity equal to the mean velocity, the flow patterns at two different distances, y_1 and $y + \Delta y$, from the wall will differ only by length and time factors. Kármán developed the velocity $V = V(y)$ in a Taylor series and ended it at the second term

$$V(y + \Delta y) = V(y) + V' \Delta y + \tfrac{1}{2} V'' \Delta y^2 \ldots$$

The characteristic data for the velocity distribution are the derivatives $\mathrm{d}V/\mathrm{d}y$ and $\mathrm{d}^2V/\mathrm{d}y^2$ and the only length which can be constructed from these quantities is the ratio $(\mathrm{d}V/\mathrm{d}y)/(\mathrm{d}V^2/\mathrm{d}y^2)$. According to Kármán's hypothesis, this ratio is proportional to the mixing length

$$l = k \frac{\mathrm{d}V/\mathrm{d}y}{\mathrm{d}^2V/\mathrm{d}y^2} \qquad \ldots.(8.34)$$

where the proportionality factor k would be a universal constant.

A simpler hypothesis for predicting l was suggested by Prandtl—near a plane wall $l = k_1 . y$, where y is the distance from the wall. Thus Kármán's hypothesis gives

$$\tau = \rho l^2 \left(\frac{\mathrm{d}V}{\mathrm{d}y}\right)^2 = \rho k^2 \frac{[\mathrm{d}V/\mathrm{d}y]^4}{[\mathrm{d}^2V/\mathrm{d}y^2]^2} \qquad \ldots.(8.35)$$

while Prandtl's gives

$$\tau = \rho k_1 \left[y \frac{\mathrm{d}V}{\mathrm{d}y}\right]^2 \qquad \ldots.(8.36)$$

On the basis of Kármán's hypothesis for flow in pipes

$$\sqrt{\frac{\tau_0}{\rho}} \sqrt{(1 - y/R)} = k \left[\frac{\mathrm{d}V}{\mathrm{d}y}\right]^2 \Big/ \left[\frac{\mathrm{d}^2V}{\mathrm{d}y^2}\right] \qquad \ldots.(8.37)$$

which can be integrated and the function $f(y/R)$ found.

First write $Z = \mathrm{d}V/\mathrm{d}y$, so that

$$\frac{\mathrm{d}Z/\mathrm{d}y}{Z^2} = \frac{k}{-V^* \sqrt{(1 - y/R)}}$$

the minus sign being inserted, since the second derivative is negative. The first integration gives

$$\frac{1}{Z} = -\frac{2kR}{V^*} \sqrt{(1 - y/R)} + C$$

The value of the constant may be determined with adequate precision by remembering that for $y \to 0$, the gradient dV/dy is large and the reciprocal may be taken as zero for all practical purposes. Thus, for $y \to 0$

$$0 = -\frac{2kR}{V^*} + C$$

therefore

$$\frac{dV}{dy} = \frac{V^*}{2kR} \cdot \frac{1}{1 - \sqrt{(1 - y/R)}}$$

To integrate again, put

$$1 - y/R = x^2 \quad \text{hence} \quad dy = -2Rx\,dx$$

Substituting and integrating yields

$$V = \frac{V^*}{2kR}\int \frac{dy}{1 - \sqrt{(1 - y/R)}} = -\frac{V^*}{k}\int \frac{x\,dx}{1 - x}$$

$$= \frac{V^*}{k}[x + \log_e (1 - x)] + C$$

Hence

$$V = \frac{V^*}{k}\{[1 - y/R] + \log_e [1 - \sqrt{(1 - y/R)}]\} + C$$

The constant may be found by substituting $V = V_m$ at the centre of the pipe where $y = R$. Hence $C = V_m$. With this value, the equation may be arranged in form of the velocity defect law

$$\frac{V_m - V}{V^*} = -\frac{1}{k}\{\log_e [1 - \sqrt{(1 - y/R)}] + \sqrt{(1 - y/R)}\} \quad \ldots . (8.38$$

Thus, the universal function based on Kármán's hypothesis is represented by the right hand side of Eq. 8.38.

On the other hand, following Prandtl's suggestion

$$\tau_0(1 - y/R) = \rho k_1^2 \left(y\frac{dV}{dy}\right)^2$$

Since the analysis is limited to the region near the wall, one may neglect the change in shear stress τ_0 across the small distance y_w and write

$$\sqrt{\tau_0/\rho} = V^* = k_1\left[y\frac{dV}{dy}\right]$$

or

$$\frac{dy}{y} = \frac{V^*}{k_1} \cdot dV$$

Hence by integration

$$V = \frac{V^*}{k_1} \log_e y + C \qquad \ldots.(8.39)$$

Results of Experiments

The velocity distribution for fully developed turbulent flow was experimentally observed by Nikuradse, who found that

$$\frac{V_m - V}{V^*} = 2{\cdot}5 \log_e R/y \qquad \ldots.(8.40)$$

Nikuradse's findings show that the equation suggested by Prandtl for the region near the wall holds for the entire cross-section.† Substituting $V = V_m$ and $y = R$ into Eq. 8.39,

$$V_m = \frac{V^*}{k_1} \log_e R + C$$

and the evaluation of the constant leads to

$$\frac{V_m - V}{V^*} = \frac{1}{k_1} \log_e R/y$$

From Nikuradse's findings, $\frac{1}{k} = 2{\cdot}5$, corresponding to the value of $k_1 \simeq 0{\cdot}4$. Changing from natural to common logarithms,

$$\frac{V_m - V}{V^*} = 5{\cdot}75 \log R/y \qquad \ldots.(8.41)$$

According to Eq. 8.41 (with the exception of a very small region near the wall) $(V_m - V)/V^*$ is indeed a universal function of y/R, independent of the Reynolds' number.

8.11 The Laminar Sublayer and the Model Flow-pattern

Eq. 8.41 gives a general form for the velocity distribution in the turbulent 'core' of pipes, or for turbulent boundary layer of a flow passing over a solid surface. Altogether different conditions prevail near the wall surface, where the thin laminar sublayer is formed. In this layer, the rate of viscous shear is large, and the cross-current velocity fluctuations are damped out, so that the Reynolds stresses are insignificant compared with the viscous stress. Farther from the

† The approximation $l = k_1 y$ near the wall is not followed across the flow. But then again, neither is τ_0 constant across the flow.

wall there is another region in which the Reynolds' stresses and the viscous stresses are of the same order of magnitude. In this region one may write for the composite stress

$$\tau = \mu \frac{dV}{dy} + \rho l^2 \left(\frac{dV}{dy}\right)^2$$

In the sublayer the first term predominates and the second term vanishes, and in a turbulent layer the second term predominates and the first term tends to zero. It then follows that in the sublayer the velocity gradient is large because the velocity rises from zero to a finite value (V_w) over a minute distance (y_w). The gradient is assumed to be uniform within this distance, so that

$$\left(\frac{dV}{dy}\right)_{\delta \to 0} = \frac{V}{y} = \frac{\tau_0}{\mu}$$

Introducing the dimensionless parameters

$$\frac{V}{V^*} \quad \text{and} \quad \frac{V^* y}{\nu}$$

and considering that $\dfrac{V}{y} = \dfrac{\tau_0}{\rho} \cdot \dfrac{\rho}{\mu} = \dfrac{V^{*2}}{\nu}$

for the laminar sublayer one obtains

$$\frac{V}{V^*} = \frac{V^* y}{\nu} \qquad \ldots . (8.42)$$

The value of $\dfrac{V^* y}{\nu}$ for $y = y_w$ (and $V = V_w$) was found to be a constant for a given flow set up. For example, for turbulent flow in smooth pipes $\dfrac{V^* y}{\nu} = 11{\cdot}6$, approximately, so that one may generally write for the laminar sublayer

$$\frac{V}{V^*} = \frac{V^* y}{\nu} = \text{CONSTANT} \qquad \ldots . (8.43)$$

With the aid of the velocity defect law (Eq. 8.33 and Eq. 8.43), it is possible to construct a hypothetical flow pattern model. The model consists of a straight line OA, representing the conditions near the wall, continued by the logarithmic velocity distribution

curve AM, as shown in *Fig. 8.36*. Whilst the velocity defect law refers to the point of maximum velocity, the hypothetical flow-pattern refers to a zero velocity datum line.

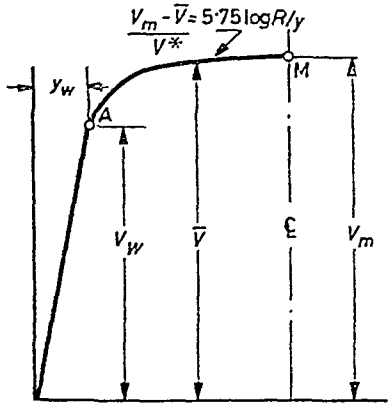

Figure 8.36

From Eq. 8.33

$$\frac{V}{V^*} = \frac{V_m}{V^*} - 5{\cdot}75 \log . \frac{R}{y} \qquad \ldots.(8.44)$$

For point A, $V = V_w$ and $y = y_w$.
Hence,

$$\frac{V_w}{V^*} = \frac{V_m}{V^*} - 5{\cdot}75 \log \frac{R}{y_w} = C$$

Since $y_w = Cv/V^*$

$$\frac{V_m}{V^*} - 5{\cdot}75 \log \frac{RV^*}{Cv} = \frac{V_m}{V^*} + 5{\cdot}75 \log C - 5{\cdot}75 \frac{RV^*}{v} = C \qquad \ldots.(8.45)$$

Hence

$$\frac{V_m}{V^*} = (C - 5{\cdot}75 \log C) + 5{\cdot}75 \log \frac{RV^*}{V}$$

Denoting $C - 5{\cdot}75 \log C$ by 'a' and substituting Eq. 8.45 into Eq. 8.44, one obtains

$$\frac{V}{V^*} = a + 5{\cdot}75 \log \frac{RV^*}{v} - 5{\cdot}75 \log \frac{R}{y}$$

$$= a + 5{\cdot}75 \log \frac{V^* y}{v}$$

In *Fig. 8.37*, Nikuradse's velocity distribution measurements are plotted, using $\frac{V}{V^*}$ and $\log \frac{V^*y}{\nu}$ as co-ordinates. It appears that the hypothetical velocity profile fits in well with the experimental

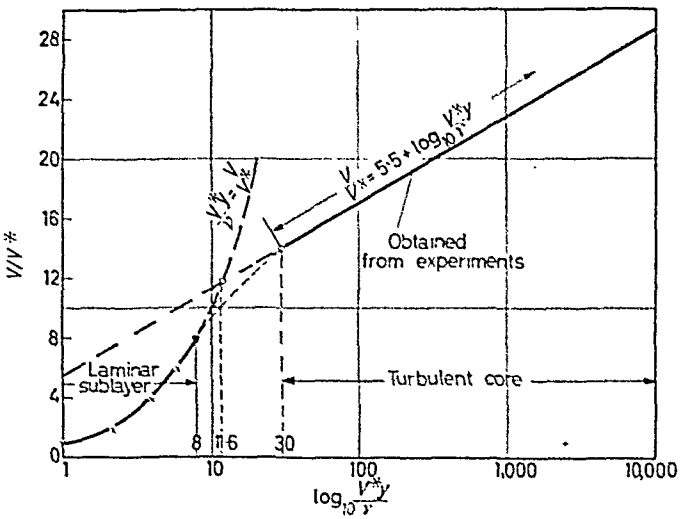

Figure 8.37

observations of Nikuradse and that the value of constant $a = 5{\cdot}5$. Hence, the equation representing the actual velocity distribution in the turbulent core of smooth pipes is given by

$$\frac{V}{V^*} = 5{\cdot}5 + 5{\cdot}75 \log \frac{V^*y}{\nu} \qquad \ldots.(8.46)$$

Conditions near the wall, representing $\frac{V}{V^*} = \frac{V^*y}{\nu}$ are also plotted on *Fig. 8.37*. The intersection of the 'laminar' curve with the 'turbulent line' occurs at $\frac{V^*y}{\nu} = 11.6$, but the points of observations show absence of [illegible] abrupt transition from laminar to turbulent. The transitio[illegible]d and whilst the value of 8 may be taken as the practi[illegible]it, the v[illegible]30 appears as a reasonable upper lim[illegible]on i[illegible] viscosity. Thus, the d[illegible] hypo[illegible] the actual velocity

distribution appears in the neighbourhood of point A, the actual conditions being represented on *Fig. 8.37* by a dotted line.

The thickness δ of laminar layer may now be calculated. Combining the relation

$$\frac{V^*\delta}{\nu} = 8 \quad \text{and} \quad \frac{V^*}{V_{av.}} = \sqrt{\frac{f}{8}} \quad \text{one obtains} \quad V_{av.}\sqrt{\frac{f}{8}}\frac{\delta}{\nu} = 8$$

Hence

$$\frac{\delta}{D} = \frac{8\sqrt{8}}{N_R\sqrt{f}} \qquad \ldots.(8.47)$$

where $N_R = V_{av.}D/\nu$

8.12 Derivation of Friction for Smooth Pipes

The friction factor defined by the Darcy equation

$$f = \frac{\Delta h_f D}{\frac{1}{2}\rho V_{av.}^2}$$

is based on the average velocity head $\frac{1}{2}\rho V_{av.}^2$. For this reason, a relationship is sought between the average and maximum velocities.

It may be shown that a formula of the same form as Eq. 8.46, with another additive constant, is valid for the velocity distribution if the average velocity is used instead of the maximum velocity. The proof is due to Prandtl.

According to Eq. 8.33, with the exception of a small region near the wall, $(V_m - V)/V^*$ is a universal function of R/y, independent of the Reynolds number. Thus, neglecting the region near the wall and integrating the velocity defect $V_m - V$ over the cross-section, we obtain

$$\int_\delta^R (V_m - V)\,\mathrm{d}A = (V_m - V_{av.})A \qquad \ldots.(8.48)$$

From the defect law

$$V_m - V = \frac{V^*}{k_1}\log_e\frac{R}{y}$$

and, since

$$\mathrm{d}A = 2\pi(R - y)\,\mathrm{d}y$$

one obtains

$$\int_\delta^R (V_m - V)\,\mathrm{d}A = -\int_\delta^R \frac{V^*}{k_1}\log_e\frac{y}{R}\,2\pi(R-y)\,\mathrm{d}y =$$

$$= \frac{2\pi}{k}V^*\left(Ry - \frac{y^2}{4}\right) - \log_e y/R\left[Ry - \frac{y^2}{2}\right]_\delta^R$$

Since δ is very small, the value of the expression $\log_e y/R\,[R/y - y^2/R^2]$ may be neglected. Hence, the value of the integral is $\frac{3}{4}R^2$, and

$$\frac{V_m - V_{av.}}{V^*} = \frac{2\pi}{k}\frac{3/4R^2}{\pi R^2} = \frac{3}{2k} = \text{CONSTANT} \quad \ldots\ldots(8.49)$$

For $k = 0{\cdot}4$, the value of the constant is 3·75. Better agreement with the experimental results is obtained if $k = 0{\cdot}368$. The discrepancy may be attributed to the omission of the small volume in the laminar layer. Hence, $3/2k = 4{\cdot}07$,

$$\frac{V_{av.}}{V_m} = \frac{V_m}{V^*} - 4{\cdot}07$$

Substituting V_m for V and R for y in Eq. 8.46, one obtains

$$\frac{V_m}{V^*} = 5{\cdot}5 + 5{\cdot}75 \log \frac{V^* R}{\nu}$$

so that

$$\frac{V_{av.}}{V^*} = 1{\cdot}43 + 5{\cdot}75 \log \frac{V^* R}{\nu} \quad \ldots\ldots(8.50)$$

The velocity distribution law for smooth pipes, as given in Eq. 8.50, may now be substituted into the expression

$$\frac{V_{av.}}{V^*} = \sqrt{\frac{f}{8}}$$

resulting in

$$\sqrt{\frac{8}{f}} = 1{\cdot}43 + 5{\cdot}75 \log \frac{R V_{av.} \sqrt{\frac{f}{8}}}{\nu} \quad \ldots\ldots(8.51)$$

Substituting the Reynolds' number based on the average velocity and the pipe diameter $N_R = \dfrac{V_{av.} D}{\nu}$ and rearranging terms yields

$$\frac{1}{\sqrt{f}} = -0{\cdot}249 + 2{\cdot}04 \log N_R \sqrt{f} \quad \ldots\ldots(8.52)$$

The results of experiments, shown in *Fig. 8.38*, give slightly different numerical constants, and the final formula is [5]

$$\frac{1}{\sqrt{f}} = \quad \ldots\ldots(8.53)$$

Discrepancy between the friction factors based on the Blasius empirical formula and the logarithmic law is shown to appear at higher Reynolds' numbers.

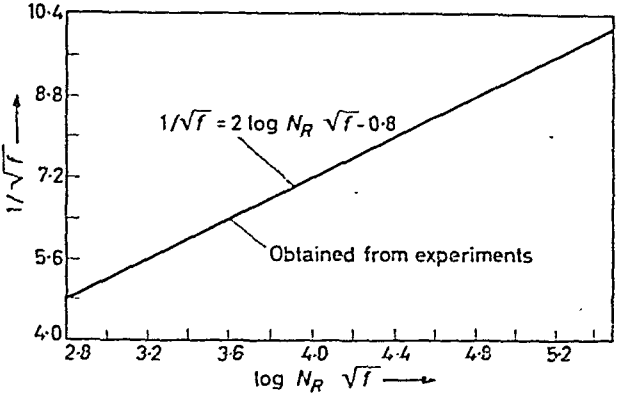

Figure 8.38

8.13 Friction in Rough Pipes

The influence of the surface roughness is not significant below a certain Reynolds' number. The physical reason for this behaviour of a rough surface seems to be that the roughness elements in this

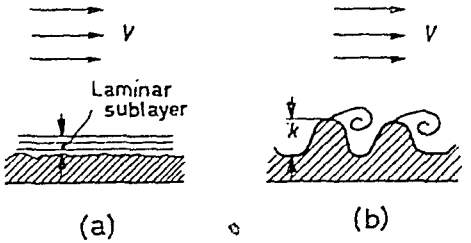

Figure 8.39

range are small in comparison with the thickness of the laminar sublayer (*Fig. 8.39a*). At higher Reynolds' numbers however, the roughness elements emerge from the laminar sublayer—like mountains emerging from a layer of fog—because the thickness of the sublayer is small. The effect is shown in *Fig. 8.39(b)*. When the height k of the roughness elements is large in comparison with the laminar sublayer, eddies are shed off the 'peaks' and the skin friction becomes proportional to the square of the velocity. This

being so, the friction factor no longer depends on the Reynolds' number. Since the eddies generated by the roughness elements increase their intensity as the size of the elements increases, the friction factor must depend on the type of the roughness. On the assumption that geometrically similar rough surfaces result in dynamically similar fluid flow patterns, one may anticipate that, by specifying the relative roughness k/D, the flow pattern is defined.

Since V_w/V^* is a variable quantity in case of rough surfaces, the distance y_w could be regarded as some function of the roughness. As a first approximation, put $y = \alpha k$, where k is the height of the roughness elements and α is a constant. As the velocity defect law is universal, it applies equally to rough surfaces and one may write for the distance $y = y_w$

$$\frac{V_w}{V^*} = \frac{V_m}{V^*} - 5{\cdot}75 \log \frac{R}{\alpha k} = \frac{V_m}{V^*} + 5{\cdot}75 \log \alpha - 5{\cdot}75 \log \frac{R}{k}$$

Substituting

$$\frac{V_m}{V^*} = \frac{V}{V^*} + 5{\cdot}75 \frac{R}{y}$$

and rearranging terms yields

$$\frac{V_w}{V^*} - 5{\cdot}75 \log \alpha = \frac{V}{V^*} - 5{\cdot}75 \log \frac{y}{k} \qquad \ldots.(8.54)$$

Hence

$$\frac{V}{V^*} = \chi + 5{\cdot}75 \log y/k \qquad \ldots.(8.55)$$

where

$$\chi = \frac{V_w}{V^*} - 5{\cdot}75 \log \alpha \qquad \ldots.(8.56)$$

Combining Eq. 8.55 with Eq. 8.46 a simple expression for χ is obtained

$$\chi = 5{\cdot}5 + 5{\cdot}75 \log \frac{V^* k}{\nu} \qquad \ldots.(8.57)$$

In *Fig. 8.40*, experimental values obtained for smooth and various rough tubes are plotted to show χ as a function of $\frac{V^* k}{\nu}$.

It appears that for smooth tubes, the experimental values agree with Eq. 8.57; with increasing roughness, the function deviates from the straight line and attains a constant value of 8·5 (approximately) for large values of $\frac{V^*k}{\nu}$. Fully developed flow with roughness is attained when $\frac{V^*k}{\nu} \geq 100$. On the other hand, if $\frac{V^*k}{\nu} \leqslant 4$,

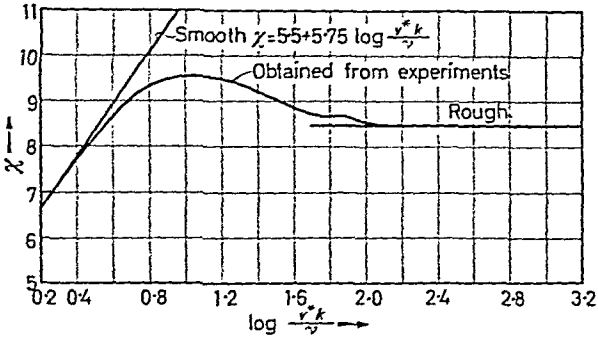

Figure 8.40

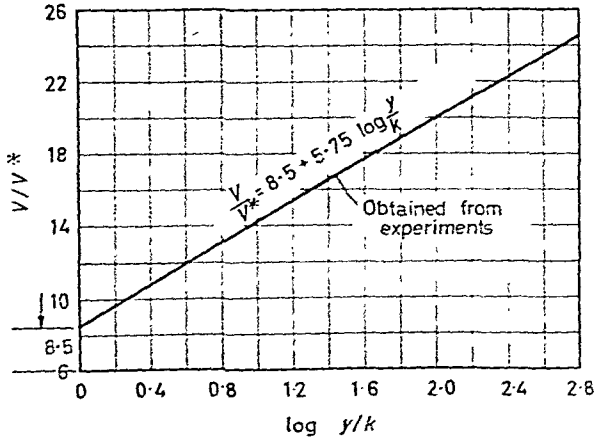

Figure 8.41

the surface is to be counted hydraulically smooth. The values of χ in *Fig. 8.40* were obtained from both velocity profile and pressure drop measurements.

In *Fig. 8.41*, V/V^* is plotted against $\log y/k$ for fully developed

rough turbulence. ($\chi = 8{\cdot}5$.) For the centre of the pipe (see Eq. 8.55)

$$\frac{V_m}{V^*} = \chi + 5{\cdot}75 \log \frac{R}{k}$$

Substituting this expression into Eq. 8.49

$$\frac{V_{av.}}{V^*} = \frac{V_m}{V^*} - C = \chi - C + 5{\cdot}75 \log \frac{R}{k} \quad \ldots.(8.58)$$

with $\chi = 8{\cdot}5$ and $C = 3{\cdot}75$

$$\frac{V_{av.}}{V^*} = \sqrt{\frac{8}{f}} = 4{\cdot}75 + 5{\cdot}75 \log \frac{R}{k}$$

or

$$\frac{1}{\sqrt{f}} = 1{\cdot}67 + 2{\cdot}02 \log \frac{R}{k} \quad \ldots.(8.59)$$

The final formula, borne out by the experiments of Nikuradse, gives

$$\frac{1}{\sqrt{f}} = 1{\cdot}74 + 2 \log \frac{R}{k} \quad \ldots.(8.60)$$

Thus, by substituting various values for R/k, the friction factor may be calculated. It is pointed out that the relation holds for fully developed turbulent flow and large Reynolds' numbers only.

Both Eq. 8.53 and Eq. 8.60 are shown graphically in *Fig. 4.4* (Chapter 4).

REFERENCES

(1) SCHLICHTLING, H., *Boundary Layer Theory*, Pergamon Press, London, 1955.
(2) GOLDSTEIN, S., *Modern Development in Fluid Dynamics*, Clarendon Press. Oxford, 1950.
(3) HOERNER, S. F., *The Aerodynamic Drag*, Author's edition.
(4) BAKHMETEFF, B., *The Mechanics of Turbulent Flow*, Princeton University Press, 1936.
(5) VON KÁRMÁN, T., *J. R. aero. Soc.*, 1937.
(6) TOWNSEND, A., 'The Structure of the Turbulent Boundary Layer,' *Proc. Camb. phil. Soc.*, 47, 1952, p. 375.

9

ELEMENTS OF WING THEORY

9.1 Introduction

ALL bodies immersed in a fluid stream experience a force. If the body is symmetrical and its axis of symmetry is parallel to the direction of flow, then the force acts in the direction of flow. Such a force was referred to as drag in the chapter on Boundary Layer Theory, and it was stated that drag was due to surface friction and wake generation. The existence of surface friction and wake generation was attributed to the boundary layer, which in turn, finds its origin in viscosity effects.

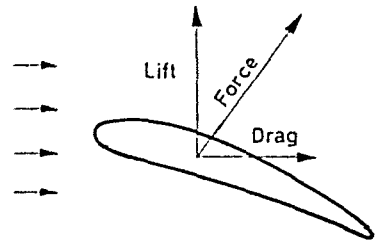

Figure 9.1—Components of aerodynamic force

In the more general case of a body immersed in a fluid stream, the direction of the force acting may differ from the flow direction as shown in *Fig. 9.1.* The force may be resolved into two components, one parallel, the other perpendicular to the direction of the flow. The component parallel to the flow is again termed drag, whilst the perpendicular component is generally called lift.

Practical fluid dynamics is interested mainly in shapes which yield high lift and low drag values. It has been found that circular arcs, 'aerofoils' and 'hydrofoils', satisfy this requirement, provided they are immersed parallel or near parallel to the fluid stream. Typical cross-sections of a circular arc, aerofoils and hydrofoils are shown in *Fig. 9.2.* Circular arcs are embodied in special axial flow fans and propellers; hydrofoils are used mainly for the blades of axial flow turbines, axial flow pumps and marine propellers. In the discussions following, the term 'wing' can be taken as referring to any of these lifting surfaces.

These three wing types have a common characteristic, namely, that the lift force increases as the angle of setting of the profile with the fluid stream is increased. This angle of setting, called the angle of attack or incidence, is generally the included angle between the

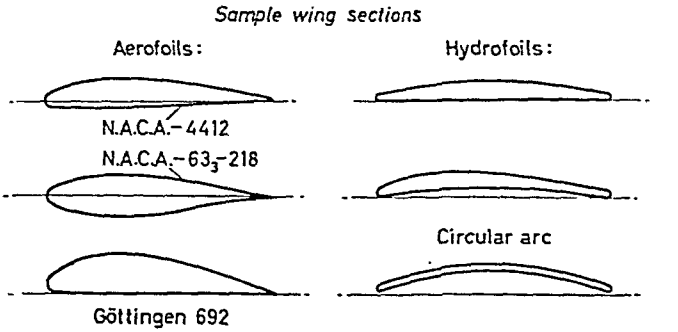

Figure 9.2

direction of fluid flow and a reference axis often chosen as the chord line of the profile. *Fig. 9.3* shows some notations frequently employed. The lift force increases linearly with increasing angle of attack up to a point; then it falls below the straight line, reaches a

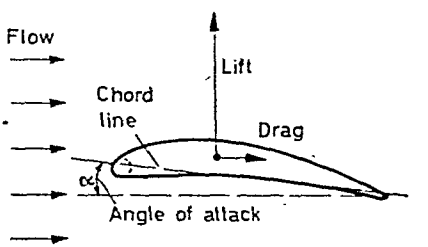

Figure 9.3

maximum and finally decreases with a further increase of angle of attack, as shown in *Fig. 9.4*. On the other hand, drag changes little whilst the angle of attack is small, but increases rapidly at larger angles of attack. There are numerous (in fact, hundreds) of different wing profiles all of which show similar characteristics, though the numerical figures of actual lift force attained at certain angles may differ considerably.

The pressure distribution around the wing section, which may be obtained experimentally, readily explains lift and drag. Wings placed in fluid streams experience (in addition to skin friction) a

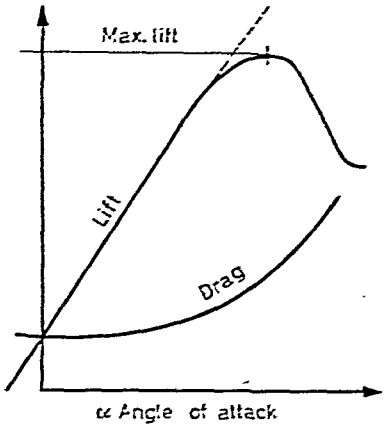

Figure 9.4—Lift and drag of a wing

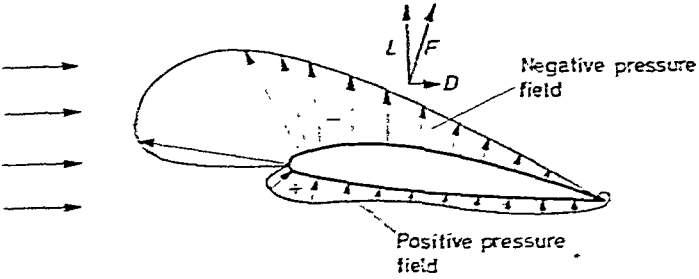

Figure 9.5—Pressure distribution around a wing section

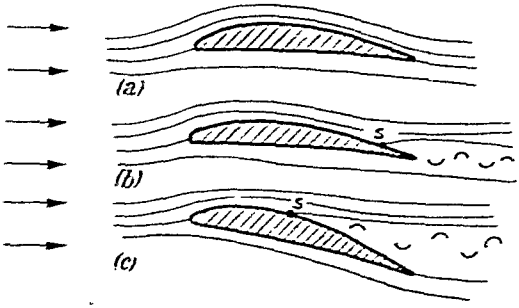

Figure 9.6—The forward movement of separation with incidence

suction on the upper surface and compression on the lower surface and the summation of all pressure and friction forces on the surface elements yields the resultant force F. This again may be resolved into components parallel and perpendicular to the stream, as shown in *Fig. 9.5*. Note that whilst pressures act normally to surfaces, friction acts tangentially.

A change in the angle of attack alters the flow pattern around the wing, resulting in a changed pressure distribution.

Wings are streamlined bodies, that is, their resistance at small angles of attack is largely due to skin friction, and the flow around the profile retains its streamline character (*Fig. 9.6a*). With increasing angle of attack a wake appears behind the body and the flow separates from the upper surface. At relatively low angles, this separation point, S, may be quite close to the rear or trailing edge (*Fig. 9.6b*), but moves forward with increasing angles of attack. Whilst the lift increases, the wake widens and drag increases too. At some stage the forward moving separation point reaches a position where lift increases no more and drag becomes very large (*Fig. 9.6c*). This phenomenon is called the stall and the angle is called the stall angle, which may be read off from *Fig. 9.4*. When the stall angle is reached the lift decreases and lift values are of less interest.

9.2 Magnus Effect and the Circulation Theory of Lift

It was stated in the preceding section (9.1) that symmetrical bodies immersed in a fluid stream, with their axis of symmetry directed parallel to the flow, experience a force acting exactly in the direction of the flow. This is due to the fact that the flow pattern around the body is symmetrical so that the pressure distribution will also be symmetrical. If, however, a symmetrical object, such as a cylinder, is placed in a fluid stream and rotated, the rotation causes a distortion of the original symmetrical flow pattern and hence a distortion of the pressure distribution. A transverse force, lift, is observed, the magnitude of which may be changed by altering either the speed of rotation or the stream velocity. The production of lift by a rotating cylinder placed in a fluid stream is known as the Magnus effect.

An explanation of the Magnus effect may be obtained from the following considerations. On the surface of the cylinder the fluid rotates with the speed of the cylinder and viscosity transmits the rotation to adjacent fluid layers. This boosts the velocity of the stream in the direction of rotation and opposes it in the reverse direction. The effect is shown in *Fig. 9.7*.

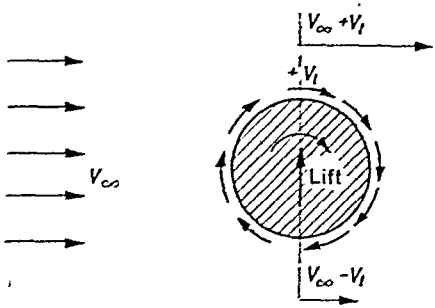

Figure 9.7—Magnus effect

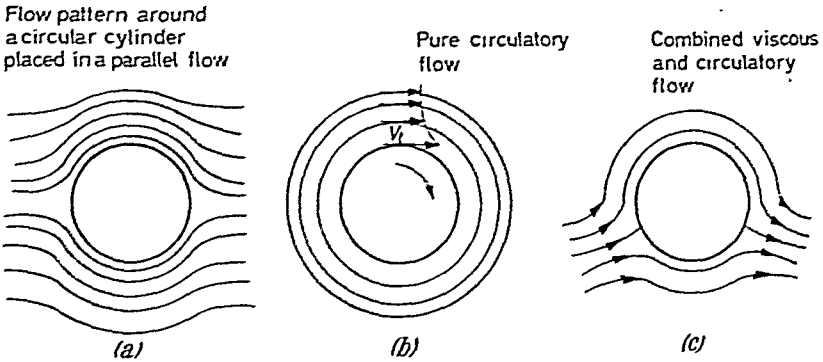

Figure 9.8

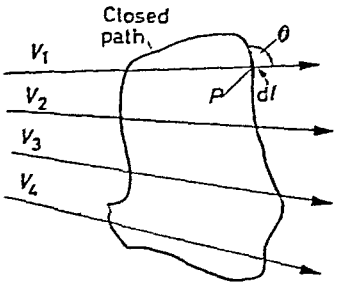

Figure 9.9—Definition of circulation

Let us place this cylinder in a parallel stream. In an ideal case the flow pattern is as illustrated in *Fig. 9.8a*. On the other hand a pure circulatory flow, resulting from a rotation, gives a flow pattern of concentric circles. A complete flow pattern may be obtained by superimposing the two fields and plotting streamlines with the aid of vector summation. The combined field is shown in *Fig. 9.8c*.

The Magnus effect was used some years ago to propel the Flettner rotor ship. Two cylinders of 9 ft. diameter and 60 ft. long were set in rotation at a speed of about 125 r.p.m. and these provided the circulatory motion, whilst natural wind supplied the parallel flow. The ship reached a speed of about 10 knots and was used for some time as a freight carrier.

The circulatory flow, or 'circulation', has since been closely connected to lift, even with the actual body rotation absent. Indeed, it has been shown that any body placed in a fluid stream may exhibit lift if a circulatory motion or 'circulation' is maintained in some way.

Having introduced the concept of circulation, it will be necessary to define it in a precise mathematical form. Consider a *closed* path drawn over any arbitrary flow field represented by velocity vectors V_1, V_2, V_3 . . . (*Fig. 9.9*). Let V be the velocity at a point of intersection P of the path with the flow pattern, ds an element of length along the path and θ the enclosed angle between V and dl (*Fig. 9.9*). Circulation, denoted as Γ, is the line integral of $V \cos \theta$. dl, taken around the path

$$\Gamma = \oint V \cos \theta \, \mathrm{d}l \qquad \ldots . (9.1)$$

As an example, let us calculate the circulation around a closed circular path of a fluid flowing in concentric circles and in such a manner that $V = A/r$† where A is a constant and r is the distance from the centre. This means that the velocity is constant along the circle at a given radius r. Since $\mathrm{d}l = r \, \mathrm{d}\phi$ and $\cos \theta = 1$

$$\Gamma = \oint_0^{\phi=2\pi} \frac{A}{r} r \, \mathrm{d}\phi = A \int_0^{2\pi} \mathrm{d}\phi = 2\pi A \qquad \ldots . (9.2)$$

It appears that the circulation of a concentric circle flow $V = A/r$ is constant and independent of the 'size' of the enclosed circular path. In fact, it may be shown that the circulation has the same value for every closed path which encloses the centre of the circles just once and has zero value for a path which excludes the centre. Note that values of the circulation may vary within other flow patterns.

† Derivation *see* Chapter 11, pp. 292, 300.

The effect of circulation on a cylinder placed in a parallel flow may be shown mathematically. This operation involves the principle of superposition which states that it is possible to build up complex flows by addition of a number of simpler flows. In considering a flow superposition, velocities of the component flows must be added at every point to obtain the final resultant flow. It may be shown† that when a cylinder of radius R is placed in a *perfect* fluid flow of velocity U, the flow pattern is symmetrical and the velocity at any point *on the surface* of the cylinder is given by $V = 2U \sin \theta$. On the other hand, a pure circulatory flow, such as described previously, would yield a velocity on the surface $V = \Gamma/2\pi \,.\, R$. The two flow patterns combined yield

$$V = 2U \sin \theta + \Gamma/2\pi R \qquad \ldots.(9.3)$$

Let us now consider the flow at a distance upstream from the cylinder where the flow is undisturbed by the presence of the body. Here the velocity of the stream is U and the static pressure p_0, whilst on the surface of the cylinder the velocity is V and the static pressure p. Applying Bernoulli's equation between the upstream section and any point on the surface

$$p_0 + \tfrac{1}{2}\rho U^2 = p + \tfrac{1}{2}\rho V^2$$

Substituting Eq. 9.3 for V and rearranging terms gives the pressure distribution around the cylinder

$$p = p_0 + \tfrac{1}{2}\rho[U^2 - (2U \sin \theta + \Gamma/2\pi R)^2] \qquad \ldots.(9.4)$$

From the pressure distribution, the transverse force may be calculated: the force on an element of unit length and of width $R \,.\, \mathrm{d}\theta$ is $pR \,\mathrm{d}\theta$: the transverse force $\mathrm{d}L$ is $pR \sin \theta \,\mathrm{d}\theta$.

Upon substitution for p (Eq. 9.4), the total transverse force is obtained by integration

$$L = \int_0^{2\pi} \{p_0 + \tfrac{1}{2}\rho[U^2 - (2U \sin \theta + \Gamma/2\pi R)^2]\} R \sin \theta \,\mathrm{d}\theta$$

As $\displaystyle\int_0^{2\pi} \sin \theta \,\mathrm{d}\theta = 0; \quad \int_0^{2\pi} \sin^3 \theta \,\mathrm{d}\theta = 0; \quad \int_0^{2\pi} \sin^2 \theta \,\mathrm{d}\theta = \pi$

$$L = -\rho U \Gamma \qquad \ldots.(9.5)‡$$

† See References.

‡ The negative sign results merely from the convention regarding a positive circulation.

Equation (9.5) known as the Kutta-Joukowski law, shows that the combination of circulation with a parallel flow results in a transverse force or lift, proportional to the fluid density, velocity and strength of circulation.

9.3 Two Dimensional Wing Theory

The Kutta-Joukowski law, derived for the simple case of a circular cylinder, has a wider range of application and holds for bodies of any shape placed in a two dimensional flow† of a perfect fluid. For wings, the following questions need answers:

(*a*) How accurately will the law hold for real (viscous) fluids?

(*b*) How is circulation originated?

(*c*) How is circulation maintained?

(*a*) Results of experiments carried out on aerofoils in wind tunnels show the existence of circulation and furnish strong evidence in favour of the theory. It was found that, except for the thin boundary layer formed on the surface, the main body of the fluid is not sensibly affected by viscosity and may be treated approximately as a perfect fluid, that is, calculations may be based on 'potential flow' theory. The relation between lift and circulation applied to real fluids agrees reasonably with the theory as long as the wing is placed at small angles of attack. Generally the Kutta-Joukowski law predicts larger lift than is found from observations and the discrepancy increases with increasing angles of attack. The reason for this discrepancy is the omission of viscosity from the theory. As one result, the law gives lift without drag and it can only be expected to apply accurately when the ratio of lift to drag is high. The existence of the boundary layer and its associated wake in real fluids also tends to make the lift less than its theoretical value.

(*b*) In two dimensional flow, circulation around a wing originates with the 'starting vortex'.

Rotating cylinders placed in flow of real fluids maintain their circulation through viscous action. Aerofoils, however, being non-rotational bodies, must have a circulation produced by different means. The process of producing circulation may be described briefly as follows: when the wing is set in motion from rest, a vortex is formed immediately downstream from the trailing edge, as shown in *Fig. 9.10.* This phenomenon takes place whenever

† Two dimensional flow demands that bodies placed in a real fluid stream either extend to infinity across the flow or end at walls.

Aerofoils tested in wind tunnels extend usually right across the working section. This is an important assumption because free ends alter the flow pattern considerably.

fluid streams of different velocities meet (*Fig. 9.11*). The fluid stream separated by the leading edge of the wing meets again at the trailing edge. At the beginning of the motion the fluid velocities are different (higher at the bottom surface than at the top) and

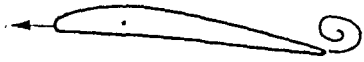

Figure 9.10—Starting vortex, forming

upon the meeting of the fluid layers a vortex is produced which is cast off soon after the wing has begun to move forward. After the start the flow rapidly adjusts itself and the two layers attain equal velocities so that no further starting vortices are shed.

Figure 9.11—Starting vortex, cast off

In order to counterbalance circulation of the starting vortex, another circulation of equal strength to the starting vortex, but of opposite sign, is set up around the wing. The sum of the circulations is zero, in accordance with Thomson's theorem, which states that

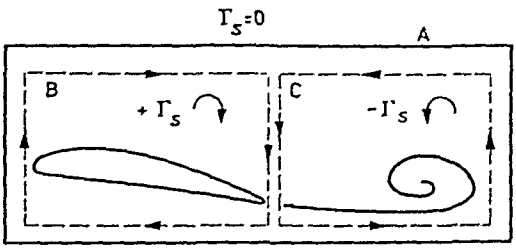

Figure 9.12—Circulation due to cast off starting vortex

circulation is independent of time. It also follows from the theorem that if around a contour circulation is zero before motion commences, it continues to be zero after the motion has started, even though finite circulations may be present within the contour. So if we take a contour around the airfoil, shown in *Fig. 9.12* as A, and divide this into two compartments, B and C, one of which

contains the starting vortex with $+\Gamma_s$ and the other, fixed relative to the wing, contains the airfoil with $-\Gamma_s$, we satisfy Thomson's theorem.†

(*c*) Flow observations made by visual methods confirm the existence of the starting vortex. A photograph showing a starting vortex is shown in *Fig. 9.13*. Viscosity effects, however, soon cause

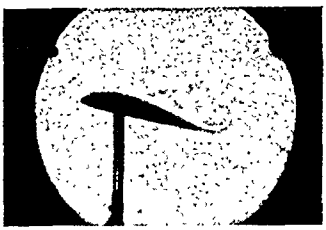

Figure 9.13—Photograph of a starting vortex.
(*By courtesy of the Aeronautical Research Council*)

the starting vortex to fuse with the surrounding fluid, turning its energy into heat, whilst the wing moving forward maintains a steady circulation. It will now be shown that this circulation depends upon the circulation in the boundary layer.

To understand the circulation in the boundary layers, consider first a section element ABCD cut out from a boundary layer (*Fig. 9.14*). Circulation in this element

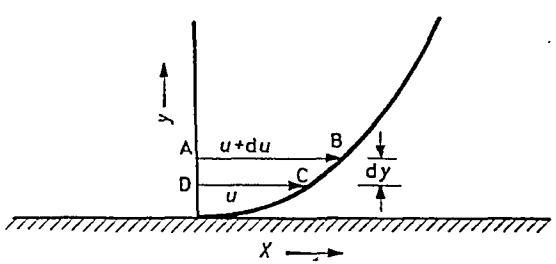

Figure 9.14

$$\oint V\,\mathrm{d}s = (U + \mathrm{d}U)\,\mathrm{d}x - U\,\mathrm{d}x = \mathrm{d}U\,\mathrm{d}x$$

Now, according to Stokes' theorem, the circulation Γ around the border of an area is equal to the sum of circulations $\Delta\Gamma$ around the

† Thomson's Theorem: In a frictionless fluid the circulation around any path which is made up of the same fluid particles is independent of the time.

elements making up that area, as shown in *Fig. 9.15.* Since boundary layers form on each side of the wing and there is circulation present in all boundary layer elements, the sum of these must be finite inside an area surrounded by a suitable border contour and the

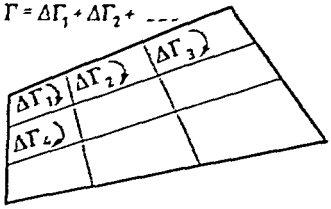

Figure 9.15

wing surface (*Fig. 9.16*). Denoting circulation on top by Γ_1 and at bottom by Γ_2, the difference $\Gamma_1 - \Gamma_2$ equals Γ the circulation strength of the starting vortex, and in fact, equals the net circulation around the wing.

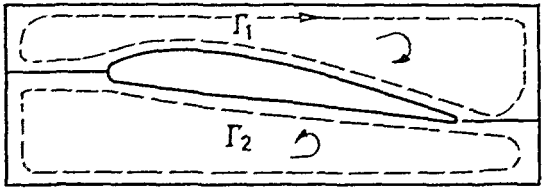

Figure 9.16—Net circulation due to boundary layer

If the circulation around the wing is changed, a fresh starting vortex is shed simultaneously which adjusts the strength of the starting vortex to the prevailing circulation level.

9.4 Coefficients of Lift and Drag

Lift and drag forces on wings may be obtained either from their pressure distribution or directly from readings on balances fitted to wind tunnels. The results are presented in form of lift and drag coefficients expressed as

lift coefficient $$C_L = \frac{L}{\frac{1}{2}\rho U^2 S} \qquad \ldots.(9.6)$$

drag coefficient $$C_D = \frac{D}{\frac{1}{2}\rho U^2 S} \qquad \ldots.(9.7)$$

The expressions are similar to the coefficient of form drag with the difference that the area S is no longer the projected area A_p normal to flow but the product of the span l and chord C (*Fig. 9.17*). Both lift and drag coefficients are frequently plotted against incidence

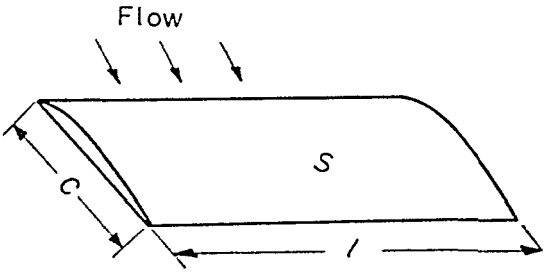

Figure 9.17—Wing plan form

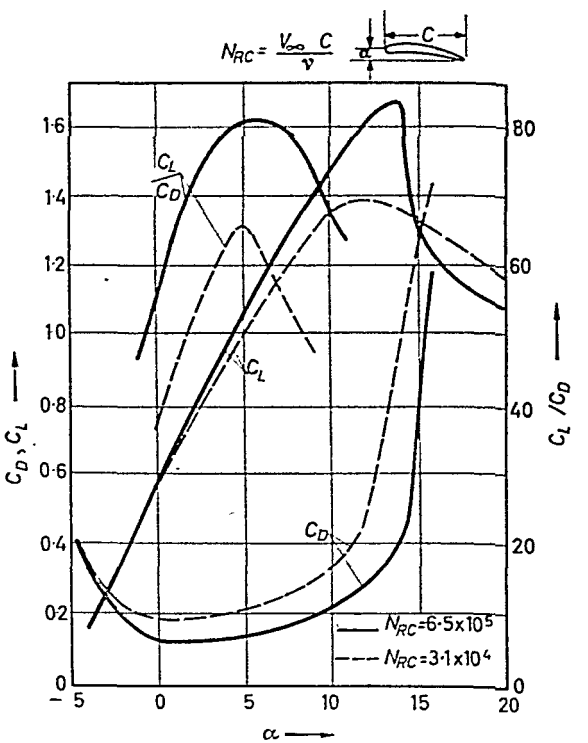

Figure 9.18—Lift and drag coefficients of a wing (two dimensional)

and a typical set of results is shown graphically in *Fig. 9.18.* Lift and drag coefficients behave similarly to the lift and drag forces and the above expressions were chosen so as to be usable, by any consistent system of units.

Both C_L and C_D are functions of the Reynolds' number N_{RC} based on the approach velocity of flow U and the chord C. For larger Reynolds' numbers (*e.g.*, 1·5 to 2 $\times$ 10^6) the variation of C_L and C_D with N_{RC} may be neglected.

9.5 Three Dimensional Wing Theory

In the following discussion, some results of the three dimensional wing theory will be described briefly.

It was stated earlier that two dimensional flow conditions demand either a wing of infinite span or a wing placed between parallel walls. Similarly the cast-off vortex must be either infinitely long or must end at the walls in a two dimensional flow. The spanwise distribution of lift is uniform for a parallel wing, that is, the value of lift per unit span is the same no matter which spanwise position is considered.

In three dimensional flow, the wing is considered of finite length, l, without walls so that the wing tips extend freely into the surrounding fluid. This affects the flow pattern and the spanwise distribution of lift, and the latter may vary from point to point along the span. Furthermore, the cast off vortex may no longer end on the walls nor will it extend to infinity. There is a theorem in ideal flow that vortex lines cannot begin or end in a fluid unless they extend to infinity or end at walls, otherwise they must form a closed path. This theorem can be usefully applied to real flow, where we frequently find vortex lines forming a closed path.

To demonstrate this concept, the airflow over the wing surface may be considered. It was stated earlier that pressure above the wing is less, and below greater than ambient (*see Fig. 9.19a*). At the wing tips the pressures equalize, however; hence there is a pressure gradient tending to make the fluid flow outwards (towards the tips) below and inwards (from the tips) above.

In plan view (*Fig. 9.19b*), the streamlines seem to cross each other, being pushed in on the top of the wing and 'sucked' out at the bottom.

As a result of this, the flow downstream from the trailing edge contains a multitude of vortices forming an entire vortex sheet. Visual observations show that this vortex sheet is not stable and rolls up at the edges, thus forming two strong concentrated 'trailing' vortices similar to those shown in *Fig. 9.20.*

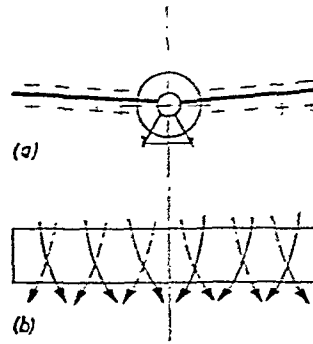

Figure 9.19

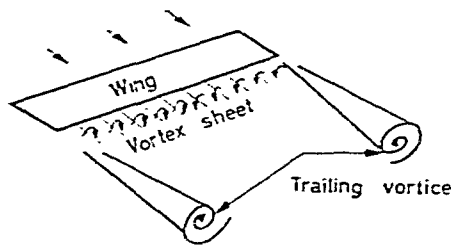

Figure 9.20

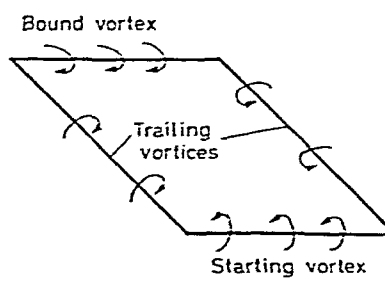

Figure 9.21

The vortex picture is now complete: there is circulation around the wing which is called a 'bound vortex' moving with the wing; the strength of the bound vortex at any point is equal to the circulation round the corresponding section of the wing; for theoretical purposes the wing itself may be replaced by the bound vortex line, the trailing vortices by the trailing vortex line and the circuit closed with the starting vortex line, as shown in *Fig. 9.21.*

To obtain the flow pattern of a moving wing of finite span, a superposition of the component flow fields is required. This can be done mathematically, but the calculations are rather elaborate and thus beyond the scope of present discussion; hence, only the essential results are noted.

The flow pattern of a cross-section of the trailing vortices shows a circulatory motion with a velocity distribution $V_r \propto \frac{\Gamma}{r}$ where r is distance from the vortex centre. When these velocities are combined

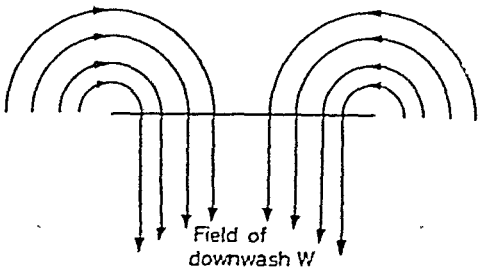

Figure 9.22

with the flow velocity downstream from the trailing edge a new flow pattern appears, showing the velocities inclined downward. The vertical component is called 'downwash' and its distribution depends on the circulation field along the span. A cross-sectional view of a downwash field is shown in *Fig. 9.22.*

9.6 Induced Drag and Lift

It appears from the preceding discussion that the finite wing produces a downwash velocity W. This must be added vectorially to the wing speed U, resulting in a deflected velocity V_i. An observer located on the wing experiences only the velocity V_i without knowing whether it actually comes from infinity or not. Hence, for the observer lift, L_i per unit span is $\rho V_i \Gamma$ and this is perpendicular to V_i, since the results of the two dimensional theory are carried over to the present case.

It appears from *Fig. 9.23* that the lift L_i, due to downwash, has a 'drag' component D_i in the flight direction, which is called 'induced' drag. From the similarity of vector triangles

$$\frac{D_i}{L} = \frac{W}{U} = \tan \varepsilon \propto \varepsilon$$

Thus the actual angle of incidence is reduced by ε, called the induced angle of incidence, giving the apparent angle of attack the value

$$\alpha_0 = \alpha - \varepsilon$$

From a physical viewpoint, the induced drag is represented by the kinetic energy of the trailing vortices as they are left behind (per unit length). In real fluids, there is still the 'form' or 'pressure' drag and frictional drag to be added to the induced drag.

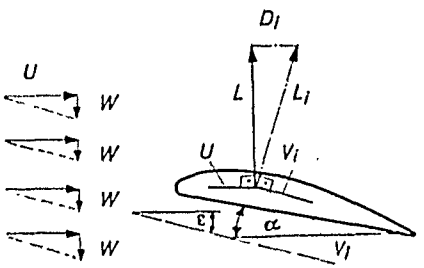

Figure 9.23—Induced drag and lift

A simple relation exists between induced drag and lift, which enables the designer to calculate lift and drag coefficients for three dimensional flow from measurements obtained on wings in two dimensional flow.
Since $L = C_L \frac{1}{2}\rho U^2 S$ similarly $D_i = C_{D_i} \frac{1}{2}\rho U^2 S$ it follows that

$$\frac{C_{D_i}}{C_L} = \frac{D_i}{L} = \frac{W}{U} \qquad \ldots\ldots(9.8)$$

To be able to use this relation, it is necessary to know the downwash velocity W distribution along the entire span. It may be shown that when the plan of the wing is elliptical or if the wings are tapered, $W \simeq$ CONST. and its value

$$W = \Gamma_0/2l \qquad \ldots\ldots(9.9)$$

A practical application of elliptical wing design was incorporated in the 'Spitfire', which had wings consisting of two semi-ellipses, as shown in *Fig. 9.24.* Elliptic wings have elliptic circulation distribution of the form

$$\Gamma = \Gamma_0 \sqrt{\left[1 - \left(\frac{x}{l/2}\right)^2\right]}$$

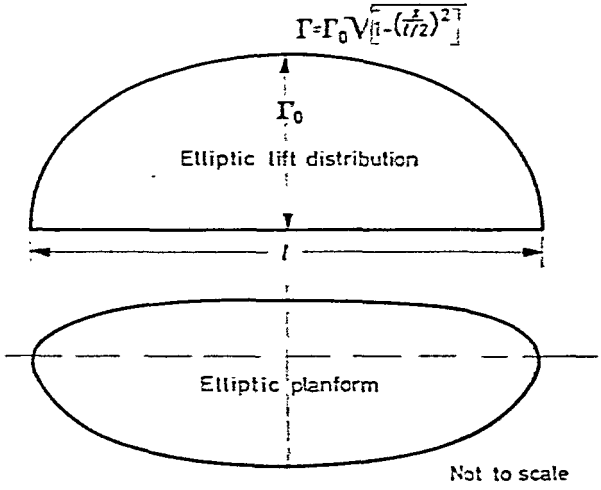

Figure 9.24

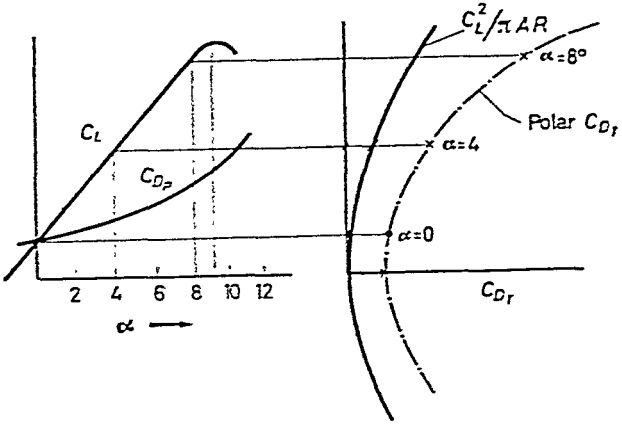

Figure 9.25

Figure 9.26

Total drag

where Γ_0 is the maximum circulation at the centre, x is distance from centre and l is the wing span. From the distribution of lift along the span, the total lift on the wing may be obtained by integration

$$L = \rho U \int_{-l/2}^{+l/2} \Gamma \, dx = \rho U \Gamma_0 \int_{-l/2}^{+l/2} \sqrt{\left[1 - \left(\frac{x}{l/2}\right)^2\right]} \, dx$$

$$= \rho U \Gamma_0 l \frac{\pi}{4} \qquad \ldots.(9.10)$$

Substituting Eq. 9.8 and 9.9 into Eq. 9.10, one obtains

$$L = C_L \tfrac{1}{2} \rho U^2 S = \rho U 2 l^2 W \frac{\pi}{4} = \tfrac{1}{2} \rho U^2 \frac{C_{D_i}}{C_L} \pi l^2$$

Upon rearranging

$$C_{D_i} = C_L^2 \cdot \frac{S}{\pi l^2} \qquad \ldots.(9.11)$$

The term l^2/S is called aspect ratio and is denoted by AR. For a rectangular wing $S = l \times c$, hence $AR = l/c$, the ratio of span to chord.

It follows that the total drag coefficient for wings in *three dimensional flow* is

$$C_{D_T} = C_{D_P} + C_{D_i} = C_{D_p} + \frac{C_L^2}{\pi AR} \qquad \ldots.(9.12)$$

where C_{D_P} is the drag coefficient in two dimensional flow and is known as the profile drag coefficient.

Clearly when $AR \rightarrow \infty$, $C_{D_T} \rightarrow C_{D_P}$.

It appears from Eq. 9.12 that induced, hence total drag, depends on the wing geometry defined by the aspect ratio. This may be illustrated by plotting C_L against C_D for a given value of AR. The procedure is as follows: first, the parabolic term $C_L^2/\pi AR$ is plotted against C_D, then corresponding profile drag figures of two dimensional flow are added which may be scaled off a C_L *versus* α graph (*Fig. 9.25*). The result appears now in form of the so called 'polar diagram' where the angles of attack are noted on the lift *versus* total drag curve, as shown in *Fig. 9.26.*

The graph may be re-plotted to give C_D and α against C_L. *Fig. 9.27* shows a series of curves for various aspect ratios, and it may be seen that an increase in an already high aspect ratio produces only a small reduction in drag.

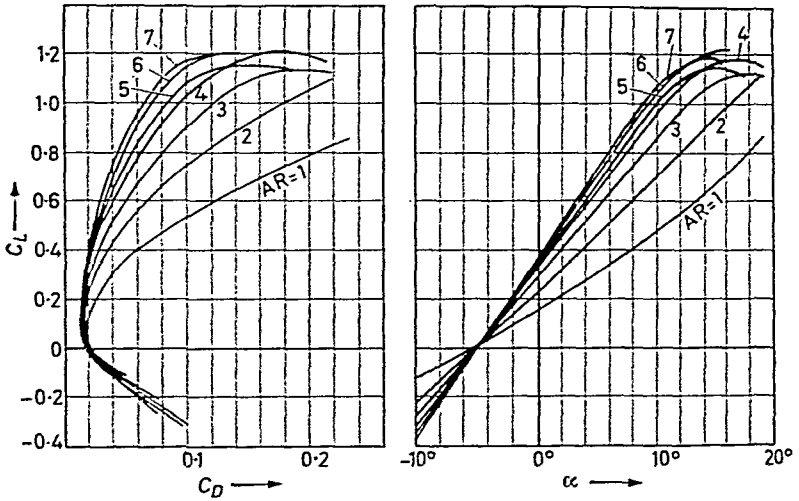

Figure 9.27—Dependence of lift and drag on aspect ratio

Examples

9.1. The wing of an aeroplane is designed to develop a lift of 10,000 lb. If the span is 35 ft. and the mean chord is 6 ft., calculate the total drag at a speed of 250 m.p.h. Assume elliptical lift distribution. $\rho = 0{\cdot}00233$ slugs/ft.^{3}

Solution.—At 250 m.p.h., $\frac{1}{2}\rho V^2 = \frac{1}{2} \times 0{\cdot}00233 \times (250 \times 1{\cdot}47)^2 = 158$ lb./ft.^{2} The wing surface $= 6 \times 35 = 210$ ft.^{2}

Hence, the lift coefficient

$$C_L = \frac{10000}{210 \times 158} = 0{\cdot}302$$

The Reynolds' number $N_R = \dfrac{250 \times 1{\cdot}47 \times 6}{1{\cdot}67 \times 10^{-4}} = 1{\cdot}32 \times 10^7$

At this N_R the drag coefficient (from two dimensional data)

$$C_D = C_{D_p} = 0{\cdot}07$$

The induced drag coefficient

$$C_{D_i} = \frac{C_L^2}{\pi AR} = \frac{0{\cdot}302^2}{\pi \times 35/6} = 0{\cdot}00494$$

Total drag coefficient

$$C_{D_t} = 0{\cdot}07 + 0{\cdot}00472 = 0{\cdot}0742$$

Hence drag

$$D = 0{\cdot}0742 \times 158 \times 210 = 2460 \text{ lb.}$$

9.2. For the same lift and speed as given in the preceding example, a smaller wing area will suffice if the lift coefficient is higher. Taking C_L at the maximum value C_L/C_D calculate the wing area and the drag.

Solution.—At maximum C_L/C_D the lift coefficient is found $C_L = 1{\cdot}05$ and $C_{D_p} = 0{\cdot}4$

Hence the wing area $S = \dfrac{10000}{158 \times 1{\cdot}05} = 60 \text{ ft.}^2$

The chord $C = \sqrt{\dfrac{60}{5{\cdot}83}} = 3{\cdot}2$ and Reynolds' number $N_R = 7 \times 10^6$

For the same aspect ratio

$$C_{Di} = \frac{1{\cdot}052}{\pi \times 5{\cdot}83} = \frac{1{\cdot}1}{\pi \times 5{\cdot}83} = 0{\cdot}06$$

Total drag coefficient

$$C_D = 0{\cdot}4 + 0{\cdot}06 = 0{\cdot}46$$

Drag

$$D = 0{\cdot}46 \times 158 \times 60 = 4370 \text{ lb.}$$

9.3. If the aspect ratio of the wing in the preceding example is increased from 5·83 to 7, calculate the reduction per cent in the induced drag coefficient. Assume the same lift coefficient.

Solution.—The reduction is

$$\Delta C_{Di} = \frac{C_L^2}{\pi}\left[\frac{1}{AR_1} - \frac{1}{AR_2}\right] = \frac{1{\cdot}05^2}{\pi}\left[\frac{1}{5{\cdot}83} - \frac{1}{7}\right] = 0{\cdot}01$$

This corresponds to $\dfrac{1}{6} = 16{\cdot}6$ per cent reduction.

REFERENCES

(1) PRANDTL, L., and TIETJENS, O. G., *Applied Hydro- and Aero-Mechanics*, McGraw-Hill, New York, 1934.
(2) STREETER, V., *Fluid Dynamics*, McGraw-Hill, New York, 1938.
(3) KUETHE, A. M., and SCHETZER, J. D., *Foundations of Aerodynamics*, John Wiley and Sons, 1950.
(4) GLAUERT, H., *Aerofoil and Airscrew Theory*, Cambridge University Press, 1937.

Problems

9.1. In a game of tennis, a ball is served so that a rotation is added to its motion of translation. If the rotation is about a horizontal axis, discuss the effect of the rotation on the flight of the ball.

9.2. Modern ships are being provided with stabilizers which substantially consist of a pair of under-water wings protruding from the hull. Calculate the righting moment and drag (power) of a pair of stabilizers fitted to 20,000 ton passenger ship travelling at a speed of 18 knots. The stabilizer wings have 6 ft. chord and are protruding 12 ft. from the hull, where the width across the ship is 60 ft. Assume $C_L = 1{\cdot}0$, $C_D = 0{\cdot}1$ (for $AR = \infty$). Density of sea water is 1·99 slugs/ft.^{3} Kinematic viscosity $\nu = 1{\cdot}3 \times 10^{-5}$ ft.^{2}/sec. Nautical mile = 6080 ft.

PART 2

10

FUNDAMENTALS OF THE FLOW OF COMPRESSIBLE FLUIDS

10.1 Introduction

THE flow of fluids under circumstances in which marked changes in density and pressure are accompanied by marked changes in velocity, and vice versa, is frequently referred to as compressible flow.

Among the fluids one generally finds that compressibility affects the flow of gases to a much larger extent than it affects liquids, particularly when high speed flow is encountered. Admittedly there is no precise boundary between high- and low-velocity flow and since all gases are easily compressible, density changes may take place even at low velocities, these, however, need not necessarily be large and a slowly moving gas may be treated as an incompressible fluid. The range may be limited depending on the accuracy required.

Marked compressibility effects appear when velocities attained are of the order of the speed of sound propagation through the gas. These effects of compressibility on the flow of gases may be observed *either* inside ducts and passages between the vanes of machines, where the flow velocity is high such as found in turbines and compressors, *or* over surfaces of bodies travelling at high speed, such as projectiles, rockets, aircraft wings, propeller blades *etc.* The following discussion will be limited to flow inside passages only, mainly because the flow over surfaces is a field beyond the scope of this text.

It is of interest to note that marked changes in pressure and velocity are also frequently encountered in liquids without a comparable change in the density. This type of phenomenon is characterized by marked accelerations rather than high velocities and the sudden changes in the flow are generally accompanied by pressure waves travelling at high speed inside the fluid. A typical example of such a pressure wave is the water-hammer produced by the sudden closing of a valve in a pipeline. Although water-hammer is a phenomenon in which compressibility effects must be taken into account it will be excluded from the present discussion because of the absence of marked density changes.

10.2 Total Energy Equation

The transformation of energy in fluids, as expressed by the Bernoulli equation, is restricted to non-frictional and incompressible flow.

A more general law governing the flow of fluids may be obtained by adding to the Bernoulli equation

$$\frac{\mathrm{d}p}{w} + \frac{V\,\mathrm{d}V}{g} + \mathrm{d}z = 0$$

the conservation of energy equation, well known from studies in thermodynamics, *i.e.*,

$$\mathrm{d}Q = \mathrm{d}E + p\,\mathrm{d}v/J$$

The combination yields

$$J\,.\,\mathrm{d}Q = \frac{\mathrm{d}p}{w} + \frac{V\,\mathrm{d}V}{g} + \mathrm{d}Z + J\,\mathrm{d}E + p\,\mathrm{d}v$$

This equation may be rearranged by considering that $1/w = v$ and that $p\,\mathrm{d}v + v\,\mathrm{d}p = \mathrm{d}(pv)$; further the sum $\mathrm{d}E + \frac{\mathrm{d}(pv)}{J} = \mathrm{d}I$, where I is commonly denoted as 'enthalpy'. Hence

$$J\,\mathrm{d}Q = J\,.\,\mathrm{d}I + \frac{V\,\mathrm{d}V}{g} + \mathrm{d}Z \qquad \ldots.(10.1)$$

Eq. 10.1 illustrates the various types of energy contained in a fluid flow, being 'enthalpic' (pressure and internal energy), kinetic and potential. It also expresses the simple fact that any change in the external heat supply $\mathrm{d}Q$ will result in changes in the component energies.

Integration of Eq. 10.1 leads to

$$\pm J\,.\,Q_{1-2} = J(I_1 - I_2) + \frac{V_1^2 - V_2^2}{2g} + Z_1 - Z_2 \quad \ldots.(10.2)$$

The symbol $\pm Q_{1-2}$ signifies a heat quantity transferred between sections 1 and 2. The positive sign denotes heat addition; the negative sign substraction of heat. Heat energy may be added to a fluid flow through the walls of the ducting, through heat transfer surfaces placed in the stream or burning fuel by injection. Heat may be subtracted by means of cooling coils or liquid sprays.

As mechanical work W is also considered as a form of heat, Q may either be replaced by its work equivalent in heat units or be combined with some work as well. Hence Eq. 10.2 may be extended

and written in a more general form

$$\pm W_{1-2} \pm J \cdot Q_{1-2} = J(I_1 - I_2) + \frac{V_1^2 - V_2^2}{2g} + Z_1 - Z_2 \quad \ldots.(10.3)$$

where the symbol $\pm W_{1-2}$ signifies the work done either on the fluid or by the fluid between sections 1 and 2. The positive sign denotes work done on the fluid; the negative sign work done by the fluid. Work on the fluid may be obtained by means of a pump or compressor and work done by the fluid takes place inside turbines or windmills.

The total energy Eq. 10.3 may be written in another form for gases. Substituting for internal energy $E = C_v\theta$ and for $p \cdot v$ the equivalent $R \cdot \theta$ one obtains

$$I = E + pv/J = C_v\theta + R\theta/J = (C_v + R/J)\theta$$

Since

$$C_p - C_v = R/J$$

it follows that enthalpy for gases

$$I = C_p\theta$$

Hence the total energy equation for gases

$$\pm W_{1-2} \pm JQ_{1-2} = JC_p(\theta_1 - \theta_2) + \frac{V_2^2 - V_1^2}{2g} + Z_1 - Z_2 \quad \ldots.(10.4)$$

The right hand side of the equation signifies the fact that the component energies of gases are: temperature, kinetic, and potential energies.

10.3 Adiabatic Flow of Gases. The Concept of Static and Stagnation Temperature

When no change of heat or work content is experienced in a gas the left hand side of Eq. 10.4 is zero. Usually changes in the potential energy may be neglected and Eq. 10.4 reduces to

$$JC_p(\theta_1 - \theta_2) + \frac{V_1^2 - V_2^2}{2g} = 0 \quad \ldots.(10.5)$$

Rearranging and dividing by $J \cdot C_p$ yields

$$\theta_1 + \frac{V_1^2}{2gJC_p} = \theta_2 + \frac{V_2^2}{2gJC_p} \quad \ldots.(10.6)$$

process no change in entropy is observed and the process is called 'isentropic'; the value of the polytropic index attains its highest limiting value when $n = \gamma = C_p/C_v$ and yields a temperature ratio

$$\theta_2'/\theta_2 = (p_2/p_1)^{\frac{\gamma-1}{\gamma}} \qquad \ldots.(10.11)$$

On the other hand, an adiabatic expansion with friction present yields values for n less than γ. Large frictional losses decrease the value of n and hence the exit velocity, whereas highly efficient nozzles have n near the value of γ. The lower limiting value of n is unity ($n = 1$) which represents no change in temperature and velocity between inlet and outlet. Such expansion may be considered a throttling process. Events may be demonstrated on a

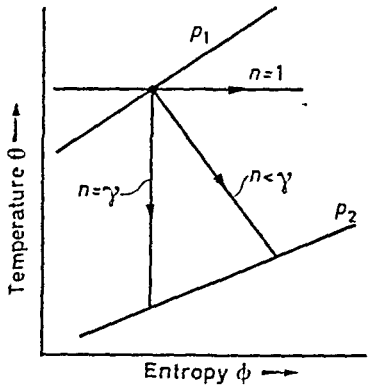

Figure 10.2—Temperature–entropy diagram for expansion processes

temperature-entropy diagram as shown in *Fig. 10.2.* Although Eq. 10.11 gives the necessary condition to obtain an exit velocity V_2 for a specified pressure ratio p_2/p_1, it will be shown that this formula alone is inadequate for the design of a nozzle and further knowledge in gas flow, relating velocities with nozzle-area changes, is required.

10.5 Velocity of Propagation of an Infinitesimal Pressure Disturbance. Speed of Sound

Consider a long straight cylinder provided with a light frictionless piston (*Fig. 10.3a*). Gas fills the space on either side of the piston and when at rest, the pressure and density of the gas are p_0 and ρ_0 respectively. At a given instant the piston is displaced to the right with a small velocity q and this movement is sufficient to set up a small disturbance (in the form of a weak pressure wave) which is

then travelling 'downstream' with a velocity a. The initial position of the piston is marked 0. During the brief time δt of piston movement the piston advances to position 1, over a distance $s = q\ \delta t$ whilst the wavefront of the disturbance advances to a position x over a distance $L = a\ .\ \delta t$. The gas 'trapped' between the piston

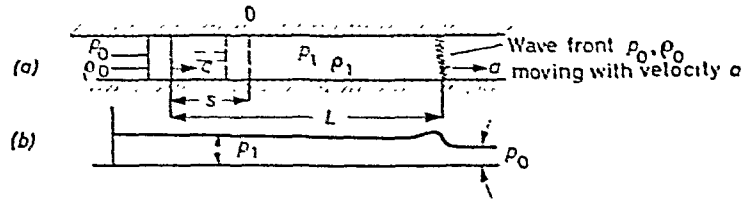

Figure 10.3—Pressure wave travelling downstream in a pipe

and the wave front is thus compressed slightly, attaining a pressure and density p_1 and ρ_1 respectively, whilst ahead of the wave front p and ρ remain unaffected (*see Fig. 10.3b*). If the cross-sectional area of the cylinder is A, the volume of the 'trapped' gas is $A(L - s)$ and its mass $A(L - s)\rho_1 = A\ \delta t(a - q)\rho_1$. This mass of gas is considered to move to the right with a continuous velocity of q and as the wave front advances the affected mass of gas increases. The momentum gained by the affected gas mass during the brief time δt is $A\ \delta t(a - q)\rho_1 q$; the time rate of change of this momentum yields a continuous force

$$F = A(a - q)\rho_1 q$$

which must be equal to the force observed across the wave front due to the pressure difference $p_1 - p_0$. Thus

$$A(p_1 - p_0) = A(a - q)\rho_1\ .\ q$$

and since $q \ll a$, $a - q \simeq a$, one obtains

$$p_1 - p_0 = a\rho_1 q \qquad \ldots.(10.12)$$

Another equation may be obtained by considering mass conservation, *i.e.*, the mass contained between piston and wave front prior to piston movement must be equal to the mass after the piston displacement, so that

$$A(a\ .\ \delta t)\rho_0 = A(a - q)\ \delta t\ .\ \rho_1$$

which yields

$$a(\rho_1 - \rho_0) = q\rho_1 \qquad \ldots.(10.13)$$

Combination of Eqs. 10.12 and 10.13 gives

$$\frac{p_1 - p_0}{\rho_1 - \rho_0} = a^2$$

Decreasing the differences $p_1 - p_0$ and $\rho_1 - \rho_0$ to infinitesimal values, $(\mathrm{d}p, \mathrm{d}\rho)$ yields

$$\frac{\mathrm{d}p}{\mathrm{d}\rho} = a^2 \quad \text{or} \quad a = \sqrt{\frac{\mathrm{d}p}{\mathrm{d}\rho}} \qquad \ldots.(10.14)$$

The symbol 'a' is referred to sound or acoustic speed although the name is misleading. Pressure waves due to sound effects of extremely low intensity, in fact infinitesimal intensity, travel with the speed defined by Eq. 10.14. Loud sound travels faster than the acoustic speed and sound waves set up by explosions may travel with speeds several times faster still.

In gases $\mathrm{d}p/\mathrm{d}\rho$ may be expressed in terms of static temperature. The slight compression of the gas may be considered as being truly isentropic so that the thermodynamic relationship $p/\rho^{\gamma} = \text{CONST.}$ will hold. Differentiating with respect to ρ yields

$$\frac{\mathrm{d}p}{\mathrm{d}\rho} = \text{CONST.} \times \gamma\rho^{\gamma-1} = \gamma \times \text{CONST.}\frac{\rho^{\gamma}}{\rho} = \gamma\frac{p}{\rho}$$

Combining this with the gas equation $p = \rho g R 0$, one obtains

$$\frac{\mathrm{d}p}{\mathrm{d}\rho} = \gamma \,.\, g \,.\, R \,.\, 0$$

hence the speed of sound

$$a = \sqrt{(\gamma g R 0)} \qquad \ldots.(10.15)$$

10.6 Mach Number

It was shown in the preceding section (Eq. 10.15) that the speed of sound a varies with the square root of the static temperature 0, (γ, g, and R being considered as constants).

Referring to a gas stream flowing with a velocity V or to an object moving with a speed V relative to a gas, a dimensionless parameter M is introduced

$$M = \frac{V}{a} = \frac{\text{velocity}}{\text{speed of sound}} = \frac{V}{\sqrt{(\gamma g R 0)}} \qquad \ldots.(10.16)$$

The symbol M stands for 'Mach' number, named after Professor Mach. The Mach number is significant in all problems concerning high speed gas flow.

Example

10.1. A jet propelled aircraft is flying at 600 m.p.h. at sea level. Calculate the Mach number and the rise in skin temperature assuming a recovery factor 0·88. Temperature = 70°F, gas constant $R = 53{\cdot}3$, $\gamma = 1{\cdot}4$.

Solution.—Mach number

$$M = \frac{1{\cdot}47 \times 600}{\sqrt{(1{\cdot}4 \times 32{\cdot}2 \times 53{\cdot}3 \times 530)}} = 0{\cdot}78$$

Temperature rise

$$\Delta\theta = 0{\cdot}88 \times \left(\frac{600}{100}\right)^2 = 31{\cdot}6°\text{C} = 55°\text{F}$$

10.7 Non-frictional Flow of Gases Inside Ducts

The following considerations will be strictly applicable to non-frictional flow and the equations derived may only be used for frictional flow when friction losses are reasonably small in comparison with other changes and may thus be neglected. The equations used will be quoted in their physical and also in log-differential form.

The continuity equation gives

$$W = A\rho g V$$

or

$$\frac{\mathrm{d}A}{A} + \frac{\mathrm{d}\rho}{\rho} + \frac{\mathrm{d}V}{V} = 0 \qquad \ldots\ldots(10.17)$$

The gas equation gives

$$p = \rho g R\theta$$

or

$$\frac{\mathrm{d}p}{p} = \frac{\mathrm{d}\rho}{\rho} + \frac{\mathrm{d}\theta}{\theta} \qquad \ldots\ldots(10.18)$$

The Mach number equation gives

$$M^2 = \frac{V^2}{\gamma g R\theta}$$

or

$$\frac{\mathrm{d}M}{M} = \frac{\mathrm{d}V}{V} - \frac{1}{2}\frac{\mathrm{d}\theta}{\theta} \qquad \ldots\ldots(10.19)$$

The isentropic pressure–density relationship gives

$$p/\rho^{\gamma} = \text{CONSTANT}$$

or

$$\frac{\mathrm{d}p}{p} - \gamma\frac{\mathrm{d}\rho}{\rho} = 0 \qquad \ldots\ldots(10.20)$$

The total energy equation, written in differential form is

$$JC_p\,\mathrm{d}\theta + V\,\mathrm{d}V/g = 0 \qquad \ldots.(10.21)$$

It will now be shown that $\mathrm{d}V/V$, $\mathrm{d}\theta/\theta$, $\mathrm{d}p/p$ may be expressed as some function of the Mach number and its log-differential $\mathrm{d}M/M$ so that $\mathrm{d}A/A$ and ultimately A may also be expressed as functions of M.

(*a*) Consider $\mathrm{d}V/V$

Dividing Eq. 10.21 by V^2 and substituting $C_p = \dfrac{\gamma}{\gamma - 1} \cdot \dfrac{R}{J}$ gives

$$\frac{\gamma}{\gamma - 1}\frac{R\,\mathrm{d}\theta}{V^2} + \frac{\mathrm{d}V}{gV} = 0$$

and as $V^2 = M^2 . (\gamma g R\theta)$

$$\frac{1}{(\gamma - 1)M^2} \cdot \frac{\mathrm{d}\theta}{\theta} + \frac{\mathrm{d}V}{V} = 0 \qquad \ldots.(10.22)$$

From Eq. 10.19 $\mathrm{d}\theta/\theta = 2(\mathrm{d}V/V - \mathrm{d}M/M)$ so that upon substitution one obtains

$$\frac{\mathrm{d}V}{V} = \frac{\mathrm{d}M/M}{1 + (\gamma - 1)M^2/2} \qquad \ldots.(10.23)$$

As M^2 is always positive, velocity and Mach number changes have the same sign.

(*b*) Consider $\mathrm{d}\theta/\theta$

Substitution of Eq. 10.23 into 10.22 leads to

$$\frac{\mathrm{d}\theta}{\theta} = \frac{-(\gamma - 1)M^2\,\mathrm{d}M}{[1 + (\gamma - 1)M^2/2]M} \qquad \ldots.(10.24)$$

Equation 10.24 shows that static temperature and Mach number changes have opposite signs.

(*c*) Consider $\mathrm{d}p/p$

Combining Eqs. 10.18 and 10.20 leads to

$$\frac{\mathrm{d}p}{p} = \frac{\gamma}{\gamma - 1} \cdot \frac{\mathrm{d}\theta}{\theta}$$

and substitution of Eq. 10.24 for $\mathrm{d}\theta/\theta$ leads to

$$\frac{\mathrm{d}p}{p} = \frac{-\gamma M^2}{1 + (\gamma - 1)M^2/2} \cdot \frac{\mathrm{d}M}{M} \qquad \ldots.(10.25)$$

Eq. 10.25 shows that pressure and Mach number changes have opposing signs.

Combining Eqs. 10.17 and 10.18 yields

$$\frac{dA}{A} = \frac{d\theta}{\theta} - \frac{dp}{p} - \frac{dV}{V} \qquad \ldots.(10.26)$$

and substitution of Eqs. 10.23, 10.24, and 10.25 into Eq. 10.26 gives

$$\frac{dA}{A} = \frac{-(1 - M^2)}{1 + (\gamma - 1)M^2/2} \cdot \frac{dM}{M} \qquad \ldots.(10.27)$$

The numerator of Eq. 10.27 shows the dependence of the sign of dA/A upon the value $(1 - M^2)$.

For subsonic flow

$$M^2 < 1, \quad 1 - M^2 > 0 \quad \text{so that } dA/A \text{ is negative}$$

Hence subsonic flow demands a decreasing cross-sectional area for acceleration (dM is positive) and vice versa;

For sonic flow

$$M^2 = 1 \quad 1 - M^2 = 0 \quad \text{so that } dA/A = 0$$

which means that in a non-frictional flow a parallel duct, called a 'throat', invariably leads to sonic flow, provided there is adequate pressure available.

For supersonic flow

$$M^2 > 1, \quad 1 - M^2 \quad \text{so that } dA/A > 0$$

Hence supersonic flow demands an increasing cross-sectional area for acceleration (dM positive) and vice versa.

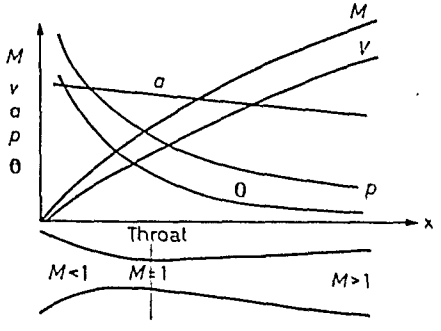

Figure 10.4—Change of flow variables along a convergent-divergent duct

In the well known convergent–divergent nozzle (frequently called the de Laval nozzle), acceleration starts with a subsonic flow in the convergent duct, attaining sonic flow at the 'throat' and supersonic flow in the divergent section. During the expansion static pressure energy is continually transformed into kinetic energy. An approximate representation of events is shown in *Fig. 10.4.*

Integration of Eq. 10.27 leads to

$$\log A = \log \left\{ \frac{(1 + (\gamma - 1)M^2/2)^{\frac{\gamma+1}{2(\gamma-1)}}}{M} \right\} + \log C$$

or

$$\frac{A_1}{A_2} = \frac{M_2}{M_1} \left\{ \frac{1 + (\gamma - 1)M_1^2/2}{1 + (\gamma - 1)M_2^2/2} \right\}^{\frac{\gamma+1}{2(\gamma-1)}} \quad \ldots.(10.28)$$

It is convenient to substitute the throat area A_{th} for A_2, where $M_2 = 1$. The resulting equation

$$\frac{A}{A_{th}} = \frac{1}{M} \left\{ \frac{1 + (\gamma - 1)M^2/2}{(\gamma + 1)/2} \right\}^{\frac{\gamma+1}{2(\gamma-1)}} \quad \ldots.(10.29)$$

may be employed for computations of area and Mach numbers and values of M for corresponding A/A_{th} may be readily found in tables.

It is noted that Eq. 10.29 may be used with limited accuracy for frictional flow in nozzles provided that the thickness of the boundary layer is taken into consideration and that the nozzle efficiency is high (n is near γ).

10.8 Temperature, Pressure and Mach Number Relationship in Non-frictional Flow

Stagnation and static temperature ratio in terms of Mach number may be obtained readily from the energy equation. Substituting $\frac{\gamma}{\gamma - 1} \cdot \frac{R}{J}$ for C_p in Eq. 10.6 one obtains

$$\frac{\gamma}{\gamma - 1} R\theta_1 + \frac{V_1^2}{2g} = \frac{\gamma}{\gamma - 1} R\theta_2 + \frac{V_2^2}{2g}$$

At a stagnation point $V_2 = 0$, $\theta_2 = T$ so that generally

$$\frac{\gamma}{\gamma - 1} \cdot R\theta + \frac{V^2}{2g} = \frac{\gamma}{\gamma - 1} RT$$

Substituting $V^2 = M^2/(\gamma g R\theta)$ and rearranging yields

$$\frac{T}{\theta} = 1 + \frac{\gamma - 1}{2} M^2 \quad \ldots.(10.30)$$

As the total energy equation holds for both frictional and non-frictional flow Eq. 10.30 also hold for both types of flow. Hence

the stagnation temperature remains the same along the flow, although the value of static temperature depends on frictional re-heating.

The ratio P/p of stagnation pressure, to static pressure, may be readily be calculated from Eq. 10.30 by considering that for isentropic state change

$$\frac{T}{\theta} = \left(\frac{P}{p}\right)^{\frac{\gamma-1}{\gamma}}$$

Hence

$$\frac{P}{p} = \left[1 + \frac{\gamma - 1}{2} M^2\right]^{\frac{\gamma}{\gamma-1}} \qquad \ldots.(10.31)$$

This Eq. 10.31 is rigorously true for conditions at a given point in a flow, but in the presence of friction P decreases along the stream. Consequently P is equal to the reservoir pressure only in frictionless flow.

10.9 The Fanno Equation

Processes taking place in a duct of constant area are of special significance. Introducing

$$\psi = \frac{W}{A} = \frac{\text{mass flow}}{\text{cross-sectional area}}$$

the continuity equation becomes

$$\psi = \rho g V$$

Substituting $V = M\sqrt{(\gamma g R\theta)}$, $\rho = p/(gR\theta)$ and $\theta = T/\left(1+(\gamma-1)\frac{M^2}{2}\right)$ in the continuity equation, upon rearranging terms, one obtains

$$\frac{\psi\sqrt{T}}{p} = \sqrt{\frac{\gamma g}{R}}\, M \sqrt{\left(1 + \frac{\gamma - 1}{2} M^2\right)} \qquad \ldots.(10.32)$$

Eq. 10.32 is known as the Fanno equation and has a variety of applications.

By plotting $\psi\sqrt{T}/p$ against M (*Fig. 10.5*) one may determine (graphically) the average Mach number in a duct at any section where the area A is known and the static pressure p and stagnation temperature T is measured. Since $\psi = W/A$, the measurement of the mass flow W by some convenient method, such as an orifice

plate or nozzle, is also required. As an example an application for determination of Mach number along a nozzle is shown in *Fig. 10.6.*

For a duct of constant cross section constant ψ lines, called

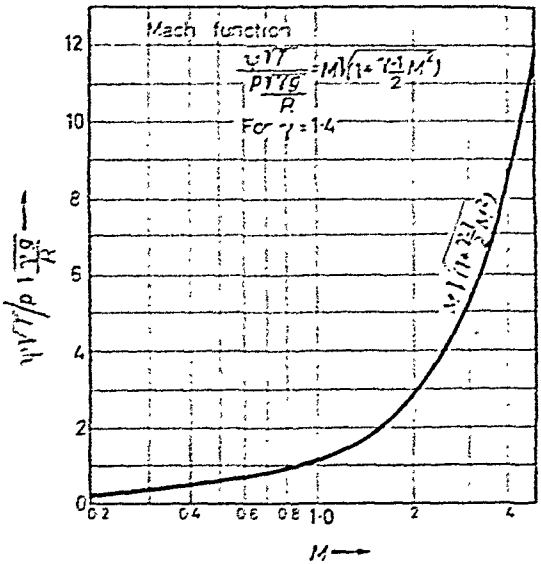

Figure 10.5

'Fanno curves', may be drawn on the temperature entropy plane. For a specified stagnation temperature the shape of all Fanno curves

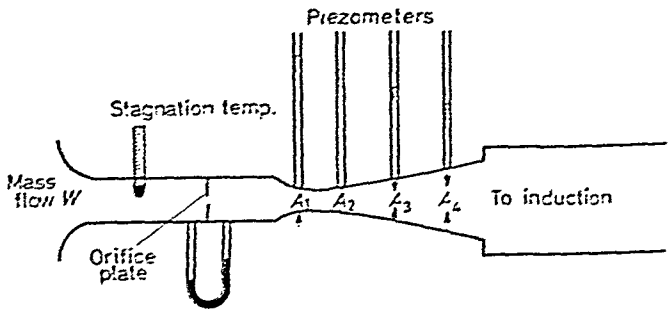

Figure 10.6

become identical; substitution of various values for ψ only displaces the curves without changing their shape. As an example Fanno

curves are shown in *Fig. 10.7*. Static temperatures and corresponding Mach numbers for this stagnation temperature are noted on the vertical ordinate.

A particular characteristic of the Fanno curves is that all vertical tangents appear at $M = 1$. For each curve entropy attains maximum at this point. Starting with a sub-sonic condition (noted as A on ψ_1 line) and following along the upper limb, or starting with

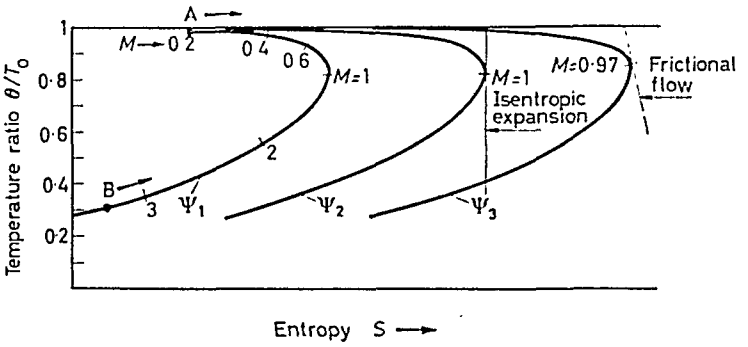

Figure 10.7—Fanno curves

a supersonic condition (noted B) and following the lower limb of the Fanno curve, the limiting entropy is reached at sonic flow. It follows, that entropy increase causes, at subsonic starting conditions, acceleration of the flow up to the speed of sound, and at supersonic starting conditions deceleration of the flow down to the speed of sound. The cause of both effects is friction and it was shown earlier that non-frictional flow in a constant area duct causes no change in M. The length of parallel ducting, over which the condition $M = 1$ is attained, is called the 'limiting length' and its value may be calculated if the friction factor f and inlet Mach number is known.

Isentropic expansion, being represented by a straight vertical line, contacts one particular ψ-line tangentially and intersects other Fanno curves. This particular ψ-line will be the 'throat' curve which is contacted at maximum entropy at $M = 1$. Other lines have lower values indicating convergent–divergent ducting. An expansion with friction and with a slight entropy increase is shown by the dotted line on *Fig. 10.7*. The curve contacts the ψ-line at a point where the Mach number is somewhat less than unity, the exact value depending on the polytropic index n. It may be shown that in case of frictional flow at the throat $M = \sqrt{[(n-1)/(\gamma-1)]}$. For example $n = 1{\cdot}35$, $\gamma = 1{\cdot}4$ values, $M = 0{\cdot}97$.

Example

10.2. Because of friction, the Mach number increases in a duct of constant cross-section from 0·3 to 0·7. Assuming adiabatic flow conditions and an initial pressure of 25 lb./in.^{2} abs., calculate the final pressure.

Solution.—Since mass flow, stagnation temperature and area are constant, it follows from the Fanno equation, that $W\sqrt{T}/A = C$

$$\therefore \quad p_1 M_1 \sqrt{\left(1 + \frac{\gamma - 1}{2} M_1^2\right)} = p_2 M_2 \sqrt{\left(1 + \frac{\gamma - 1}{2} M_2^2\right)}$$

Hence

$$p_2 = p_1 \frac{M_1}{M_2} \sqrt{\left(\frac{1 + (\gamma - 1)M_1^2/2}{1 + (\gamma - 1)M_2^2/2}\right)} = 25 \times \frac{0{\cdot}3}{0{\cdot}7} \times \sqrt{\frac{1{\cdot}018}{1{\cdot}098}} = 10{\cdot}3 \text{ lb./in.}^2 \text{ abs}$$

10.10 Frictional Losses in Parallel Pipes

It was stated in the preceding section that friction accelerates a subsonic and decelerates a supersonic stream. In a subsonic stream pressure, static temperature and density decrease while velocity and Mach number increase: thus the flow expands along the pipe. In a supersonic stream pressure, static temperature and density increase while velocity and Mach number decrease: hence the gas is being compressed along the flow. For both subsonic and supersonic inlet conditions, the limiting condition at the outlet is sonic flow.

The Reynolds' number changes follow the Mach number changes. Since mass flow $A \cdot V \cdot \rho$ is constant along the flow, any change in the Reynolds' number is due only to changes in viscosity†. Changes in the Reynolds' number result in changes of the friction factor, hence in a compressible fluid stream the friction factor generally varies along the flow.

For the purpose of calculations of the friction factor f, it is necessary to distinguish between short and long parallel pipes. Results obtained from experiments on short parallel pipes ($L/D = 150$) show that large changes in the flow conditions take place mainly near the outlet as shown in *Fig. 10.8.* Thus, for approximate calculations, the friction factor could be considered as constant along the pipe provided fully developed turbulent flow prevails. This may hold for long pipes and the value of f thus may be obtained satisfactorily from friction factor charts. In short pipes, however, the flow is undeveloped and a considerable discrepency

† For air $\mu = \mu_0 \dfrac{0{\cdot}312 + \theta^{3/2}}{\theta + 120} \times 10^{-7}$ where θ is in °C.

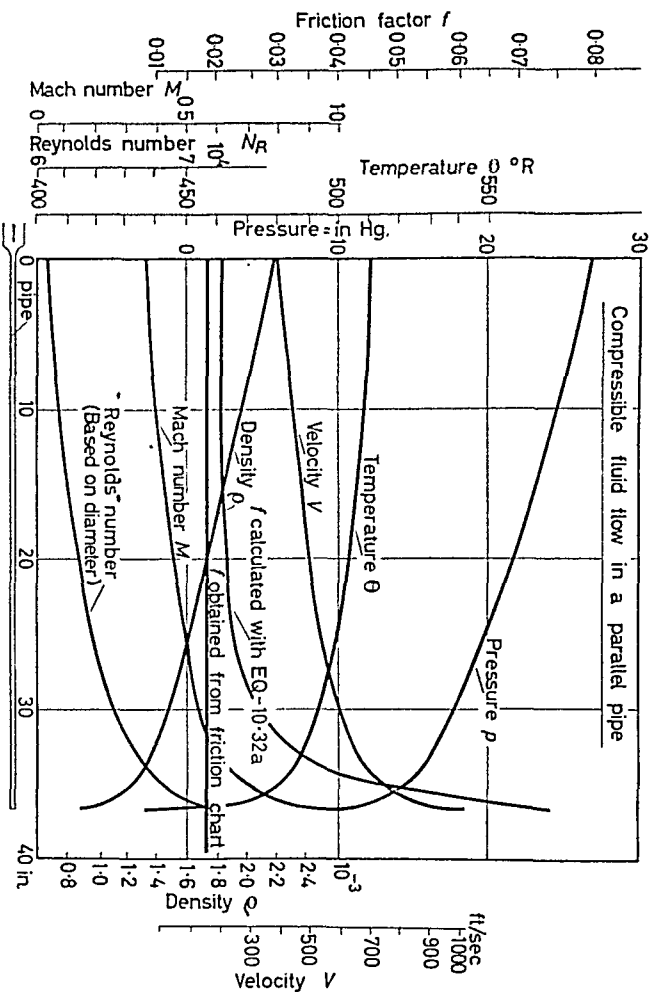
Friction factor f
0·001
0·002
0·003
0·004
0·005
0·006
0·007
0·008
Mach number M
0
0·5
1·0
Reynolds number N_R
6
7
10^6
400
450
500
550
Temperature θ °R
Pressure in Hg.
10
20
30
Compressible fluid flow in a parallel pipe
Pressure p
Temperature θ
Velocity V
Density ρ
Mach number M
"Reynolds" number (Based on diameter)
f calculated with EQ. 10·32a
f obtained from friction chart
0 pipe
10
20
30
40 in.
Distance along pipe
10^-3
1·8
2·0
2·2
2·4
1·6
1·4
1·2
1·0
0·8
Density ρ
ft/sec
300
500
700
900
1000
Velocity V

Figure 10.8

exists between values obtained from friction factor charts and values obtained from the experiments calculated with the formula†

$$f = \frac{D}{4(x_2 - x_1)}\left[\frac{1}{\gamma}\left\{\frac{1+\frac{\gamma-1}{2}M_1^2}{M_1^2} - \frac{1+\frac{\gamma-1}{2}M_2^2}{M_2^2}\right\} - \frac{\gamma+1}{2\gamma}\log_e\left\{\frac{M_2^2}{M_1^2}\cdot\frac{1+\frac{\gamma-1}{2}M_1^2}{1+\frac{\gamma-1}{2}M_2^2}\right\}\right] \quad \ldots.(10.32a)$$

where M_2 is distant x_2 from inlet
M_1 is distant x_1 from inlet.

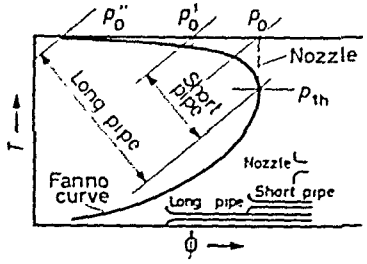

Figure 10.9

Since the data on friction factors of undeveloped flow are, at present, incomplete, calculations of frictional losses in short pipes are rather unreliable.

Representation of pressure changes on the $T - \phi$ plane in a convergent nozzle, a short and a long pipe for a constant specific mass flow (ψ = CONST.), is shown in *Fig. 10.9.* It may be seen that, for $M = 1$ *at exit*, the reservoir pressure P_0 at inlet to the nozzle must be at least $\left(\frac{2}{\gamma+1}\right)^{\frac{\gamma-1}{\gamma}} p_{th}$ this being the lowest value of P_0. If this convergent nozzle is fitted with a short or long parallel pipe, the inlet stagnation pressure is required to be higher so that P_0' and P_0'' etc. are pushed further to the left on the Fanno curve.

10.11 The Convergent–Divergent Nozzle. Effects of Variation of Back Pressure

The convergent–divergent duct, known as the Laval nozzle, plays a significant role in turbines and other machines and in the light

† The derivation of this formula is rather long and is therefore omitted from the text.

of the preceding sections a more detailed study of the flow conditions will now be made. Non-frictional flow will be assumed.

Consider first the flow conditions at the throat, the divergent section being removed. Denoting pressure, temperature and density in the reservoir, from which the stream issues, as P_0, T_0 and ρ_0 respectively, and substituting at the throat $M = 1$ into the Fanno equation, one obtains

$$W = \frac{p_{th}}{\sqrt{T_0}} A_{th} \sqrt{\frac{\gamma g}{R}} \sqrt{\frac{\gamma + 1}{2}} \quad \ldots.(10.33)$$

where A_{th} is the area and p_{th} the pressure at the throat. It follows from Eq. 10.31 that

$$\frac{p_{th}}{P_0} = \left(\frac{2}{\gamma + 1}\right)^{\frac{\gamma}{\gamma - 1}} \quad \ldots.(10.34)$$

so that Eq. 10.33 may be written

$$W = K \,.\, A_{th} \frac{P_0}{\sqrt{T_0}} \text{ where } K = \sqrt{\frac{\gamma g}{R}\left(\frac{2}{\gamma + 1}\right)^{\frac{\gamma+1}{\gamma-1}}} \quad \ldots.(10.35)$$

For air $\gamma = 1{\cdot}4$ and the value of $K = 0{\cdot}51$ so that

$$W = 0{\cdot}51 \,.\, A_{th} \frac{P_0}{\sqrt{T_0}}$$

The static temperature θ_{th} at the throat may be obtained from Eq. 10.30

$$\theta_{th} = \frac{2}{\gamma + 1} T_0 \quad \ldots.(10.36)$$

and the density at the throat may be obtained upon substituting Eq. 10.34 and 10.36 into the gas equation

$$\rho_{th} = \left(\frac{2}{\gamma + 1}\right)^{\frac{1}{\gamma - 1}} \frac{P_0}{gRT_0} \quad \ldots.(10.37)$$

The following conclusions may be made:

1. Provided sonic flow is attained at the throat, the mass flow is proportional to the reservoir pressure and inversely proportional to the half power of the stagnation temperature.

2. Sonic flow is attained at the throat if the static pressure $p_{th} = 2/(\gamma + 1)^{\gamma/(\gamma-1)} P_0$. If the nozzle discharges into the surroundings (without the diverging section) the surrounding pressure, called back pressure, must be equal to or *less* than p_{th}. On this assumption, a variation of the back pressure results in no change of the mass flow.

3. The flow velocity at the throat depends only on the stagnation temperature as may be seen by considering that for $M = 1$

$$V = \sqrt{(\gamma g R \theta_{th})} = \sqrt{\left(\frac{2\gamma}{\gamma + 1} g R T_0\right)}$$

4. Density varies directly with P_0 and inversely with T_0.

When the convergent nozzle is provided with the divergent section, expansion of the gas continues along the divergent duct without affecting conditions at the throat. The Mach number at the exit may be obtained by solving Eq. 10.31 for M

$$M_e = \sqrt{\left[\frac{2}{\gamma - 1}\left\{\left(\frac{P_0}{p_e}\right)^{\frac{\gamma}{\gamma-1}} - 1\right\}\right]} \qquad \ldots.(10.37)$$

Emphasis is laid on the requirement that the static exit-pressure p_e in the nozzle must be equal to the back pressure. For this exit Mach number the nozzle area may be calculated from Eq. 10.29.

Once p_e is specified, variation of the back pressure p_a influences exit conditions considerably.

5. If the back pressure is lower than the static pressure inside the nozzle at exit, a further expansion of the gas takes place outside the nozzle resulting in an increase in the stream velocity, the excess pressure $p_e - p_a$ being converted into kinetic energy. The mass flow (being entirely defined by the throat conditions), and the flow inside the nozzle remain unchanged.

6. If the back pressure rises above p_e, flow conditions inside the nozzle change at the exit. Velocity and Mach number decrease whilst the pressure rises until at exit p_e becomes equal to p_a. The mass flow remains unchanged as long as p_a is less than the pressure at the throat.

The change of flow conditions takes place through the setting up, *inside the nozzle*, of a pressure wave, called a 'shock wave' which abruptly changes supersonic into subsonic flow. In going along the nozzle we find: subsonic expansion between inlet and throat, followed by supersonic expansion between throat and shock wave, and finally subsonic diffusion between shock and exit. There is a sudden pressure rise across the shock followed by a gradual pressure rise downstream. The effect is shown in *Fig. 10.10.*

The shock wave itself may be located between the throat and the exit and between these limiting positions its exact location depends on the value of p_a.

An increase of back pressure p_a results in the shock being moved towards the throat and once the condition $p_a = p_{th}$ is attained the shock disappears. For values of $p_a < p_{th}$ the nozzle behaves like a

Venturi and the mass flow, hitherto unchanged, decreases. The other limiting position for a shock wave inside the nozzle is in the

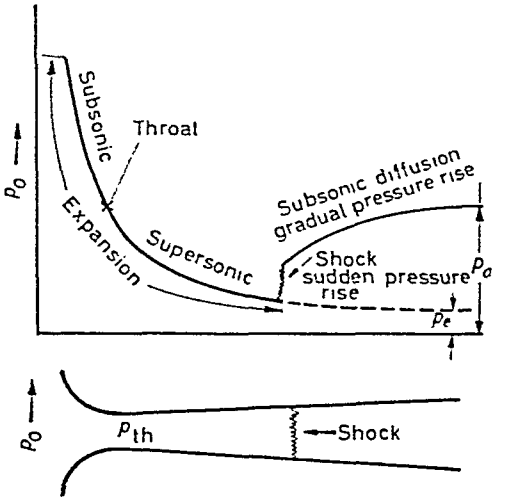

Figure 10.10—Pressure changes along a convergent–divergent nozzle

exit plane. This condition defines a back pressure p_a^+ and it will be shown in Section 10.14 that external oblique shocks begin to

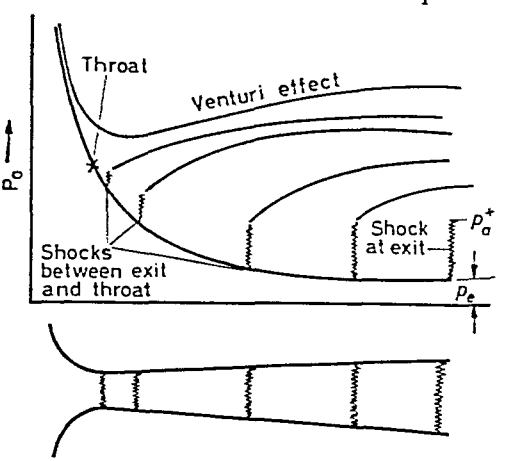

Figure 10.11—The effects of shock location on pressure distribution in a divergent nozzle

appear outside the nozzle once the back pressure falls below p_a^+. These effects are shown in *Fig. 10.11.*

A Laval nozzle with incorrect back pressure functions inefficiently and the stream loses much of its momentum through the shock. Detailed study of shock waves is presented in successive chapters.

10.12 Normal Shock Waves

It was stated in the preceding Section 10.11 that rising back pressure results in a shock wave being set up inside the divergent section of a Laval nozzle. The type of shock is said to be 'normal' when the plane of the shock is substantially perpendicular to the

Figure 10.12—A normal shock situated between oblique shock formations. (*By courtesy of the Institution of Mechanical Engineers*)

direction of flow. On the other hand a shock is said to be 'oblique' when the plane is inclined to the direction of flow. On passing through the shock there is a sudden (discontinuous) rise, not only in pressure, but also in density, static temperature, and entropy; Mach number and velocity drop sharply across the shock. Shocks set up in nozzles are stationary in steady flow, as long as the pressures are kept constant.

Physically, a shock wave is a pressure wave of finite thickness, calculated to be of the order of 10^{-4} in.; it follows that the shock thickness is of the order of the mean free path.

A shock must always be compressive and Mach number always decreases across a shock, the upstream Mach number being supersonic. Normal shocks do not usually appear without being accompanied by other shocks of oblique formation. This may also be observed in the vicinity of solid walls where the stream outside the boundary layer is supersonic; a fine net of oblique shocks may be seen, this being the result of interaction between main shock and boundary layer. In *Fig. 10.12* oblique shock waves, springing from

wedges, a normal shock and reflected oblique shocks are shown. In *Fig. 10.13* a shock boundary layer interaction is shown.

Consider now a normal shock inside a duct. Upstream of the shock the flow is supersonic with velocity V_1, pressure p_1, density ρ_1,

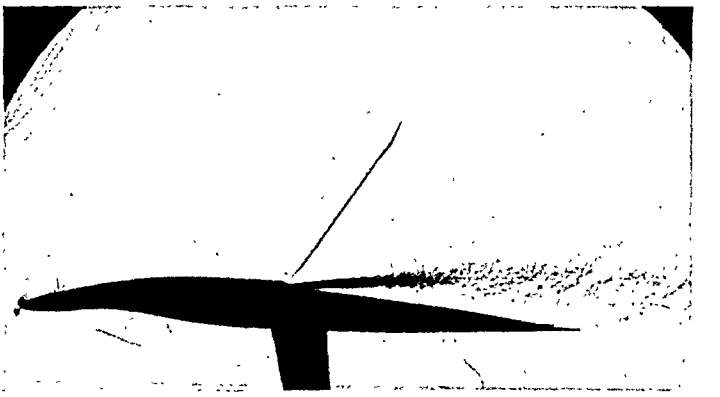

Figure 10.13—Shock over a wing. (Incidence 6°, upstream Mach number 0·84, transition fixed at leading edge). (*By courtesy of N.P.C. Crown copyright reserved*)

temperature θ_1, downstream from the shock subsonic conditions prevail with velocity V_2, pressure p_2, density ρ_2 and temperature θ_2. In passing through the shock (see *Fig. 10.14*) the gas loses momentum

Figure 10.14

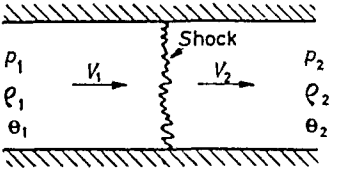

proportionally to the velocity change $V_1 - V_2$ so that a force is experienced in the direction of the flow which is balanced by the pressure difference $p_2 - p_1$ across the shock. (The action is somewhat similar to a sheet of plywood being held firmly against a constant barrage of oranges.) For a cross-section of unit area $A = 1$ the continuity equation gives the mass flow as

$$\rho_1 V_1 = \rho_2 V_2 \qquad \ldots\ldots(10.38)$$

Accordingly, the momentum equation is

$$p_2 - p_1 = \rho_1 V_1 (V_1 - V_2) \qquad \ldots\ldots(10.39)$$

The total energy remains constant across the shock

$$JgC_p\theta_1 + \frac{V_1^2}{2} = JgC_p\theta_2 + \frac{V_2^2}{2} = T_0' \qquad \ldots.(10.40)$$

where $T_0' = JgC_pT_0$, T_0 being the stagnation temperature on both sides of the shock.

Substituting $R\gamma/(\gamma - 1)J$ for C_p and p/ρ . R for $g\theta$ in Eq. 10.40 gives

$$\frac{\gamma}{\gamma - 1}\frac{p_1}{\rho_1} + \frac{V_1^2}{2} = \frac{\gamma}{\gamma - 1}\frac{p_2}{\rho_2} + \frac{V_2^2}{2} = T_0' \qquad \ldots.(10.41)$$

and upon rearranging

$$\frac{\gamma}{\gamma - 1}\left(\frac{p_2}{\rho_2} - \frac{p_1}{\rho_1}\right) = \tfrac{1}{2}(V_1^2 - V_2^2) \qquad \ldots.(10.42)$$

To eliminate $V_1^2 - V_2^2$ multiply both sides of Eq. 10.39 by $(V_1 + V_2)$ and divide by $\rho_1V_1 = \rho_2V_2$

$$\frac{p_2 - p_1}{\rho_1V_1}(V_1 + V_2) = (V_1 - V_2)(V_1 + V_2) = V_1^2 - V_2^2$$

and upon rearranging

$$V_1^2 - V_2^2 = (p_2 - p_1)\left[\frac{V_1}{\rho_1V_1} + \frac{V_2}{\rho_2V_2}\right]$$

$$= (p_2 - p_1)\left[\frac{1}{\rho_1} + \frac{1}{\rho_2}\right] \qquad \ldots.(10.43)$$

Combining Eq. 10.42 with 10.43 yields

$$\frac{\gamma}{\gamma - 1}\left[\frac{p_2}{\rho_2} - \frac{p_1}{\rho_1}\right] = \tfrac{1}{2}(p_2 - p_1)\left[\frac{1}{\rho_1} + \frac{1}{\rho_2}\right]$$

Upon rearranging and solving for p_2/p_1 one obtains

$$\frac{p_2}{p_1} = \frac{1 - \dfrac{\rho_2}{\rho_1}\dfrac{\gamma + 1}{\gamma - 1}}{\dfrac{\rho_2}{\rho_1} - \dfrac{\gamma + 1}{\gamma - 1}} \qquad \ldots.(10.44)$$

Solving for ρ_2/ρ_1 the same equation yields

$$\frac{\rho_2}{\rho_1} = \frac{1 + \dfrac{\gamma + 1}{\gamma - 1}\dfrac{p_2}{p_1}}{\dfrac{\gamma + 1}{\gamma - 1} + \dfrac{p_2}{p_1}} \qquad \ldots.(10.45)$$

These are the equations of Rankine and Hugoniot first used in studies of ballistics. These equations will be used in due course.

Consider now Eq. 10.41; it follows that

$$\frac{p_1}{\rho_1} = \frac{\gamma - 1}{\gamma}\left[T_0' - \frac{V_1^2}{2}\right] \quad \text{and} \quad \frac{p_2}{\rho_2} = \frac{\gamma - 1}{\gamma}\left[T_0' - \frac{V_2^2}{2}\right]$$

With these values of p/ρ the momentum equation becomes

$$\begin{aligned} V_1 - V_2 = \frac{p_2 - p_1}{\rho_1 V_1} &= \frac{1}{V_2}\left(\frac{p_2}{\rho_2}\right) - \frac{1}{V_1}\left(\frac{p_1}{\rho_1}\right) \\ &= \frac{1}{V_2}\left[\frac{\gamma - 1}{\gamma}\left(T_0' - \frac{V_2^2}{2}\right)\right] - \frac{1}{V_1}\left[\frac{\gamma - 1}{\gamma}\left(T_0' - \frac{V_1^2}{2}\right)\right] \\ &= (V_1 - V_2)\frac{\gamma - 1}{\gamma}\left[\frac{T_0'}{V_1 V_2} + \frac{1}{2}\right] \qquad \ldots.(10.46) \end{aligned}$$

To appreciate the significance of Eq. 10.46 a new parameter, called the critical speed of sound a^* is introduced. In a gas stream a^* is attained at some point where the fluid velocity V becomes equal to the local sound velocity a. For example, in a convergent–divergent nozzle $V = a^*$ at the throat. Substituting $V = a^*$ in Eq. 10.41 and remembering that $a^2 = \gamma p/\rho$

$$\frac{a^{*2}}{\gamma - 1} + \frac{a^{*2}}{2} = \frac{\gamma + 1}{2(\gamma - 1)}a^{*2} = T_0' \qquad \ldots.(10.47)$$

With this value of T_0 Eq. 10.46 becomes

$$V_1 - V_2 = (V_1 - V_2)\frac{\gamma - 1}{\gamma}\left[\frac{\gamma + 1}{2(\gamma - 1)} \cdot \frac{a^{*2}}{V_1 V_2} + \frac{1}{2}\right] \qquad \ldots.(10.48)$$

One obvious solution to this is $V_1 - V_2 = 0$. The other is

$$V_1 V_2 = a^{*2} \qquad \ldots.(10.49)$$

Eq. 10.49 is of fundamental importance, for it gives the velocity change across the shock wave. With the aid of this relationship, the pressure, density, temperature, and Mach number changes across the shock may be expressed in terms of Mach number M_1 in front of the shock.

Pressure Change Across a Normal Shock

The energy equation may be written as

$$\frac{c_1^2}{\gamma-1}-\frac{V_1^2}{2}=T_t=\frac{\gamma+1}{2(\gamma-1)}c^{*2}$$

Dividing by V_1^2 and substituting $M_1^2=V_1^2/c_1^2$ yields

$$\frac{1}{\gamma-1}\frac{1}{M_1^2}-\frac{1}{2}=\frac{\gamma+1}{2(\gamma-1)}\left(\frac{c^*}{V_1}\right)^2$$

and solving for V_1/c^* gives

$$\left(\frac{V_1}{c^*}\right)^2=\frac{\gamma+1}{\gamma-1-2/M_1^2} \qquad \ldots\ldots(10.50)$$

Similarly

$$\left(\frac{V_2}{c^*}\right)^2=\frac{\gamma+1}{\gamma-1-2/M_2^2} \qquad \ldots\ldots(10.51)$$

It follows from Eq. 10.49 that

$$\left(\frac{V_2}{V_1}\right)=\left(\frac{c^*}{V_1}\right)^2 \quad \text{or} \quad \frac{V_2}{V_1}=\left(\frac{V_1}{c^*}\right)^2$$

hence Eq. 10.49 becomes

$$\frac{V_2}{V_1}=\frac{\gamma-1}{\gamma-1-2/M_1^2} \qquad \ldots\ldots(10.52)$$

Substituting this value of V_2/V_1 for p_2/p_1 in Eq. 10.44, one obtains

$$\frac{p_2}{p_1}=\frac{\dfrac{\gamma+1}{\gamma-1}\dfrac{V_2}{V_1}-1}{\dfrac{\gamma+1}{\gamma-1}-\dfrac{V_2}{V_1}}=\frac{\dfrac{\gamma+1}{\gamma-1}\left[\dfrac{\gamma-1}{\gamma-1-2/M_1^2}\right]-1}{\dfrac{\gamma+1}{\gamma-1}-\dfrac{\gamma-1}{\gamma-1-2/M_1^2}}$$

Upon simplifying we obtain the pressure ratio across the normal shock

$$\frac{p_2}{p_1}=\frac{2\gamma}{\gamma+1}M_1^2-\frac{\gamma-1}{\gamma+1} \qquad \ldots\ldots(10.53)$$

Density Ratio Across a Normal Shock

The density ratio across the shock follows from Eq. 10.52

$$\frac{\rho_2}{\rho_1} = \frac{V_1}{V_2} = \frac{(\gamma + 1)M_1^2/2}{1 + \frac{\gamma - 1}{2} M_1^2} \qquad \ldots\ldots(10.54)$$

Static Temperature Ratio Across Normal Shock

From the gas equation

$$\frac{\theta_2}{\theta_1} = \frac{p_2}{p_1} \cdot \frac{\rho_1}{\rho_2}$$

Upon substitution of Eqs. 10.53 and 10.54, one obtains

$$\frac{\theta_2}{\theta_1} = \frac{[2\gamma M_1^2 - (\gamma - 1)][2 + (\gamma - 1)M_1^2]}{(\gamma + 1)^2 M_1^2} \qquad \ldots\ldots(10.55)$$

Mach Number Downstream from a Normal Shock

The Mach number immediately downstream from the normal shock may be obtained by first re-writing Eq. 10.49, so that

$$\left(\frac{V_1}{a^*}\right)^2 \left(\frac{V_2}{a^*}\right)^2 = 1$$

and then substituting Eq. 10.50 and 10.51. Thus

$$\left[(\gamma - 1) + \frac{2}{M_1^2}\right]\left[(\gamma - 1) + \frac{2}{M_2^2}\right] = (\gamma + 1)^2$$

Solving for M_2^2 yields

$$M_2^2 = \frac{1 + \frac{\gamma - 1}{2} M_1^2}{\gamma M_1^2 - \frac{\gamma - 1}{2}} \qquad \ldots\ldots(10.56)$$

Eq. 10.56 shows that for a normal shock the downstream Mach number is always subsonic. If the upstream Mach number becomes very large M_2 approaches a limiting value. This may be calculated

by dividing the right hand side of Eq. 10.56 by M_1^2 and letting M_1 tend to ∞. The limiting value is

$$M_2 = \sqrt{\frac{\gamma - 1}{2\gamma}}$$

Fig. 10.15 shows Eqs. 10.53, 10.54, 10.55, and 10.56 plotted against M_1 for air. ($\gamma = 1{\cdot}4$)

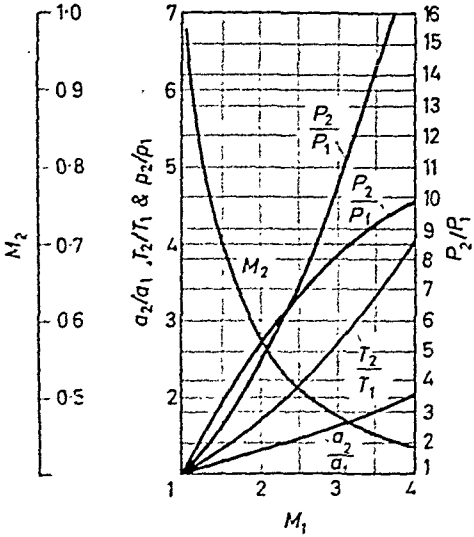

Figure 10.15—Changes of flow variables across a normal shock wave. (*By courtesy of the Institution of Mechanical Engineers*)

Example

10.3. Calculate the Pitot pressure of an air stream flowing at 1350 ft./sec. Assume that the bow wave set up ahead of the tube is detached, the centre part being considered as a normal shock. Ambient pressure = 14·7 lb./in.^{2} abs., static temperature = 70°F.

Solution.—Upstream of the shock, the Mach number

$$M_1 = \frac{1350}{\sqrt{(1{\cdot}4 \times 32{\cdot}2 \times 53{\cdot}3 \times 530)}} = 1{\cdot}195$$

Pressure rise across the shock

$$\frac{p_2}{p_1} = \frac{2 \times 1{\cdot}4}{1{\cdot}4 + 1} 1{\cdot}195^2 - \frac{1{\cdot}4 - 1}{1{\cdot}4 + 1} = 1{\cdot}404$$

Downstream from the shock the Mach number

$$M_2 = \frac{1 + \dfrac{1{\cdot}4 - 1}{2} 1{\cdot}195^2}{1{\cdot}4 \times 1{\cdot}195^2 - \dfrac{1{\cdot}4 - 1}{2}} = 0{\cdot}716$$

Hence the ratio of stagnation to static pressure, downstream from the shock (isentropic deceleration)

$$\frac{P_0}{p_2} = \left(1 + \frac{\gamma - 1}{2} M_2^2\right)^{\gamma/\gamma - 1} = (1 + 0{\cdot}2 \times 0{\cdot}716^2)^{3{\cdot}5} = 1{\cdot}442$$

Hence the total pressure rise

$$\frac{P_0}{p_1} = \frac{p_2}{p_1} \times \frac{P_0}{p_2} = 1{\cdot}404 \times 1{\cdot}442 = 2{\cdot}025$$

$$\therefore \qquad P_0 = 2{\cdot}025 \times 14{\cdot}7 = 29{\cdot}8 \text{ lb./in.}^2 \text{ abs.}$$

10.13 Entropy Change Across a Normal Shock

From the definition of entropy, it follows that

$$\mathrm{d}\phi = \frac{\mathrm{d}Q}{\theta} = \frac{\mathrm{d}E}{\theta} + \frac{p\mathrm{d}v}{J\theta}$$

Substituting $\mathrm{d}E = C_V\,\mathrm{d}\theta$, $pv = R\theta$

$$\mathrm{d}\phi = C_V \frac{\mathrm{d}\theta}{\theta} + \frac{R}{J}\frac{\mathrm{d}v}{v}$$

Again, since

$$\frac{\mathrm{d}\theta}{\theta} = \frac{\mathrm{d}v}{v} + \frac{\mathrm{d}p}{p} \quad \text{and} \quad C_p - C_V = \frac{R}{J}$$

$$\mathrm{d}\phi = C_p \frac{\mathrm{d}v}{v} + C_V \frac{\mathrm{d}p}{p}$$

Integration between limits 1 and 2 leads to

$$\Delta\phi = \phi_2 - \phi_1 = C_V \left[\gamma \,.\, \log_e \frac{v_2}{v_1} + \log_e \frac{p_2}{p_1}\right]$$

$$= C_V \log_e \left(\frac{\rho_1}{\rho_2}\right)^2 \left(\frac{p_2}{p_1}\right) \qquad \ldots\ldots(10.57)$$

Substituting Eqs. 10.53 and 10.54 in Eq. 10.57 yields

$$\Delta\phi = C_V \log_e \left\{\left[\frac{(\gamma - 1)M_1^2 + 2}{(\gamma + 1)M_1^2}\right]^{\gamma}\left[\frac{2\gamma}{\gamma + 1} M_1^2 - \frac{\gamma - 1}{\gamma + 1}\right]\right\} \qquad \ldots\ldots(10.58)$$

The entropy change across a normal shock may conveniently be plotted against M_1 as shown in *Fig. 10.16.* The change is small for lower values of M_1 and increases rapidly with increasing M_1. It

may be of interest to note that no entropy change will result with an initial Mach number lower than 1†. Flow across the normal

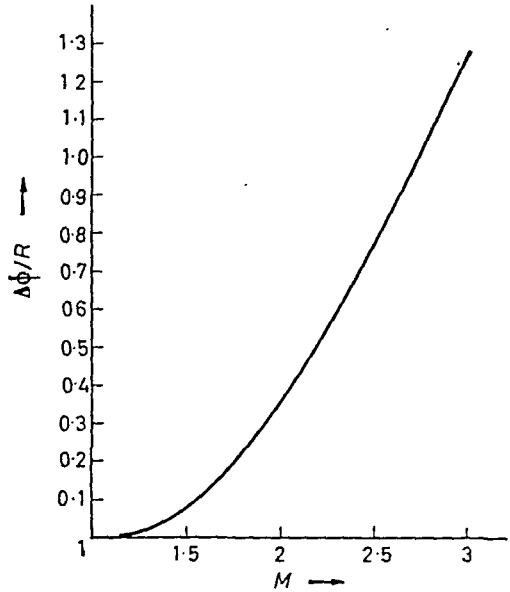

Figure 10.16—Entropy change across a normal shock wave

shock satisfies the energy and continuity equations as well as the Fanno equation. There is no area change, the shock being extremely thin, so the shock may be represented by a jump from point (1)

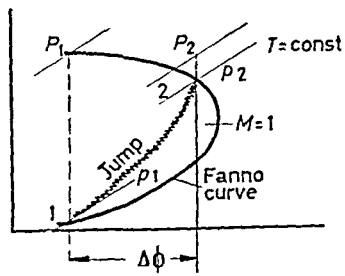

Figure 10.17—Representation of a shock jump on the temperature entropy plane

on the supersonic limb of a Fanno curve to point (2) on the subsonic limb of that curve as shown in *Fig. 10.17*. Once the

† If M_1 were negative Eq. 10.58 would yield a negative value of $\Delta\phi$ which would contravene the second law of thermodynamics.

initial Mach number is specified the position of the downstream state of flow may be found on the $T - \phi$ plane with the aid of Eqs. 10.53 and 10.58.

Whilst the stagnation temperature remains constant across a shock, the stagnation pressure P decreases. This effect may be seen in *Fig. 10.17*, and the change may be calculated by considering that

$$P_1 = p_1 \left[1 + \frac{\gamma - 1}{2} M_1^2\right]^{\gamma/\gamma - 1}$$

and

$$P_2 = p_2 \left[1 + \frac{\gamma - 1}{2} M_2^2\right]^{\gamma/\gamma - 1}$$

so that

$$\frac{P_1}{P_2} = \frac{p_1}{p_2} \left[\frac{1 + (\gamma - 1)M_1^2/2}{1 + (\gamma - 1)M_2^2/2}\right]^{\gamma/\gamma - 1} \quad \ldots . (10.59)$$

where p_1/p_2 may be obtained from Eq. 10.53 and M_2 from Eq. 10.56.

10.14 Oblique Shock Waves

An oblique shock wave occurs when a supersonic flow has to turn through a finite angle. The theory of oblique shocks is more complex than that of normal shocks and is beyond the scope of this text. However, a brief descriptive summary of the types most frequently encountered in high speed flow will be presented.

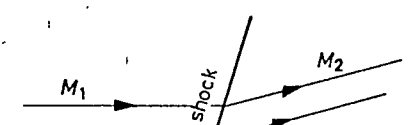

Figure 10.18—Oblique shock (compressive)

Consider first a supersonic stream flowing past a thin wedge so that the stream is deflected through a small angle. The streamlines, set parallel to the wall, change their direction suddenly and this abrupt change is brought about by an oblique shock inclined at a certain angle to the flow as shown in *Fig. 10.18*. This type of shock is *compressive* because it decelerates the flow downstream. On the other hand if a supersonic stream turns around a sharp corner, the

change of direction is effected gradually and the streamlines follow a curved path as shown in *Fig. 10.19*. There are two main waves marking the beginning and ending of the changes of flow direction. Inside these a whole fan of fine oblique waves change the flow and this gradual transformation is considered isentropic. This type of wave pattern causes expansion so that downstream the Mach number is greater and the pressure lower than the corresponding upstream values.

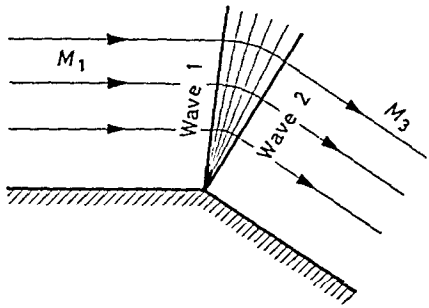

Figure 10.19—Oblique waves (expansive)

Unlike normal shocks, oblique shocks do not generally change the flow from supersonic to subsonic, so that the flow downstream from oblique shocks normally retains its supersonic condition. If a thin double wedge is placed in a supersonic stream, one may observe oblique waves attached to the leading edge (*Fig. 10.20a*); a 'thick' double wedge 'pushes' the wave to the front of the leading edge and a detached bow wave results (*Fig. 10.20b*). The enclosed angle $2e$

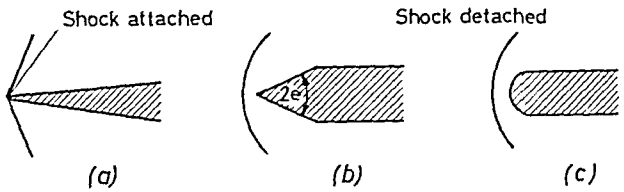

Figure 10.20—Attached and detached waves

of the double wedge, at which the wave becomes detached, may be calculated. Similar detached bow waves may be observed in front of blunt objects (*Fig. 10.20c*).

A projectile moving with a speed slightly above Mach number one sets up a shock nearly normal and well ahead of the leading edge (*Fig. 10.21a*). At higher speeds the wave becomes oblique and may

become attached (*see Fig. 10.21b*); one may observe, in addition, a set of waves in the wake.

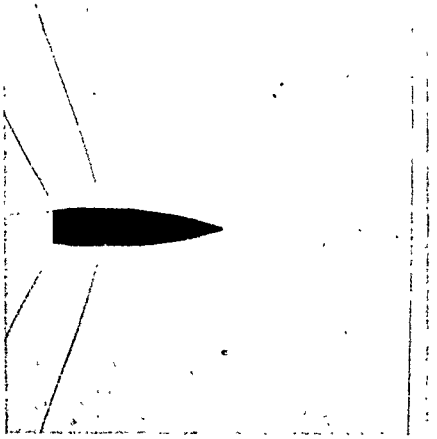

Figure 10.21a—Normal shock well ahead of projectile ($M = 1{\cdot}004$)

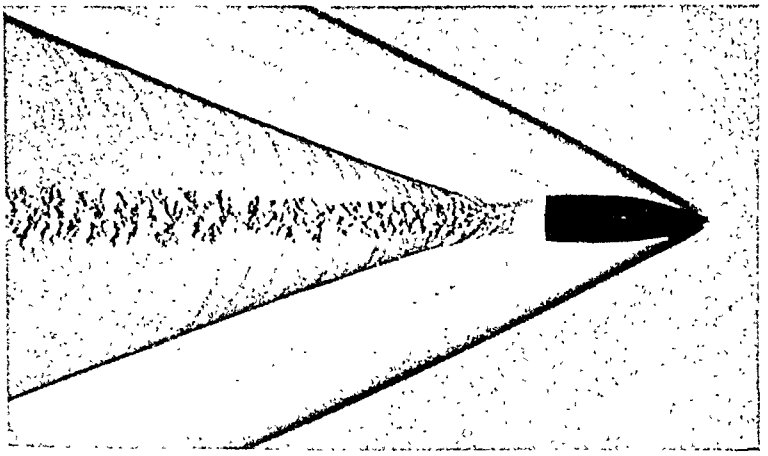

Figure 10.21b—Oblique shock attached to projectile

When an oblique wave contacts a solid wall a reflected wave results. A sudden change in direction of the boundary surface causes a supersonic flow to set up an incident wave which turns the flow parallel to the boundary; the opposite wall then 'reflects' the incident wave which returns the flow to the original direction.

Each change of direction brings about a change in the Mach number as shown in *Fig. 10.22.*

Reflection effects on oblique shock waves intersecting each other are shown in *Fig. 10.23.* The waves, having intersected each other, change their angle of setting to the flow in such way that the final stream becomes parallel to the original flow direction.

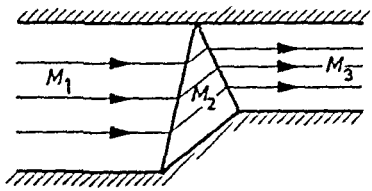

Figure 10.22—Reflected waves

A more complex shock pattern may be observed at the exit of a nozzle when the pressure at the end of the nozzle is greater than the pressure of the surroundings into which the nozzle discharges.

In the case of a nozzle ending with a *parallel wall* one may observe oblique shocks (O) which spring from the corners (C) and intersect a normal shock (N). They are then reflected (R) towards the flow

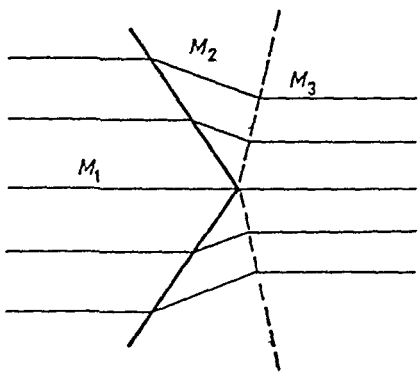

Figure 10.23—Intersecting waves

boundary (B). Whilst the Mach M_1 number changes across the normal shock to M_2, it changes to M_3 across the oblique shock and to M_4 across the reflected wave. A discontinuity of velocity appears between the stream regions M_4 and M_2 and this results in a 'slip surface' (S). This slip surface consists substantially of a thin vortex sheet which, having traversed a short distance, diffuses into the surrounding stream (*see Fig. 10.24*).

If the pressure is sufficiently high at the parallel nozzle exit, a chain of successive shock patterns may be observed in the jet, substantially similar to that shown in *Fig. 10.24* (*see Fig. 10.25*). The complete physical picture is complex, nevertheless it is obvious that surplus energy (unexpended) in the flow is destroyed through a succession of shocks.

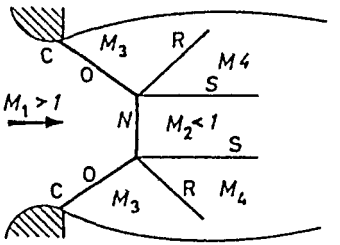

Figure 10.24

Focussing attention on the central core of the flow, an approximate explanation of the events may be obtained. The first shock causes a deceleration of the flow to subsonic condition and this is accompanied by a decrease in the stagnation pressure and an increase in entropy. The stream which surrounds the core is supersonic, having passed through oblique waves. It 'activates'

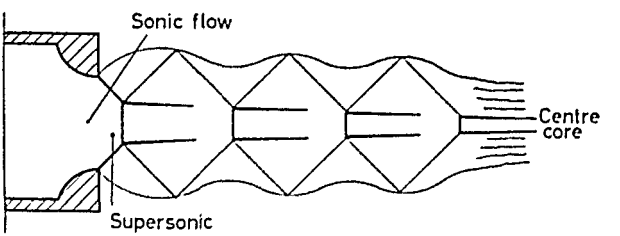

Figure 10.25
(*By courtesy of the Director, R.A.E., Farnborough*)

the core through the slip surface to attain higher speed and in this action the flow is aided by a further expansion so that the stream again attains supersonic conditions. A second shock appears with a further decrease of stagnation pressure and increase in entropy. The process is then repeated until the stagnation pressure decreases to the limiting value, after which there is insufficient energy left in the stream to attain supersonic flow. The end of the jet diffuses into the surroundings at low speed. The approximate representation

on the $T - \phi$ plane is shown in *Fig. 10.26.* A similar state change is thought to occur in some types of throttling processes.

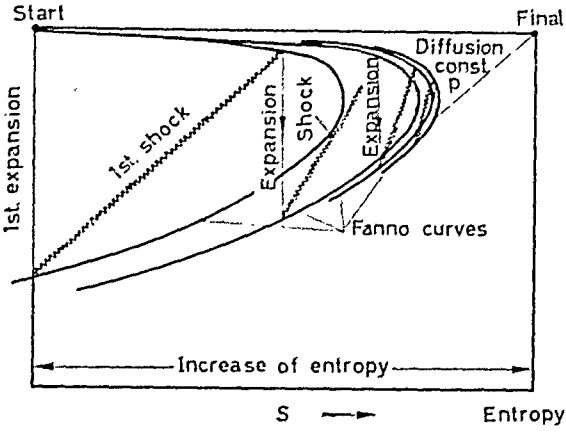

Figure 10.26

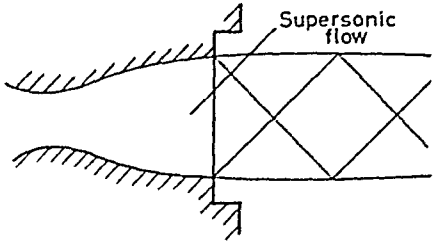

Figure 10.27

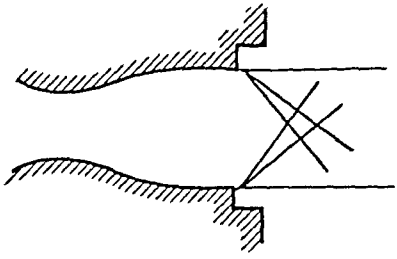

Figure 10.28—Oblique wave pattern at exit from a nozzle

Oblique shock wave patterns appear at theex it of convergent-divergent nozzles when the pressure at the nozzle exit is higher or lower than the back pressure (*see Fig. 10.11*). The pattern changes with the variation of pressure as shown in *Figs. 10.27* and *10.28.*

In *Fig. 10.29* shock waves photographed in cascade blading are shown.

Figure 10.29—Shock waves in a cascade.
(*From* R. & M. 2792 *by permission of the Controller, H.M.S.O.*)

Examples

10.4. Air discharges from a reservoir into the atmosphere through a convergent–divergent nozzle of circular cross-section.

Calculate:

(*a*) The diameter of the nozzle at the exit for 'shockless' flow condition if a Mach number $M = 2$ is to be obtained, assuming frictionless flow and a throat diameter $D_{th} = 0{\cdot}5$ in.

(*b*) The correct pressure in the reservoir assuming the atmospheric pressure to be 14·7 lb./in.^{2} The temperature of the air in the reservoir is 70°F.

(*c*) If the jet impinges on a flat plate placed vertically to the flow, calculate the force of the impact.

Data: $\gamma = 1{\cdot}4$, $g = 32{\cdot}2$ ft./sec., $R = 53{\cdot}3$ ft. lb. per lb. °R.

Solution.—(*a*) The exit area to throat area ratio

$$\frac{A_e}{A_{th}} = \frac{1}{2}\left[\frac{1 + (1{\cdot}4 - 1)2^2/2}{(1{\cdot}4 + 1)/2}\right]^{\frac{1{\cdot}4+1}{2(1{\cdot}4-1)}} = 1{\cdot}67$$

$\therefore$ Exit diameter $D_e = D_{th}\sqrt{1{\cdot}67} = 0{\cdot}645$ in.

(*b*) For non-frictional process, the ratio of stagnation to static pressure

$$\frac{P}{p} = \left[1 + \frac{1{\cdot}4 - 1}{2} \times 2^2\right]^{\frac{1{\cdot}4}{1{\cdot}4-1}} = 7{\cdot}8$$

Hence pressure in the reservoir $P = 14{\cdot}7 \times 7{\cdot}8 = 114{\cdot}6$ lb./in.^{2} abs.

(*c*) To obtain the impact force, the mass flow through the nozzle and the exit velocity must be calculated.

From the Fanno equation, mass flow

$$W' = \frac{0{\cdot}5^2\pi}{144 \times 4} \times \frac{114{\cdot}6 \times 144}{\sqrt{530}} \times \sqrt{\frac{1{\cdot}4 \times 32{\cdot}3}{53{\cdot}3}} \times \left[\frac{2}{1{\cdot}4 + 1}\right]^{\frac{1{\cdot}4+1}{2(1{\cdot}4-1)}}$$

$$= 0{\cdot}52 \text{ lb./sec.}$$

Exit velocity

$$V_e = M_e\sqrt{(\gamma R g \theta_e)} = M_e\sqrt{(\gamma R g)}\sqrt{\frac{T_0}{1 + [(\gamma - 1)/2]M_e^2}}$$

$$\therefore \quad V_e = 2\sqrt{(1{\cdot}4 \times 53{\cdot}3 \times 32{\cdot}2)}\ \sqrt{530/1 + [(1{\cdot}4 - 1)/2]2^2} = 1680 \text{ ft./sec.}$$

Hence force

$$F = \frac{W'}{g} V_e = \frac{0{\cdot}52 \times 1680}{32{\cdot}2} = 27{\cdot}2 \text{ lb.}$$

10.5. Calculate the energy efficiency of a normal shock, if upstream of the shock the following flow conditions are maintained:

static pressure	$p_1 = 2$ lb./in.^{2}
Mach number	$M_1 = 1{\cdot}8$
static temperature	$\theta = 530°$R. $\gamma = 1{\cdot}4$.

Solution.—The energy efficiency of the shock is given by

$$\eta = \frac{\theta_2' - \theta_1}{\theta_2 - \theta_1}$$

which may be written

$$\eta = \frac{\theta_2'/\theta_1 - 1}{\theta_2/\theta_1 - 1}$$

where θ_2 is the actual temperature downstream from the shock and θ_2' is a temperature attained in the case of isentropic compression. Both θ_2 and θ_2' lie on the same $p_2 =$ CONST. line (*see Fig. 10.30*).

To obtain p_2 first calculate the pressure ratio across the shock

$$\frac{p_2}{P_1} = \frac{2 \times 1{\cdot}4}{1{\cdot}4 + 1} \times 1{\cdot}8^2 - \frac{1{\cdot}4 - 1}{1{\cdot}4 + 1} = 3{\cdot}62$$

The density ratio across the shock

$$\frac{\rho_2}{\rho_1} = \frac{[(1{\cdot}4 + 1)/2] \times 1{\cdot}8^2}{1 + [(1{\cdot}4 - 1)/2] \times 1{\cdot}8^2} = 2{\cdot}35$$

M_1 may be obtained from the shock area to throat area ratio,

$$\frac{A_{sh}}{A_{th}} = \frac{1}{M_1}\left[\frac{1 + 0{\cdot}2 \times M_1^2}{1{\cdot}2}\right]^{3{\cdot}5} = \frac{1{\cdot}3}{1}$$

Trial and error leads to

$$M_1 = 1{\cdot}61 \text{ approx.}$$

The pressure ratio across the shock may now be calculated:

$$p_2/p_1 = 1{\cdot}166 \times 1{\cdot}61^2 - 0{\cdot}166 = 2{\cdot}89$$

The static pressure in front of the shock

$$p_1 = \frac{14{\cdot}7}{[1 + 0{\cdot}2 \times 1{\cdot}61^2]^{3{\cdot}5}} = 3{\cdot}39 \text{ lb./in.}^2 \text{ abs.}$$

Hence

$$p_2 = 2{\cdot}89 \times 3{\cdot}39 = 9{\cdot}73 \text{ lb./in.}^2 \text{ abs.}$$

The Mach number downstream from the shock

$$M_2^2 = \frac{1 + 0{\cdot}2 \times 1{\cdot}61^2}{1{\cdot}4 \times 1{\cdot}61^2 - 0{\cdot}2} = 0{\cdot}441$$

$$\therefore \qquad M_2 = \sqrt{0{\cdot}441} = 0{\cdot}664$$

The Mach number M_3 at exit may again be obtained from the area ratio

$$\frac{1{\cdot}5}{1{\cdot}3} = \frac{0{\cdot}664}{M_3}\left[\frac{1 + 0{\cdot}2M_3^2}{1 + 0{\cdot}2 \times 0{\cdot}664^2}\right]^3$$

Trial and error yields

$$M_3 = 0{\cdot}53$$

Since the stagnation pressure remains constant downstream from the shock

$$P_2 = p_2[1 + (\gamma - 1)M_2^2/2]^{\gamma/(\gamma-1)} = p_3[1 + (\gamma - 1)M_3^2/2]^{\gamma/(\gamma-1)}$$

$$9{\cdot}43[1 + 0{\cdot}2 \times 0{\cdot}441]^{3{\cdot}5} = p_3[1 + 0{\cdot}2 \times 0{\cdot}53^2]^{3{\cdot}5}$$

$$\therefore \qquad p_3 = 10{\cdot}85 \text{ lb./in.}^2 \text{ abs.}$$

REFERENCES

(1) LIEPMANN, H. W., and PUCKETT, A. E., *Aerodynamics of a Compressible Fluid*, John Wiley and Sons, 1947.
(2) HYLTON, W. F., *High Speed Aerodynamics*, Longmans Green, 1952.
(3) SHAPIRO, A., *The Dynamics and Thermodynamics of Compressible Fluid Flow*, Ronald Press, New York, 1953.

Problems

10.1. Compressed air flows from a pressure vessel through a suitably shaped convergent–divergent nozzle into a tube of uniform cross-sectional area and thence is discharged into the atmosphere. Conditions allow the flow to become supersonic at the entry to the tube.

Neglecting the effects of friction in the nozzle, calculate the 'limiting length' of the tube, that is, the length sufficient for friction to produce sonic flow at the outlet. (Use Eq. 10.32*a*.)

The following conditions prevail:

Pressure in the tank: 150 lb./in.^{2} abs; temperature 70°F.

Atmospheric pressure: 14·7 lb./in.^{2} abs.

Data:

Throat diameter in the convergent-divergent nozzle: 1 in.

Tube diameter: 1·25 in.

10.2. Prove the expression

$$\frac{1}{V}\frac{\mathrm{d}V}{\mathrm{d}x} = \frac{1}{1 - M^2}\left[\frac{f\gamma}{2m}M^2 - \frac{1}{A}\frac{\mathrm{d}A}{\mathrm{d}x}\right]$$

show that in a duct of uniform cross-sectional area, friction accelerates subsonic flow and decelerates a supersonic stream.

Symbols: V = velocity of stream, x = distance along axis of duct, M = Mach number, f = friction factor, m = hydraulic radius, A = cross-sectional area of duct.

10.3. Because of friction the Mach number decreases in a duct of constant cross-section from 1·5 to 1·3. Assuming adiabatic flow conditions and an initial pressure of 5 lb./in.^{2} abs., calculate the exit pressure.

10.4. Air discharges from a reservoir into the atmosphere through a convergent nozzle of circular cross-section having a short parallel exit. Calculate the exit velocity, volume flow, and mass flow, assuming adiabatic frictionless flow.

Data:

Exit diameter of nozzle 1 in.

Pressure in the reservoir 50 lb./in.^{2} abs.

Temperature in the reservoir 70°F.

How will the above quantities vary if the reservoir pressure is increased to 100 lb./in.^{2} abs?

10.5. A Laval nozzle discharging steam is operated so that a normal shock is located at the exit. If the ratio of stagnation to back pressure is 8, calculate the Mach number immediately upstream of the shock. γ steam = 1·3.

10.6. The exit-to-entry area ratio of a divergent duct is 1·4 and the Mach numbers are 1·7 at inlet and 0·5 at exit. Assuming frictionless flow determine the shock location and calculate the efficiency considering the duct as a diffuser. (Note diffuser efficiency is defined as the ratio of static pressure rise to dynamic pressure decrease, thus

$$\eta_d = \frac{p_2 - p_1}{\frac{1}{2}\rho(V_1^2 - V_2^2)}$$

where suffices 1 and 2 refer to conditions at inlet and outlet respectively. $\frac{1}{2}\rho V^2 = \frac{1}{2}p\gamma M^2$.)

PART 3

11

ROTODYNAMIC MACHINERY

11.1 Introduction

THE collective name 'rotodynamic' applies to a group of machines which function through rotary action. Transformation of fluid energy into mechanical work or mechanical work into fluid energy is obtained by means of rotating impellers. Although the basic theory is substantially the same for all of these machines, one distinguishes between two groups *viz.*, pumps and turbines. Pumps deliver fluids at the expense of power input ($+W$), turbines supply power at the expense of fluid energy ($-W$). In centrifugal pumps the fluid pressure develops radially to the axis of rotation whilst in axial flow pumps the stream remains parallel to the axis. Pumps are called *fans* if they deliver gases at low pressures and compressors or superchargers if they deliver gases at higher pressure. Similarly, in radial turbines (*e.g.*, Francis) the fluid gives up energy in radial direction to the axis of rotation whilst in axial flow turbines (*e.g.*, Kaplan) the stream remains parallel to the axis.

Work and fluid energy relationship may be derived from Eq. 10.4, Chapter 10. Since $Q_{1-2} = 0$

$$\pm W_{1-2} = J(I_1 - I_2) + \frac{V_1^2 - V_2^2}{2g} + Z_1 - Z_2 \qquad \ldots.(11.1)$$

For incompressible fluids $dE = 0$ and $w = \text{CONST.}$ hence enthalpy change $dI = v\,dp/J$ so that Eq. 10.1 becomes

$$\pm W_{1-2} = \frac{p_1 - p_2}{w} + \frac{V_1^2 - V_2^2}{2g} + Z_1 - Z_2 \qquad \ldots.(11.2)$$

11.2 Description of Centrifugal Pumps

Centrifugal pumps consist substantially of one or several impellers rotating in a suitably shaped casing. In single stage pumps a single impeller rotates in a casing of spiral or volute form (*Fig.*

whilst in multistage pumps two or more impellers are fitted to a common shaft (*Fig. 11.2*). Fluid enters the impeller axially through the eye, the flow continuing radially and discharging around the entire circumference into the casing. In passing through the impeller the fluid receives energy from vanes (*Fig. 11.2a*) incorporated in the impeller, resulting in an increase of both pressure and velocity. The kinetic energy of the fluid leaving the impeller is partially transformed into pressure inside the casing.

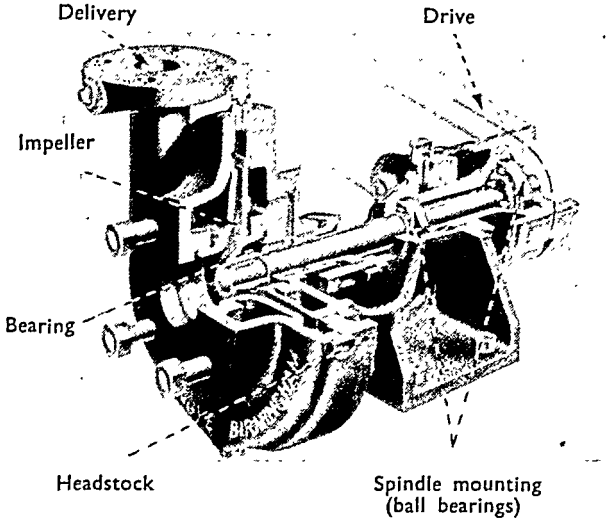

Figure 11.1—(By courtesy of Tangye Ltd.)

According to requirements, a variety of pump designs exist in practice such as single and double suction pumps, turbine pumps, mixed flow pumps, and so on. If the impeller is surrounded by diffuser vanes, we speak of turbine pumps probably because its construction is similar to that of turbines having guide vanes (*Fig. 11.3*). The function of the diffuser is to guide the fluid, whereas in volute type pumps the fluid, after leaving the impeller, discharges freely into the casing. In double inlet pumps, fluid enters from two sides as if two impellers were placed back to back, thus doubling discharge for the same head (*Fig. 11.4*). Mixed flow pumps are designed for large discharge and limited lift requirements; the impeller passages being wide the flow has radial and axial components as well (*Fig. 11.5*). Again, in multi-stage pumps the

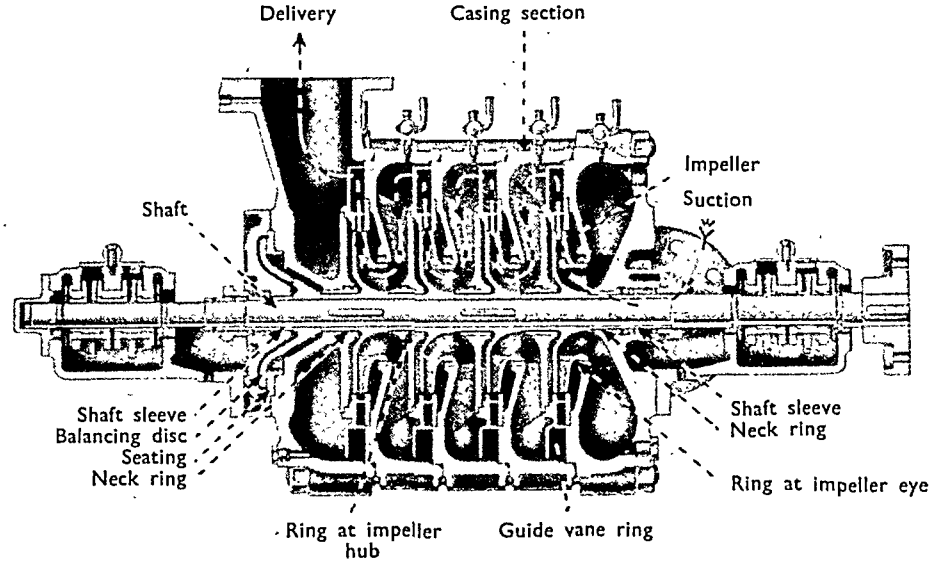

Figure 11.2—(By courtesy of Tangye Ltd.)

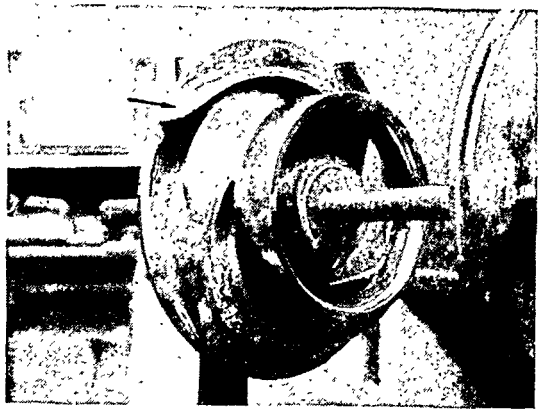

Figure 11.2a—Centrifugal pump impeller showing shape of vane

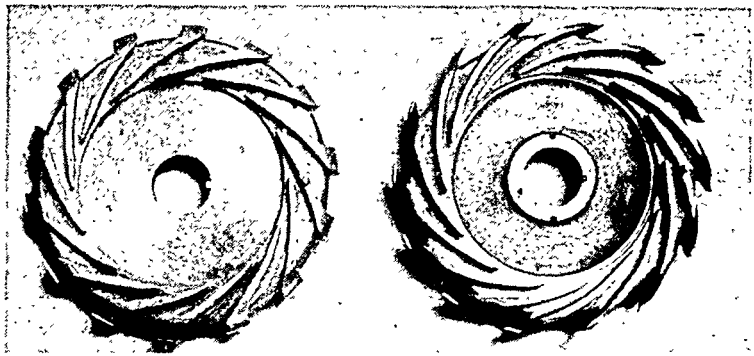

Figure 11.3—Diffuser guide vanes
(By courtesy of Escher Wyss)

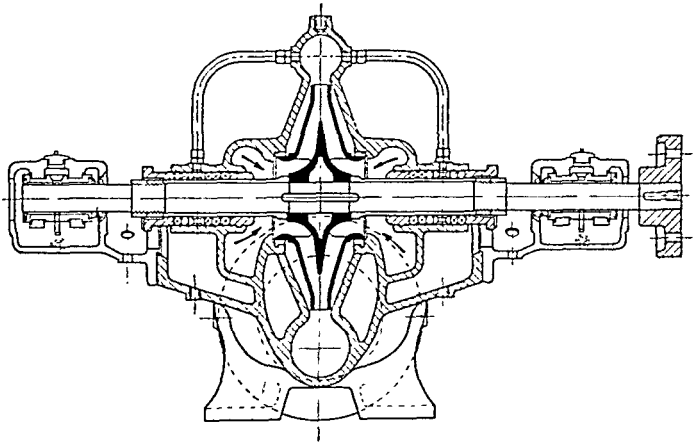

Figure 11.4—Double inlet pump
(By courtesy of Tangye Ltd.)

discharge is the same as for one stage but the total head developed is the product of the lift of one stage times the number of stages. In each stage the fluid discharged from the impeller is returned to the eye of the impeller of the next stage through suitably shaped passages (*Fig. 11.2*).

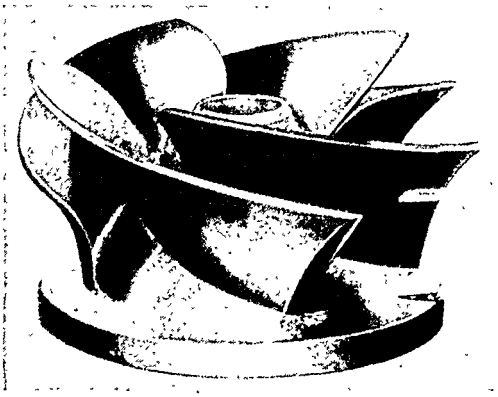

Figure 11.5—Mixed flow impeller
(*By courtesy of Escher Wyss*)

11.3 The Euler Equation

Consider a simple impeller consisting of two circular discs with their centre in line and with their plane perpendicular to an axis of rotation (*see Fig. 11.6*). Straight vanes are fitted between the

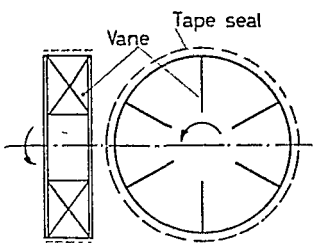

Figure 11.6—Simple impeller

discs and the passages so formed are filled with a fluid. Consider the discs first sealed with a tape around the perimeter so that no fluid can escape when the impeller is set in rotation. Owing to centrifugal action the fluid exerts a force on the seal. If the seal is now suddenly removed the fluid contained in the impeller

discharges at once owing to the action of this centrifugal force. A continuous flow may be obtained by providing one of the discs with an opening to which a simple supply line is connected as shown in *Fig. 11.7.*

After priming the impeller and pipeline and setting the impeller in rotation the fluid discharged causes a partial vacuum in the centre. Fluid is then driven up through the supply line by the atmospheric pressure to replace that discharged outwards by centrifugal action.

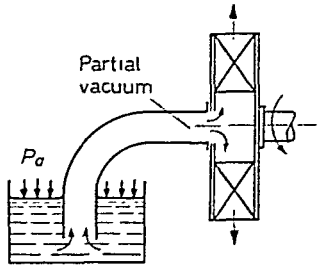

Figure 11.7

Work done on the fluid may be calculated from consideration of the moment of momentum. Momentum is obtained from the pressure force applied to the fluid by vanes whilst flowing through the passages. As a result of this action the fluid (in transit) develops a rotation, frequently called 'whirling.' As the peripheral speed of the impeller increases radially the rotational or whirl velocity (V_w) also increases with increasing radius.

Consider a fluid element weighing 1 pound in passing through a passage. Its whirl velocity at radius r is V_w, hence its momentum

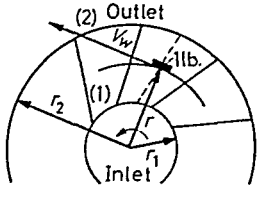

Figure 11.8

is V_w/g. The fluid enters the impeller at radius r_1 and leaves the impeller at r_2 hence its momentum changes from V_{w1}/g to V_{w2}/g (*Fig. 11.8*). The change of moment of the momentum between passage inlet and outlet is $\frac{V_{w2}}{g} r_2 - \frac{V_{w1}}{g} r_1$ which must be equal to

the torque applied to the impeller

$$T = \frac{V_{w2}}{g} r_2 - \frac{V_{w1}}{g} r_1$$

The power required for driving the impeller (per pound of fluid per second) is obtained by multiplying the torque, T, with the angular speed ω

$$H_E = T\omega = \frac{V_{w2}}{g} (r_2\omega) - \frac{V_{w1}}{g} (r_1\omega)$$

The bracketed terms $r_2\omega$ and $r_1\omega$ are actually the peripheral speeds of the impeller V_{t2}, V_{t1} at outlet and inlet respectively. Hence

$$H_E = \frac{V_{t2}V_{w2} - V_{t1}V_{w1}}{g} \qquad \ldots.(11.3)$$

Equation 11.3 is known as the Euler equation and the quantity H_E is the Euler lift. The dimension of H_E is ft.lb./sec. per lb./sec. fluid flowing or simply ft. This is the possible maximum lift developed in impellers for a non-frictional flow.

11.4 Construction of Velocity Vector Diagrams

In order to calculate the Euler lift, whirl velocities V_{w1}, V_{w2}, must be found. These may be obtained from velocity vector diagrams.

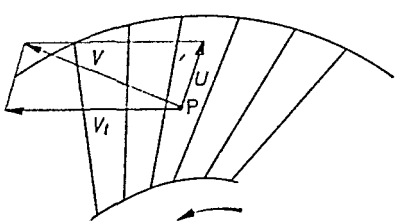

Figure 11.9—Velocity vector diagram

Consider an impeller in which the number of vanes is large, so that the passages are closely spaced and the fluid flowing in the passages follows the path outlined by the vanes. In such 'narrow' passages an even velocity distribution may be assumed.

A fluid element flowing in a passage at a point P has a 'relative' velocity U, which is parallel to the direction of the passage at that point, and a peripheral velocity V_t due to the rotation of the impeller. The 'relative' velocity would be seen by an observer moving with the impeller. The resultant velocity vector called the absolute velocity V, is the vectorial sum of V_t and U as shown in *Fig. 11.9.*

The absolute velocity V may again be resolved into two components V_r and V_w, V_r being the radial speed of the fluid and V_w the whirl velocity (*Fig. 11.10*). The vector diagram given in *Figs. 11.9* and

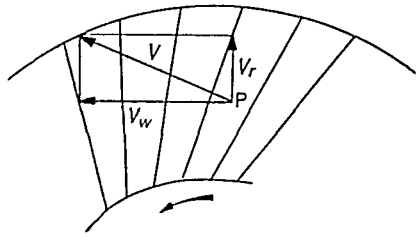

Figure 11.10—Velocity vector diagram

11.10 may be superimposed as shown in *Fig. 11.11*. With the aid of vector diagrams the quantities V_{t1}, V_{w1}† and $V_{t2}V_{w2}$ may be obtained graphically and upon substitution in Eq. 11.3 the Euler lift, H_E be obtained.

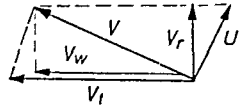

Figure 11.11—Velocity vector diagrams, superimposed

Construction of Vector Diagrams

In the following examples the general principle of constructing vector diagrams is applied to forward, radial and backward curved vane impellers. The name of the types of impellers refers to the outer vane tip angle β_2 enclosed between the tangents drawn to

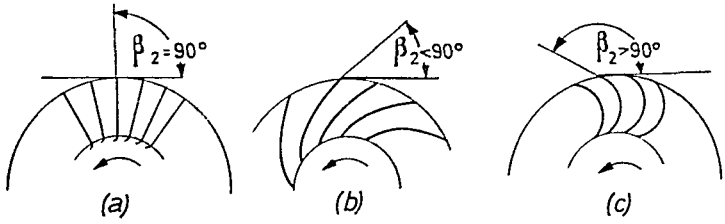

Figure 11.12—Types of impeller vanes

the outer vane tip and to the outer circle. When the angle $\beta_2 = 90°$, the vane is called radial: when $\beta_2 < 90°$ the vane is called backward curved and when $\beta_2 > 90°$ the vane is called forward curved, (*see Fig. 11.12, a, b,* and *c*). The procedure to be followed is simple:

† Since V_{w1} is usually zero for the design point, V_{t1}, V_{w1} may be neglected; *see* Section 11.6, paragraph on separation losses.

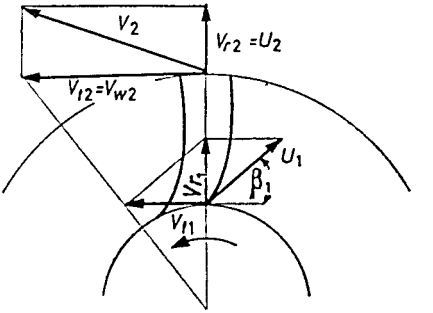

Figure 11.13—Velocity vector diagram, radial vanes

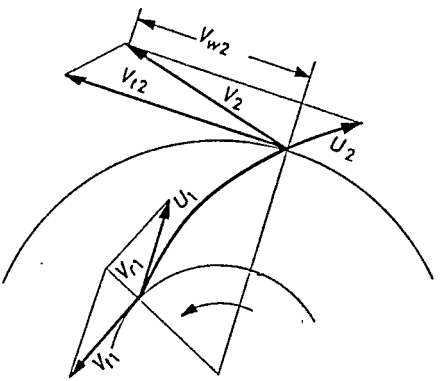

Figure 11.14—Velocity vector diagram, backward curved vane

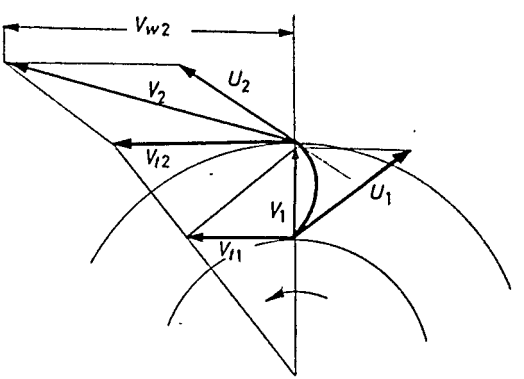

Figure 11.15—Velocity vector diagram, forward curved vanes

assuming that the vane shape is given, first the outlet peripheral speed vector V_{t2} and relative speed vector U_2 is drawn. The resultant absolute velocity V_2 is again resolved into V_{w2} and V_{r2} and the procedure is repeated for the inlet. Since $V_t = \omega r$ the vector V_{t1} may simply be obtained by drawing a straight line from the tip of V_{t2} to the centre of rotation. Note that for radial vanes $V_{w2} = V_{t2}$ whereas for forward curved vanes $V_{w2} > V_{t2}$ (*see Figs. 11.13, 11.14,* and *11.15*).

11.5 Practical Impellers. The Relative Eddy. Correction of the Euler Lift

An impeller with a large number of vanes could only be considered as hypothetical. The number of vanes employed in impellers of conventional design is usually limited, and the passages widen

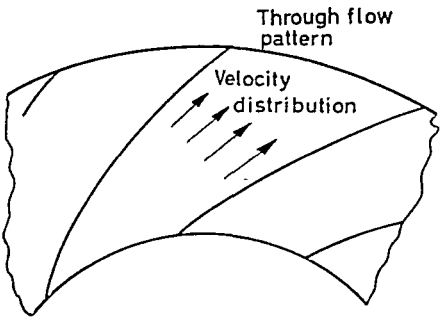

Figure 11.16

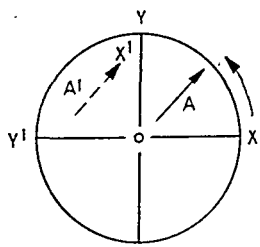

Figure 11.17

considerably from inlet to outlet. The velocity distribution becomes uneven, the stream velocity being lowest on the concave side and highest on the convex side of curved vanes (*see Fig. 11.16*). In addition, inertia effects cause further distortion in the flow pattern.

Inertia effects on the fluid in a rotating impeller may be explained by considering the fluid momentarily enclosed in the impeller. For this demonstration a simple impeller provided with four vanes will be used, as shown in *Fig. 11.17.* Consider an arbitrary direction fixed relatively to the fluid which, at a given instant is marked by an arrow A. After giving the impeller a quarter turn rotation counterclockwise, the segment moved to position marked X^1–Y^1–O. During this movement the fluid, owing to its inertia does not experience any rotation so that the arrow, shown by the dotted line, still points in the same direction. As a result a counterclockwise

circulatory motion is set up inside the segment relative to the impeller, which is called the 'relative eddy.' The same effects on the fluid are maintained if the fluid is allowed to flow through the passages.

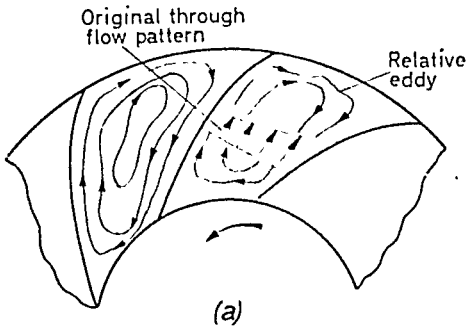

Figure 11.18a—Relative eddy (left) superimposed on through flow

The streamlines due to the relative eddy may be superimposed in the original 'through-flow' pattern, resulting in a further distortion of the velocity distribution. The inward flow of the circulation

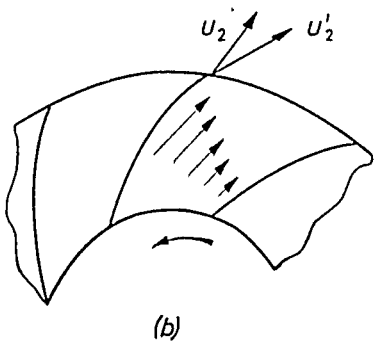

Figure 11.18b—Resulting flow pattern (due to relative eddy)

opposes whilst the outward flow helps the through flow as shown in *Fig. 11.18a*. The velocity distribution and the resultant relative velocity vector U_2, is shown in *Fig. 11.18b*.

Since U_2' is turned away from U_2 in the sense of rotation of the relative eddy, the whirl velocity decreases as illustrated in *Fig. 11.19*. The relative eddy thus decreases the lift developed in the pump

and this is taken into account by the correction factor λ † defined as

$$\lambda = \frac{V_w \text{ actual}}{V_w \text{ Euler}}$$

Hence the total lift H_t developed by the impeller $H_t = \lambda H_E$.

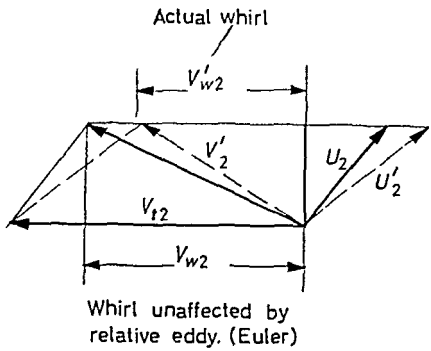

Figure 11.19

11.6 Energy Losses in Pumps

Energy losses in pumps may be divided into three categories: (*a*) hydraulic, (*b*) volumetric, and (*c*) mechanical losses. These must be compensated by an appropriate power input to the pump.

Hydraulic losses refer to energy consumed by friction and flow separation.

Frictional losses are experienced partly in the impeller passages, and partly in the passages of the casing. Frictional losses follow the relationship given by the Darcy equation, hence

$$H_f = \text{CONST.} \times V_r^2 \propto Q^2.$$

Separation losses appear mainly at the inlet to the impeller. To understand the mechanism of these losses consider the fluid which enters the impeller through the 'eye' in the axial direction free of rotation. As the flow turns gradually in the radial direction it contacts the vane inlet edge and a sudden impact is experienced which marks the beginning of the whirling motion of the fluid. Under this impact the flow changes direction from V_r to V_1 and the flow separates from the vane at inlet with a consequent loss of

† Formulae for the calculation of λ have been put forward by Stodola, Buseman, and Pfleiderer. There is little evidence to show which gives the best results in practice. Discrepancy between theory and measurements varies considerably. See footnote p. 301.

energy. The phenomenon is frequently called 'shock' loss. The flow separation and the inlet velocity vector diagram, illustrating the change in flow direction, is shown in *Fig. 11.20.* It is possible

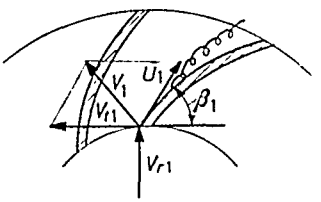

Figure 11.20—Entry shock in impellers

to obtain flow conditions without the appearance of separation. This condition, called 'shock-free entry' is satisfied if the direction of the absolute velocity V_1 at vane inlet remains radial, as shown in *Fig. 11.21.*

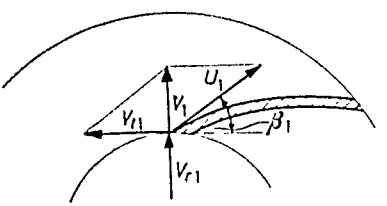

Figure 11.21—Shock-free entry

For a specified discharge, shock-free entry may be obtained by suitably adjusting vane inlet angle β_1. Thus shock-free entry really means zero whirl at inlet, and the discharge at which this occurs is called the design discharge or design point Q_d. It is noted that shock losses increase in proportion with $(Q - Q_d)^2$.

Hydraulic losses decrease the total lift developed by the impeller and this must be taken into consideration when the impeller is designed. As the total lift is the sum of the actual lift and the hydraulic losses, *i.e.*, $H_t = H_a + h_f$ the hydraulic efficiency may be defined as

$$\eta_H = \frac{H_a}{H_t} = \frac{H_a}{H_a + H_f} \qquad \ldots.(11.6)$$

Volumetric losses refer to energy losses due to leakage effects. Fluid recirculates through the tip clearance and seal separating the impeller from the casing, this being due to flow from higher to

lower pressure zones (*see Fig. 11.22*). The amount of fluid is usually small for the correct clearance but may be quite considerable if the impeller is worn. If ΔQ is the recirculating quantity and Q_a is the actual discharge, the total volume flowing through the impeller is $Q_a + \Delta Q$.

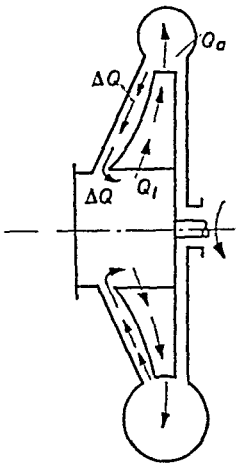

Figure 11.22—Schematic section of pump showing recirculating fluid

The volumetric losses may be expressed by the volumetric efficiency η_V defined by

$$\eta_V = \frac{Q_a}{Q_t} = \frac{Q_a}{Q_a + \Delta Q} \qquad \ldots.(11.7)$$

Note that the value of recirculation is largest when the valve on the discharge side of the pump is closed. This accounts for the relatively high power required to drive a pump at shut-off condition. *Mechanical losses* refer to energy losses due to fluid friction acting on the impeller, and gland and bearing friction.

The fluid, contained between the shrouding of the impeller and the casing, adheres to both surfaces owing to viscosity and when the impeller rotates, an energy loss, frequently called 'disc friction', results. It may be shown that energy loss due to disc friction is $\propto N^3 D^5$.

The value of bearing friction depends on the type and number of bearings employed, whilst the gland friction depends mostly on the tightness of the packing.

Mechanical losses are taken into account by the mechanical efficiency η_m.

11.7 Overall Efficiency and Power Required for Driving Pumps

Consider a fluid column of height H_a moving upward in a pipe of cross-section A, with a velocity V. (*Fig. 11.23*). The weight of the fluid above the cross-section A is $p \,.\, A$ where $p = H_a w$. The

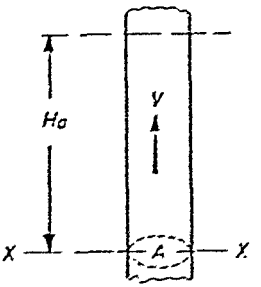

Figure 11.23

pump continuously lifts the fluid column with a velocity V to a height H_a. Thus the actual work done by the fluid per second

$$W_a = p \,.\, A \,.\, V = H_a \,.\, w \,.\, A \,.\, V = H_a \,.\, w \,.\, Q_a$$

$A \,.\, V$ being the actual discharge Q_a. Because of hydraulic, volumetric, and mechanical losses, the input power applied to the impeller shaft

$$W_t = \frac{H_t \,.\, w \,.\, Q_t}{\eta_m}$$

The overall efficiency of the pump

$$\eta_0 = \frac{\text{actual work done by fluid}}{\text{shaft power}} = \frac{H_a \,.\, W \,.\, Q_a}{H_t \,.\, W \,.\, Q_t / \eta_m}$$

Introducing the hydraulic and volumetric efficiencies (Eqs. 11.5 and 11.6) one obtains

$$\eta_0 = \eta_H \times \eta_V \times \eta_m \qquad \ldots\ldots(11.8)$$

Hence the overall efficiency of the pump is the product of the hydraulic, volumetric and mechanical efficiencies. From the above, the shaft power required for driving pumps

$$P = \frac{Q_a w H_a}{550 \eta_0} \text{ (h.p.)} \qquad \ldots\ldots(11.9)$$

11.2 Qualitative Analysis of Pump Characteristics. Design Point

Pump characteristics generally relate to the performance of a pump under varying working conditions. Usually the power and efficiency are plotted against discharge for a constant speed and a typical set of curves is shown in Fig. 11.24. It appears that the head H_t

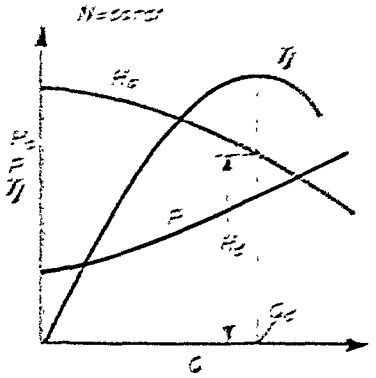

Figure 11.24—Pump characteristics

decreases and power consumption P increases with increasing discharge. The overall efficiency increases from zero to a maximum value, then decreases again. The value of the design discharge Q_d is marked on the horizontal ordinate under the efficiency peak and the design head H_d is shown on the vertical ordinate erected over the design point.

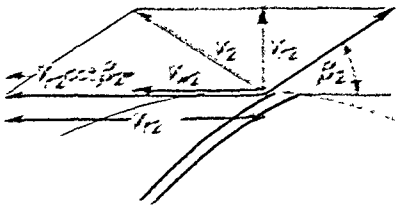

Figure 11.25

In order to explain the behaviour of these curves, consider an impeller rotating at constant speed. Neglecting the whirl at inlet the Euler head becomes

$$H_E = \frac{V_{w2}V_{r2}}{g}$$

From the outlet velocity vector diagram (Fig. 11.25), the whirl

velocity V_{w2} may be expressed in terms of the radial velocity V_{r2} and the vane tip angle β_2

$$V_{w2} = V_{t2} - V_{r2} \cot \beta_2$$

Again, the radial velocity at outlet $V_{r2} = Q/A_p$ where A_p is the area around the perimeter open to fluid flow. With these values the Euler lift

$$H_E = \frac{V_{t2}^2}{g} - \frac{V_{t2} \cot \beta_2}{gA_p} Q = a - bQ$$

where $a = \frac{V_{t2}^2}{g}$ and $b = \frac{V_{t2} \cot \beta_2}{gA_p}$. As the values of a and b are constant for constant speed, the slope of the Euler lift line will depend on the value of the vane tip angle. With increasing discharge, the Euler lift decreases for values of $\beta_2 < 90°$, increases for $\beta_2 > 90°$ and remains constant for $\beta = 90°$, as shown in *Fig. 11.26.*

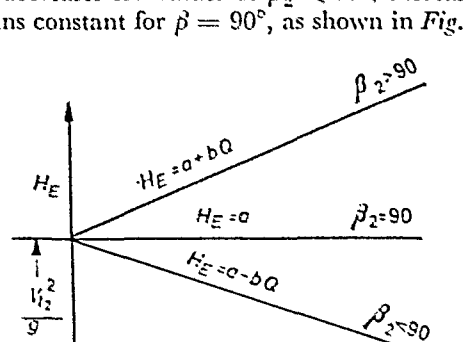

Figure 11.26—Pump characteristics for non-frictional flow (Euler)

Consider for example an impeller with backward curved vanes. When the Euler lift is corrected for relative eddy effects the total lift line ($H_t = \lambda H_E$) is obtained. (*Fig. 11.27*). Frictional losses in the passages are represented by curve F, (loss proportional to Q^2). and when the shock loss is subtracted from F, the actual lift H_a is obtained. As shock losses are a minimum when the inlet whirl is zero, the actual lift curve touches the F line above the design discharge Q_d.

The hydraulic efficiency curve may be obtained with the aid of curves H_a and H_t from the relationship $\eta_H = H_a/H_t$. Note that at zero discharge the hydraulic efficiency has still a finite value.

In *Fig. 11.28* the component efficiencies η_H, η_V, η_m and the resulting product η_0 are plotted against discharge Q.

The energy losses in pumps expressed in terms of power are represented in *Fig. 11.29*.

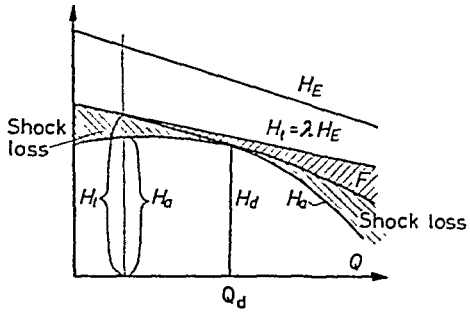

Figure 11.27—Development of actual characteristics, showing design point Q_d

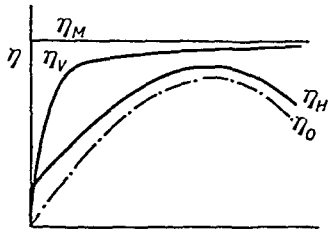

Figure 11.28—Variation of component efficiencies with discharge

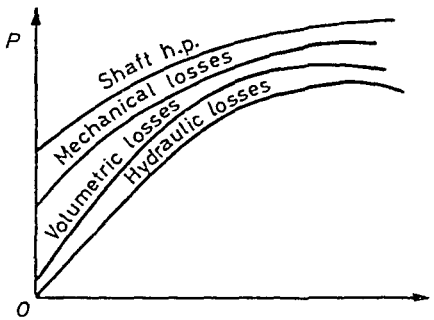

Figure 11.29—Representation of losses in pumps

11.9 Free Vortex. Absolute Path

On leaving the impeller the fluid loses momentum with increasing radius in accordance with the principle of conservation of momentum and its absolute velocity decreases, thus converting kinetic into

pressure energy. This may be shown from the following: consider at position A, a fluid element of mass dm leaving the perimeter of an impeller with absolute velocity V_2, whirl V_{w2} and radial speed V_{r2} (*Fig. 11.30*). Having travelled over to position B, its absolute

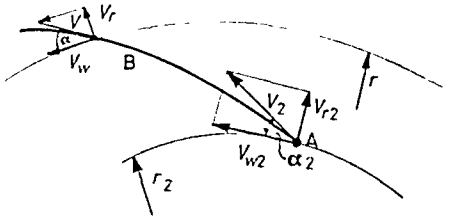

Figure 11.30—Absolute path of fluid leaving impeller

velocity will be V, whirl V_w and radial speed V_r at radius r. The centrifugal force acting on the fluid element is balanced by a pressure difference dp acting on the surface element δA in the radial direction (*Fig. 11.31*) so that in equilibrium

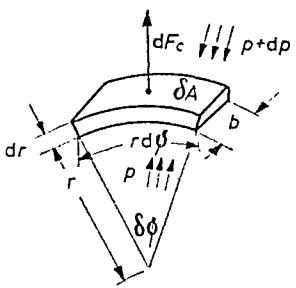

Figure 11.31—Fluid element

$$dF_C = dm \frac{V_w^2}{r} = \delta A \,.\, dp$$

where $$\delta A = r \,.\, \delta\phi \,.\, b$$

Substituting

$$dm = (r\,\delta\phi\, b)\, dr\rho$$

one obtains

$$\frac{dp}{p} = V_w^2 \frac{dr}{r} \qquad \ldots.(11.10)$$

Combining the Bernoulli equation $\mathrm{d}p/\rho + V\,\mathrm{d}V = 0$ with Eq. 11.10 leads to

$$\frac{\mathrm{d}V_w}{V_w} + \frac{\mathrm{d}r}{r} = 0$$

Integration gives

$$\log [V_w r] = \text{CONST.}$$

or

$$V_w = \frac{C_1}{r} \qquad \ldots.(11.11)$$

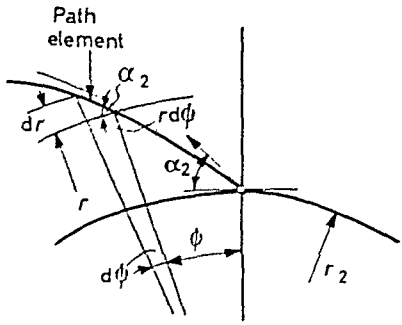

Figure 11.32

Equation 11.11 is characteristic of the so called 'free' vortex in which the whirl varies inversely with the radius. The continuity equation may now be applied and on the assumption that the fluid leaving the impeller flows between parallel walls, spaced distance b_2 apart

$$Q = 2\pi r_2 b_2 V_{r2} = 2\pi r b_2 V_r$$

or

$$V_{r2} r_2 = V_r r = C_2 \qquad \ldots.(11.12)$$

Dividing Eq. 11.11 with 11.12 gives

$$\tan \alpha = \frac{V_w}{V_r} = \frac{C_1}{C_2} \times \frac{V_{r2}}{r_2} = C_3 = \tan \alpha_2$$

It appears that a decrease in V_w is accompanied by a proportional decrease in V_r because α is independent of r.

It is of interest to trace the absolute path of the fluid leaving the impeller. The absolute path is seen by an observer stationary with respect to fixed surroundings. The absolute path of the fluid between the parallel walls is known to be a logarithmic spiral and the equation for it may be obtained by considering a path element (*Fig. 11.32*).

From similarity of triangles

$$\tan \alpha_2 = \frac{dr}{r\, d\phi}$$

Integration leads to

$$r = r_2 e^{\tan \alpha_2 \phi} \qquad \ldots.(11.13)$$

The spiral flow pattern† around the entire circumference of the impeller is shown in *Fig. 11.33.*

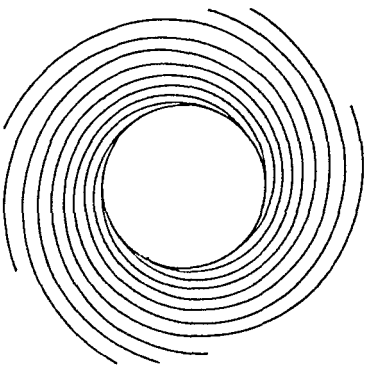

Figure 11.33—Spiral flow pattern around pump impeller

11.10 Impeller Design Based on First Principles

The design of pumps may be considered a highly specialized field so that the finer details are beyond the scope of this text. The engineer who faces the problem of designing a new pump relies on empirical data which may not be readily available and which may also vary considerably with the type of design. Besides, calculations of the performance characteristics of a pump meet with difficulties and reliable results may only be obtained from actual tests. Nevertheless for the purpose of guidance a brief summary of a simple design procedure, followed by a worked example, will be presented here on the assumption that values of the relative eddy factor and of the component efficiencies are available.

Impeller diameter

Assuming zero whirl at inlet the total head developed by the impeller

$$H_t = \lambda H_E = \frac{H_d}{\eta_H} = \frac{V_{t2} V_{w2}}{g}$$

† A detailed paper on Flow Patterns is by J. F. Peck: 'Investigations Concerning Flow Conditions in a Centrifugal Pump', *Proc. Instn mech. Engrs.* Vol. 164, 1951.

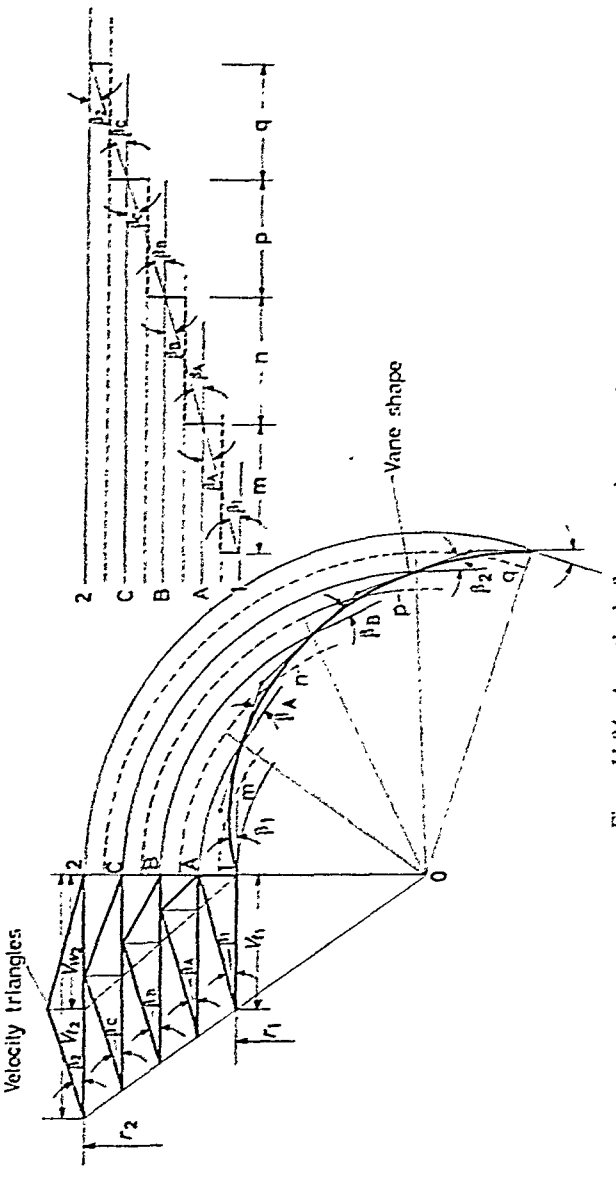

Figure 11.34—A method of constructing vane shape

To be able to calculate the peripheral speed V_{t2}, the value of V_{w2} may be assumed to be a fraction of V_{t2}, *i.e.*, $V_{w2} = \zeta V_{t2}$.

Hence
$$\frac{H_d}{\eta_H} = \frac{\zeta V_{t2}^2}{g}$$

Since $V_{t2} = \dfrac{D_2 \pi N}{60}$, the impeller diameter

$$D_2 = \frac{60}{\pi N} \sqrt{\frac{H_d \cdot g}{\eta_H \cdot \zeta}} \qquad \ldots . (11.14)$$

The rotational speed N of the impeller may be estimated approximately with the aid of the specific speed graph, details of which will be discussed in Art. 11.12.

Vane Shape

The approximate vane shape may be obtained from velocity vector diagrams. Values of V_{t2}, V_{w2} and V_{r2} are assumed to be known. For all practical purposes the whirl velocity may be assumed to vary linearly with the radius, so that

$$V_w = \frac{r - r_1}{r_2 - r_1} V_{w2}$$

First, assuming that the radial velocity remains constant, velocity vector diagrams are constructed at the vane inlet and outlet and for a number of intermediate stations. In *Fig. 11.34* three intermediate stations are shown. From these vector diagrams the vane angles are obtained.

The second step is to arrange the relative velocity vectors in a single line with the aid of the vane angles. This is shown on the right hand side of *Fig. 11.34*. The distance between stations 1, A, B, C, 2 is halved and the vane angles, measured at the respective stations, carry over two successive half-stations. The half-stations are shown by dotted lines. This procedure yields lengths m, n, p, q shown by heavy dotted lines.

The third step is to measure these lengths along the circular paths of the half-stations. Finally, with the aid of the vane angles an envelope is found which yields the approximate vane shape.

Other Proportions

Proportions such as the passage width between vanes and passage depth between shrouding are established by calculations aided by graphical methods. Consider sections of an impeller as shown in *Fig. 11.35.*

The variation of passage width S and passage depth b is shown on the sectional elevation A–A and on the side elevation respectively. Since the passage width S increases with the radius, the depth b decreases, owing to the constancy of V_r.† If the number of vanes is Z the area open for fluid flow is $Z \,.\, S \,.\, b$ so that the actual quantity

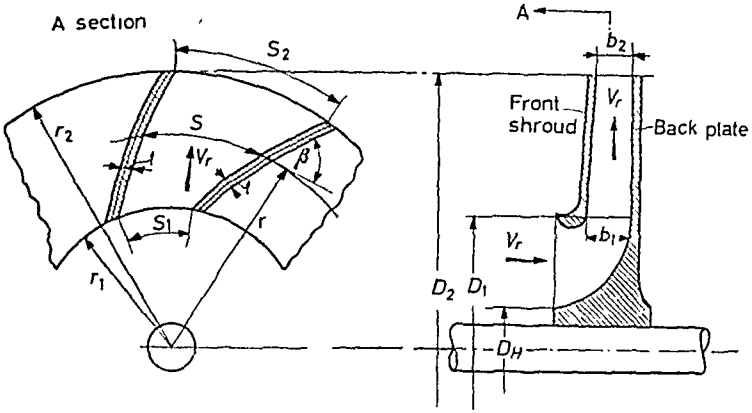

Figure 11.35—Sectional views of pump impeller

$$Q_t = \frac{Q_d}{\eta_V} = ZSbV_r$$

where
$$S = \frac{2\pi r}{Z} - \frac{t}{\sin\beta} \qquad \ldots.(11.15)$$

In practice the backplate is usually flat, and the curved shape of the front shroud may be obtained from the relationship.

$$b = \frac{Q_d}{\eta_V ZSV_r} \qquad \ldots.(11.16)$$

The hub diameter D_h may be obtained from the continuity

$$\frac{\pi}{4}D_1^2 - \frac{\pi}{4}D_H^2 = \frac{Q_d}{\eta_V V_r}$$

whence
$$D_h = \sqrt{\left(D_1^2 - \frac{4}{\pi}\frac{Q_d}{\eta_V V_r}\right)} \qquad \ldots.(11.17)$$

Pump Casing

In volute pumps the casing usually consists of parallel walls near the impeller in which a large portion of the kinetic energy is converted into head and an outer volute chamber of increasing

† Sometimes V_r decreases about 10 per cent.

cross-sectional area (usually of circular form) in which the fluid is collected around the perimeter and directed towards the outlet (*see Fig. 11.36*). The stream between the parallel walls may be considered a spiral.

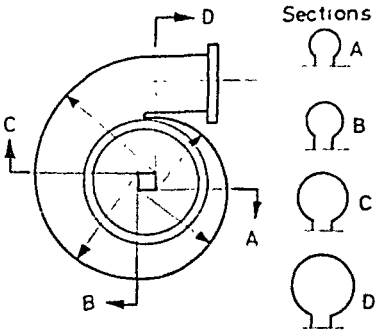

Figure 11.36—Side elevation and sectional views of pump casing

Example

11.1. A certain single-stage centrifugal pump delivers water at the rate of 200 ft.^{3}/sec. against a head of 444 ft. at 455 r.p.m.

Assuming 90 per cent overall efficiency, calculate:

(*a*) The power required for driving the pump;

(*b*) The outer diameter of the impeller assuming that the actual whirl velocity is 0·575 times the peripheral speed and both the mechanical and volumetric efficiencies are 98 per cent;

(*c*) Draw to scale the outlet (and inlet) velocity triangles assuming a 'relative eddy factor' of 0·765 and a radial velocity of 30 ft./sec. and find the blade angles β_2 and β_1.

(*d*) Find vane width b_1 and b_2.

Solution.—(*a*) Power required $= \dfrac{200 \times 62{\cdot}4 \times 444}{0{\cdot}90 \times 550} = 11{,}200$ h.p.

(*b*) Hydraulic efficiency $\eta_H = \dfrac{\eta_0}{\eta_v \eta_m} = \dfrac{0{\cdot}90}{0{\cdot}98^2} = 0{\cdot}936$

$$\frac{H_d}{\eta_H} = \frac{444}{0{\cdot}936} = 0{\cdot}575\,\frac{V_{t2}^2}{32{\cdot}2}$$

$$\therefore \qquad V_{t2} = \sqrt{\frac{444 \times 32{\cdot}2}{0{\cdot}936 \times 0{\cdot}575}} = 163{\cdot}5 \text{ ft./sec.}$$

Since $V_{t2} = D_2 \pi N/60$

$$D_2 = \frac{163{\cdot}5 \times 60}{\pi \times 455} = 6{\cdot}92 \text{ ft.}$$

(*c*) whirl velocity $= 0{\cdot}575 \times 163{\cdot}5 = 94$ ft./sec. The theoretical whirl $\frac{94}{0{\cdot}765} = 123$ ft./sec. Assume $V_{r2} = 30$ ft./sec. outlet angle $\beta_2 = \tan^{-1}\frac{30}{163{\cdot}5 - 123} = 36° 30'$

Assuming $D_1 = D_2/2 = 6{\cdot}92/2 = 3{\cdot}46$ ft.

$$V_{t1} = 163{\cdot}5/2 = 81{\cdot}75 \text{ ft./sec.}$$

inlet angle $\beta_1 = \tan^{-1}\frac{30}{81{\cdot}75} = 20°$

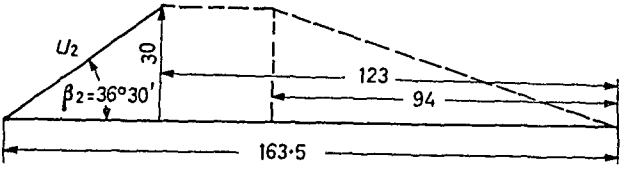

Figure 11.37

(*d*) Assuming $Z = 8$ blades and $t = 0{\cdot}5$ in.

$$S_1 = \frac{3{\cdot}46\pi}{8} - \frac{0{\cdot}5}{12 \times \sin 20°} = 1{\cdot}238 \text{ ft.}$$

$$\therefore \quad b_1 = \frac{200}{0{\cdot}98 \times 8 \times 1{\cdot}238 \times 30} = 0{\cdot}685 \text{ ft.}$$

$$S_2 = \frac{6{\cdot}92\pi}{8} - \frac{0{\cdot}5}{12 \times \sin 36\frac{1}{2}°} = 2{\cdot}65 \text{ ft.}$$

$$b_2 = \frac{200}{0{\cdot}98 \times 8 \times 2{\cdot}65 \times 30} = 0{\cdot}321 \text{ ft.}$$

11.11 Similarity Laws for Centrifugal Pumps

Performance characteristics of pumps are obtained generally from experiments. The usual procedure is to measure the lift H developed and the power P applied to the shaft for a constant rotational speed whilst the discharge is varied over a desired range. This procedure may be repeated for different (constant) speeds provided a variable speed motor is available for driving the pump. A set of performance curves obtained from actual tests on a pump

for different constant speeds ranging from 1,000 r.p.m. to 2,000 r.p.m. is shown in *Fig. 11.38.*

By applying the laws of similarity to pumps, the performance of geometrically similar machines may be predicted from tests obtained on any one machine belonging to that family. The term 'family' relates to geometrically similar machines of different sizes, so that one member of the family is merely an enlargement or reduction in size of the other. In modern practice performance variations caused by change of speed, modifications of design or the behaviour

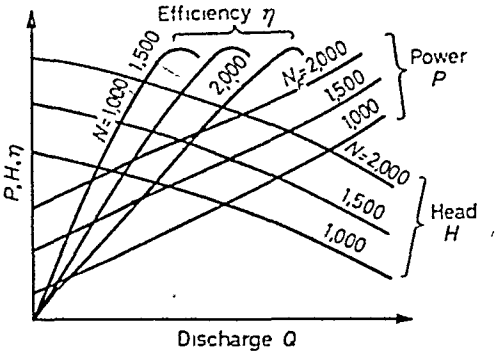

Figure 11.38—Pump characteristics for different speeds

of radically new designs are frequently determined first on models of convenient size before the prototype, usually larger than the model, is produced.

These laws of similarity again lead to non-dimensional curves and as a result, the multitude of curves, such as shown in *Fig. 11.38* may be reduced to single lines. By applying the principles of dimensional analysis (*see* Chapter 7), a set of non-dimensional performance parameters may be deduced. By noting the relevant variables: Q, N, H, P, D, ρ, μ, k (surface roughness) and by choosing D, N, ρ, as independent variables, one obtains

$$\Pi_Q = \frac{Q}{ND^3} \qquad \text{(discharge parameter)} \qquad \ldots.(11.18)$$

$$\Pi_H = \frac{Hg}{N^2D^2} \qquad \text{(lift parameter)} \qquad \ldots.(11.19)$$

$$\Pi_P = \frac{P}{\rho N^3 D^5} \qquad \text{(power parameter)} \qquad \ldots.(11.20)$$

Supplementary parameters are

$$\epsilon = \frac{k}{D} \qquad \text{(relative surface roughness)} \quad \ldots.(11.21)$$

$$N_R = \frac{D^2 N \rho}{\mu} \qquad \text{(Reynolds' number)} \quad \ldots.(11.22)$$

The overall efficiency, $\eta_0 = QwH/P$ may be expressed in terms of the discharge, lift and power parameters

$$\eta_0 = \frac{\Pi_Q \Pi_H}{\Pi_P} \quad \ldots.(11.23)$$

The usual practice is to plot Π_H, Π_P and η_0 against Π_Q as shown in *Fig. 11.39.* It may be seen that the shape of the curves is substantially similar to those shown in *Fig. 11.38.*

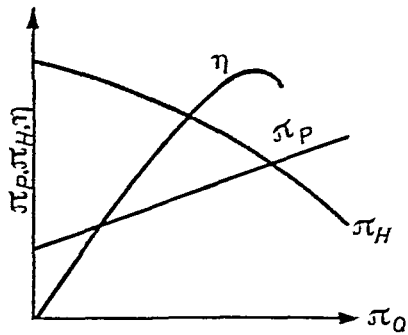

Figure 11.39—Non-dimensional characteristics

Provided that: (*a*) geometric similarity is satisfied, (*b*) relative surface roughness is the same for all sizes, and (*c*) effects of changes in the Reynolds' number are taken into consideration,† *the performance curves of all sizes of machines of the same family, for any rotational speed, lift etc., may be represented by these non-dimensional curves.* Naturally different families have different curves, characteristic only of the type represented.

Non-dimensional parameters may be applied to various types of problems, such as the prediction of performance of a machine at different speeds, different lift, or for the prediction of performance of a prototype from test results obtained from experiments on

† 'The influence of Reynolds' number on the performance of turbo-machinery.' by Davis, Kottas and Moody, *Trans. A.S.M.E.* 1951 p. 499.

models and so on. These problems may roughly be divided into two categories.

Category A

The performance variations are effected at corresponding speeds, that is, complete similarity prevails. In this case no change in the parameters is experienced and the following equations apply:

$$\frac{Q_1}{N_1 D_1^3} = \frac{Q_2}{N_2 D_2^3} \qquad \ldots.(11.24)$$

$$\frac{H_1}{N_1^2 D_1^2} = \frac{H_2}{N_2^2 D_2^2} \qquad \ldots.(11.25)$$

$$\frac{P_1}{\rho_1 N_1^3 D_1^5} = \frac{P_2}{\rho_2 N_2^3 D_2^5} \qquad \ldots.(11.26)$$

$$N_{R1} = N_{R2} \qquad \ldots.(11.27)$$

$$e_1 = e_2 \qquad \ldots.(11.28)$$

where suffix 1 applies to the unchanged (original) and suffix 2 applies to the changed conditions. It is sometimes convenient to use suffices m and p for model and prototype respectively. In other words, at the corresponding speed, suffices 1, 2 or m, p refer to one particular point on the non-dimensional curves, which need not be used at all. (*See* Examples, p. 313.)

Category B

The performance variations result in a change of the parameters (Π_Q, *etc.*); in this case scale effect is present and suffices 1, 2 or m, p refer to two particular but different points which lie on the non-dimensional curves.

11.12 The Specific Speed of Pumps

Having obtained the characteristics of a number of different families the selection of type and size most suitable for a specific purpose may be obtained through the use of non-dimensional performance curves.

For the purpose of selection of a type of pump, the concept of 'specific speed', is used. The specific speed, denoted by the symbol N_s, may be obtained from Eqs. 11.18 and 11.19 by eliminating the size variable D, thus

$$N_s = \frac{\Pi_Q^{1/2}}{\Pi_H^{3/4}} = N \frac{Q^{1/2}}{(Hg)^{3/4}}$$

In practice the runner speed is usually given in r.p.m., discharge in gal./min., lift in feet and g is omitted, being a constant, so that specific speed

$$N_s = \text{r.p.m.} \times \frac{(\text{gal./min.})^{1/2}}{(\text{lift})^{3/4}} \qquad \ldots.(11.29)$$

It must be clearly borne in mind that the specific speed is not a speed in the ordinary sense of implying a rate of movement but is a convenient expression which indicates what is usually called the type or family of impeller.

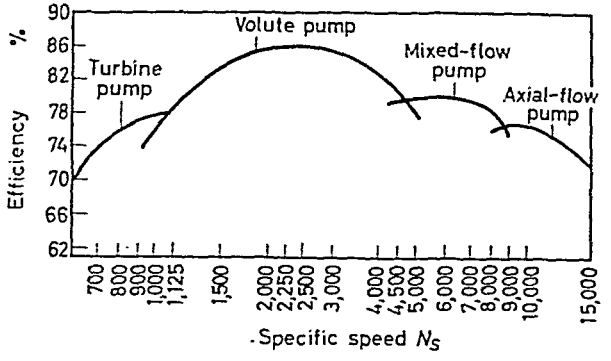

Figure 11.40—(By courtesy of the Institution of Mechanical Engineers)

As the specific speed is obtained from the discharge and lift parameters, Π_Q and Π_H respectively, a relationship between specific speed and the overall efficiency will exist. One may plot for each family of pumps $\Pi_Q^{1/2}/\Pi_H^{3/4}$ against Π_Q and read off the graph the corresponding efficiency values. The results may be represented in a composite chart showing efficiencies of different impeller types plotted against specific speed† (*Fig. 11.40*).

It appears that each family of pumps has a certain range of specific speed, characteristic to the type of impeller; for example the specific speed ranges between 600–1,200 for turbine pumps, a characteristic feature of these being high lift and low delivery; volute and mixed flow pumps fall in the category of medium lift and delivery, the specific speed range being between 1,200–10,000; again, axial flow pumps have high specific speeds, 10,000–15,000 and over, because of their low lift and high discharge.

Within the specific speed range the efficiency attains maximum value at a particular value of specific speed, and this particular

† Sherwell, T. Y. and Pennington, R., Centrifugal Pump Characteristics, *Proc. Instn. mech. Engrs*, vol. 123, 1932.

speed is frequently referred to as the 'wheel number'. A variety of impeller types with their wheel numbers are shown in *Fig. 11.41*.

Results of more recent research on pump efficiency are represented in *Fig. 11.42*, showing pump discharge as an additional parameter.

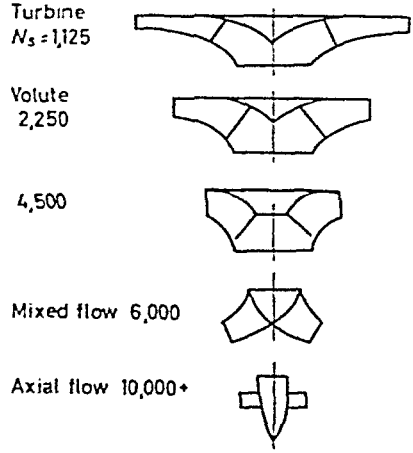

Figure 11.41—Impeller shapes showing dependence on wheel number

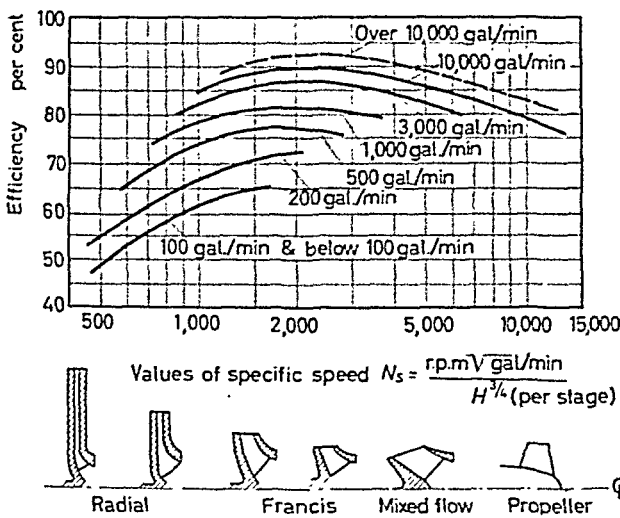

Figure 11.42—Specific speed–efficiency chart for centrifugal pumps. (*By courtesy of McGraw-Hill, New York*)

The curves show a trend towards increased efficiency with higher discharges and a marked falling off at low discharges. This is

attributable to leakage losses through the annular clearances between impeller and casing. Larger pumps have relatively smaller clearances which accounts for their higher efficiency.

Since the maximum efficiency point provides the most economical working conditions it is desirable to run the pump as near as possible at the speed defined by the 'wheel number'. For example, in the case of a turbine'pump, wheel number $N_s = 1{,}200$, specified discharge 200 gal./min., lift 120 ft. the most economic running speed would be at

$$N = N_s \frac{H^{3/4}}{Q^{1/2}} = 1{,}200 \times \frac{120^{3/4}}{(200)^{1/2}} = 3{,}120 \text{ r.p.m.}$$

Such a speed, however, may not necessarily be available particularly when we consider pumps which are directly driven by a.c. motors. In the case of this example the nearest available speed of an a.c. motor might be 2,880 r.p.m. giving a specific speed $N_s = 2{,}880 \times 14{\cdot}2/37 = 1{,}110$ obviously one would have to be content with an efficiency figure somewhat less than the maximum.

11.13 Selection of Impeller Size

It was shown in the preceding section that specific speed charts lead to selection of impeller type. For the calculation of the diameter on the basis of non-dimensional performance characteristics,† one may eliminate speed N from Eqs. 11.18 and 11.19 resulting in

$$\frac{\sqrt{\Pi_H}}{\Pi_Q} = \frac{[Hg/N^2D^2]^{1/2}}{Q/ND^3} = D^2 \frac{(Hg)^{1/2}}{Q} \qquad \ldots\ldots(11.30)$$

With values of Π_H and Π_Q obtained from curves of non-dimensional performance, $\sqrt{\Pi_H}/\Pi_Q$ may be calculated and the results plotted against Π_Q as shown in *Fig. 11.43.*

It follows from Eq. 11.30 that for a specified discharge and lift, the diameter of the impeller

$$D = \left[\left(\frac{\sqrt{\Pi_H}}{\Pi_Q}\right)\left(\frac{Q}{Hg}\right)\right]^{1/2} \qquad \ldots\ldots(11.31)$$

The particular value of $\sqrt{\Pi_H}/\Pi_Q$ at which the efficiency peaks yield the 'best diameter' whilst other values of $\sqrt{\Pi_H}/\Pi_Q$ yield diameters either smaller or larger than the 'best'. With the aid of Eq. 11.30 one may plot efficiency and speed against diameter for a specified discharge and lift as shown in *Fig. 11.44.* It appears that

† The calculation of impeller diameter from first principles was shown in Section 11.10.

diameters smaller than the 'best' require higher speeds, whilst larger diameters require lower speeds. Selection may be made on the basis of (*a*) cost of installation, (*b*) economy of operation, and (*c*) noise generation. The latter view is rather important in the case of fans used in ventilation of buildings where restrictions imposed

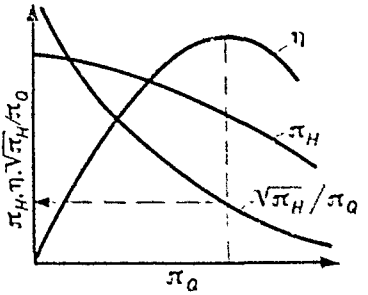

Figure 11.43

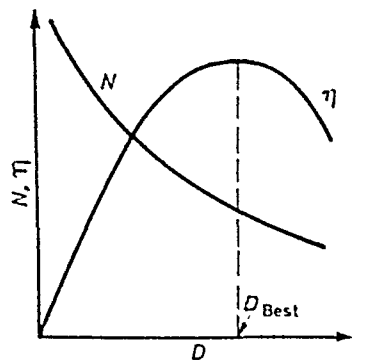

Figure 11.44

on noise level limit the speed of the impeller. On the other hand the cost of machines increases with increasing size whilst the lowest running cost is obtained with the selection of best diameter.

Examples

Category A. Corresponding speed. Small change in speed N.

11.2. A single centrifugal pump discharges 0·26 ft.^{3} of water per sec. producing a head of 48 ft. A squirrel-cage motor drives the pump and the tachometer registers 1,420 r.p.m. (due to slip). At this speed the brake horse power necessary to drive the pump is 4·5. If the number of revolutions is increased to 1,450 per min., find the corrected discharge, head and brake horse power.

Solution.—For increased speed

$$\eta_1 = \eta_2$$

$$Q_2 = Q_1 \frac{N_2}{N_1} = 0{\cdot}26 \times \frac{1{,}450}{1{,}420} = 0{\cdot}266 \text{ cusec.}$$

$$H_2 = H_1 \left(\frac{N_2}{N_1}\right)^2 = 48 \times \left(\frac{1{,}450}{1{,}420}\right)^2 = 50{\cdot}2 \text{ ft.}$$

$$P_2 = P_1 \left(\frac{N_2}{N_1}\right)^3 = 4{\cdot}5 \times \left(\frac{1{,}450}{1{,}420}\right)^3 = 4{\cdot}81 \text{ h.p.}$$

Category A. Corresponding speed. Speed and size changed

11.3. A certain water pump tested at 2,000 r.p.m. discharged 6·0 ft.^{3}/sec. against a head of 340 ft. At this capacity the input power was 250 h.p.

If a geometrically similar pump twice the size runs at 1,500 r.p.m. finds its discharge, head and power for the same efficiency.

Solution.—

$$\eta_1 = \eta_2$$

$$Q_2 = Q_1 \left(\frac{N_2}{N_1}\right)\left(\frac{D_2}{D_1}\right)^3 = 6 \times \frac{1{,}500}{2{,}000} \times \left(\frac{2}{1}\right)^3 = 36 \text{ cusec.}$$

$$H_2 = H_1 \left(\frac{N_2}{N_1}\right)^2\left(\frac{D_2}{D_1}\right)^2 = 340 \times \left(\frac{1{,}500}{2{,}000}\right)^2 \times \left(\frac{2}{1}\right)^2 = 764 \text{ ft.}$$

$$P_2 = P_1 \left(\frac{N_2}{N_1}\right)^3\left(\frac{D_2}{D_1}\right)^5 = 250 \times \left(\frac{1{,}500}{2{,}000}\right)^3 \times \left(\frac{2}{1}\right)^5 = 3{,}375 \text{ h.p.}$$

Category B. Changes in parameters Π_Q, Π_H, Π_P. $\eta_1 \neq \eta_2$.

11.4. An exhaust fan driven by a motor at a speed of 1,635 r.p.m. delivers air at the rate of 3,180 ft.^{3}/min., against a static pressure of 3·5 in. W.G.

It is proposed to increase the supply to 4,920 ft.^{3}/min. and the static head to 6 in. W.G.

Calculate the power necessary to drive the fan, (*i*) before, (*ii*) after the increase of supply.

The non-dimensional characteristics of the fan are given in *Fig. 11.45.*

The diameter of the impeller is 21 in. Density of air is 0·0023 slugs/ft.^{3}

Solution.—(*i*) Since

$$D = 21 \text{ in.} = 1{\cdot}75 \text{ ft.}, \quad D^2 = 3{\cdot}05, \quad D^3 = 5{\cdot}32$$

Prior to change

$$\Pi_{Q_1} = \frac{3{,}180}{1{,}635 \times 5{\cdot}32} = 0{\cdot}365$$

From the graph the efficiency $= \eta_1 = 0{\cdot}375$

Thus power required

$$P_1 = \frac{3{,}180 \times 3{\cdot}5 \times 5{\cdot}2}{33{,}000 \times 0{\cdot}375} = 4{\cdot}7 \text{ h.p.}$$

(*ii*) At the increased supply and head

$$\frac{\sqrt{\Pi_{H_2}}}{\Pi_{Q_2}} = \frac{3{\cdot}05 \times (6 \times 5{\cdot}2/0{\cdot}0023)}{4{,}920/60} = 4{\cdot}34$$

Using the $\sqrt{\Pi_H}/\Pi_Q$ curve on the graph the corresponding $\Pi_Q = 0{\cdot}392$ and the efficiency

$$\eta_2 = 0{\cdot}31$$

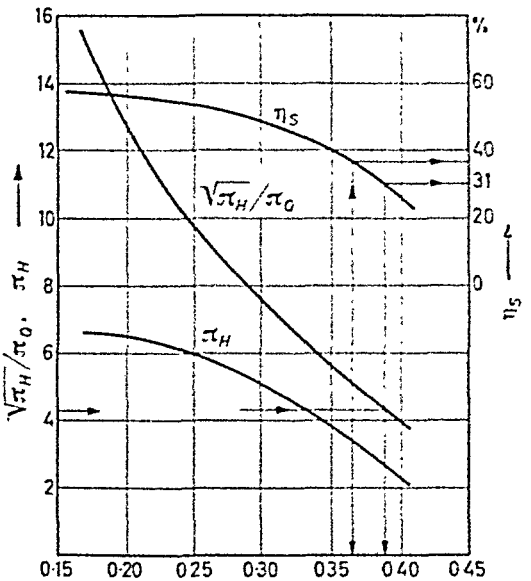

Figure 11.45

At the increased speed power required

$$P_2 = \frac{4{,}920 \times 6 \times 5{\cdot}2}{33{,}000 \times 0{\cdot}31} = 15 \text{ h.p.}$$

The increased speed may be calculated with Π_Q

$$N_2 = \frac{Q_2}{\Pi_Q D^3} = \frac{4{,}920}{0{\cdot}392 \times 5{\cdot}32} = 2{,}350 \text{ r.p.m.}$$

11.15 Cavitation in Centrifugal Pumps†

In pumps carrying liquids, a phenomenon termed 'cavitation' is frequently encountered. As a result of the dynamics of motion the pressure varies along the path of the flowing liquid, and, in

† A survey on Cavitation was recently made by F. A. L. Winternitz. *See* M.E.R.L. Fluids Report No. 40 August 1955. *See also* Ref. 5.

particular, low pressure regions are encountered at points where high local velocities are observed. If conditions are such that the static pressure attains the vapour pressure of the liquid, vaporization results. In centrifugal pumps these low pressure regions are mostly observed at the inlet to the impeller (*Fig. 11.46*) where the liquid is locally accelerated over the vane surfaces.

Where vaporization occurs small cavities or bubbles filled with vapour form near the points of lowest pressure. Subsequently these expand whilst moving forward with the flow and then suddenly collapse on reaching zones of higher pressures. Experiments show

Figure 11.46—Cavitation at impeller blade inlet. Instantaneous pictures of impeller with transparent sectors. (*By courtesy of C. J. Weir Ltd. and the Institute of Engineers and Shipbuilders*)

that the rate of growth and collapse of these bubbles is extremely high and the local pressures, resulting from the sudden collapse of the bubbles near the surfaces, are of the order of thousands of pounds per square inch.

The undesirable features of cavitation are:

(1) pitting of the surfaces which is due to the continuous hammering action of the collapsing cavities;

(2) marked drop in efficiency, owing to vapour formation which increases the volume of the fluid;

(3) knocking and vibration of the machine resulting in noise, emanating from cavitation zones.

11.16 Net Positive Suction Head

In order to avoid cavitation it is necessary to ensure that the lowest pressure regions are maintained above vapour pressure.

Consider a pump taking liquid from reservoir A and discharging into reservoir B as shown in *Fig. 11.47*. The height of the free surface level of reservoir A is Z_A and that of B is Z_B, above datum.

By adding the frictional losses and the kinetic head to the static lift $Z = Z_B - Z_A$ one obtains the total lift, H, of the pump. The total lift itself may be considered as the sum of the 'suction' lift, H_s, and the discharge lift, H_D.

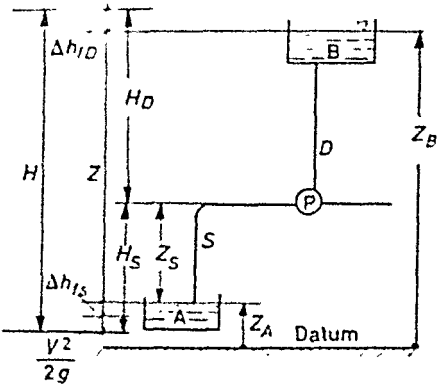

Figure 11.47—Simple line diagram of a pump head

In order to discover the effect of suction lift on pump performance, the pump may be tested with various suction lifts whilst keeping the total lift constant. This may be done, for example, by gradually

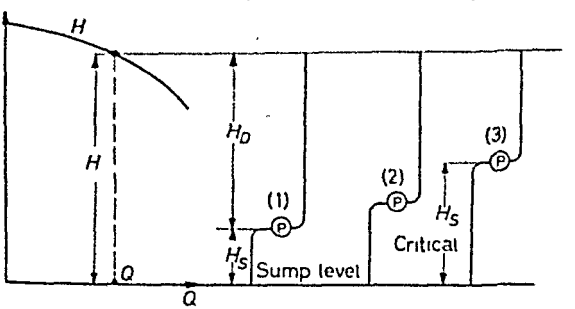

Figure 11.48

increasing the height of the pump above 'sump' level. Results of such experiments show, that when the height of the pump is *below* a certain critical value (H_{sc}) no change is experienced in its performance so that lift, discharge and efficiency remains constant (*see Fig. 11.48* pump position 1 and 2). At the critical height however, the performance of the pump begins to deteriorate and eventually the flow may break down. (*Fig. 11.48* position 3.)

The cause for this breakdown may be explained by noting that

the liquid is driven to the pump by atmospheric pressure so that at impeller inlet the static pressure may be well below atmospheric. When the 'limiting height' is reached, this pressure becomes equal to the vapour pressure, the fluid vaporizes, and the pump cavitates.

In order to control cavitation, it is necessary to maintain the inlet pressure to the pump at or above a certain critical value.

Consider a pump taking fluid from a sump with a free surface below the pump centre (*Fig. 11.49*).

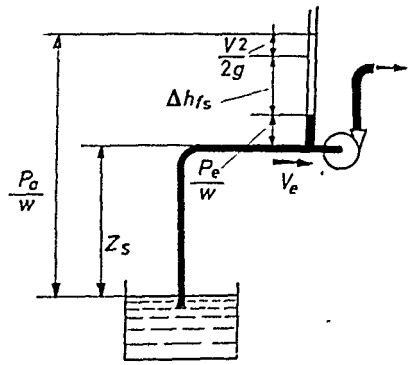

Figure 11.49

Writing the energy equation between free surface and pump inlet one obtains

$$\frac{p_a}{w} - Z_s = \frac{p_e}{w} + \frac{V_e^2}{2g} + \Delta h_{fs} \qquad \ldots.(11.32)$$

where Δh_{fs} is the frictional loss in the line and p_e is the absolute static pressure at pump inlet.

The value of p_e is critical from the point of view of cavitation, and *at the limit of safe operation* p_e must be greater than the vapour pressure p_v by an amount equal to that required by the fluid for the increase of its velocity head when entering the impeller. This amount is called the 'net suction head', H_{sv}, so that we may write

$$\frac{p_e}{w} = \frac{p_v}{w} + H_{sv}$$

Substituting this into Eq. 11.32, and rearranging terms gives

$$H_{sv} = \frac{p_a}{w} - \left[Z_s + \frac{V^2}{2g} + \Delta h_{fs}\right] - \frac{p_v}{w} \qquad \ldots.(11.33)$$

or

$$H_{sv} = H_a - H_s - H_v \qquad \ldots.(11.34)$$

where H_a is the atmospheric head, H_s is the suction lift, and H_v is the 'vapour' head.

It appears from Eq. 11.34 that the net inlet head, frequently referred to as the net positive suction head (N.P.S.H.), is in fact the difference between the static inlet head and the head corresponding to the vapour pressure of the liquid.

11.17 The Thoma Cavitation Parameter

The critical value of the net suction head which marks the onset of cavitation is determined experimentally. It is found that cavitation will occur for approximately the same value of the relative

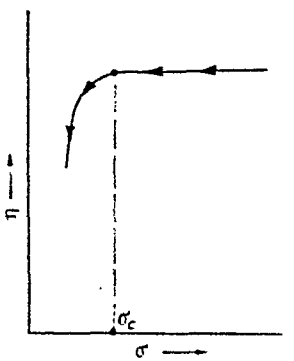

Figure 11.50—Point of critical condition

inlet velocity U_1 when operating conditions are varied. Since, as shown in section 11.16, the net suction head H_{sv} is related to U_1^2, it may also be related to the total lift of the pump H, because both U_1^2 and H are proportional to $(ND)^2$.

On the basis of the above considerations Thoma introduced a cavitation parameter defined as

$$\sigma = \frac{H_{sv}}{H} = \frac{H_a - H_v - H_s}{H} \qquad \ldots.(11.35)$$

The significance of the cavitation parameter appears from experiments which show that for specified working conditions cavitation sets in at approximately the same critical value of σ. This critical value is obtained from tests carried out with various suction lifts whilst keeping the total lift, discharge and speed constant. From the results thus obtained efficiency may be plotted against σ as shown in *Fig. 11.50*; the point where the efficiency begins to drop marks the critical value $\sigma = \sigma_c$, which represents the minimum at which it is possible to maintain cavitation-free running conditions.

The test procedure may be repeated for different sets of H, Q, N values and the resulting σ_c may be plotted against specific speed. In *Fig. 11.51*, $\log \sigma$ against $\log N_s$ chart, the critical points obtained from experiments fall inside a narrow band which may be regarded as the dangerous zone, whilst the region above the 'limit' line will be free of cavitation.

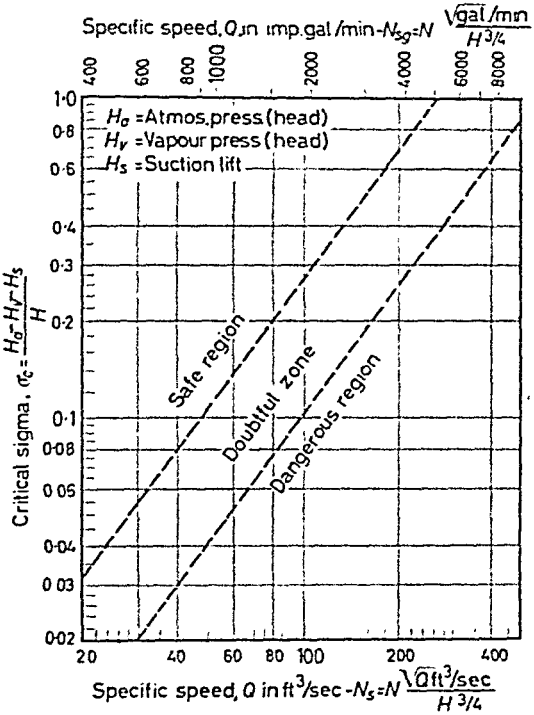

Figure 11.51—Cavitation chart for centrifugal pumps (first stage). (*By courtesy of McGraw-Hill, New York*).

The graph is useful for the calculation of cavitation limits. Combining Eq. 11.33 with Eq. 11.35, the minimum safe setting of a pump may be determined from

$$\pm Z_{sc} = \frac{p_a}{w} - \left[\sigma_c H + \frac{V_e^2}{2g} + \Delta h_{fs} + \frac{p_v}{w}\right] \quad \ldots\ldots(11.36)$$

Note that if the r.h.s. of Eq. 11.36 is positive, the pump may be placed above sump level, if negative, it must be set below the sump and so allow gravity to contribute to overcoming cavitation.†

† The bracketed term in Eq. 11.36 must always be positive.

Cavitation may be studied on models and the results employed for the prediction of performance of the prototype. Whilst the use of *Fig. 11.52* may be recommended for general practice, experiments on models yield more accurate results; this applies *e.g.*, to larger projects where the high cost of installation of prototypes justifies the additional expense incurred in building models.

Generally, flow similarity applies if Eqs. 11.24 to 11.28 are satisfied, which implies that

$$N_{s\,\text{model}} = N_{s\,\text{prototype}} \qquad \ldots\ldots(11.37)$$

and cavitation similarity conditions are satisfied if, *in addition*,

$$\sigma_{\text{model}} = \sigma_{\text{prototype}} \qquad \ldots\ldots(11.38)$$

Worked examples illustrate the use of these equations.

Examples

11.5. A single stage centrifugal pump is required to deliver water at the rate of 200 ft.^{3}/sec. against a head of 4,000 ft. at 450 r.p.m. A positive suction lift including the velocity head, and friction is to be 10 ft. As the impeller diameter is 6·8 ft. and the pump is too large for laboratory tests, a model with 18 in. impeller is to be tested at a reduced head of 320 ft.

Calculate the speed, discharge and suction lift for the laboratory tests.

Solution.—For dynamic similarity we may use

$$\left(\frac{H}{N^2D^2}\right)_{\text{m}} = \left(\frac{H}{N^2D^2}\right)_{\text{p}}$$

whence

$$N_{\text{m}} = N_{\text{p}}\frac{D_{\text{p}}}{D_{\text{m}}}\sqrt{\frac{H_{\text{m}}}{H_{\text{p}}}} = 450 \times \frac{6{\cdot}8}{1{\cdot}5} \times \sqrt{\frac{320}{400}} = 1{,}825 \text{ r.p.m.}$$

Similarly, for kinematic similarity

$$\left(\frac{Q}{ND^3}\right)_{\text{m}} = \left(\frac{Q}{ND^3}\right)_{\text{p}}$$

whence

$$Q_{\text{m}} = Q_{\text{p}}\left(\frac{N_{\text{m}}}{N_{\text{p}}}\right)\left(\frac{D_{\text{m}}}{D_{\text{p}}}\right)^3 = 200 \times \frac{1{,}825}{450} \times \left(\frac{1{\cdot}5}{6{\cdot}8}\right)^3 = 8{\cdot}65 \text{ cusecs.}$$

For cavitation similarity

$$\sigma_{\text{m}} = \sigma_{\text{p}}$$

Since the cavitation parameter for the prototype

$$\sigma_{\text{p}} = \frac{H_a - H_v - H_s}{H_{\text{p}}} = \frac{(14{\cdot}7 - 0{\cdot}5)144/62{\cdot}4 - 10}{400} = 0{\cdot}107$$

for the model with the same water

$$\sigma_{\text{m}} = 0{\cdot}107 = \frac{14{\cdot}7 - 0{\cdot}5)144/62{\cdot}4 - H_{s\text{m}}}{320}$$

$$\therefore \qquad H_{s\text{m}} = 1{\cdot}45 \text{ ft.}$$

Hence the model should be tested with a positive suction lift of 1·45 ft.

11.6. A centrifugal pump is to deliver water at a rate of 150 gal./min. against a head of 60 ft. The speed is 1,440 r.p.m.

Calculate the limiting height of the pump above the sump level at which cavitation free, safe operation may be expected. Assume a straight, vertical suction pipe of $2\frac{1}{2}$ in. internal diameter made of galvanized iron, the intake being 3 ft. below the water surface; the pipe is fitted with a strainer at intake and with a standard 90° bend at the inlet to the pump.

Data: water temperature 80°F; kinematic viscosity $= 0{\cdot}93 \times 10$ ft./sec.; k bend $= 0{\cdot}25$; k strainer $= 2{\cdot}0$; atmospheric pressure 14·7 lb./in.^{2} abs.; vapour pressure 0·5 lb./in.^{2} abs.

Solution.—Specific speed $N_s = 1{,}440 \times \sqrt{(150/60 \times 6{\cdot}24)}/60^{\frac{3}{4}} = 42{\cdot}5$. For this N_s the critical value of the cavitation parameter $\sigma_c = 0{\cdot}087$.

Hence $\sigma H = 0{\cdot}087 \times 60 = 5{\cdot}23$

Since $H_a = 14{\cdot}7 \times 144/62{\cdot}4 = 33{\cdot}8$ ft.

$h_v = 0{\cdot}5 \times 144/62{\cdot}4 = 1{\cdot}15$ ft.

the suction lift

$$H_s = 5{\cdot}23 + 1{\cdot}15 - 33{\cdot}8 = -27{\cdot}4 \text{ ft.}$$

Velocity in the line

$V = 0{\cdot}4 \times 144 \times 4/2{\cdot}5^2\Pi = 11{\cdot}8$ ft./sec.; $V^2/2g = 11{\cdot}8^2/64{\cdot}4 = 2{\cdot}14$

Reynolds' number

$$N_R = \frac{11{\cdot}8 \times 2{\cdot}5 \times 10^5}{12 \times 0{\cdot}93} = 2{\cdot}65 \times 10^5$$

For galvanized iron

$$k = 0{\cdot}0005 \text{ ft.}, \quad D/k = 2{\cdot}5/0{\cdot}0005 \times 12 = 416$$

From friction charts (see *e.g.*, Rouse chart) friction factor $f = 0{\cdot}025$.

The suction lift

$$H = Z_s + V^2/2g + \text{losses}, \quad \text{where } Z_s = l - 3$$

l being the length of the suction line.

Hence

$$27{\cdot}4 = (l - 3) + V^2/2g\left[1 + k_b + k_s + f\frac{l}{D}\right]$$

$$= (l - 3) + 2{\cdot}14[1 + 0{\cdot}25 + 2 + 0{\cdot}025l/2{\cdot}5/12]$$

$$\therefore \quad l = 18{\cdot}7 \text{ ft.}$$

Limiting height $Z_s = 15{\cdot}7$ ft.

11.18 Centrifugal Fans

The theory of centrifugal fans is substantially the same as that of centrifugal pumps. There are, however, differences in construction,

apart from the difference in the working fluid, pumps being used for liquids and fans for gaseous substances.

Most of the fans manufactured at the present time are fabricated from sheet steel. Simplicity of design predominates over efficiency requirements, although some types of fan attaining 90 per cent efficiency are now being successfully manufactured commercially. Variations in design appear in the impeller which according to requirements, may incorporate forward, radial or backward curved vanes. The casing is invariably of the volute form. Generally speaking, fans have wider impellers than pumps.

The characteristic features of the three standard types are given in the following table:

Impeller type	Forward	Radial	Backward
Width–diameter ratio (B/D)	0·5–0·6	0·35–0·45	0·25–0·45
Number of vanes	16–20	6–8	8–12
Pressures, in. W.G. (max.)	3–4	16–18	5–6
Application	Ventilation *etc.*	Mill exhaust *etc.*	Air conditioning *etc.*
Efficiency (max.)	55–60	60–70	75–90

Figures 11.52, 11.53, 11.54 and *11.55* show the general features and performance characteristics of these types, whilst efficiency and specific speed characteristics are shown in *Fig. 11.56.*

11.19 Static and Total Pressure and Efficiency of Fans

The volume of flow through a duct system depends on its frictional resistance and a relation between flow rate and resistance may be plotted to give a curve, called the system characteristics. The intersection of the system characteristics with the fan pressure characteristics yields the volume flow at the point of operation.

It must be borne in mind, however, that resistance is generally expressed in terms of static pressure whilst the overall performance of the fan (or pump for that matter) is based on the total pressure (the sum of static and kinetic head) the reason being that the impeller imparts total energy to the fluid. In pumps the kinetic head is usually negligible in comparison with the total lift, but in the case of fans the flow velocities are comparatively high and the kinetic head may be a considerable proportion of the total energy.

As a result it is customary to plot both the total and the static pressures against volume flow and the intersection of the static pressure curve with the system characteristics yields the point of operation (*Fig. 11.57*). Furthermore, it is also customary to differentiate between static efficiency η_s and total efficiency η_s.

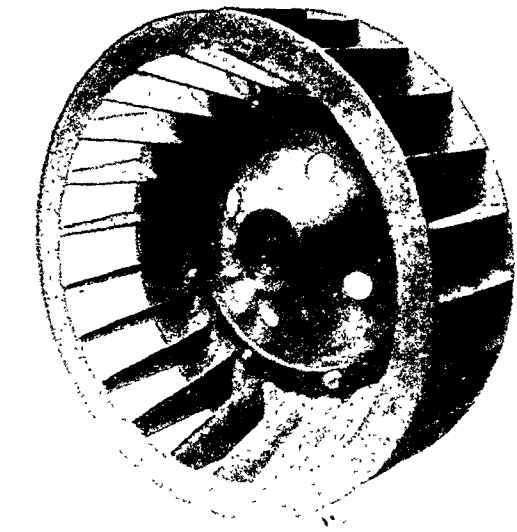

Figure 11.52—Forward curved fan impeller.
(By courtesy of Aerex Ltd.)

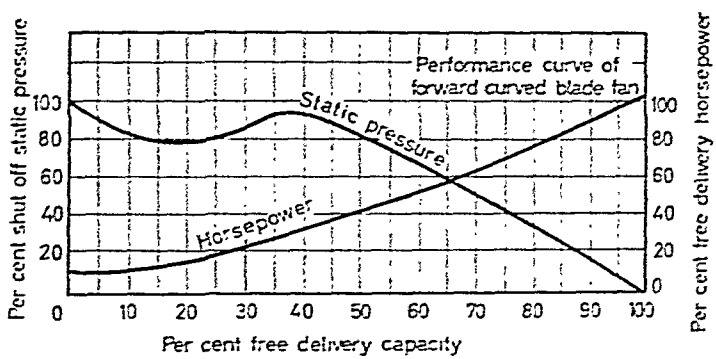

Figure 11.53

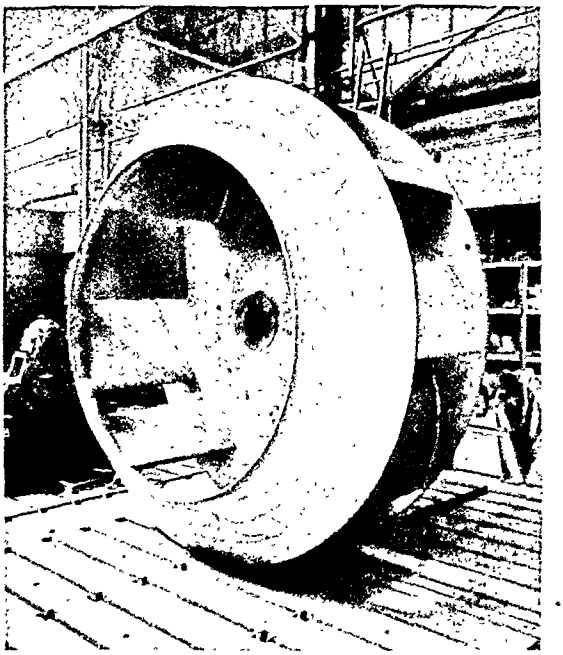

Figure 11.54—Backward curved fan impeller.
(*By courtesy of Aerex Ltd.*)

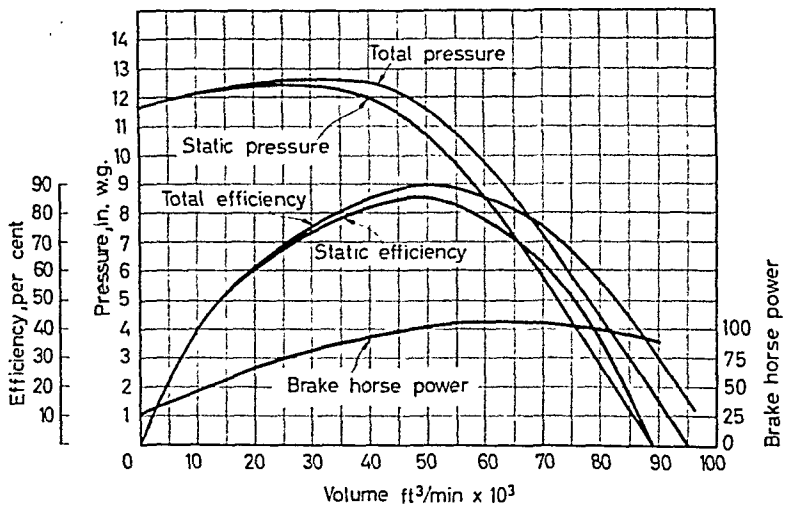

Figure 11.55

Denoting the static and total pressure rise of the fan by Δp_s and Δp_t respectively, the power required

$$P = \frac{Q\Delta p_s}{550\eta_s} = \frac{Q\Delta p_t}{550\eta_t}$$

hence

$$\frac{\eta_t}{\eta_s} = \frac{\Delta p_t}{\Delta p_s} \qquad \ldots.(11.39)$$

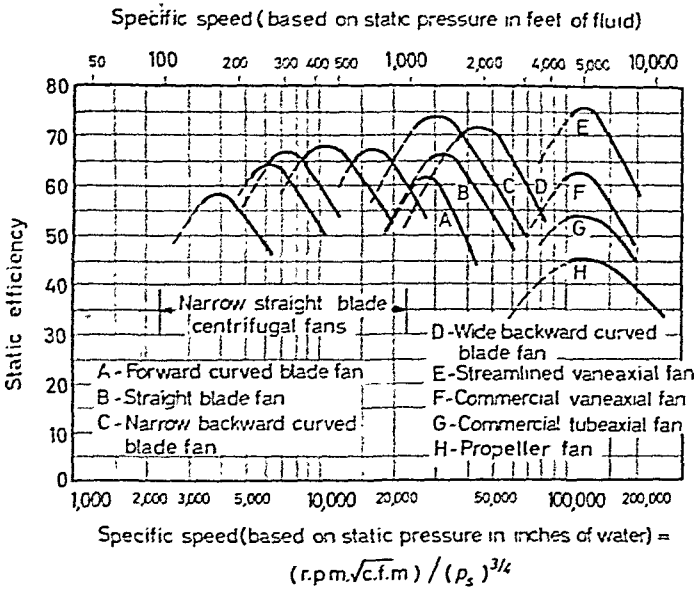

Figure 11.56—(By courtesy of Buffalo Forge)

It is of interest to note that the static efficiency curve peaks at a lower volume flow than the total efficiency curve. Therefore, assuming that the point of operation falls under the static efficiency peak, the fan does not necessarily operate at maximum total efficiency.

In general, the use of the 'total' performance curves would be more satisfactory than the static, because the latter depends on the size of the fan exit area A_e.† This may be shown by referring the performance to the exit. Assuming zero total pressure at fan inlet

† Exit area of fan housing (scroll, volute).

and using suffix e for exit, the total pressure rise

$$\Delta p_{te} = \Delta p_{se} + \tfrac{1}{2}\rho V_e^2 = \Delta p_{se} + \tfrac{1}{2}\rho\,(Q/A_e)^2$$

or $$\Delta p_{te}/\Delta p_{se} = \eta_t/\eta_s = 1 + \tfrac{1}{2}\rho/\Delta p_{se}\,(Q/A_e^2)$$

Introducing

$$\frac{\Delta p_{te}}{\rho N^2 D^2} = \Pi_{Ht}, \quad \frac{\Delta p_{se}}{\rho N^2 D^2} = \Pi_{Hs}, \quad \frac{Q}{ND^3} = \Pi_Q$$

one obtains $$\frac{\eta_t}{\eta_s} = \frac{\Pi_{Ht}}{\Pi_{Hs}} = 1 + \tfrac{1}{2}\varepsilon^2 \frac{\Pi_Q^2}{\Pi_{Hs}} \qquad \ldots.(11.40)$$

where $$\varepsilon = D^2/A_e$$

It appears that whilst Π_{Ht} and η_t are constant for a given impeller, Π_{Hs} and η_s depend on the value of ε. In other words the variation of exit area causes a variation of the static performance

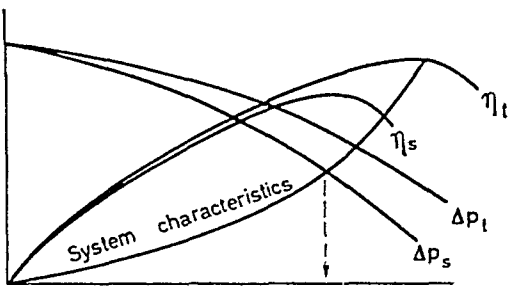

Figure 11.57—Static and total efficiency plotted against discharge

of the fan. Since larger exit areas allow for an increase in the static performance it is customary either to provide fans with diffusers at the exit, or to make the scroll wider than required from aerodynamic considerations and thus save the extra cost of the diffuser.

REFERENCES

(1) Wislicenus, G. F., *Fluid Mechanics of Turbomachinery*, McGraw-Hill, New York, 1947.
(2) Church, A., *Centrifugal Pumps and Blowers*, J. Wiley and Son, London, 1945.
(3) Pfleiderer, C., Strömungsmachinen, Springer, Berlin, 1952.
(4) Stepanoff, A. J., *Centrifugal and Axial Flow Pumps*, McGraw-Hill, New York, 1947.
(5) 'Cavitation in Hydrodynamics' *N.P.L. Symposium*, H.M.S.O., 1956.
(6) Davis, C. V., Ed., *Handbook of Hydraulics*, McGraw-Hill, New York, 1952.

Examples

11.7. The air conditioning of a building requires a centrifugal fan (blower) capable of handling air at the rate of 10,000 ft.^{3}/min. against a static head of $1\frac{1}{2}$ in.W.G. The runner of the fan is a 'forward curved design' and consists of a large number of blades.

A geometrically similar fan was tested in the laboratory and the results of the readings are plotted in non-dimensional form on *Fig. 11.58.* With the aid of this graph and assuming maximum efficiency, calculate:

(*a*) the diameter of the runner
(*b*) the speed (r.p.m.)
(*c*) the power required for driving the fan.

The density of air is 0·00233 slugs/ft.^{3}

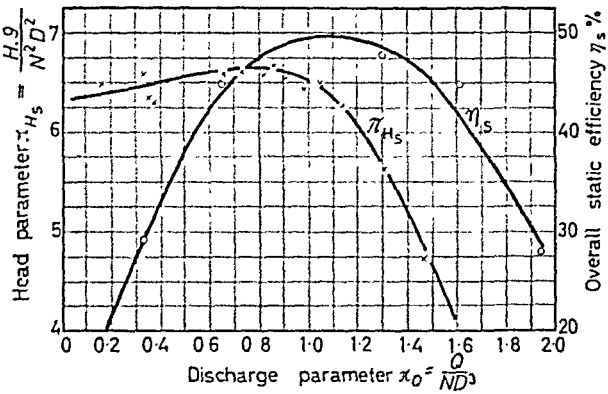

Figure 11.58

Solution.—It appears from the graph that for maximum efficiency $\eta_{max} = 0{\cdot}497$

$$\Pi_H = 6{\cdot}35, \quad \Pi_Q = 1{\cdot}1$$

Elimination of N leads to

$$\frac{\sqrt{\Pi_H}}{\Pi_Q} = \frac{\sqrt{6{\cdot}35}}{1{\cdot}1} = 2{\cdot}3$$

$$\therefore \quad \frac{D^2\sqrt{\Delta p/\rho}}{Q} = \frac{D^2\sqrt{1{\cdot}5 \times 5{\cdot}2/0{\cdot}00233}}{10{,}000/60} = 2{\cdot}3$$

(*a*) $$\therefore \quad D = 2{\cdot}56 \text{ ft.}$$

(*b*) $$N = \frac{Q}{\Pi_Q D^3} = \frac{10{,}000}{1{\cdot}1 \times (2{\cdot}56)^3} = 526 \text{ r.p.m.}$$

(*c*) $$P = \frac{10{,}000 \times 1{\cdot}5 \times 5{\cdot}2}{550 \times 60 \times 0{\cdot}495} = 4{\cdot}78 \text{ h.p.}$$

11.8. A building requires a centrifugal fan (blower) capable of handling air at a rate of 2,000 ft.^{3}/min. against a total head of 1·5 in. water. The fan is driven by a motor at 1,500 r.p.m. The runner of the fan is a 'forward curved' design and consists of a large number of circular arc blades. Assuming that the hydraulic efficiency of the fan is 55 per cent and that the whirl velocity is twice the peripheral speed of the runner,
Calculate:

(*a*) the diameter of the runner

(*b*) the power required for driving the fan.

(*c*) Draw to scale the inlet and outlet velocity triangles, and find the blade angles at inlet and outlet, assuming that the width of the runner is equal to half of its diameter and approximately only 50 per cent of this width is effective (that is the air passing through the runner fills only half of the width). The radial dimension of the blades is one tenth of the runner diameter.

Neglect volumetric and mechanical losses, and discount the effect of the relative eddy.

The specific weight of air is 0·075 lb./ft.^{3}

Solution.—Convert the pressure into feet of air

$$1{\cdot}5 \text{ in. W.G.} = 1{\cdot}5 = \frac{62{\cdot}4}{12} = 7{\cdot}8 \text{ lb./ft.}^2$$

$$\therefore \quad H = \frac{7{\cdot}8}{0{\cdot}075} = 104 \text{ ft.}$$

Lift developed

$$H = \frac{V_{t2}V_{w2}}{g} \cdot \eta_H$$

where $V_{w2} = 2V_{t2}$ and η_H is the assumed hydraulic efficiency.
Hence

$$104 = \frac{2V_{t2}^2}{32{\cdot}2} \times 0{\cdot}55$$

$$\therefore \quad V_{t2} = 55{\cdot}2 \text{ ft./sec.}$$

Since

$$V_{t2} = \frac{D_2 \Pi N}{60}$$

$$\therefore \quad D_2 = \frac{60 \times 55{\cdot}2}{\Pi \times 1{,}500} = 0{\cdot}701 \text{ ft.} = 8{\cdot}5 \text{ in.}$$

Width of the impeller

$$b_2 = D_2/2 = 4{\cdot}25 \text{ in.}$$

Effective width

$$b_2/2 = 2{\cdot}125 \text{ in.}$$

The radial velocity is found from the discharge and from the effective flow area,

$$V_{r2} = \frac{Q}{A_{\text{eff}}} = \frac{2{,}000 \times 144}{60 \times 2{\cdot}125 \times 8{\cdot}5 \times \Pi} = 38{\cdot}1 \text{ ft./sec.}$$

The radial dimension of the vanes $= 8{\cdot}5/10 = 0{\cdot}85$ in.
For shockless inflow $V_{w1} = 0$.
At the inlet to the vanes the tangential velocity

$$V_{t1} = \frac{D_1 \Pi N}{60} = \frac{(8{\cdot}5 - 2 \times 0{\cdot}85)\Pi \times 1{,}500}{60 \times 12} = 38 \text{ ft./sec.}$$

and the radial velocity (from continuity)

$$V_{r1} = \frac{8{\cdot}5}{5{\cdot}8} \times 38{\cdot}1 = 56 \text{ ft./sec.}$$

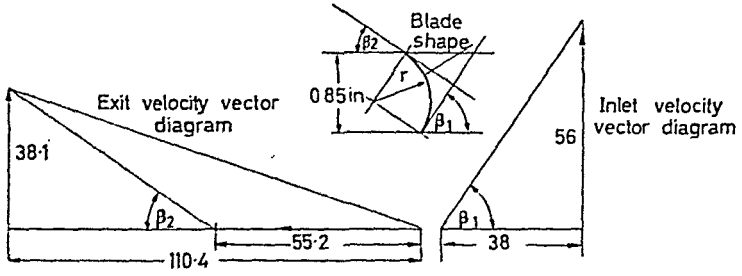

Figure 11.59

$$\text{Vane angles} \quad \beta_2 = \tan^{-1}\frac{38{\cdot}1}{55{\cdot}2} = 34°20'$$

$$\beta_1 = \tan^{-1}\frac{56}{38} = 55°48'$$

Problems

11.1. Show, by simple reasoning, that decreasing the supply by throttling on the discharge side of a centrifugal pump lessens the dangers of cavitation, whereas throttling on the intake side increases the danger.

11.2. A single stage centrifugal pump operating at constant speed draws water from a sump and is located 25 ft. above the free surface level. The suction line is 27 ft. long and it incorporates one bend and a strainer at intake.

With the aid of the head v. discharge data given below, establish the approximate discharge at which the pump may no longer operate free of cavitation. Assume a constant friction factor.

Data:

Bend loss $k = 0{\cdot}25$

Strainer $k = 2{\cdot}0$

Friction factor $f = 0{\cdot}02$

Pipe diameter (internal) = 2 in.

Pump data:

Speed 1,440 r.p.m.

Discharge, ft.^{3}/sec	0·107	0·133	0·160
Head, ft.	66	61	54

Atmospheric pressure, 14·7 lb./in.^{2}abs.

Vapour pressure, 0·5 lb./in.^{2}abs.

11.3. A prototype centrifugal fan is to deliver air at a rate of 26,000 ft.^{3}/min. against a static pressure of 13 in. W.G. at a speed of 650 r.p.m. Assuming a static efficiency of 60 per cent the power required to drive this fan would be 89 h.p. approximately. The diameter of the fan would be 72 in.

It is proposed to build a geometrically similar fan on $\frac{1}{6}$th scale of the prototype and test this under dynamically similar conditions.

You are required to report on the practicability of these tests, submitting the corresponding figures of the model, that is, fan shaft diameter, speed, discharge, power, and pressure.

The shaft diameter may be calculated from the expression

$$d = 4{\cdot}6\sqrt[4]{\frac{\text{h.p.}}{\text{r.p.m.}}}$$

and it is suggested to keep only as close as practicable to the formula.

11.4. The power output of a gas turbine is 840 h.p. at 13,750 r.p.m. The dry weight of the engine is 760 lb., its diameter 27 in. and length 57 in. The fuel consumption is 79 gal./hr., and the air consumption 13·5 lb./sec.

The engine is to form the 'prototype' for a projected 'geometrically similar' unit of 160 h.p.

Calculate the approximate (*a*) r.p.m., (*b*) dry weight, (*c*) diameter and length, (*d*) fuel and air consumptions for the scale model, assuming the blade speed in the scale engine to be three-quarters of those in the prototype.

Indicate in what respects the estimated figures may be 'out of scale'.

11.5. A fluid particle leaves the outer perimeter of a centrifugal impeller at a peripheral speed of 100 ft./sec. and a radial speed of 20 ft./sec. What will be the absolute velocity of this particle after it has travelled a radial distance of $\frac{1}{2}$ in. from the perimeter of the impeller without any interference? The diameter of the impeller is 10 in.

11.6. The feedwater pump of a boiler under consideration is a 'turbine' pump consisting of several stages.

Calculate the approximate number of stages necessary to obtain 250 lb./in.^{2} pressure (gauge) and find the power necessary to drive the pump at a discharge of 300 gal./min.

Make the following assumptions:

Diameter of the impeller, 10 in.

Motor speed, 1,440 r.p.m.

Hydraulic efficiency, 92 per cent

Mechanical efficiency, 95 per cent

Volumetric efficiency, 90 per cent

Actual exit whirl velocity, 55 per cent of peripheral speed

11.7. A four-stage centrifugal pump supplying water is to be designed for the following conditions:

Delivery: 500 gal./min.

Head: 150 lb./in.^{2}

r.p.m.: 1,440.

Calculate:

(*a*) the diameter, width and vane angles of the impeller at inlet and outlet, assuming shockless inflow conditions;

(*b*) the power necessary to drive the pump.

Assume that the actual whirl velocity is approximately 60 per cent of the tangential (peripheral) speed and the relative eddy factor is 0·76; assume a radial velocity 20 ft./sec.

The hydraulic efficiency is to be established with the aid of specific speed graph. Assume 90 per cent volumetric and 95 per cent mechanical efficiency. Tabulate the results.

Exercise

(*a*) Differentiate between 'forced' and 'free' vortex. Prove, that in a 'free' vortex the 'whirl' velocity is inversely proportional to the radius.

(*b*) List the 'losses' affecting the performance of centrifugal pumps. Discuss briefly all factors causing the losses. Show that the factors can be grouped into three groups and that the overall efficiency of a centrifugal pump is ultimately the product of three component efficiencies.

(*c*) What is the specific speed of a pump? Discuss briefly its use.

(*d*) Discuss the effect of the relative eddy on centrifugal pump performance. Explain first the phenomenon then, by drawing the outlet velocity triangle at the tip of a vane, show graphically the variations caused.

12

AXIAL FLOW MACHINERY

12.1 Introduction

In an axial flow machine the fluid passes through in a substantially axial direction. The impeller blades are enclosed by a cylindrical duct of sufficient length to provide uniform flow on both the upstream and downstream sides. Upstream from the impeller, the duct is usually provided with a bell-mouthed intake to avoid sudden contraction of the stream, whilst immediately downstream

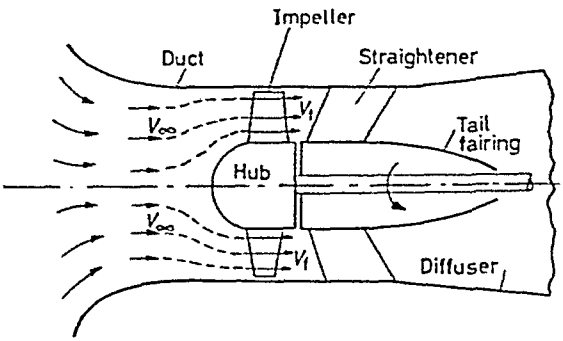

Figure 12.1

from the impeller straightener vanes are employed to remove the whirling motion of the fluid. Since the flow contracts on approaching the impeller a suitably shaped hub is provided in front of the rotor and downstream from the straightener vanes a tail-fairing aids diffusion (*Fig. 12.1*). A cut-away view of a large installation and a fan rotor is shown in *Fig. 12.2*.

Several theories exist for the design of axial flow machines. The more accurate ones are rather complex and therefore are beyond the scope of this text. An approximate theory however, called the 'isolated blade theory' is presented in the following discussion.

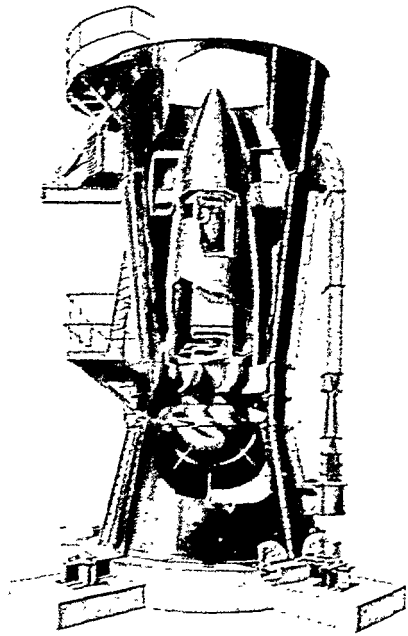

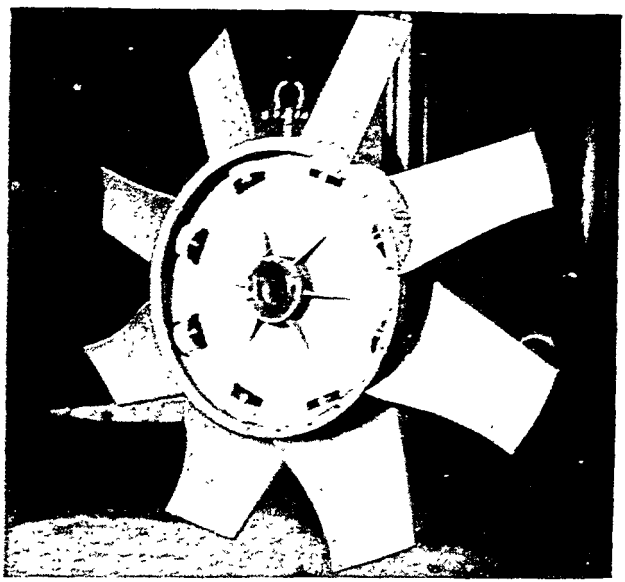

Figure 12.2—(Top) A large axial flow fan installation, *(Bottom)* Adjustable pitch axial flow rotor. *(By courtesy of Aerex Ltd.)*

12.2 Isolated Blade Theory

This theory assumes that (*a*) the blades are sufficiently spaced apart for multiplane interference to be negligible; (*b*) the fan is ducted and the tip clearance is small; with these assumptions the blades may be considered as isolated two dimensional wings; (*c*) the rotation of the flow downstream from the impeller is small.

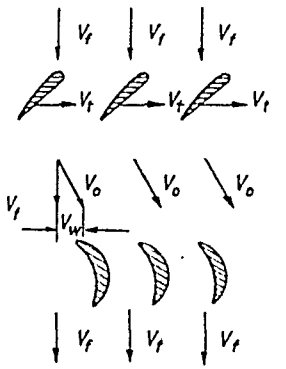

Figure 12.3—Rotor blades and straightener vanes

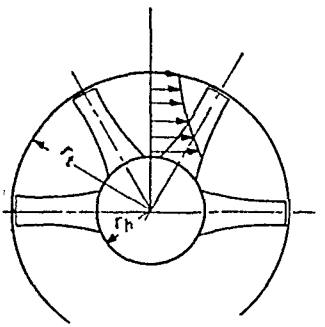

Figure 12.4—Front view of rotor

In passing through the rotating blades the fluid is deflected, resulting in rotation of the whole fluid mass downstream. This rotation, superimposed on the axial flow causes the absolute flow velocity to increase from V_f to V_0 (*Fig. 12.3*). The role of the straightener blades is to remove this rotation, so that downstream from the straighteners the flow velocity is again V_f.

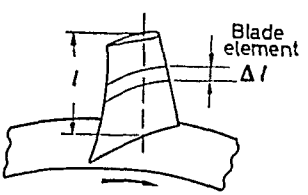

Figure 12.5—Single blade showing blade element

The measure of rotation is the whirl velocity V_w which must follow the law of the free vortex, *i.e.*, $V_w = c/r$. Accordingly the whirl is largest near the root of the blade and is smallest at the tip (*Fig. 12.4*). This is one reason why correctly designed blades are twisted along the blade axis.

Consider a blade element of length Δl (*Fig. 12.5*), moving with tangential speed V_t. A fluid particle approaching the leading edge

of the blade section with a velocity V_f will slide along the inner blade surface and leave with an absolute velocity V_0 at the trailing edge (*Fig. 12.6*). Thus two velocity vector diagrams may be constructed, one at inlet to and one at outlet from the blade. The base of both triangles is the same and also the through flow velocity erected perpendicularly to V_t remains the same. The relative

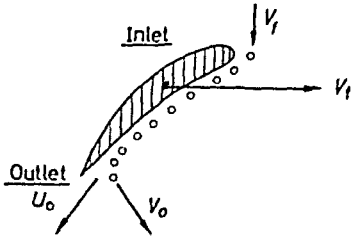

Figure 12.6

velocities U_{in}, U_0 are obtained upon completion of the vector triangles as shown in *Fig. 12.7a* and *b*. The change in shape of the vector diagrams is due to the whirl V_w.

The two diagrams may be superimposed (*Fig. 12.7c*) and the mean value of the relative velocities $\bar{U}_m \cong (U_{in} + U_{out})/2$ be obtained.

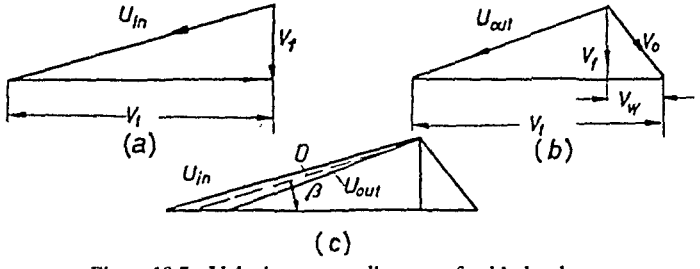

Figure 12.7—Velocity vector diagrams for blade element

The results of the general wing theory may now be applied and it is assumed that the blade element under consideration is a wing section set at an angle of incidence to the mean relative velocity $\bar{U}_m$ (*Fig. 12.8*). The setting angle of the blade with the plane of rotation is $\alpha + \beta$ where β is the angle enclosed between $\bar{U}_m$ and V_t.

According to wing theory the blade experiences a lift force L, perpendicular to $\bar{U}_m$, and a drag force D, parallel with $\bar{U}$. The resultant force R may be resolved into two components T and F, T being the axial thrust, and F being the force parallel to the plane of rotation.

From the vector diagram shown in *Fig. 12.8* it appears that

$$F = L \sin \beta + D \cos \beta$$

To maintain rotation, the power to be applied to a blade element

$$\Delta P = FV_t = [L \sin \beta + D \cos \beta] V_t$$

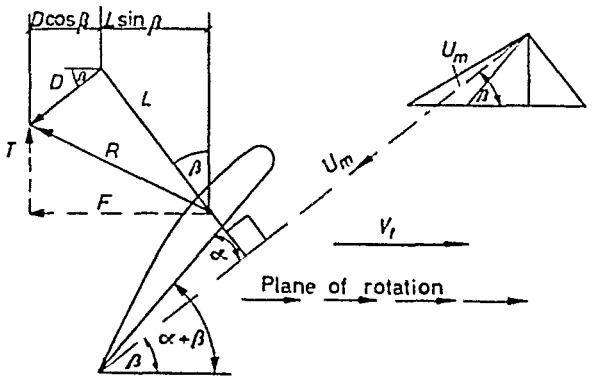

Figure 12.8

Introducing lift and drag coefficients, defined by Eqs. 9.6 and 9.7, one obtains

$$L = C_L \times \tfrac{1}{2} \rho \bar{U}_m^2 \times (c \, \Delta l)$$
$$D = C_D \times \tfrac{1}{2} \rho \bar{U}_m^2 \times (c \, \Delta l)$$

where area S is the product of the blade element spanwise length Δl and chord c. Thus,

$$\Delta P = (c \, \Delta l) \times \tfrac{1}{2} \rho U_m^2 [C_L \sin \beta + C_D \cos \beta] V_t$$

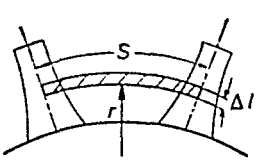

Figure 12.9

The total mass flow across the impeller may be divided so that each blade element receives a due share; accordingly the mass flow allotted for a blade element (*Fig. 12.9*).

$$\Delta m = S \, \Delta l \rho g V_f$$

where s is the blade spacing at radius r. For an impeller employing z blades

$$s = (2\pi r)/z$$

Hence the power imparted to the fluid by a blade element per pound of fluid flowing is

$$\frac{\Delta P}{\Delta m} = \frac{c\bar{U}_m^2[C_L \sin\beta + C_D \cos\beta]V_t}{sgV_f}$$

The next important step is to equate $\Delta P/\Delta m$ with the Euler lift $V_t V_w/g$; this may be done because the power imparted to the fluid reappears in the stream in a form of rotational energy. Accordingly

$$\frac{V_t V_w}{g} = \frac{c\bar{U}_m^2[C_L \sin\beta + C_D \cos\beta]V_t}{sgV_f}$$

Substituting $\sin\beta = V_f/\bar{U}_m$, reducing and rearranging terms yields

$$V_w = \frac{\bar{U}_m[C_L + C_D \cot\beta]}{2s/c} \qquad \ldots.(12.1)$$

It appears from Eq. 12.1 that both the lift and drag coefficients affect the whirl. Introducing $\gamma = C_L/C_D$ Eq. 12.1 may be written as

$$V_w = \frac{\bar{U}_m C_L}{2s/c}\left[1 + \frac{\cot\beta}{\gamma}\right]$$

For large values of γ, say $\gamma \geqslant 20$, and assuming $\beta \cong 45°$, the error introduced by neglecting $1/\gamma$ is not greater than about 5 per cent, so that for approximate calculations

$$V_w \cong \frac{\bar{U}_m C_L}{2S/c} \qquad \ldots.(12.2)$$

where S/c is the pitch–chord ratio.†

Eq. 12.2 may be employed in establishing a simple relationship for the calculation of blade chord. Denoting the hydraulic efficiency of the blade element at radius r by η_b, and substituting Eq. 12.2 for V_w in the Euler equation, one obtains

$$\frac{H}{\eta_b} = \frac{V_t \bar{U}_m C_L}{g2s/c}$$

Since $V_t = D\pi N/60$, $s = D\pi/z$, upon substituting and rearranging terms, one obtains

$$c = \frac{120\ \mathrm{Hg}}{C_L N z \eta_b \bar{U}_m} \qquad \ldots.(12.3)$$

12.3 Efficiency Considerations

The overall increase in energy supplied by an axial flow unit is made up of an increase of the total lift through the rotating blades

† Values of the pitch-chord ratio should be equal to or greater than one. With values below one multiplane interference may appear.

and a small decrease due to frictional losses in the straightener, *i.e.*,

$$H = H_b - H_s$$

where H_b is the lift imparted by the impeller and H_s is the head loss in the straightener. Accordingly, the efficiency of operation of the combined blade and straightener elements may be written† as

$$\eta_{Comb} = \frac{V_f}{V_t}\left[\frac{\dfrac{C_L}{C_D} - \dfrac{V_f}{V_t}}{\dfrac{C_L}{C_D}\cdot\dfrac{V_f}{V_t} + 1} - \frac{1}{\dfrac{C_{Ls}}{C_{Ds}}}\right]$$

where C_L/C_D applies to the blade and C_{Ls}/C_{Ds} to the straightener element. Since it will be the object of good straightener design to

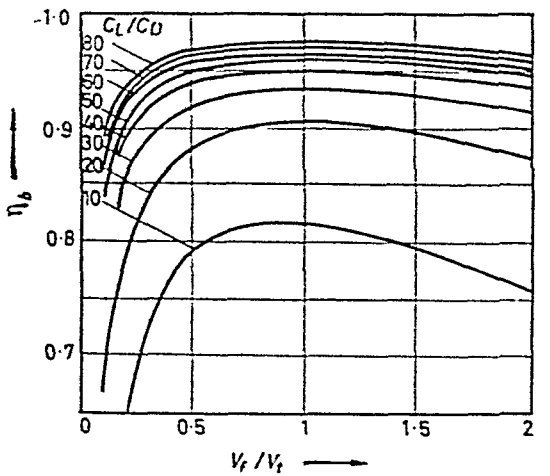

Figure 12.10—Blade element efficiency

make the second term negligibly small compared with the first, then one may expect the general characteristics leading to high blade-element efficiency to be obtained with sufficient accuracy, from

$$\eta_b \cong \frac{\dfrac{V_f}{V_t}\left[\dfrac{C_L}{C_D} - \dfrac{V_f}{V_t}\right]}{\dfrac{C_L}{C_D}\cdot\dfrac{V_f}{V_t} + 1} \qquad \ldots\ldots(12.4)$$

Curves based on Eq. 12.4 are given in *Fig. 12.10* and they indicate that the primary consideration for high efficiency is the choice of

† Patterson, G. N. 'Ducted Fans', *Australian Council of Aeronautics Report* 7, 1944.

V_f/V_t in the neighbourhood of the value 1·0. Provided this is satisfied, the choice of any $C_L/C_D \geqslant 40$ will be sufficient to ensure *blade* efficiency around the 90 per cent mark.

An allowance for 2–5 per cent loss in the straighteners may be made in advance (so as to ensure higher whirl velocity) and a certain increase in power, due to mechanical losses, (bearing and drive friction) may be allowed for. Volumetric losses, on the other hand, are considered non-existent in axial flow machines.

12.4 Blade Design based on Constant Element Efficiency

Results of the isolated blade theory apply to both axial flow pumps and fans. Once the design lift H and speed N are specified and the number of blades is assumed, Eq. 12.3 reduces to

$$c = \frac{\text{CONST.}}{C_L \eta_b \bar{U}} \qquad \ldots\ldots(12.5)$$

Since C_L, η_b and $\bar{U}_m$ are interdependent, the calculation of c is carried out step-by-step.

1. Divide the blade into a suitable number of elements and find the mean tangential velocities. It is noted that all calculations in these steps are carried out for each element.

2. Assume a reasonable value of η_b (which will remain constant along the blade) and calculate the whirl velocity from the relationship $V_w = Hg/V_f\eta_b$.

3. Calculate the through flow velocity from the relationship

$$V_f = \frac{Q}{\frac{\pi}{4}(D_T^2 - D_H^2)}$$

where D_T, D_H are the tip and hub diameters respectively.

4. Complete the construction of velocity vector diagrams and find the value of the mean relative velocities $\bar{U}$.

5. With aid of Eq. 11.4 find values of C_L/C_D using the assumed blade efficiency η_b.

6. Select a suitable wing profile† and from the data provided draw a graph of C_L and C_L/C_D against incidence α. With the calculated values of C_L/C_D (step 5) find C_L and α. Assume a Reynolds' number. A sample graph for a R.A.F. type 6 section D profile is shown in *Fig. 12.11.*

† Hydrofoils for pumps and aerofoils for fans. Where this data refers to a wing of finite aspect ratio it must first be corrected to the two dimensional case. For this see Eq. 9.12 and Example 9.3.

7. With the values of C_L, η_h and $\bar{U}_m$, find the chord c and the profile setting angle $\alpha - \beta$.

8. With the chord c and mean velocity $\bar{U}_m$, check the assumed value of the Reynolds' number. (Note $N_R = c \cdot \bar{U}_m/\nu$.)

9. Check the pitch–chord ratio for overlapping.

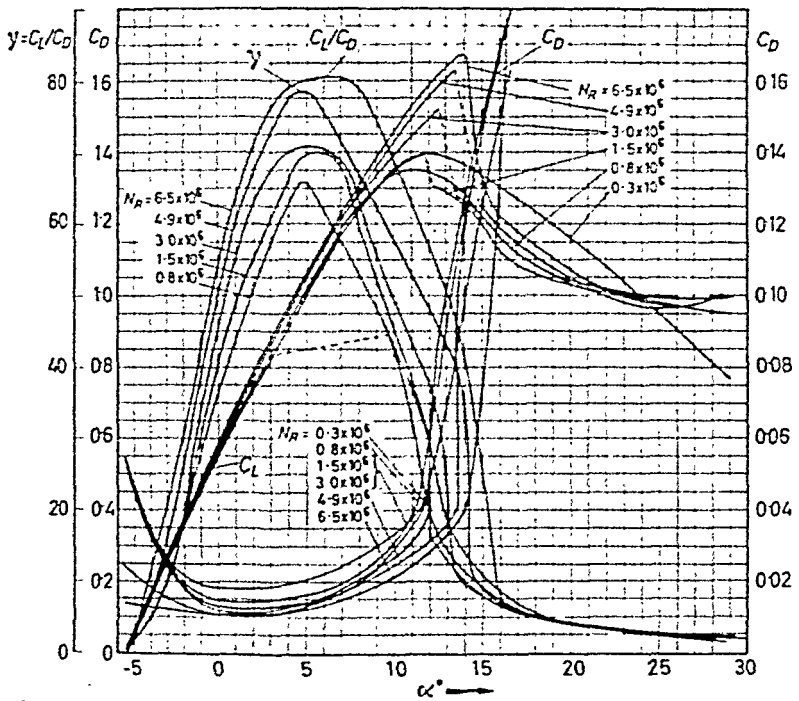

Figure 12.11—Characteristic curves for fan blade element (R.A.F. 6 type section).

12.5 Cavitation in Axial Flow Pumps

The considerations governing cavitation in axial flow pumps are somewhat different from those previously considered in the case of centrifugal pumps, and Thoma's cavitation parameter is not applicable. Generally, axial flow pumps are more susceptible to cavitation than centrifugal pumps and achievement of cavitation-free running conditions presents one of the main problems of design.

Conditions for cavitation may be obtained directly with the aid of a non-dimensional pressure coefficient, defined as

$$K_p = \frac{p_z - p_s}{\frac{1}{2}\rho \bar{U}_m^2}$$

where p_s is the pressure at the blade surface at a point where a suction peak occurs, p_2 is the undisturbed, free stream pressure at the impeller section and $\bar{U}$ is the mean relative velocity over the blade, (all variables being at a radius r).

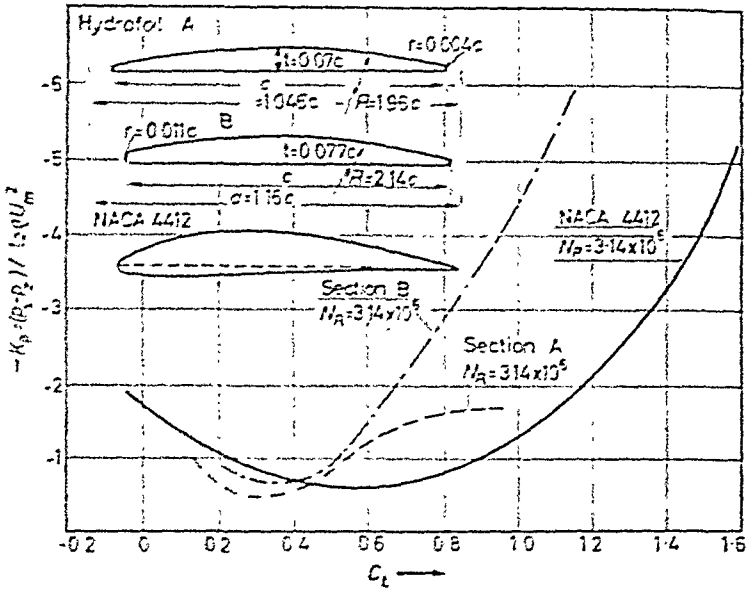

Figure 12.12—Variation of peak suction pressure coefficient with lift coefficient. [*Adapted from A.R.L. (Melbourne) Aero. Note 70*]

Cavitation sets in when the suction peak pressure p_s approaches vapour pressure p_v so that the *critical* value of the pressure coefficient

$$K_{p\,crit} = \frac{p_2 - p_v}{\frac{1}{2}\rho \bar{U}_{r1}^2} \qquad \ldots\ldots(12.6)$$

Since the pressure distribution around the blade and the lift force acting are closely connected, it is reasonable to relate the critical value of the pressure coefficient to the lift coefficient C_L. In *Fig. 12.12* results of experiments on the critical value of the pressure coefficient are plotted against lift coefficient for two types of hydrofoil. While the zone of incipient cavitation is in the vicinity of the curves (as shown by the shaded areas) the zone of fully established cavitation lies below the curves.

The types of wings which are most suitable as blade profiles for axial flow pumps are characterized by low suction peaks and are frequently referred to as hydrofoils in contrast to aerofoils which

have higher suction peaks. Hydrofoils have sharp leading edges and are therefore more resistant to cavitation although some sacrifice in efficiency must be accepted at off design-point conditions.

Generally cavitation sets in at the blade tip since the relative velocities are highest there and these are squared in the expression.

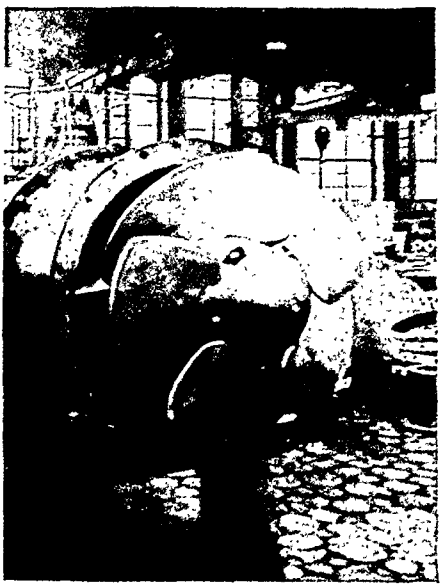

Figure 12.13—Axial flow pump impeller.
(*By courtesy of Escher Wyss*)

For this reason the lift coefficient must be kept as low as possible resulting in a large chord (*Fig. 12.13*). On the other hand cavitation-free running at the design point does not secure freedom from cavitation at reduced flow. In the case of fixed blade impellers, when the discharge is reduced, the angle of attack between relative velocity and blade will increase. Therefore C_L increases and cavitation may set in again. In this case cavitation may first occur at some point other than the blade tip.

The undisturbed stream pressure may be determined from

$$\frac{p_z}{w} = \frac{p_a}{w} + Z - \left\{\frac{V_f^2}{2g} + \text{losses}\right\} \qquad \ldots.(12.7)$$

where Z is the submergence of the blade *i.e.*, the distance of its centre below the free surface.

Example

12.1. An axial flow fan incorporating 12 blades of 'aerofoil' cross-section delivers air at atmospheric conditions at a rate of 21,900 ft.³/min.; at 960 r.p.m. The static pressure rise across the fan is to be 1·15 in. W.G. The tip diameter of the fan is 40 in. and the hub diameter 20 in. Assuming 90 per cent blade efficiency, calculate the chord and profile setting angle at the tip and hub. The 'aerofoil' is R.A.F. 6D type for which the C_L, C_D and C_L/C_D curves are given in *Fig. 12.14.*

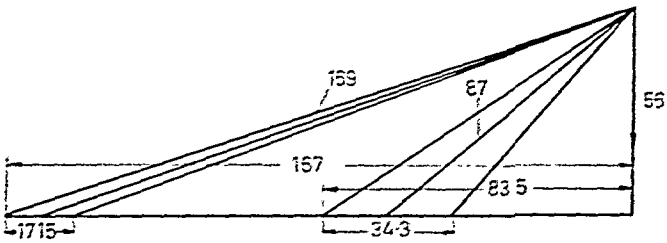

Figure 12.14

Solution.—Steps of calculations carried out as in Section 11.4.

(1) Peripheral speed at tip $V_t = \dfrac{40 \times \pi \times 960}{12 \times 60} = 167$

$$\text{at hub } V_h = \frac{20 \times \pi \times 960}{12 \times 60} = 83{\cdot}5$$

(2) Assumed blade efficiency $\eta_h = 90$ per cent.

$$\text{Whirl velocity at tip } V_w = \frac{1{\cdot}15 \times 5{\cdot}2 \times 32{\cdot}2}{0{\cdot}9 \times 0{\cdot}075 \times 167} = 17{\cdot}15$$

$$\text{at hub } V_w = 2 \times 17{\cdot}15 = 34{\cdot}3$$

(3) Through flow velocity $V_f = \dfrac{21{,}900 \times 4 \times 144}{\pi(40^2 - 20^2)} = 56$

(4) From the velocity vector diagram the mean relative velocity at tip $\bar{U}_m = 169$ and at hub $\bar{U}_m = 87$.

(5) The through flow–peripheral velocity ratio

$$\text{at tip } \frac{V_f}{V_t} = \frac{56}{167} = 0{\cdot}335, \text{ at hub} = 0{\cdot}670$$

(6) The lift–drag coefficient ratios

$$\text{at tip } \frac{C_L}{C_D} = \frac{0{\cdot}9 - 0{\cdot}335}{(0{\cdot}335)(0{\cdot}1)} = 37, \text{ at hub} = \frac{0{\cdot}9 - 0{\cdot}670}{(0{\cdot}670)(0{\cdot}1)} = 23{\cdot}5$$

(7) Reynolds' number assumed $N_R = 5 \times 10^5$

Lift coefficient at tip $C_L = 0{\cdot}73$, at hub $= 0{\cdot}46$

Incidence at tip $\alpha = 0°$, at hub $= -1\frac{1}{2}°$

$$\text{Chord } c = \frac{120}{960} \times \frac{1{\cdot}15 \times 5{\cdot}2 \times 32{\cdot}2}{12 \times 0{\cdot}9 \times 0{\cdot}075} \times \frac{1}{(C_L U_m)} = \frac{29{\cdot}8}{C_L U_m}$$

$$\text{Chord at tip } \frac{29{\cdot}8 \times 12}{0{\cdot}73 \times 169} \simeq 3 \text{ in. at hub} \simeq 9 \text{ in.}$$

Setting angle at tip $\alpha + \beta = 19°30'$, at hub $= 40 - 1\frac{1}{2} = 38°30'$

(8) Reynolds' number at tip $\frac{3 \times 167}{12 \times 1{\cdot}67} \times 10^4 = 2{\cdot}5 \times 10^5$

$$\text{at hub} = \frac{9 \times 87}{12 \times 1{\cdot}67} \times 10^4 = 3{\cdot}9 \times 10^5$$

(9) Hub pitch–chord ratio $\frac{20 \times \pi}{12 \times 9} = 0{\cdot}585 < 1$. Because of the overlapping it may be recommended to increase the hub diameter and repeat the calculations.

Problems

12.1. Determine, at the tip, the magnitude and direction of the air velocity downstream from an axial flow fan. (No guide vanes employed.)

The following data are available:

Air delivery: 15,660 ft.^{3}/min.
Total pressure rise across the fan: 1·08 in. W.G.
Efficiency of the fan: 70 per cent.
Tip diameter: 35 in.
Hub diameter: 18 in.
Revolutions per minute: 960
Air temperature: 70°F.

12.2. An axial flow fan incorporating 8 blades of aerofoil cross-section delivers air at atmospheric conditions at a rate of 13,700 ft.^{3}/min. at 1,440 r.p.m. The static pressure across the fan is $1\frac{3}{4}$ in. W.G. The tip diameter is 35 in., the hub 18 in. Assuming a reasonable blade efficiency, calculate the chord and profile setting angle at the tip and hub.

12.3. For the ventilation of a mine a long straight vertical circular duct is used and an axial flow fan is fitted inside the duct to maintain the air-flow.

With the data provided, calculate:

(*a*) the resistance of the duct;

(*b*) the power required to drive the fan;

(*c*) the number of stages in the fan;

(*d*) the leading dimensions of the fan (number of blades, chord at tip and hub, profile setting angles, *etc.*)

Data:

Duct diameter: 27·5 in., material galvanized iron.
Length of duct: 1,300 ft.
Delivery: 8,000 ft.^{3}/min.
Motor speed: 1,440 r.p.m.
Spec. weight of air: 0·075 per ft.^{3}
Fan overall efficiency: 80 per cent (allowing 10 per cent for frictional losses).
Entry loss k: = 0·1.
Lift coefficient C_L–angle of attack ratio:

α	0	4	8	$9\frac{1}{2}$
C_L	0·48	0·80	1·13	1·2

Neglect Reynolds' number effects.

12.4. An axial flow fan unit incorporates two impellers, one rotating in the opposite direction to the other (contra-rotation). The air enters the first impeller in an axial direction and leaves with a free vortex superimposed on the (axial) flow. Thence the air passes through the second impeller which removes the vortex motion, so that downstream from the second impeller the flow conditions are similar to the conditions in front of the first impeller. Draw the velocity triangles for both impellers, assuming that the energy imparted to the air is equal in both stages.

12.5. An axial flow pump is to deliver water at the rate of 100 ft.^{3}/sec. against a head of 15 ft. when running at 500 r.p.m.

Calculate the leading dimensions of the pump impeller and the profile setting angles of the vanes.

The tip-to-hub diameter ratio may be taken as 2, and the efficiency may be estimated with the aid of *Fig. 12.10.*

Determine which regions on the blade are affected by cavitation if the water temperature is 80°F, and the pump impeller is set 3 ft. above sump level. Use *Fig. 12.12.* Employ hydrofoil profile for the blades.

13

HYDRAULIC TURBINES

13.2 Introduction

HYDRAULIC turbines fall into that group of rotodynamic machinery which converts fluid pressure into useful power. The fluid medium is invariably water and its supply to the turbine must come from a certain height above the installation. Since the power is proportional to the product of supply Q and head H, it is evident that a given power requirement specifies the product $Q \cdot H$. For the QH product to remain constant one needs: (*a*) either values of high H and low Q or (*b*) low H and high Q. It will be shown in the following discussions that class (*a*) will be satisfied by the use of action (impulse) turbines and class (*b*) by reaction turbines. This classification is rather broad as there is some overlapping of conditions when both action or reaction turbines may be used.

13.2 Action (Impulse) Turbine Theory

In impulse turbines the head available is first completely converted into kinetic energy in one or more nozzles; the emerging jet then successively engages suitably shaped vanes called buckets spaced at

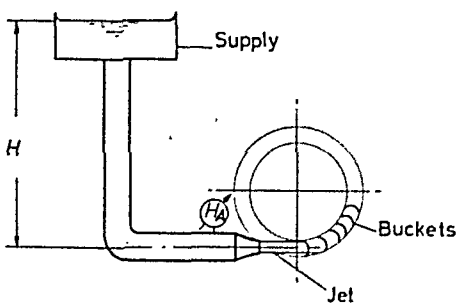

Figure 13.1—Schematic diagram of an impulse turbine.

equal pitch, which deflect the stream, and a force is created due to the change in momentum. The vanes are fitted to the perimeter of a circular disc which maintains steady rotation resulting from the tangential jet force (*see Fig. 13.1*). It is noted that the jet leaving the nozzle is surrounded by atmospheric pressure which also prevails both on entering and leaving the vane system.

The jet force acting on the vanes and the resulting power may be calculated from the change of momentum of the jet and the peripheral speed of the vanes. Consider first the simple case of a jet issuing from a nozzle with a velocity V_j, impinging tangentially on a vane which deflects the jet through 180° (*Fig. 13.2*).

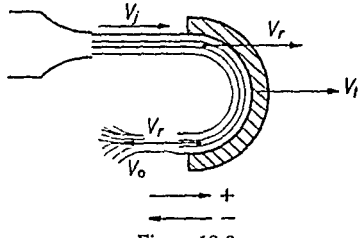

Figure 13.2

Since the vane moves away from the jet with velocity V_t, the relative velocity between vane and jet $V_r = V_j - V_t$. Neglecting friction, the force acting on the vane

$$F = Q\rho(V_1 - V_2) = Q\rho[(V_r)_{in} - (-V_r)_{out}]$$

Since

$$V_r = |V_j - V_t|_{in} = |V_j - V_t|_{out}$$

the force

$$F = 2Q\rho(V_j - V_t) \qquad \ldots.(13.1)$$

The resulting (ideal) power

$$P = FV_t = 2Q\rho(V_j - V_t)V_t \qquad \ldots.(13.2)$$

For given V_j, P attains a maximum value when

$$\frac{dP}{dV_t} = 2Q\rho(V_j - 2V_t) = 0$$

that is, when

$$\frac{V_t}{V_j} = \frac{1}{2} \qquad \ldots.(13.3)$$

At this vane speed the absolute outlet velocity $V_0 = 0$, in other words, the kinetic energy of the water that drops into the tailrace is a minimum. The specific power $P/\sqrt{2gH}$ plotted against V_t/V_j shows zero power at both $V_t/V_j = 0$ and $V_t/V_j = 1$ (*see Fig. 13.3*). In the first case the wheel is at rest and in the second case it attains the speed of the jet. This speed is called the 'run-away' speed and the vanes are running away from the jet with the same velocity.

The jet velocity may be calculated from $V_j = C_v\sqrt{(2gH_A)}$ where H_A is the available head. If H_A is assumed constant at the nozzle entry, power regulation may only be obtained by varying the discharge Q, since the rotational speed of the wheel is constant.

For this purpose the nozzle is provided with an adjustable needle which controls the diameter of the jet (*Fig. 13.4*). The coefficient C_v of the nozzle is about 0·985.

The standard impulse turbine at the present time is the Pelton wheel. In this design Pelton provided the buckets with a central splitter which divides the jet into two halves and the water leaving encloses an angle θ with the plane of rotation. The value of θ

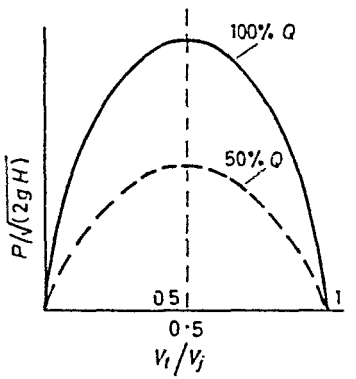

Figure 13.3

varies between 4 and 7°. Because of this angle the force is somewhat reduced and it is easy to see that

$$F = Q\rho[(V_j - V_t)_{in} - [-(V_j - V_t)_{out} \cos \theta]$$

$$= Q\rho(V_j - V_t)(1 + \cos \theta) \qquad \ldots.(13.4)$$

A further reduction of the force is due to friction, acting between the stream and the bucket walls which slows down the relative velocity V_r. This may be taken into consideration by means of a loss coefficient k. Writing the Bernoulli equation for the inlet and outlet of the vane, one obtains

$$\frac{(V_j - V_t)^2_{in}}{2g} = \frac{(V_j - V_t)^2_{out}}{2g} + k\frac{(V_j - V_t)^2_{out}}{2g}$$

so that

$$(V_j - V_t)_{out} = \frac{(V_j - V_t)_{in}}{\sqrt{(1 + k)}} \qquad \ldots.(13.5)$$

The theoretical power

$$P = Q\rho(V_j - V_t)\left(1 + \frac{\cos \theta}{\sqrt{(1 + k)}}\right)V_t \qquad \ldots.(13.5)$$

still attains its maximum value when $V_t/V_j = \frac{1}{2}$. It is noted, however, that windage and other mechanical losses cause the power peak to appear earlier (normally at a value of $V_t/V_j = 0{\cdot}45$).

The hydraulic efficiency of the Pelton wheel is given by

$$\eta_H = \frac{2P}{Q\rho V_j^2}$$

Substituting for P from Eq. 13.5 one obtains

$$\eta_H = 2\left[\frac{V_t}{V_j} - \left(\frac{V_t}{V_j}\right)^2\right]\left(1 + \frac{\cos\theta}{\sqrt{(1+k)}}\right) \quad \ldots.(13.6)$$

Maximum efficiency is attained when

$$\frac{d\eta_H}{dV_t} = 0$$

that is when

$$\frac{V_t}{V_j} = \frac{1}{2}$$

With this value the maximum hydraulic efficiency of the wheel

$$\eta_{max} = \frac{1}{2}\left(1 + \frac{\cos\theta}{\sqrt{(1+k)}}\right) \quad \ldots.(13.7)$$

Mechanical losses, resulting from windage and bearing friction, may be taken into account by the mechanical efficiency η_m.

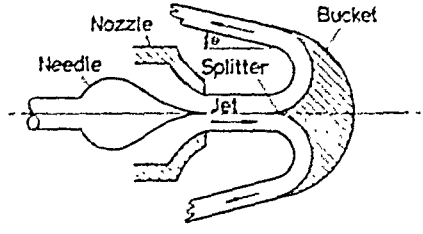

Figure 13.4—Pelton needle nozzle and bucket

Assuming that no leakage occurs, the overall efficiency $\eta_0 = \eta_H \cdot \eta_m$ and the shaft horse-power based on the available head

$$P = \frac{QwH_A\eta_0}{550} \quad \text{(h.p.)} \quad \ldots.(13.8)$$

Note that the power expression Eq. 13.8 differs from the pump power required, (Eq. 11.9) in that the overall efficiency now appears in the numerator.

13.3 Optimum Penstock Diameter

Impulse turbines are generally operating under a fairly large head. This requires a long penstock† in which the frictional losses may be considerable (*Fig. 13.5*). The jet diameter d_j is governed by

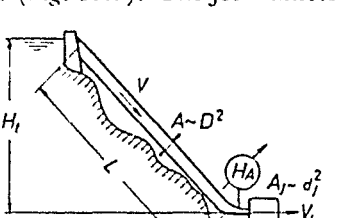

Figure 13.5—Schematic arrangement of Pelton turbine plant

power requirements or availability of water supply. The optimum diameter of the penstock D_p may be calculated by considering frictional losses and the power of the jet.

Considering pipe friction losses only, the available head at inlet to the nozzle,

$$H_A = H_t - H_f$$

where H_t is the total head and

$$H_f = f\frac{L}{D}\frac{V^2}{2g}.$$

Since the power of the jet

$$P_j = QwH_A/550$$

and

$$Q = a_j V_j$$

one obtains

$$P_j = \frac{wa_jV_j}{550}\left[H_t - f\frac{L}{D}\frac{V_j^2}{2g}\frac{a_j^2}{A^2}\right] \qquad \ldots.(13.9)$$

Differentiating with respect to a_j and equating to zero gives

$$\frac{dP_j}{da_j} = H_t - 3f\frac{L}{D}\frac{V_j^2}{2g}\frac{a_j^2}{A^2} = 0$$

whence

$$H_t = 3H_f$$

Thus power attains its maximum when the frictional loss H_f equals $\frac{1}{3}H_t$. This implies that the available head $H_A = \frac{2}{3}H_t = V_j^2/2g$.

† It is known that penstocks up to a mile long have been built.

Substituting this result into Eq. 13.9 (noting that $A^2 \propto D^4$) one obtains the optimum diameter of the penstock

$$D_p = (2fLd_j^4)^{\frac{1}{5}} \qquad \ldots.(13.10)$$

Eq. 13.10 may be solved for the jet diameter giving maximum power when

$$d_j = \left(\frac{D_p^5}{2fL}\right)^{\frac{1}{4}} \qquad \ldots.(13.11)$$

Thus for a specified penstock diameter the jet attains maximum power at a particular value of the jet size. The significance of Eq. 13.11 lies in the fact that *small* jets are powerless, because the discharge is small although the jet speed is high, and large jets are again powerless if the jet velocity is small *even if* the discharge is high.

Example

13.1. The supply to a nozzle is 18 in. diameter and 1,000 ft. long. If the mouth of the nozzle is 100 ft. below the water level in the supply reservoir taking $f = 0{\cdot}025$, what diameter of nozzle would give maximum kinetic energy of the issuing water per second and what is the horse-power of the jet. (Neglect all losses other than pipe friction.)

Solution.—For maximum kinetic energy

$$d = \sqrt[4]{\frac{(1{\cdot}5)^5}{2 \times 0{\cdot}025 \times 1{,}000}} = 0{\cdot}624 \text{ ft.} = 7{\cdot}5 \text{ in.}$$

Head available at jet

$$H = \tfrac{2}{3}H_t = 66{\cdot}6 \text{ ft.}$$

Jet speed

$$V_j = \sqrt{(64{\cdot}4 \times 66{\cdot}6)} = 65{\cdot}5 \text{ ft./sec.}$$

Discharge

$$Q = \frac{0{\cdot}624^2 \times \Pi \times 65{\cdot}5}{4} = 2{\cdot}01 \text{ ft.}^3\text{/sec.}$$

Jet power

$$P = \frac{2{\cdot}01 \times 62{\cdot}4 \times 65{\cdot}5}{550} = 152 \text{ h.p.}$$

Exercise

Also calculate the jet power with any other jet diameter.

13.4 Specific Speed and Wheel–jet Diameter Relationships

The specific speed for turbines is obtained by eliminating the wheel diameter from the power and head parameters (Eqs. 11.19 and 11.20). Thus

$$N_s = \frac{\Pi_P^{1/2}}{\Pi_H^{5/4}} = N\frac{P^{1/2}}{\rho^{1/2}g^{5/4}H_A^{5/4}}$$

Ignoring the constants

$$N_s = N \frac{\sqrt{(HP)}}{H^{5/4}} \qquad \ldots\ldots(13.12)$$

Results of tests made on single nozzle Pelton turbines show a limited range of specific speed for high efficiency; (*see Fig. 13.6*)

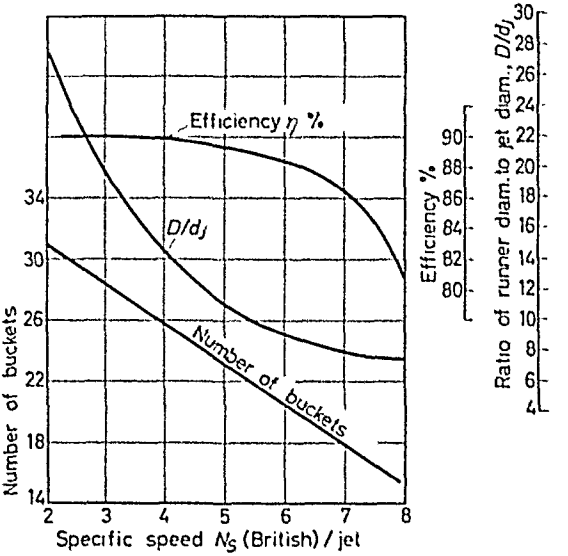

Figure 13.6—(By courtesy of English Electric)

generally $N_s = 2$–7 is recommended. The highest efficiency attained is about 88 per cent at approximately $N_s = 4{\cdot}5$.

The relationship between jet and wheel pitch diameter D affects the specific speed hence the efficiency of the turbine. This may be shown by substituting into Eq. 13.12 the following expressions

(i) $$HP = \frac{QwH_t\eta_0}{550} = \frac{\pi w d_j^2 V_j^3 \eta_0}{4 \times 550 \times 2g}$$

(ii) $$N = \frac{60V_t}{\pi D}$$

Hence

$$N_s = \frac{60(2g^{3/4})\sqrt{w}}{2\sqrt{\pi} \times 550} \sqrt{\eta_0} C_v^{3/2} \left(\frac{V_t}{V_j}\right) \frac{d_j}{D}$$

With standard numerical values of w, g, C_v

$$N_s \simeq 129\sqrt{\eta_0} \left(\frac{V_t}{V_j}\right) \frac{d_j}{D} \qquad \ldots\ldots(13.13)$$

Finally, substituting into Eq. 13.13 $\eta_0 = 0{\cdot}88$, $V_f/V_j = 0{\cdot}45$ and $N_s = 4{\cdot}5$ one obtains the optimum wheel–jet diameter ratio

$$\frac{D}{d_j} \cong 11 \text{ (approximately)} \qquad \ldots\ldots(13.14)$$

Note that the D/d_j ratio decreases with increasing N_s and vice versa. For example $N_s = 2$, $D/d_j = 28$; for $N_s = 7$, $D/d_j = 6{\cdot}5$. Again, a large D/d_j results in a low speed wheel whilst the lower values of D/d are limited by bucket design considerations.

13.5 Pelton Turbine Designs

Pelton turbines are usually arranged with horizontal shafting supporting single or twin runners. Power may be derived from a single jet (*Fig. 13.7*) or from twin jets (*Fig. 13.8*), although some

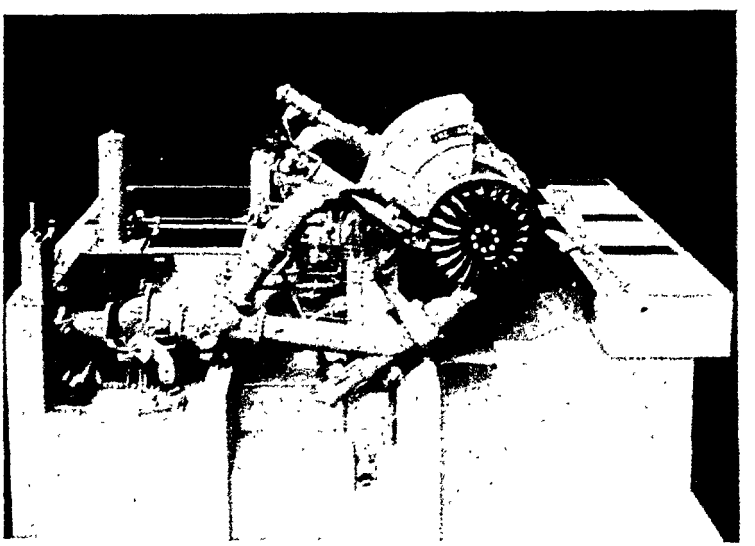

Figure 13.8—Twin jet Pelton turbine.
(*By courtesy of English Electric*)

designs embody as many as four jets. The nozzle incorporating the needle (*Fig. 13.9*) must be carefully streamlined to produce parallel flow at exit and the surfaces must be smooth to reduce losses resulting from friction. In order to keep the boundary layer as thin as possible the velocity should be increased quickly at the nozzle tip and for this reason the nozzle must be short.

The buckets may be cast in one piece with the disc (*Fig. 13.10*), or may be separately cast, machined and bolted to the disc. In designing the buckets care must be taken that no water is allowed to pass through the wheel without reacting fully on the buckets. To avoid shock losses upon contact with the jet the buckets must

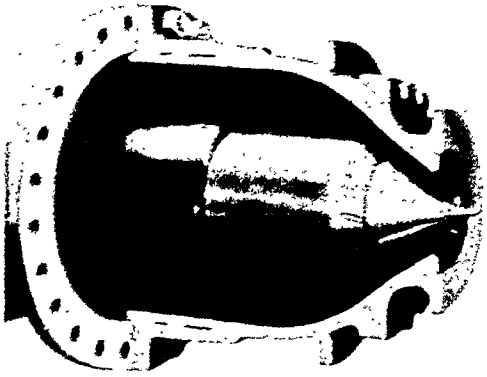

Figure 13.9—Nozzle and needle of a Pelton turbine. (By courtesy of English Electric)

be carefully shaped. Their number and size depends to some extent upon jet diameter although experiments indicate that a large number of buckets is desirable. Details of design are beyond this text and may be found in the literature.†

The casing, housing the wheel and nozzle, is usually made in two parts and is open at the bottom to allow the water to escape freely into the tailwater.

Example

13.2. A Pelton turbine is to supply a net output of 100 kilowatts. If the total head available is 600 ft. and the penstock is 800 ft. long, calculate:

(*a*) the jet horsepower for maximum hydraulic (wheel) efficiency assuming that water leaves the bucket at an angle $\theta = 10°$ and that generator efficiency is 92 per cent, mechanical efficiency is 95 per cent;
(*b*) the discharge, allowing $\frac{1}{2}$ of the total head for frictional losses;
(*c*) the velocity and the diameter of the jet;
(*d*) diameter and speed of the wheel;
(*e*) the diameter of the penstock.

† *See* Engineering News, Feb. 10, 1910, a paper by S. J. Zwoiki, *or* Marks Mechanical Engineering Handbook.

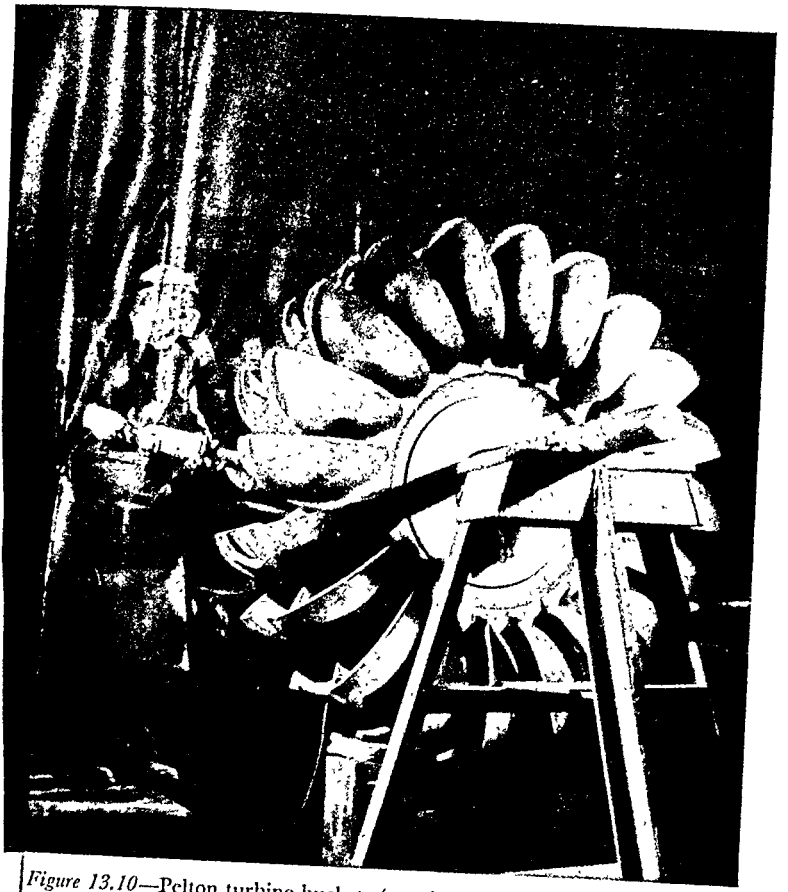

Figure 13.10—Pelton turbine buckets (cast in one piece with the disc)
(*By courtesy of English Electric*)

sume a wrought iron pipe. Kinematic viscosity $= 1{\cdot}16 \times 10^{-5}$ ft.²/sec.
coefficient in buckets $k = 0{\cdot}25$.
$= 1{\cdot}36$ h.p.

lution.—(*a*) Maximum hydraulic efficiency

$$\eta_H = \tfrac{1}{2}\left(1 + \frac{\cos\theta}{\sqrt{(1 + 0{\cdot}25)}}\right) = 0{\cdot}936$$

$\therefore$ overall efficiency $\eta_0 = 0{\cdot}936 \times 0{\cdot}95 = 0{\cdot}89$

$$\text{Required jet power} = \frac{1{\cdot}36 \times 100}{0{\cdot}89 \times 0{\cdot}92} = 167 \text{ h.p.}$$

(*b*) Since the available head is $H_{av} = \frac{2}{3}H_t = \frac{2}{3} \times 600 = 400$ ft.

$$\text{Jet power} = 167 = \frac{Q \times 62{\cdot}4 \times 400}{550}$$

$\therefore$ The discharge $Q = 3{\cdot}68$ cusecs.

(*c*) Jet velocity $V_j = 0{\cdot}985 \times \sqrt{(64{\cdot}4 \times 400)} = 158{\cdot}8$ ft./sec.

$$\text{Jet diameter } d_j = \sqrt{\frac{4}{\pi} \times \frac{3{\cdot}68}{158{\cdot}8}} = 0{\cdot}172 \text{ ft.} = 2{\cdot}07 \text{ in.}$$

(*d*) For max. efficiency peripheral speed $V_t = 0{\cdot}45 \times 158{\cdot}8 = 71{\cdot}5$ ft./sec.

$$DN = \frac{60 \times 71{\cdot}5}{\pi} = 1370$$

For

$N =$	500	750	1,000
$D =$	2·74	1·83	1·37
$\frac{D}{d_j} =$	15·9	10·6	7·95

Choose $N = 750$ r.p.m. specific speed $= 750 \dfrac{\sqrt{(167 \times 0{\cdot}92)}}{400^{5/4}} = 5{\cdot}25$

(*e*) Assume friction factor: $f = 0{\cdot}015$
Diameter of penstock

$$D_P = (2 \times 0{\cdot}015 \times 800 \times 0{\cdot}172^4) = 0{\cdot}46 \text{ ft.} = 5{\cdot}5 \text{ in.}$$

Check frictional losses.

13.6 Reaction Turbines

In reaction turbines the head available is partially transformed into kinetic energy in a set of stationary guide vanes, the balance being transformed inside the runner. Whilst in the impulse turbine the jet engages a few vanes at a time and leaves the rest rotating in the surrounding air, in the reaction turbine fluid fills the runner passages completely.

Two distinct types of reaction turbines are being produced at the present time: the Francis and the Kaplan.

Francis

The principle of operation of the Francis type turbines is similar to a centrifugal pump working under reversed flow conditions, namely the fluid entering the 'discharge' end and leaving the eye. Whilst in centrifugal pumps a whirl is developed in the impeller and subsequently transformed into pressure, in reaction turbines one portion of the head available is first transformed into a whirl and is subsequently converted into power inside the runner. The other portion of the head is employed for the acceleration the

relative velocity of the water passing through the channels formed by the runner vanes. The vanes themselves are curved surfaces.

The principal features of a particular Francis turbine are shown in *Fig. 13.11.* Water first enters a spiral casing† from which it flows

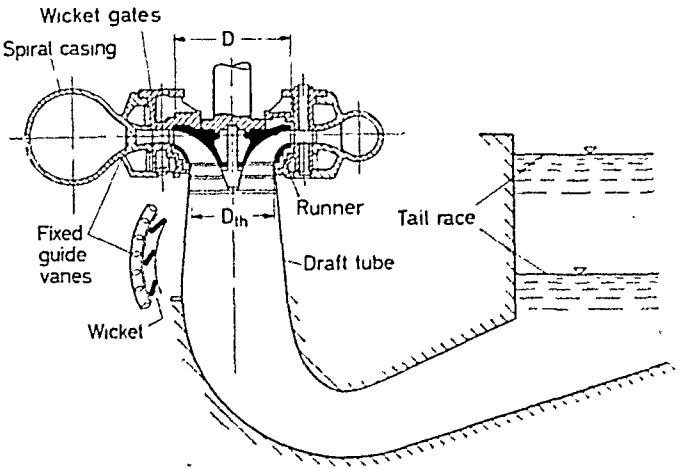

Figure 13.11—Schematic section of a Francis turbine

radially through a set of fixed guide vanes arranged in the form of a ring around a second inner ring of adjustable guide vanes, frequently called wicket gates. The flow turns inside the runner and leaves in the axial direction; it then enters the diffuser or draft tube and finally discharges into the tail-race.

At the throat of the draft tube the pressure may be well below atmospheric which compensates for the height at which the turbine runner is set. The draft tube serves a dual purpose: it reduces the velocity from throat to exit and permits the turbine to be set above the level of the tail water.

Kaplan

The principle of operation of the Kaplan type turbine is similar to an axial flow pump in which the stream passes over blades of hydrofoil cross-section.‡ The guide vanes for the Kaplan turbine are arranged in the same way as for the Francis and produce a

† Spiral casing for high pressure turbines and open flame type for moderate heads.

‡ HUTTON, S. P. 'Aerofoil theory applied to the design of Kaplan turbine blades,' *Proc. Instn. Mech. Engrs*, 163, 1950, p. 89.

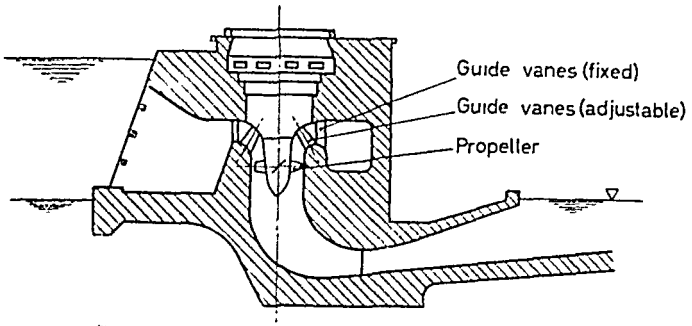

Figure 13.12—Schematic section of a Kaplan turbine

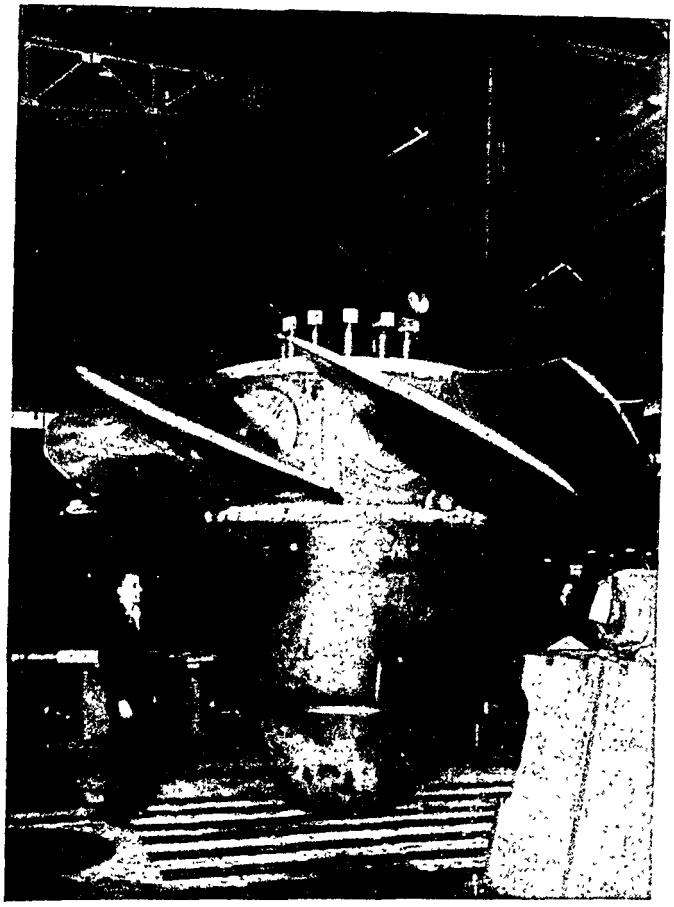

Figure 13.13—Runner for a 35,000 h.p. Kaplan turbine.
(*By courtesy of English Electric*)

whirl (*Fig. 13.12*). The runner itself (*Fig. 13.13*) is found at the throat of the ducting and a considerable space exists between the ends of the guide vanes and the leading edge of the propeller. Within this space the flow direction changes from radial to axial and simultaneously the flow pattern approaches, but does not fully

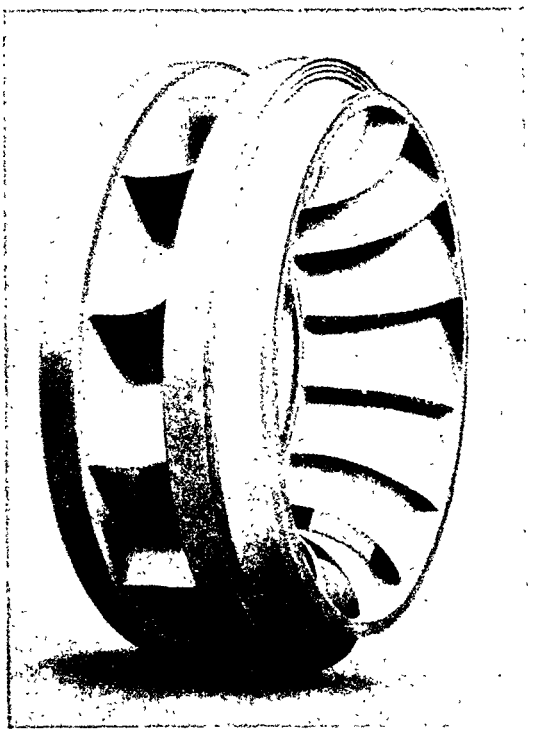

Figure 13.14—Francis turbine runner showing inlet and discharge side. (*By courtesy of English Electric*)

attain, the free vortex state. Tests show that at the inlet to the propeller the whirl velocity is not exactly inversely proportional to the radius because the flow had not had time to reach the ideal state of radial equilibrium before entering the wheel blading. The runner blades remove this whirl and transform it into useful power. The advantage of Kaplan turbines over the Francis type lies in the fact that both guide vane and blade setting angles can be adjusted simultaneously to compensate for changing flow or load conditions whilst the Francis turbine with fixed blade runners (*Fig. 13.14*) can

only change the wicket gate setting. Thus, off-design-point operation results in shock losses in the Francis turbine with a subsequent loss in efficiency, whilst the Kaplan maintains optimum operation over a wider range of loading. It is noted that the speed of these machines is held constant under changes of load.

13.7 Velocity Vector Diagrams and Application of Euler's Equation

Velocity vector diagrams for the low specific speed Francis turbines are similar in construction to those shown in the section on centrifugal pumps. For Francis runners with high specific speeds these simple two-dimensional diagrams become three dimensional because of the mixed flow character of the stream. In Kaplan turbines the behaviour of the flow is even more complex† and both theory and test results appear to be closely guarded commercial secrets. It is known, however, that the design of modern Kaplan blading is based on wing theory, applied so as to take cascade (blade interference) effects into account.

Referring to the low specific speed Francis turbine the wicket gates are at an angle α to produce a whirl V_{w1}, thus increasing the radial velocity at runner inlet from V_{r1} to V_1. At the runner blade inlet, the relative velocity U_1, drawn parallel to the tip, the tangential (peripheral) speed of the runner V_{t1}, and the absolute inlet velocity V_1 complete the inlet velocity vector diagram (*Fig. 13.15*). Assuming the whirl velocity to be zero at runner outlet,‡ the absolute exit velocity V_2 becomes radial. In this case the ideal power developed by the runner may be obtained from the equation,

$$H_{av} = \frac{V_{t1} V_{w1}}{g} \text{ ft.lb./lb.}$$

Introducing the hydraulic efficiency η_H, the 'internal' power

$$H_i = H_{av} \cdot \eta_H \qquad \ldots . (13.15)$$

Therefore, the actual whirl velocity at inlet

$$V_{w1} = \frac{H_{av} \cdot g \cdot \eta_H}{V_{t1}} \qquad \ldots . (13.16)$$

It is of interest to note that in turbines (unlike in pumps) the relative eddy effects need not be considered, because the whirl is developed in a stationary vane system.

† For qualitative information see: 'The importance of cavitation in the development of high pressure Kaplan turbine blading' *Escher-Wyss News*, Vol. XX, 1946, 47, p. 17.

‡ It was found in practice that best efficiency is obtained when a small whirl is retained at the exit. The small whirl improves the efficiency of the draft tube.

The available head may be calculated, considering the total difference in elevation H_t minus the frictional losses in the ducting

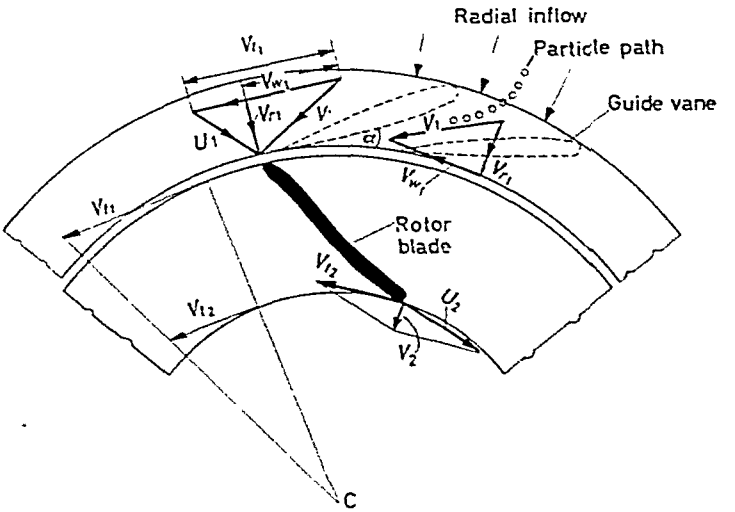

Figure 13.15—Inlet and outlet velocity vector diagrams of a Francis turbine

and the velocity head lost in the tailrace at the point of discharge (*see Fig. 13.16*).

$$H_{ar} = H_t - H_f - \frac{V_0^2}{2g} \qquad \ldots.(13.17)$$

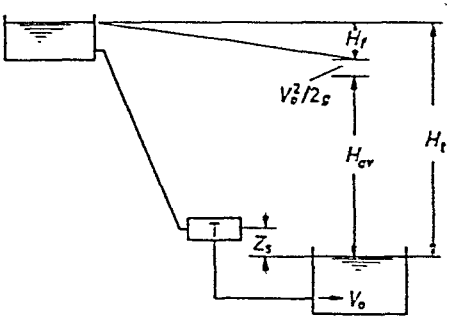

Figure 13.16—Simple line diagram of a reaction turbine plant

13.8 Turbine Selection and Runner Design on the Basis of Specific Speed

There are two sets of curves which provide a basis for turbine selection. The first graph gives the range of specific speed of the

various turbines for a given application (head) (*Fig. 13.17*). This graph is a summary of modern turbine building practice and it facilitates the selection of a turbine type. It shows, for example, that for heads over 1,500 ft. only, the Pelton wheel is recommended; for heads between 1,500 ft. and 200 ft. there is a choice between Pelton or Francis. From 200 ft. to 100 ft. the choice lies between Francis and Kaplan.

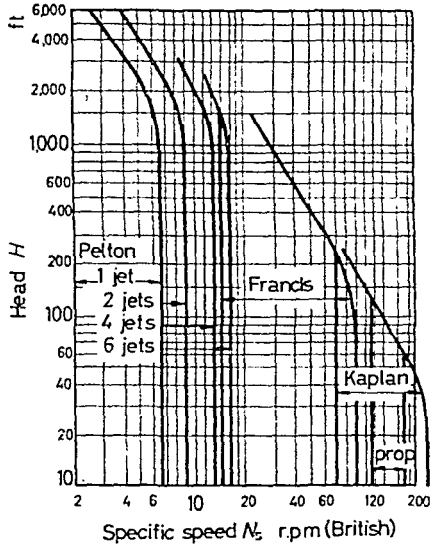

Figure 13.17—Chart for turbine selection
(*From Kempe's Engineers' Year Book*)

The second graph (*Fig. 13.18*), gives the maximum efficiencies obtained in practice and shows the variation of efficiency with specific speed. This graph indicates the range of specific speed at which the various types operate most favourably.

The specific speed of Francis turbines lies between the approximate limits 10–90 and that of the Kaplan between 70–180 (British units).

The shape of the Francis runners and their relative dimensions are greatly influenced by the specific speed. Typical runner profiles are shown in *Fig. 13.19a*, *b* and *c*. It appears that in low specific speed Francis runners the ratio of outside diameter to the eye or throat diameter, D/D_{th}, is well over one (*Fig. 13.19a*), whilst around $N_s = 45$–50 the ratio is one (*Fig. 13.19b*), hence $D = D_{th}$; above this N_s the D_{th} appears to be larger than D (*Fig. 13.19c*). The

inlet passage width to diameter ratio, B/D, also increases with specific speed. Changes of the relative dimensions and of runner

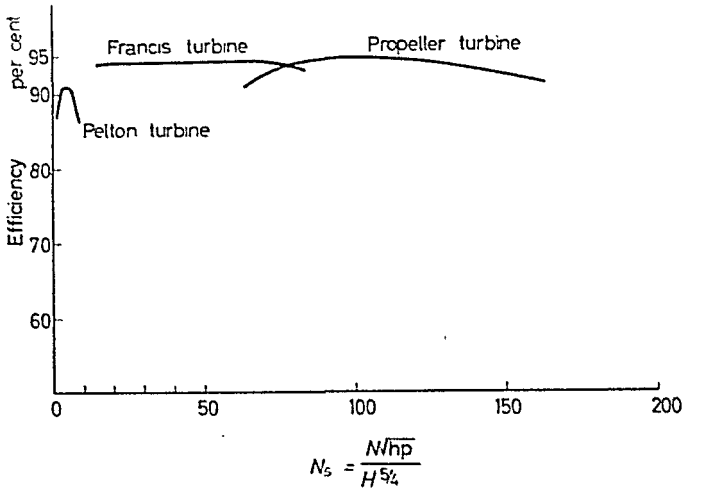

Figure 13.18—Specific speed-efficiency graph of water turbines. (*By courtesy of English Electric*)

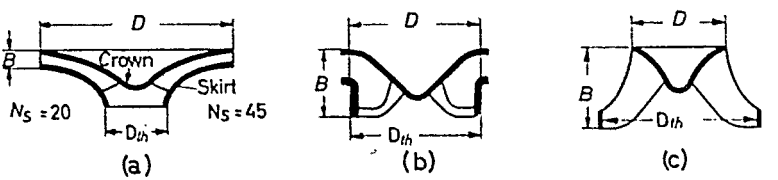

Figure 13.19—Variation of Francis runner shape with specific speed

coefficients with specific speed appear from curves shown in *Fig. 13.20.* The runner coefficient is defined by

$$\phi = \frac{V_t}{\sqrt{(2gH_{av})}}$$

where V_t is the tangential speed of the runner at a given diameter.

There are curves for four coefficients, each representing a point on the runner. The suffix i denotes crown and the suffix 0 denotes the skirt. Suffices 1 and 2 denote passage inlet and outlet respectively.

Similar curves are given for the Kaplan turbine in *Fig. 13.21.*

These curves may serve as a guide in estimating the leading dimensions of the runner without going into detailed calculations

of the vane design, which is a drafting board problem. Ultimately the results must be checked by laboratory tests, which really means

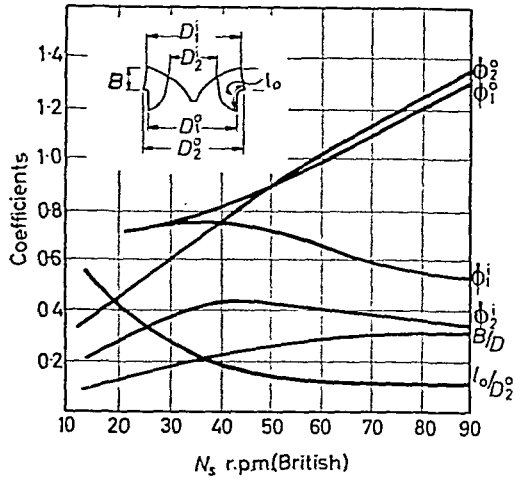

Figure 13.20—Runner coefficients for Francis runners. (*From Kempe's Engineers' Year Book*)

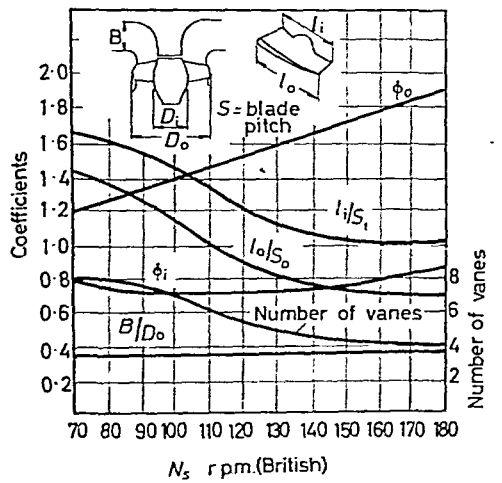

Figure 13.21—Runner coefficients and number of vanes for Kaplan runners. (*From Kempe's Engineers' Year Book*)

that scale model testing of turbines has become standard practice nowadays because turbines built for large power output are costly projects and their performance must be guaranteed by the makers.

13.9 Similarity Relationships and Cavitation of Reaction Turbines

With the aid of Eqs. 11.18, 11.19, and 11.20, results obtained on model turbines may be applied for the prediction of the performance of the prototype. It is essential not only that the geometrical reproduction of the turbine be true to scale, but also that a complete

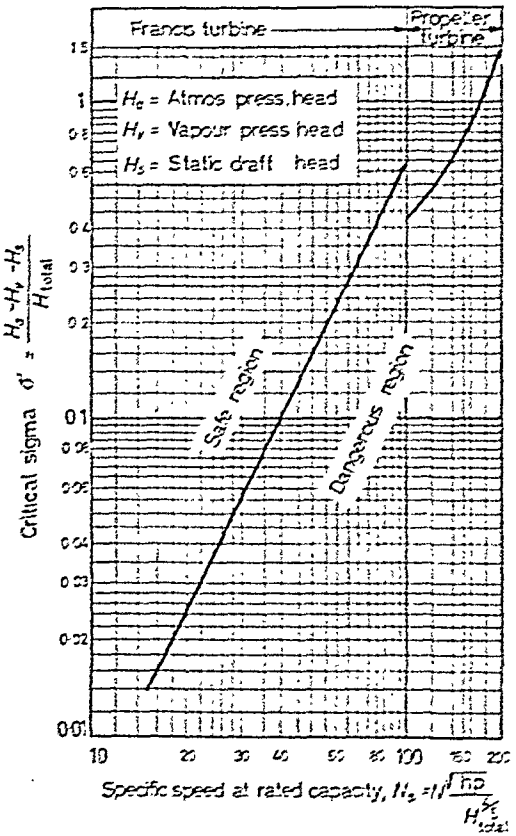

Figure 13.22—Cavitation chart for turbines. *(By courtesy of McGraw-Hill, New York.)*

similarity of flow conditions be established at the turbine approaches and at the turbine outlet. Finally, similarity of cavitation should be observed and scale effects taken into account.

Similarity of cavitation is satisfied with Eqs. 11.37 and 11.38. For the checking of setting height, Z_s, a critical cavitation limit

line for Francis and Kaplan turbines is given in *Fig. 13.22.* As is apparent from the diagram the cavitation parameter σ is the same expression as given by Eq. 11.35.

It appears from *Fig. 13.22* that turbines, like pumps, show increased susceptibility to cavitation at higher specific speeds. For this reason the setting of high specific speed machines above tail-water level is more critical than that of low specific speed machines,

Figure 13.23—Cavitation in a Kaplan model turbine.
(*By courtesy of Escher Wyss*)

and it may so happen that the runner must be submerged below the level of the tail-water. Cavitation in a Kaplan model turbine is shown in *Fig. 13.23.*

Scale effects *i.e.,* discrepancies in performance owing to a difference of the Reynolds numbers may be corrected by applying a step-up formula. A number of such step-up formulae are recommended. The formula by Moody gives the overall efficiency

relations between model and prototype (suffices m and p respectively) in terms of the runner diameters, thus

$$\frac{1-\eta_m}{1-\eta_p} = \left(\frac{D_m}{D_p}\right)^{1/5} \qquad \ldots\ldots(13.18)$$

The formula by Ackeret gives the hydraulic efficiency relations in terms of the Reynolds' numbers,

thus

$$\frac{1-\eta_{Hm}}{1-\eta_{Hp}} = \tfrac{1}{2}\left[1+\left(\frac{N_{Rm}}{N_{Rp}}\right)^{1/5}\right] \qquad \ldots\ldots(13.19)$$

where

$$N_R = D \times \sqrt{(2gH_{ar})}/\nu$$

The above formulae are strictly applicable only to the point of optimum performance.

Example

13.3. A hydraulic turbine is required to utilize a supply of 55 ft.^{3}/sec. under an available head of 200 ft. The turbine will be used directly coupled to a 50 cycle alternator. Place the runner 10 ft. above the tail water and provide for a possible water temperature of 80°F (at sea level).

Select a suitable type of turbine and calculate:

(*a*) the power of the turbine;

(*b*) the rotational speed;

(*c*) the leading dimensions of the runner for cavitation-free operating conditions and the mean inlet vane angle.

Assume 93 per cent overall efficiency and 99 per cent mechanical efficiency.

Note: The relation between number of poles p, frequency f and rotational speed is given by $N = 120f/p$.

Solution.—(*a*) $$P = \frac{55 \times 62{\cdot}4 \times 200 \times 0{\cdot}93}{550} = 1{,}160 \text{ h.p.}$$

(*b*) Specific speed

$$N_s = N\frac{\sqrt{1{,}160}}{200^{5/4}} = 0{\cdot}0453\,N$$

Question of N:

Calculate cavitation parameter

$$\sigma = \frac{34 - 1{\cdot}16 - 10}{200} = 0{\cdot}114$$

Safe region line intersects 0·114 at $N_s = 50$ so that a Francis turbine will be used.

The speed $N = 50 \times 750/34 = 1{,}100$ gives $120 \times 50/1{,}100 = 5{\cdot}4$ poles.

For safe operation use $N = 1{,}000$ r.p.m. so that number of poles $= 6$.
For this speed $N_s = 1{,}000 \times 34/750 = 45{\cdot}3$.
(c) For $N_s = 45{\cdot}3$ the design constants are (British practice)

$$\phi_1^e = 0{\cdot}85 \qquad \phi_2^e = 0{\cdot}82$$
$$\phi_1^i = 0{\cdot}75 \qquad \phi_2^i = 0{\cdot}43$$
$$B/D_2^e = 0{\cdot}23 \qquad l_0/D_2^e = 0{\cdot}17$$

Since $\sqrt{(2gH_{ar})} = \sqrt{(64{\cdot}0 \times 200)} = 114$

$$V_{f1}^e = 0{\cdot}85 \times 114 = 97 \text{ ft./sec.}$$

and
$$D_1^e = \frac{60 \times 97}{\Pi \times 1{,}000} = 1{\cdot}85 \text{ ft.} = 22{\cdot}2 \text{ in.}$$

Then by proportion

$$D_2^e = 0{\cdot}82/0{\cdot}85 \times 22{\cdot}2 = 21{\cdot}5 \text{ in.}$$
$$D_1^i = 0{\cdot}75/0{\cdot}85 \times 22{\cdot}2 = 19{\cdot}6 \text{ in.}$$
$$D_2^i = 0{\cdot}43/0{\cdot}85 \times 22{\cdot}2 = 11{\cdot}2 \text{ in.}$$
$$B = 21{\cdot}5 \times 0{\cdot}23 = 4{\cdot}95 \text{ in.}$$
$$l_0 = 21{\cdot}5 \times 0{\cdot}17 = 3{\cdot}65 \text{ in.}$$

Radial velocity at runner inlet (using $D_m = D_1^i + D_1^e/2$)

$$V_f = \frac{55 \times 144}{20{\cdot}9\Pi \times 4{\cdot}95} = 24{\cdot}3 \text{ ft./sec.}$$

Whirl velocity at inlet (using mean peripheral speed)

$$V_{w} = \frac{200 \times 32{\cdot}2 \times 0{\cdot}94}{91} = 66{\cdot}6$$

Inlet vane angle

$$\beta_1 = \tan^{-1} \frac{V_f}{V_{f1} - V_{w1}} = \tan^{-1} \frac{24{\cdot}3}{91 - 66{\cdot}6} \simeq 45^\circ$$

REFERENCES

(1) Braikevitch, M., and Adler, G. F. W., *Kempe's Engineers Year Book* (section on Water Turbines) p. 945.
(2) Davis, C. V., Ed., *Handbook of Applied Hydraulics*, McGraw-Hill, New York, 1952.
(3) Tenot, A., *Turbines Hydrauliques et Regulateurs Automatiques de Vitesse*, Libraire de l'enseignement Technique, Vol. III, Paris, 1935.
(4) Pfleiderer, C., Die Wasserturbinen, Springer, 1948.
(5) Winternitz, F. A. L., 'Cavitation in Turbomachines', *M.E.R.L. Report*, No. 40, 1955.

Problems

13.1. A turbine is to operate under a head of 500 ft. and is to develop 5,000 h.p. at 600 r.p.m. The efficiency is expected to be 90 per cent.

A model of the turbine is to be built to a scale of 1 : 9 and the head available for testing is 25 ft. What would be the speed of the model and what will be its approximate water consumption and power output? Briefly state your reasons for any assumption made.

13.2. In a hydro electric power project, it is proposed to instal two turbines each providing 5,000 kW output. The supply available is approximately 300,000 gal./min.

Calculate:

(*a*) the approximate head required at the inlet to the turbine assuming 92 per cent overall efficiency;

(*b*) the rotational speed, and the leading dimensions of a suitable turbine for cavitation free operating conditions.

Place the runner 10 ft. above tail water level and base your calculations on 80°F water temperature.

Note: The relation between number of poles p, frequency and rotational speed is given by $N = 120 f/p$.

13.3. A propeller turbine is to develop 5,000 h.p. under an available head of 30 ft.

Assuming a suitable specific speed, calculate:

(*a*) the approximate height of the runner above the tailwater for cavitation free operating conditions, (water temperature 80°F neglecting losses in the draft tube)

(*b*) the rotational speed, and the diameter of the runner;

(*c*) the discharge through the turbine assuming an efficiency of 92 per cent.

INDEX